HOLLOW SECTIONS IN STRUCTURAL APPLICATIONS

by J. Wardenier

Hollow Sections in Structural Applications

Prof.dr. J. Wardenier
Delft University of Technology
The Netherlands

Comité International pour le Développement
et l'Etude de la Construction Tubulaire

Review Committee

Prof.Dr. J.M. Aribert	France	
Prof.Dr. G. Hancock	Australia	
Prof.Dr. Y. Kurobane	Japan	
Prof.Dr. D.A. Nethercot	U.K.	
Prof.Dr. E. Niemi	Finland	
Prof.Dr. J.A. Packer	Canada	
Prof.Dr. R.S. Puthli	Germany	
Prof.Dr. J.L. Ramirez	Spain	
Prof.Dr. J. Rondal	Belgium	
Mr J. Ocio	Spain	Chairman, CIDECT Promotions Group
Mr. N.F. Yeomans	U.K.	Chairman, CIDECT Technical Commission

HOLLOW SECTIONS IN STRUCTURAL APPLICATIONS

by J. Wardenier

PREFACE

Professor Jaap Wardenier has had an enormous impact on the design methods for tubular steel structures in the late 20th. century. The Rectangular Hollow Section is veritably his progeny and it has grown up to be a respectable member of the steel society under his tutelage. Indeed, his output has been so prolific that all subsequent researchers on Rectangular Hollow Sections might well be deemed but footnotes to Wardenier.

Professor Wardenier is universally renowned for his leadership role in international unity efforts to standardize hollow section design rules, particularly while Chair of the International Institute of Welding (IIW) Subcommission XV-E on Tubular Structures, from 1981 to 1991. Similarly, his constant support of CIDECT activities over three decades, whether serving as a Member or Chair of Working Groups, and Member or Chair of the Technical Commission, has been a vital component of its success.

In the 1980s and 1990s a number of technical books and guides for design with hollow sections have been produced, beginning of course with his own landmark treatise, "*Hollow Section Joints*", in 1982. These books and guides were almost totally directed at the practicing engineer and the complexity of the formulations is perplexing to the novice. So, it is quite fitting that - having scaled to the top of the research mountain - Professor Wardenier can see the big picture so well that he can now paint a smaller version for the newcomer to the field., the student. This book hence fits this role admirably and this "text for students" is a much-needed contribution to the literature on tubular steel structures. The content and presentation is generally oriented to "graduate level" structural engineering students, or those in about Year 5 of their university studies. In addition to being invaluable for a specialist course on "Tubular Steel Structures", parts of the book would be excellent for more introductory-level courses on steel behaviour and design. Aside from succinctly telling the important principles for the behaviour of tubular structures, the book is nicely presented with numerous colour illustrations. The material included is an international consensus of knowledge on the topic at the turn of the Millenium: as such it is an ideal reference book too for all structural design engineers, as well as being a "student text".

Professor Jeffrey A. Packer
Chair, International Institute of Welding Subcommission XV-E on Tubular Structures

Mr. Noel F. Yeomans
Chair, CIDECT Technical Commission

December 2001.

Acknowledgement

This book serves as a background for students in Structural and Civil Engineering.
Since the available hours for teaching Steel Structures and particularly Tubular Structures vary from country to country, this book has been written in a modular form. To cover the needs in the various countries, a committee was established to review the material. Although the material is mainly based on the Eurocodes, the setup makes it easy to change the lectures and relate them to other (national) codes.

I wish to thank the review committee for their constructive comments during the preparation of this book. In particular I would like to thank my colleagues Prof. Packer, Prof. Puthli and Mr. Yeomans for their very detailed checks and suggestions. I am very grateful that Prof. Packer was willing to check the language in detail.

Appreciation is further extended to the authors of the various CIDECT Design Guides and to CIDECT itself for making parts of these design guides or background information for this book available.

Grateful acknowledgement is made to the contributions of Delft University of Technology in particular for the typing by Mrs van der Wouden and the excellent preparation of the figures and the layout by Dr. Liu.

Finally, I wish to thank CIDECT for the initiative in sponsoring the writing of this book and producing the CD-ROM.

Delft, December, 2000
J. Wardenier

Contents

Symbols

A	cross sectional area
A_a	cross sectional area of the structural steel in a composite column
A_c	cross sectional area of concrete in a composite column
A_m	surface area of a steel member/unit length
A_m	cross section parameter for torsion
A_{net}	net cross sectional area
A_s	cross sectional area of the reinforcement in a composite column
A_v	shear area
B_e	effective chord length in ring model
C_K	efficiency parameter for K-joints
C_T	efficiency parameter for T-joints
C_X	efficiency parameter for X-joints
CTOD	Crack Tip Opening Displacement
E	modulus of elasticity
E_a	modulus of elasticity for the steel section in a composite column
E_d	energy dissipation
E_{cm}	modulus of elasticity for concrete in a composite column
E_s	molulus of elasticity for the reinforcement in a composite column
I	moment of inertia
I_a	moment of inertia for the steel section in a composite column
I_b	moment of inertia for a beam
I_c	moment of inertia for the concrete in a composite column
I_s	moment of inertia for the reinforcement in a composite column
I_t	torsional moment of inertia
J_{AA}	load ratio for multiplanar joint
L_b	length of beam
$L_{co\theta}$	buckling length under fire condition
L_o	measured length of a tensile test specimen
M	moment
M_b	beam bending moment
$M_{c,Rd}$	design bending moment capacity of a member
M_e	elastic moment capacity
M_f	moment in flange
M_{fi}	maximum applied end moment in the fire situation
M_j	joint bending moment
$M_{j,Rd}$	joint moment capacity
$M_{j,Sd}$	joint moment loading
$M_{p\ell}$	plastic moment capacity
$M_{p\ell,f}$	plastic moment capacity of a flange
$M_{p\ell,Rd}$	beam plastic moment capacity
$M_{t,Rd}$	design torsional moment capacity of a member
M_y	elastic yield moment capacity
N	axial load
N	number of cycles
$N_{b,Rd}$	design buckling capacity of a member
$N_{cr,\theta}$	buckling resistance under fire conditions
N_{cr}	elastic Euler buckling load
N_{eq}	equivalent axial load
$\mathbf{N_i^*}$	joint design resistance, expressed as an axial force in member i
N_{fi}	axial force in the fire situation

$N_{G.Sd}$	permanent part of the acting design force in a composite column
N_i	applied axial force in member i (i = 0, 1, 2, 3)
N_i	number of cycles to failure
N_{nc}	compression resistance of gross cross section at room temperature
$N_{p\ell}$	axial load capacity of a member
$N_{p\ell,Rd}$	design yield capacity of a member
N_{Sd}	(acting) design normal force
N_o	chord load
$N_{o,gap}$	reduced axial load resistance, due to shear, in the cross section of the chord at the gap
N_{op}	chord "preload" (additional axial force in the chord member at a connection which is not necessary to resist the horizontal components of the brace member forces)
$N_{t, Rd}$	design tensile capacity of a member
N_1 (J_{AA} = 0)	axial load capacity for J_{AA} = 0
N_1 (J_{AA})	axial load capacity for a particular J_{AA}
N_{1u}	axial ultimate load capacity based on the load in member 1
O_v	overlap, O_v = q/p x 100%
R	stress or load ratio
R_{AZ}	reduction of area
R_d	design resistance at room temperature
R(t)	capacity under fire condition
S	static moment to neutral axis
SCF	stress concentration factor
S_d	design action
$S_{j,ini}$	initial rotational stiffness of a joint
S_o	cross sectional area of a standard tensile test specimen (in mm^2)
V	volume of a steel member/unit length
V_f	shear load on flange
$V_{p\ell}$	plastic shear load capacity
$V_{p\ell,f}$	plastic shear capacity of a flange
$V_{p\ell,Rd}$	design plastic shear capacity
V_{Sd}	factored design shear load
W	section modulus
W_o	chord elastic section modulus
W_{eff}	effective section modulus
$W_{e\ell}$	elastic section modulus
$W_{p\ell}$	plastic section modulus
W_t	section modulus for torsion
a	throat thickness of a weld
b	width of a plate
b	external side length of a rectangular hollow section
b_e	effective width of brace member
b_{ep}	effective punching shear width
$b_{e,ov}$	effective width for overlapping brace member connected to overlapped brace member
b_i	external width of a brace i (i = 1, 2 or 3)
b_j	width of overlapped brace j
b_o	external width of a chord
b_m	effective width of a web of an I section chord
b_m	average width of an RHS (b-t)
b_w	effective width of a web
c	a correction factor used for columns to obtain the effective degree of utilization
c, c_o, c_1	coefficients
d	external diameter of a hollow section

d_i	external diameter of a brace i (i = 1, 2 or 3)
d_o	external diameter of a chord
d_r	concrete cover to reinforcement
e	eccentricity
$f_{b,Rd}$	design buckling stress
f_{cd}	design strength of the concrete in a composite column
f_{ck}	characteristic concrete cylinder strength in N/mm^2
f_k	buckling stress for chord side wall (general)
f_{kn}	buckling stress
f(n')	function which incorporates the chord prestress in the joint strength equation
f_{sd}	design strength of the reinforcement in a composite column
f_{sk}	characteristic strength of the reinforcement in a composite column
f_u	specified ultimate tensile strength
f_{uo}	ultimate tensile stress of the chord
f_y	specified design yield strength
f_{ya}	average design yield strength of a cold formed section
f_{yb}	yield strength of the basic material of a hollow section
f_{yd}	design yield strength
f_{yi}	design yield strength of a brace i (i = 1, 2 or 3)
f_{yo}	design yield strength of a chord
f(20)	strength at room temperature
f(θ)	strength in the fire condition
g	gap between the braces of a K-, N- or KT joint at the connection face of the chord
g'	$\frac{g}{t_o}$
h_i	external depth of a brace i (i = 1, 2 or 3)
h_o	external depth of a chord
h_m	average depth of an RHS (h-t)
h_z	moment arm
h_1	depth of plate or depth of an I or RHS section brace
k	a moment modification factor
ℓ	length
ℓ_A	circumferential parameter for torsion
ℓ_i	length of yield line i
ℓ_k	buckling length
m	slope of $\Delta\sigma$-N curve
m_p	plastic moment per unit length
n	$\frac{N_o}{A_o \cdot f_{yo}} + \frac{M_o}{W_o \cdot f_{yo}}$
n'	$\frac{N_{op}}{A_o \cdot f_{yo}} + \frac{M_o}{W_o \cdot f_{yo}}$
n_i	applied number of cycles
p	internal pressure
p	length of projected contact between overlapping brace and chord without the presence of the overlapping brace
p_s	amount of reinforcement
q	projected length of overlap between braces of a K- or N-joint at the chord face
q	uniform distributed loading
q, q_1, q_2	loadings
r	radius of gyration
r	inside corner radius of rectangular or square hollow sections

r	ratio of the smaller to the larger end moment ($-1 \le r \le +1$)
r_j	load bearing capacity in fire of a single component of a composite cross-section
r_o	radius of a chord member (I, U or RHS)
t	time
t	thickness; wall thickness
t_i	wall thickness of a brace i (i = 1, 2 or 3)
t_j	thickness of overlapped brace j
t_o	wall thickness of a chord or "through member" (e.g. column)
α	non-dimensional factor for the effectiveness of the chord flange in shear
β	diameter or width ratio between braces and chord: $\beta = \frac{d_1}{d_o}$ or $\frac{b_1}{b_o}$ (T, Y, X); $\beta = \frac{d_1+d_2+d_3}{3d_o}$ or $\frac{b_1+b_2+b_3}{3b_o}$ (KT)
γ	half diameter or width to thickness ratio of the chord, $\gamma = d_o/2t_o$ or $b_o/2t_o$
γ_a	partial safety factor for the steel section in a composite column
γ_c	partial safety factor for concrete in a composite column
γ_s	partial safety factor for the reinforcement in a composite column
γ_m	material or joint partial safety factor
δ , δ_1	deformation
δ	section parameter (steel contribution ratio)
$\Delta\sigma$	stress range
$\Delta\sigma_{geom}$	geometrical stress range
$\Delta\sigma_{nom}$	nominal stress range
ϵ	coefficient for local buckling
η	brace member depth to chord width ratio $\eta = h_i/b_0$
θ	temperature
θ_s	steel temperature
θ_i	acute angle between brace member i (i = 1, 2, 3) and the chord
λ	slenderness of a member under compression
λ_E	Euler slenderness
$\bar{\lambda}$	relative slenderness ratio
μ	degree of utilization
μ	related bending capacity
μ_y	related bending capacity about y axis
μ_z	related bending capacity about z axis
σ	stress
σ_a	stress in steel member of a composite column
σ_c	stress in concrete part of a composite column
σ_o	stress in chord
σ_{op}	prestress in chord
σ_r	stress in the reinforcement of a composite column
σ_{min}	minimum stress
σ_{max}	maximum stress
σ_{joint}	geometrical stress at the joint
σ_{nom}	nominal stress in a member
τ	brace to chord thickness ratio $\frac{t_i}{t_o}$
τ	shear stress
τ_{Rd}	design bond stress

χ	reduction factor for buckling
χ_d	ratio between design force and plastic moment capacity of a composite section
χ_n	corrected χ factor for effect of end moment ratio
χ_{min}	buckling coefficient according to curve "c" of EC3 Part 1 or any equivalent national buckling curve
Φ_i	rotation in a yield line

1. INTRODUCTION

Design is an interactive process between the functional and architectural requirements and the strength and fabrication aspects. In a good design, all these aspects have to be considered in a balanced way. Due to the special features of hollow sections and their connections it is even here of more importance than for steel structures of open sections. The designer should therefore be aware of the various aspects of hollow sections.

Many examples in nature show the excellent properties of the tubular shape with regard to loading in compression, torsion and bending in all directions, see Figs. 1.1 and 1.2. These excellent properties are combined with an attractive shape for architectural applications (Figs. 1.3 and 1.4). Furthermore, the closed shape without sharp corners reduces the area to be protected and extends the corrosion protection life (Fig. 1.5).

Another aspect which is especially favourable for circular hollow sections is the lower drag coefficients if exposed to wind or water forces. The internal void can be used in various ways, e.g. to increase the bearing resistance by filling with concrete or to provide fire protection. In addition, the heating or ventilation system sometimes makes use of the hollow section columns.

Although the manufacturing costs of hollow sections are higher than for other sections, leading to higher unit material cost, economical applications are achieved in many fields. The application field covers all areas, e.g. architectural, civil, offshore, mechanical, chemical, aeronautical, transport, agriculture and other special fields. Although this book will be mainly focused on the background to design and application, in a good design not only does the strength have to be considered, but also many other aspects, such as material selection, fabrication including welding and inspection, protection, erection, in service inspection and maintenance.

One of the constraints initially hampering the application of hollow sections was the design of the joints. However, nowadays design recommendations exist for all basic types of joints, and further research evidence is available for many special types of joints.

Based on the research programmes carried out, CIDECT (Comité International pour le Développement et l'Etude de la Construction Tubulaire) has published design guides [1 to 8] for use by designers in practice. Since these design guides are all together too voluminous for education purposes and do not provide the theoretical background, it was decided to write this special book as a background for students in structural and civil engineering.

1.1 HISTORY AND DEVELOPMENTS

The excellent properties of the tubular shape have been recognised for a long time; i.e. from ancient time nice examples are known. An outstanding example of bridge design is the Firth of Forth Bridge in Scotland (1890) with a free span of 521 m, shown in Fig. 1.6. This bridge has been built up from tubular members made of rolled plates which have been riveted together, because other fabrication methods were at that time not available for these sizes.

In that century the first production methods for seamless and welded circular hollow sections were developed. In 1886, the Mannesmann brothers developed the skew roll piercing process (Schrägwalzverfahren), shown in Fig. 1.7, which made it possible to roll short thick walled tubulars.

This process, in combination with the Pilger Process (Pilgerschrittverfahren, Fig. 1.8), developed some years later, made it possible to manufacture longer thinner walled seamless hollow sections.

In the first part of the previous century, the Englishman Whitehouse developed the fire welding of circular hollow sections. However, the production of welded circular hollow sections became more important after the development of the continuous weld process in 1930 by the American Fretz Moon (Fig. 1.9). Especially after the Second World War, welding processes have been perfected, which made it possible for hollow sections to be easily welded together.

The end cutting required for fitting two circular hollow sections together was simplified considerably by the development by Müller of a special end preparation machine (Fig. 1.10).

For manufacturers who did not have such end cutting machines, the end preparation of circular hollow sections remained a handicap.

A possibility to avoid the connection problems was the use of prefabricated connectors, e.g. in 1937

Mengeringhausen developed the Mero system. This system made it possible to fabricate large space structures in an industrialized way (Fig. 1.11).
In 1952 the rectangular hollow section was developed by Stewarts and Lloyds (now Corus Tubes). This section, with nearly the same properties as the circular hollow section, enables the connections to be made by straight end cuttings.

In the fifties, the problems of manufacturing, end preparation and welding were solved and from this point of view the way to a successful story was open. The remaining problem was the determination of the strength of unstiffened joints.

The first preliminary design recommendations for truss connections between circular hollow sections were given by Jamm [45] in 1951. This study was followed by several investigations in Japan [46,47], the USA [48,49,50] and Europe [30,32,33,35,38,39,40,42,44]. The research on connections between rectangular hollow sections started in Europe in the sixties, followed by many other experimental and theoretical investigations. Many of these were sponsored by CIDECT. Besides these investigations on the static behaviour, in the last 25 years much research was carried out on the fatigue behaviour and other aspects, such as concrete filling of hollow sections, fire resistance, corrosion resistance and behaviour under wind loading.

1.2 DESIGNATION

The preferred designations for structural applications are:

- structural hollow sections (SHS)
- circular hollow sections (CHS)
- rectangular hollow sections (RHS)

In Canada and the USA it is common to speak about Hollow Structural Sections (HSS) instead of (SHS).

1.3 MANUFACTURING OF HOLLOW SECTIONS

As mentioned, hollow sections can be produced seamless or welded. Seamless hollow sections are made in two phases, i.e. the first phase consists of piercing an ingot and the second one consists of the elongation of this hollow bloom into a finished circular hollow section. After this process, the tube can go through a sizing mill to give it the required diameter. Besides the Mannesmann process, other processes are used, most of them based on the same principle [31,32].

Nowadays, welded hollow sections with a longitudinal weld are mainly made with electrical resistance welding processes or with an induction welding process, shown in Fig. 1.12. A strip or plate is shaped by rollers into a cylindrical shape and welded longitudinally. The edges are heated e.g. by electrical resistance. The rollers push the edges together, resulting in a pressure weld. The outer part of the weld is trimmed immediately after welding.

Rectangular hollow sections are made by deforming circular hollow sections through forming rollers, as shown in Fig. 1.13. This can be done hot or cold and seamless or longitudinally welded circular hollow sections can be used.
It is common practice to use longitudinally welded hollow sections. For the very thick sections, seamless sections may be used.

Square or rectangular hollow sections are sometimes made by using channel sections, which are welded together or by shaping a single strip to the required shape and closing it by a single weld, preferably in the middle of a face.

Large circular hollow sections are also made by rolling plates through a so-called U-O press process shown in Fig. 1.14. After forming the plates to the required shape, the longitudinal weld is made by a submerged arc welding process.

Another process for large tubulars is to use a continuous wide strip, which is fed into a forming machine at an angle to form a spirally formed circular, see Fig. 1.15. The edges of the strip are welded together by a submerged arc welding process resulting in a so-called spirally welded tube.

More detailed information about the manufacturing processes and the limitations in sizes can be obtained from [31,32].

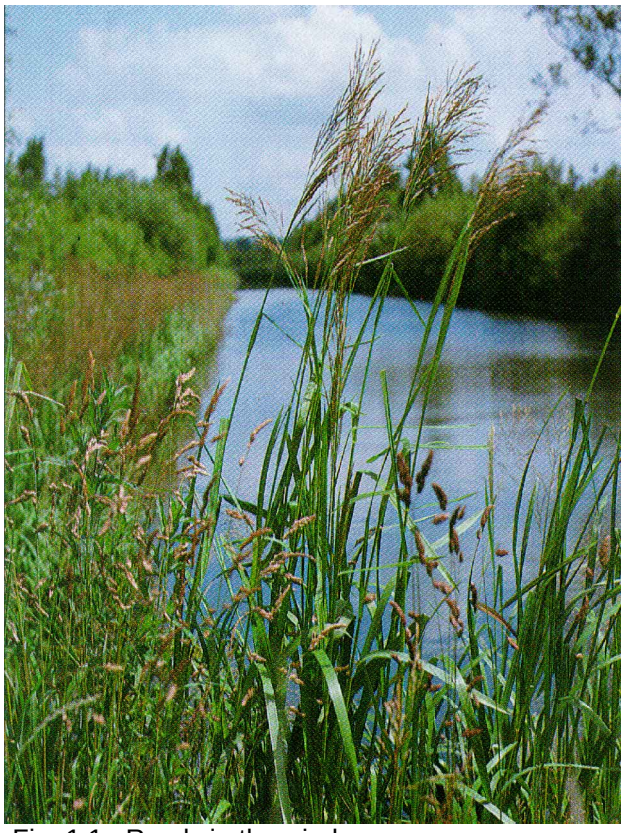

Fig. 1.1 Reeds in the wind

Fig. 1.2 Bamboo

Fig. 1.3 Pavilion in Seville

Fig. 1.4 Movable Bridge, Delft

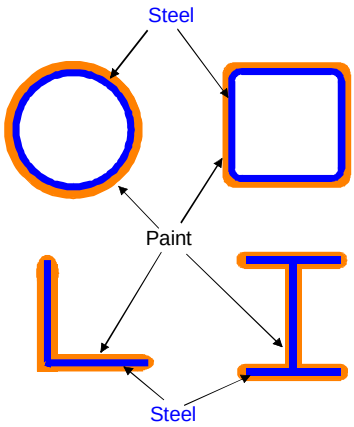

Fig. 1.5 Paint surface for hollow sections vs open sections

Fig. 1.6 Firth of Forth bridge

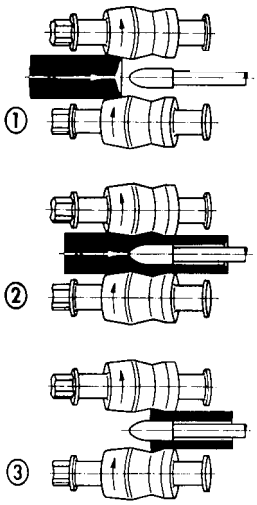

Fig. 1.7 Skew roll piercing process (Schrägwalzverfahren)

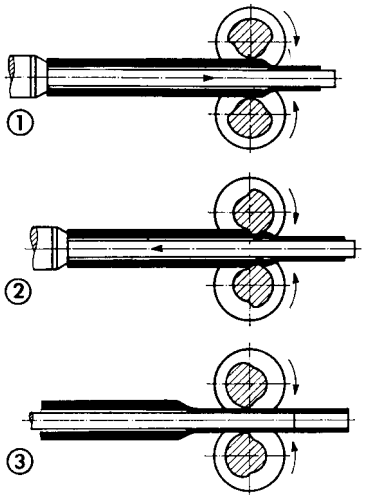

Fig. 1.8 Pilger Process (Pilgerschritt)

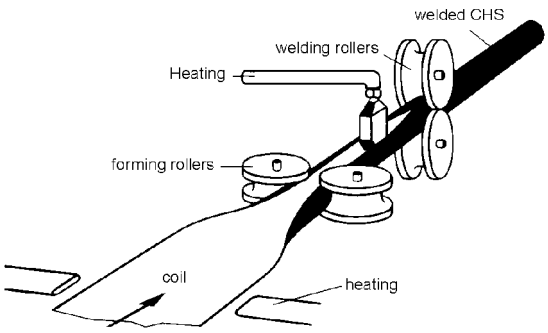

Fig. 1.9 Fretz Moon process

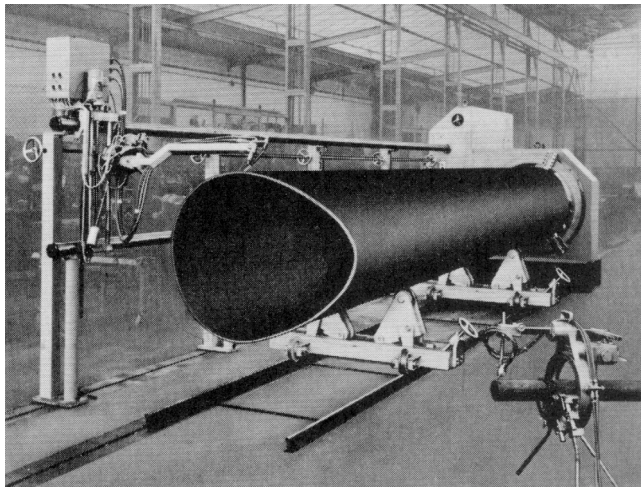

Fig. 1.10 End cutting machine

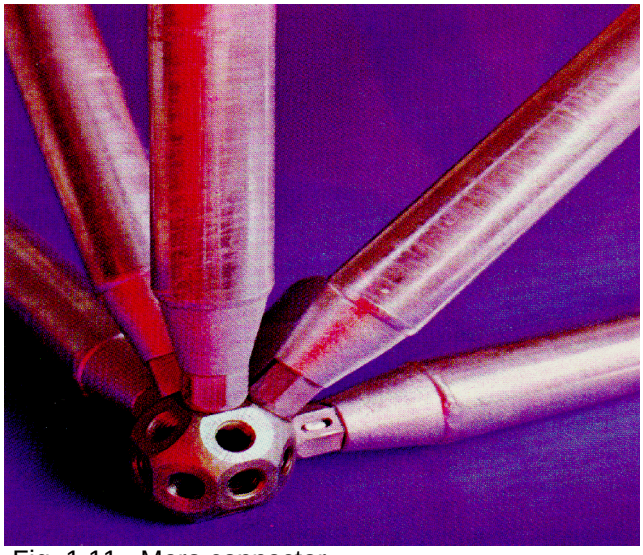

Fig. 1.11 Mero connector

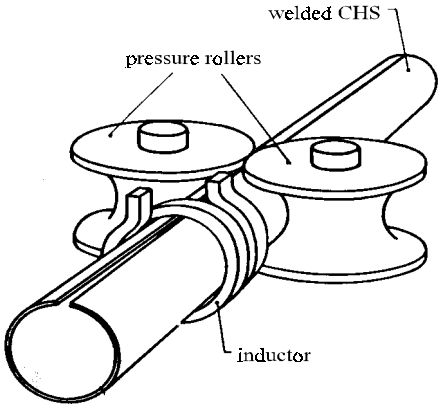

Fig. 1.12 Induction welding process

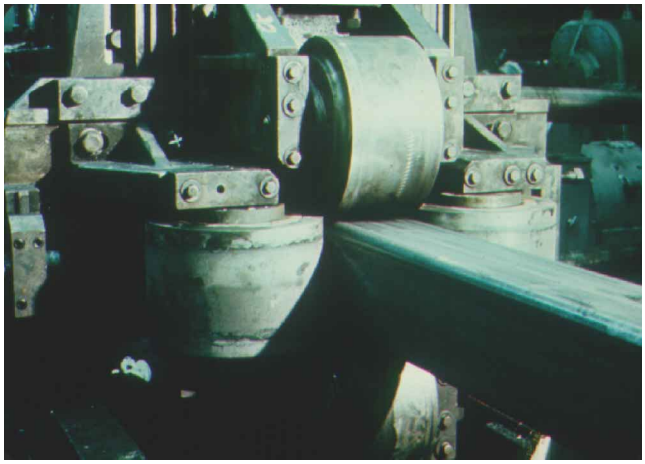

Fig. 1.13 Manufacturing of rectangular hollow sections

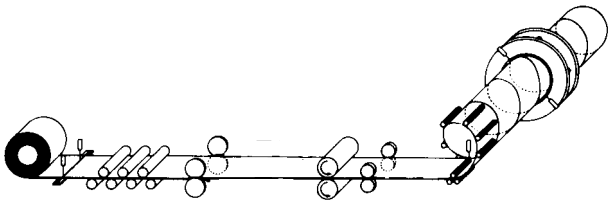

Fig. 1.15 Spirally welded CHS

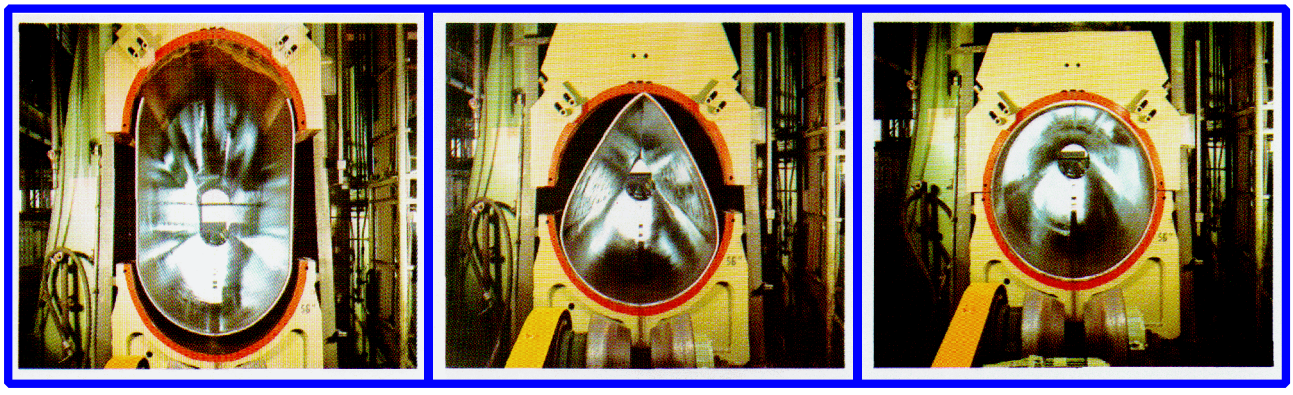

Fig. 1.14 Forming of large CHS

2. PROPERTIES OF HOLLOW SECTIONS

2.1 MECHANICAL PROPERTIES

Hollow sections are made of similar steel as used for other steel sections, thus in principle there is no difference, and the mechanical properties are given in standards [26 to 29].
Tables 2.1a and 2.2a show, as an example, the mechanical properties according to the European standard EN 10210-1 for hot finished structural hollow sections of non-alloy and fine grain structural steels. The cold formed sections are given in EN 10219-1: Cold formed welded structural hollow sections of non-alloy and fine grain structural steels (see tables 2.1b and 2.2b). As shown, the requirements of EN 10210-1 and EN 10219-1 are almost identical.

Hollow sections can also be produced in special steels, e.g. high strength steel with yield strengths up to 690 N/mm^2 or higher, weathering steels and steel with improved or special chemical compositions, etc.

Generally, the design of members is based on yield, since the deformation under loads becomes excessive. In statically indeterminate structures, yielding of members or yielding at particular locations provides redistribution of loads. In this case, sufficient deformation capacity or rotation capacity is required. E.g. a tensile member made of ductile steel can be brittle if a particular cross section is weakened, e.g. by holes in such a way that this cross section fails before the whole member yields. It is therefore required that yielding occurs first. This shows that the yield to ultimate tensile strength ratio is also important, especially for structures with very non uniform stress distributions, which is a situation that occurs in tubular joints. Some codes, such as Eurocode 3 [12], require the following condition for the specified minimum values:

$$\frac{f_u}{f_y} \geq 1.2 \qquad (2.1)$$

This is only one aspect for ductility. In the case of impact loading, the steel and members should also behave in a ductile manner. That is why a requirement based on the standard Charpy test is also given in tables 2.1.a and 2.2.a.

Nowadays, more refined characterisation methods also exist to characterise the ductility of cracked bodies, e.g. the CTOD (Crack Tip Opening Displacement) method. These characterisation methods are generally used for pressure vessels, transport line pipes and offshore applications, which are beyond the scope of this book.

Another characterisation is sometimes required for thick walled sections which are loaded in the thickness direction. In this case, the strength and ductility in the thickness direction should be sufficient to avoid cracking, called lamellar tearing, see Fig. 2.1.
This type of cracking is caused by non metallic manganese-sulphide inclusions. Thus, if the sulphur content is very low or the sulphur is joined with other elements such as calcium (Ca), such a failure can be avoided.
Indirectly this is obtained by requiring a certain reduction of area R_{AZ} in the tensile test. For example, R_{AZ} = 35 means that in the tensile test the cross sectional area at failure has been reduced by 35% compared to the original cross sectional area.

In most structural steel specifications the yield strength, ultimate tensile strength, elongation and in some specifications also the Charpy V values are specified. Design standards or specifications give further limitations for the f_u/f_y ratio, whereas depending on the application more restrictive requirements may be given related to CTOD values or the properties in the thickness direction (Z quality).
Another aspect is the effect of cold forming on the mechanical properties of the parent steel. In the case of cold forming of hollow sections, the yield strength and to a lesser extent the ultimate tensile strength are increased, especially in the corners, as shown in Fig. 2.2. Further, the yield to ultimate tensile ratio is increased and the elongation somewhat decreased.
If the specifications specify the properties based on the finished product, these properties have been already taken into account. However, some specifications specify the material properties of the parent material. In this case, the increased yield strength can be taken into account for design.

The method for the determination of the increased yield strength given in Eurocode 3 is based on the work of Lind and Schroff [51]. Here it is assumed that the product of the cold formed area times the increase of yield strength is nearly constant. Thus, a small corner radius produces a small cold formed area with a large cold forming effect and consequently a large increase in yield strength, and a large corner radius does just the

opposite. Based on research work [51] it can be assumed that in every corner of 90° the yield strength f_{yb} is increased over a length of 7t to the ultimate tensile strength of the parent material. The total increase over the section $4(7t)t(f_u-f_y)$ can be averaged over the section, resulting in an average yield strength f_{ya}, as shown in table 2.3 and Fig. 2.2.
In those cases where the RHS sections are made from a CHS section a considerable increase in yield strength of the flat sides may also occur.
If the yield stress of the finished product is used this increase is automatically included.

It is noted that the cold formed sections should satisfy the requirements for minimum inside corner radius to guarantee sufficient ductility, see table 2.4 for fully aluminium killed steel.

Sometimes cold formed hollow sections are annealed or stress relieved immediately after cold forming. EN 10210-1 states that *"the standard EN 10210-1 applies to hot finished hollow sections formed hot with or without subsequent heat treatment or formed cold with subsequent heat treatment to obtain equivalent metallurgical conditions to those obtained in the hot formed product."*

2.2 STRUCTURAL HOLLOW SECTION DIMENSIONS AND DIMENSIONAL TOLERANCES

The dimensions and sectional properties of structural hollow sections have been standardised in ISO standards ISO 657-14 [20] and ISO 4019 [21] for hot formed and cold formed structural hollow sections respectively.

Various national standards are available which may contain these and other sizes. In Europe the two applicable standards are EN 10210-2 'Hot finished structural hollow sections of non-alloy and fine grain structural steels - tolerances, dimensions and sectional properties' and EN 10219-2 'Cold formed welded structural hollow sections of non-alloy and fine grain structural steels - tolerances, dimensions and sectional properties'.

The majority of manufacturers of structural hollow sections do not produce all the sizes shown in these standards. It should also be noted that other sizes, not included in these standards, may be produced by some manufacturers.

The tolerances on dimensions and shape are given in ISO 657-14 and ISO 4019 for circular and rectangular (including square) sections respectively. Again, various national standards are also applicable and these may or may not contain the same tolerances.

In Europe the tolerances are contained within EN 10210-2 and EN 10219-2 respectively for hot finished and cold formed sections, see Tables 2.5a and 2.5b. The majority of the tolerances given in EN 10219-2 are the same as those in EN 10210-2. Where differences do occur, these are indicated in table 2.5b.

Due to additional mass and length tolerances, considerable variations may occur between the various national standards [52].

Although circular, square and rectangular hollow sections are the generally-used shapes; other shapes are sometimes available. For example, some tube manufacturers deliver the shapes given in Table 2.6. However, these shapes are not dealt with further in this book.

2.3 GEOMETRICAL PROPERTIES

2.3.1 Tension

The design capacity $N_{t,Rd}$ of a member under a tensile loading depends on the cross-sectional area and the design yield strength, and is independent of the sectional shape. In principle, there is no advantage or disadvantage in using hollow sections from the point of view of the amount of material required. The design capacity is given by:

$$N_{t,Rd} = \frac{A \cdot f_y}{\gamma_M} \quad (2.2)$$

where
γ_M is the partial safety factor.

If the cross section is weakened by bolt holes, the net cross section should also be checked in a similar way as for other sections, e.g. acc. to [12]:

$$N_{t,Rd} = \frac{A_{net} \cdot f_u}{\gamma_M} \cdot 0.9 \quad (2.3)$$

The factor 0.9 may vary from country to country depending on the partial factor γ_M used. Where ductile behaviour is required (e.g. under seismic loading), the plastic resistance shall be less than the ultimate resistance at the net section of fastener holes, i.e.:

$0.9\ A_{net} \cdot f_u > A \cdot f_y$

2.3.2 Compression

For centrally loaded members in compression, the critical buckling load depends on the slenderness λ and the section shape.

The slenderness λ is given by the ratio of the buckling length ℓ and the radius of gyration r.

$$\lambda = \frac{\ell}{r} \quad (2.4)$$

The radius of gyration of a hollow section (in relation to the member mass) is generally much higher than that for the weak axis of an open section. For a given length, this difference results in a lower slenderness for hollow sections and thus a lower mass when compared with open sections.

The buckling behaviour is influenced by initial eccentricities, straightness and geometrical tolerances as well as residual stresses, nonhomogeneity of the steel and the stress-strain relationship.

Based on an extensive investigation by the European Convention for Constructional Steelwork and CIDECT, "European buckling curves" (Fig. 2.3 and table 2.7) have been established for various steel sections including hollow sections. They are incorporated in Eurocode 3.

The reduction factor χ shown in Fig. 2.3 is the ratio of the design buckling capacity to the axial plastic capacity.

$$\chi = \frac{N_{b,Rd}}{N_{pl,Rd}} = \frac{f_{b,Rd}}{f_{yd}} \quad (2.5)$$

where

$$f_{b,Rd} = \frac{N_{b,Rd}}{A} \text{ (the design buckling strength)} \quad (2.6)$$

$$f_{yd} = \frac{f_y}{\gamma_M} \quad (2.7)$$

The non-dimensional slenderness $\bar{\lambda}$ is determined by

$$\bar{\lambda} = \frac{\lambda}{\lambda_E} \quad (2.8)$$

$$\text{where } \lambda_E = \pi \sqrt{\frac{E}{f_y}} \text{ (Euler slenderness)} \quad (2.9)$$

The buckling curves for the hollow sections are classified according to table 2.7.

Most open sections fall under curves "b" and "c". Consequently, for the case of buckling, the use of hot-formed hollow sections generally provides a considerable saving in material.

Fig. 2.4 shows for a buckling length of 3 m a comparison between the required mass of open and hollow sections for a given load.

It shows that in those cases in which loads are small, leading to relatively slender sections, hollow sections provide a great advantage (considerably lower use of material). However, if loads are higher, resulting in low slendernesses, the advantage (in %) will be lower.

The overall buckling behaviour of hollow sections improves with increasing diameter or width to wall thickness ratio. However, this improvement is limited by local buckling. To prevent local buckling, d/t or b/t limits are given e.g. in Eurocode 3, see table 2.8.

In the case of thin walled sections, interaction between global and local buckling should be considered.

In addition to the improved buckling behaviour due to the high radius of gyration and the enhanced design

buckling curve, hollow sections can offer other advantages in lattice girders. Due to the torsional and bending stiffness of the members in combination with joint stiffness, the effective buckling length of compression members in lattice girders with K-gap joints can be reduced (Fig. 2.5). Eurocode 3 recommends an effective buckling length for hollow section brace members in welded lattice girders equal to or less than 0.75ℓ, see [2,12], in which ℓ represents the system length. Other codes, e.g. API [15] give a buckling length of 0.8ℓ.

For lattice girders with overlap joints no test results are available and for the time being the buckling length is assumed to be the system length. For chords 0.9 times the system length for in-plane buckling or 0.9 times the length between the supports is taken as the buckling length.

Laterally unsupported chords of lattice girders (see Fig. 2.6) have a reduced buckling length due to the improved torsional and bending stiffness of the tubular members [53,54]. These factors make the use of hollow sections in girders even more favourable.

2.3.3 Bending

In general, I and H sections are more economical under bending about the major axis (I_{max} larger than for hollow sections). Only in those cases in which the design stress in open sections is largely reduced by lateral buckling do hollow sections offer an advantage.

It can be shown by calculations that lateral instability is not critical for circular hollow sections and for rectangular hollow sections with b/h >0.25 (with bending about the strong axis), which are normally used.

It is apparent that hollow sections are especially favourable compared to other sections if bending about both axes is present.

Hollow sections used for elements subjected to bending can be more economically calculated using plastic design. However, then the sections have to satisfy more restricted conditions to avoid premature local buckling. Like other steel sections loaded in bending, different moment-rotation behaviours can be observed.

Fig. 2.7 shows various moment-rotation diagrams for a member loaded by bending moments.

The moment-rotation curve "1" shows a moment exceeding the plastic moment and a considerable rotation capacity. Moment-rotation curve "2" shows a moment exceeding the plastic moment capacity; but after the maximum, the moment drops immediately, so that little moment-rotation capacity exists. Moment-rotation curve "3" represents a capacity lower than the plastic moment capacity, which, however, exceeds the elastic yield moment capacity. In the moment-rotation curve "4" the capacity is even lower than the elastic yield moment capacity. The effect of the moment-rotation behaviour is reflected in the classification of cross sections as shown in table 2.8. The cross section classification is given in limits for the diameter or width to thickness ratio, i.e. d/t, b/t or h/t.

The limits are based on experiments and given as:

$$\frac{d}{t} \le c \cdot \frac{235}{f_y} \qquad \text{for CHS} \qquad (2.10)$$

$$\frac{b}{t} \le c \cdot \sqrt{\frac{235}{f_y}} \qquad \text{for RHS} \qquad (2.11)$$

with f_y in N/mm^2 and c depending on the section class, the cross section and the loading.

The cross section classes 1 and 2 can develop the plastic moment capacity up to the given b/t or d/t limits with bi-linear stress blocks, whereas the moment capacity of the cross section classes 3 and 4 is based on an elastic stress distribution (see Fig. 2.8). The difference between the cross section classes 1 and 2 is reflected in the rotation capacity. After reaching the plastic moment capacity, the cross section class 1 can keep this capacity after further rotation, whereas the capacity of the cross section class 2 drops after reaching this capacity. As a consequence, the moment distribution in the structure or structural component should be determined in an elastic way for structures made of sections with cross section classes 2, 3 or 4. For structures made of sections with cross sections in class 1, a plastic moment distribution can be adopted, but an elastic moment distribution is still permissible (and in some countries more common).

Detailed information about the cross sectional classification is given in [2].

Recent research by Wilkinson and Hancock [56] has shown that especially the limits for the web slenderness have to be reduced considerably and that the limits of Eurocode 3 for the h/t ratio are unsafe.

For a beam fully clamped at both ends and subjected to a uniformly distributed loading q, it means that after reaching the plastic moment capacity at the ends, the beam can be loaded until a further plastic hinge occurs at mid span (see Fig. 2.9).

For the class 4 cross section the maximum stress is determined by local buckling and the stress in the outer fibre is lower than the yield strength f_y. Alternatively, an effective cross sectional area based on the yield strength may be determined.

In the absence of shear forces or if the shear forces do not exceed 50% of the shear capacity $V_{pl,Rd}$, the effect of shear may be neglected and the bending moment capacity about one axis is given by:

$$M_{c,Rd} = \frac{W_{pl} \cdot f_y}{\gamma_M} \quad \text{for cross section classes 1 or 2} \qquad (2.12)$$

$$M_{c,Rd} = \frac{W_{el} \cdot f_y}{\gamma_M} \quad \text{for cross section class 3} \qquad (2.13)$$

$$M_{c,Rd} = \frac{W_{eff} \cdot f_y}{\gamma_M} \quad \text{for cross section class 4} \qquad (2.14)$$

When the shear force exceeds 50% of the shear capacity, combined loading has to be considered, see e.g. Eurocode 3.

2.3.4 Shear

The elastic shear stress can be determined with simple mechanics by:

$$\tau = \frac{V_{Sd} \cdot S}{2 \cdot I \cdot t} \le \frac{f_y}{\sqrt{3}} \qquad (2.15)$$

Fig. 2.10 shows the elastic stress distribution. The design capacity based on plastic design can be easily determined based on the Huber-Hencky-Von Mises criterion by assuming the shear yield strength in those parts active for shear.

$$V_{pl,Rd} = A_v \cdot \frac{f_y}{\sqrt{3}} \cdot \frac{1}{\gamma_M} \qquad (2.16)$$

with $A_v = A \cdot \frac{h}{b+h}$ for rectangular sections

(or just $2\,h \cdot t$) with V in the direction of h.

$A_v = \frac{2}{\pi} \cdot A$ for circular sections

2.3.5 Torsion

Hollow sections, especially CHS, have the most effective cross-section for resisting torsional moments, because the material is uniformly distributed about the polar axis. A comparison of open and hollow sections of nearly identical mass in table 2.9 shows that the torsional constant of hollow sections is about 200 times that of open sections.

The design capacity is given by:

$$M_{t,Rd} = W_t \cdot \frac{f_y}{\sqrt{3}} \qquad (2.17)$$

Circular hollow sections:

$$I_t \approx \frac{\pi}{4} (d-t)^3 \cdot t \qquad (2.18)$$

$$\text{with } W_t = \frac{2I_t}{d-t} \cong \frac{\pi}{2} (d-t)^2 \cdot t \qquad (2.19)$$

Rectangular hollow sections [57]:

$$I_t = \frac{t^3 \cdot \ell_A}{3} + \frac{4 A_m^2 \cdot t}{\ell_A} \qquad (2.20)$$

with:

$$\ell_A = 2(h_m + b_m) - 2 r_m (4 - \pi) \qquad (2.21)$$

$$A_m = b_m \cdot h_m - r_m^2 (4 - \pi) \qquad (2.22)$$

with $W_t = \dfrac{I_t}{t + 2\dfrac{A_m}{\ell_a}}$ (2.20[a])

For thin walled rectangular hollow sections eq. 2.20[a] can be approximated by:

$W_t = 2\, h_m \cdot b_m \cdot t$
(2.23)

The first term in eq. 2.20 is generally only used for open sections however, research [57] has shown that the given formula fits the test results best.

2.3.6 Internal pressure

The circular hollow section is most suitable to resist an internal pressure p.
The design capacity per unit length, shown in Fig. 2.11, is given by:

$$p = f_y \cdot \frac{2t}{d-2t} \cdot \frac{1}{\gamma_M} \qquad (2.24)$$

For transport pipelines, the γ_M value may be considerably larger than for other cases, depending on the hazard of the product, the effect of failure on the environment and the inspectability. The design capacities for RHS sections subjected to internal pressure are much more complicated; reference can be made to [58].

2.3.7 Combined loadings

Various combinations of loadings are possible, e.g. tension, compression,bending, shear and torsion.

Depending on the cross sectional classification, various interaction formulae have to be applied. Reference can be made to the relevant codes, e.g. Eurocode 3. It is too extensive to deal with all these formulae in this lecture book, however, the interaction of the various loads in the cross section can be based on the Huber-Hencky-Von Mises stress criterion [60].

For the member checks other interaction formulae apply, see e.g. [12, 60].

2.4 DRAG COEFFICIENTS

Hollow sections, especially circular hollow sections, have a striking advantage for use in structures exposed to fluid currents, i.e. air or water.

The drag coefficients are much lower than those of open sections with sharp edges (see Fig. 2.12 and table 2.10) [31, 33, 61].

2.5 CORROSION PROTECTION

Structures made of hollow sections offer advantages with regard to corrosion protection. Hollow sections have rounded corners (Fig. 2.13) which result in a better protection than sections with sharp corners. This is especially true for the joints in circular hollow sections where there is a smooth transition from one section to another. This better protection increases the protection period of coatings against corrosion.

Structures designed in hollow sections have a 20 to 50% smaller surface to be protected than comparable structures made using open sections. Many investigations [62] have been carried out to assess the likelihood of internal corrosion. These investigations, carried out in various countries, show that internal corrosion does not occur in sealed hollow sections.

Even in hollow sections which are not perfectly sealed, internal corrosion is limited. If there is concern about condensation in an imperfectly sealed hollow section, a drainage hole can be made at a point where water can drain by gravity.

2.6 USE OF INTERNAL VOID

The internal void in hollow sections can be used in various ways, e.g. to increase the compressive resistance by filling with concrete, or to provide fire protection. In addition, the heating or ventilation system is sometimes incorporated into hollow section columns. The possibilities of using the internal space are briefly described below.

2.6.1 Concrete filling

If the commonly-available wall thicknesses are not sufficient to meet the required load bearing resistance,

the hollow section can be filled with concrete. For example, it may be preferable in buildings to have the same external dimensions for the columns on every floor. At the top floor, the smallest wall thickness can be chosen, and the wall thickness can be increased with increasing load for lower floors. If the hollow section with the largest available wall thickness is not sufficient for the ground floor, the hollow section can be filled with concrete to increase the load bearing resistance.

A very important reason for using concrete-filled hollow sections is that the columns can be relatively slender. Design rules are given in e.g. Eurocode 4 [13].

Concrete filling of hollow sections contributes not only to an increase in load bearing resistance, but it also improves the fire resistance duration. The extensive test projects carried out by CIDECT and ECSC have shown that reinforced concrete-filled hollow section columns without any external fire protection like plaster, vermiculite panels or intumescent paint, can attain a fire life of even 2 hours depending on the cross-section ratio of the steel and concrete, reinforcement percentage of the concrete and the applied load, see Fig. 2.14 [4].

2.6.2 Fire protection by water circulation

One of the modern methods for fire protection of buildings is to use water-filled hollow section columns.

The columns are interconnected with a water storage tank. Under fire conditions, the water circulates by convection, keeping the steel temperature below the critical value of 450°C. This system has economical advantages when applied to buildings with more than about 8 storeys. If the water flow is adequate, the resulting fire resistance time is virtually unlimited.

In order to prevent freezing, potassium carbonate (K_2CO_3) is added to the water. Potassium nitrate is used as an inhibitor against corrosion.

2.6.3 Heating and ventilation

The inner voids of hollow sections are sometimes used for air and water circulation for heating and ventilation of buildings. Many examples in offices and schools show the excellent combination of the strength function of hollow section columns with the integration of the heating or ventilation system. This system offers maximization of floor area through elimination of heat exchangers, a uniform provision of warmth and a combined protection against fire.

2.6.4 Other possibilities

Sometimes hollow section chords of lattice girder bridges are used for conveying fluids (pipe bridge).
Sometimes in buildings the rain water downpipes go through the hollow section columns (Fig. 2.15) or in other cases electrical wiring is located in the columns. The internal space can also be used for prestressing a hollow section.

2.7 AESTHETICS

A rational use of hollow sections leads in general to structures which are cleaner and more spacious. Hollow sections can provide slender aesthetic columns, with variable section properties but flush external dimensions. Due to their torsional rigidity, hollow sections have specific advantages in folded structures, V-type girders, etc..

Lattice construction, which is often made of hollow sections directly connected to one another without any stiffener or gusset plate, is often preferred by architects for structures with visible steel elements. However, it is difficult to express aesthetic features in economic comparisons. Sometimes hollow sections are used only because of aesthetic appeal, whilst at other times appearance is less important, see e.g. Fig. 2.16a and Fig. 2.16b.

Table 2.1a EN 10210-1 Hot Finished Structural Hollow Sections Non-Alloy Steel Properties

Steel designation	Minimum yield strength N/mm²			Minimum tensile strength N/mm²		Min. elong.% on gauge $L_o = 5.65\sqrt{S_o}$ t ≤ 40 mm*		Charpy Impact strength (10x10 mm)	
	t≤16 mm	16<t≤40 mm	40<t≤65 mm	t<3mm	3≤t≤65 mm	Long.	Trans.	Temp. °C	J
S235JRH	235	225	215	360-510	340-470	26	24	20	27
S275J0H S275J2H	275	265	255	430-580	410-560	22	20	0 -20	27 27
S355J0H S355J2H	355	345	335	510-680	490-630	22	20	0 -20	27 27

* for thicknesses above 40 mm, these values are reduced

Table 2.1b EN 10219-1 Cold Formed Welded Structural Hollow Sections Non-Alloy Steel - Steel Property different from EN 10210-1

Steel designation	Min. longitudinal elongation, % all thicknesses, t_{max} = 40 mm
S235JRH	24
S275J0H S275J2H	20
S355J0H S355J2H	20

For sections ≤ 60 x 60 mm and equivalent round and rectangular sections, the

Table 2.2a EN 10210-1 Hot Finished Structural Hollow Sections - Fine Grain Steel Properties

Steel designation	Minimum yield strength N/mm²			Minimum tensile strength N/mm²	Min. elong.% on gauge $L_o = 5.65\sqrt{S_o}$ t ≤ 65 mm*		Charpy Impact strength (10x10 mm)	
	t≤16 mm	16<t≤40 mm	40<t≤65 mm	t≤65mm	Long.	Trans.	Temp. °C	J
S275NH S275NLH	275	265	255	370-540	24	22	-20 -50	40 27
S355NH S355NLH	355	345	335	470-630	22	20	-20 -50	40 27

Table 2.2b EN 10219-1 Cold Formed Welded structural Hollow Section Fine Grain Steel - Steel Property different from EN 10210-1

Steel designation	Feed stock condition* M	
	Min. Tensile strength	Min. longitudinal elongation
S275MH S275MLH	360 - 510	24
S355MH S355MLH	450 - 610	22
S460MH S460MLH	530 - 720	17

M: refers to thermal mechanical rolled steels.

** : Min. Elong. % on gauge* $L_o = 5.65\sqrt{S_o}$

For sections ≤ 60 x 60 mm and equivalent round and rectangular sections, the minimum elongation is 17% for all steel grades and section thicknesses.

Table 2.3 Increase in yield strength due to cold-forming of RHS sections [12]

Average yield strength:

The average yield strength f_{ya} may be determined from full size section tests or as follows:

$$f_{ya} = f_{yb} + (k \cdot n \cdot t^2/A) \cdot (f_u - f_{yb})$$

where

f_{yb}, f_u = specified tensile yield strength and ultimate tensile strength of the basic material (N/mm^2)
t = material thickness (mm)
A = gross cross-sectional area (mm^2)
k = coefficient depending on the type of forming (k = 7 for cold forming)
n = number of 90° bends in the section with an internal radius < 5 t (fractions of 90° bends should be counted as fractions of n)
f_{ya} should not exceed f_u or 1.2 f_{yb}

The increase in yield strength due to cold working should not be utilised for members which are annealed* or subject to heating over a long length with a high heat input after forming, which may produce softening.

Basic material:
Basic material is the flat hot rolled sheet material out of which sections are made by cold mechanical forming.

* Stress relief annealing at more than 580 °C or for over one hour may lead to deterioration of the mechanical properties, thus hot dip galvanizing at about 460 °C gives no reduction of the increased stresses.

Table 2.4 Minimum inner corner radii of full aluminium (≥0.02%) killed cold finished RHS [12]

Steel grade		Wall thickness t (mm)	minimum r/t (r = inside corner radius)
Acc. to EN 10219 [29]	Previous designation		
S 235, S 355, S 275	Fe 360, Fe 430, Fe 510	24 12 10 6	3.0 2.0 1.5 1.0

Table 2.5a EN 10210-2 Hot Finished Structural Hollow Sections - Tolerances

Section type		Square/rectangular	Circular
Outside dimension		the greater of ± 0.5 mm and ± 1% but not more than 10 mm	
Thickness	Welded	-10%	
	Seamless	-10% and -12.5% at max. 25% cross section	
Mass	Welded	± 6% on individual lengths	
	Seamless	-6%; +8%	
Straightness		0.2% of the total length	
Length (exact)		+10 mm, -0 mm, but only for exact lengths of 2000 to 6000 mm	
Out of roundness			2% for d/t ≤ 100
Squareness of sides		90°, ± 1°	-
Corner radii	Outside	3.0 t max.	
Concavity/convexity		± 1% of the side	-
Twist		2 mm + 0.5 mm/m	-

Table 2.5b EN 10219-2 Cold Formed welded structural Hollow Sections - Tolerance Variations from EN 10210-2

Section type		Square/rectangular	Circular	
Outside dimension		b < 100 mm: the greater of ± 0.5mm and ± 1% 100 mm ≤ h, b ≤ 200 mm: ± 0.8%, b > 200 mm: ± 0.6%	± 1%, min. ± 0.5 mm max. ± 10 mm	
Concavity/convexity		max. 0.8% with min. of 0.5 mm	-	
Outside corner radii		t ≤ 6 mm 1.6 to 2.4t 6 mm < t ≤ 10 mm 2.0 to 3.0t t > 10 mm 2.4 to 3.6t	-	
Thickness	Welded	t ≤ 5 mm: ± 10% t > 5 mm: ± 0.5 mm	For d ≤ 406.4 mm, t ≤ 5 mm: ± 10% t > 5 mm: ± 0.5mm	For d > 406.4 mm, ± 10%, max. 2 mm
Mass		± 6%	± 6%	
Straightness		0.15% of the total length	0.20% of the total length	

Table 2.6 Special shapes available

	triangular	hexagonal	octagonal	flat - oval	elliptical	half-elliptical
shape						

Table 2.7 European buckling curves according to manufacturing processes

Cross section	Manufacturing process	Buckling curves
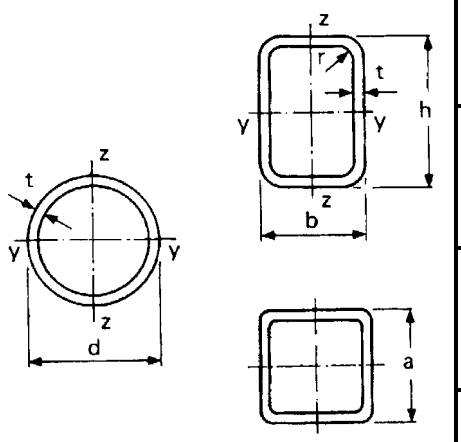	Hot finished $f_y \geq 420$ N/mm^2	a_o
	Hot finished	a
	Cold formed (f_{yb}* used)	b
	Cold formed (f_{ya}** used)	c

* f_{yb} = yield strength of the basic material
** f_{ya} = yield strength of the material after cold forming

Table 2.8 b/t, h/t and d/t limits for the cross section classes 1, 2 and 3 (for $r_0 = 1.5t$)

			class	1				2				3			
cross section	load type	considered element	f_y(N/mm^2)	235	275	355	460	235	275	355	460	235	275	355	460
RHS	compression*	compression		45	41.6	36.6	32.2	45	41.6	36.6	32.2	45	41.6	36.6	32.2
RHS	bending	compression		36	33.3	29.3	25.7	41	37.9	33.4	29.3	45	41.6	36.6	32.2
RHS	bending [1]	bending		1)	1)	1)	1)	1)	1)	1)	1)	1)	1)	1)	1)
CHS	compression and/or bending			50	42.7	33.1	25.5	70.0	59.8	46.3	35.8	90.0	76.9	59.6	46

* There is no difference between b/t and h/t limits for the classes 1, 2 and 3, when the whole cross section is only under compression.
* Class 3 limits appear when whole section is in compression.
1) Recent research [56] has shown that the Eurocode limits for the web slenderness should be reduced considerably, e.g. for class 1 to : $\frac{(h-2t-2r_i)}{t} \leq 70 - \frac{5(b-2t-2r_i)}{6t}$

Table 2.9 Torsional strength of various sections

Section		Mass (kg/m)	Torsion constant I_t (10^4 mm^4)
	UPN 200	25.3	11.9
	INP 200	26.2	13.5
	HEB 120	26.7	13.8
	HEA 140	24.7	8.1
	140x140x6	24.9	1475
	168.3x6	24.0	2017

Table 2.10 Drag coefficients for I-profiles and hollow sections depending on Reynold's number

Section	Drag coefficient
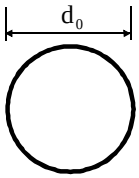	0.5 - 1.2
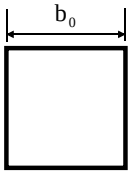	0.6 - 2.0
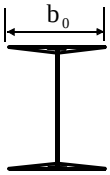	2.0

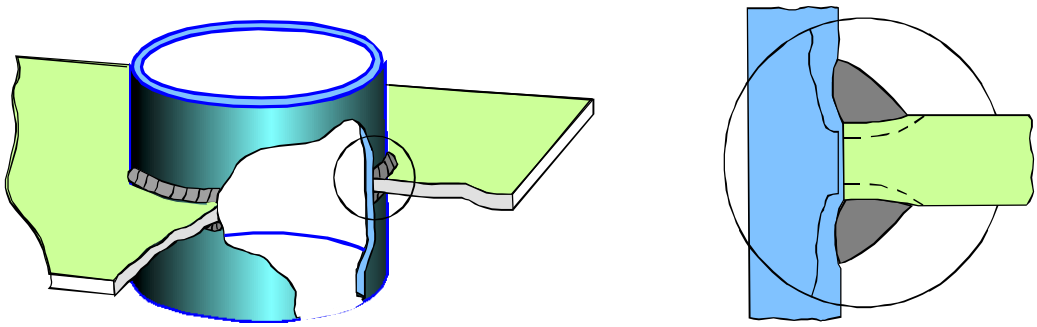

Fig. 2.1 Lamellar tearing

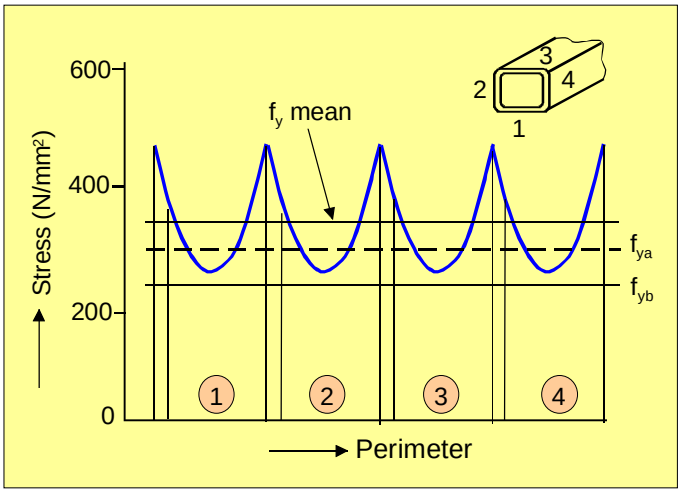

Fig. 2.2 Influence of cold forming on the yield strength for a square hollow section of 100x100x4 mm

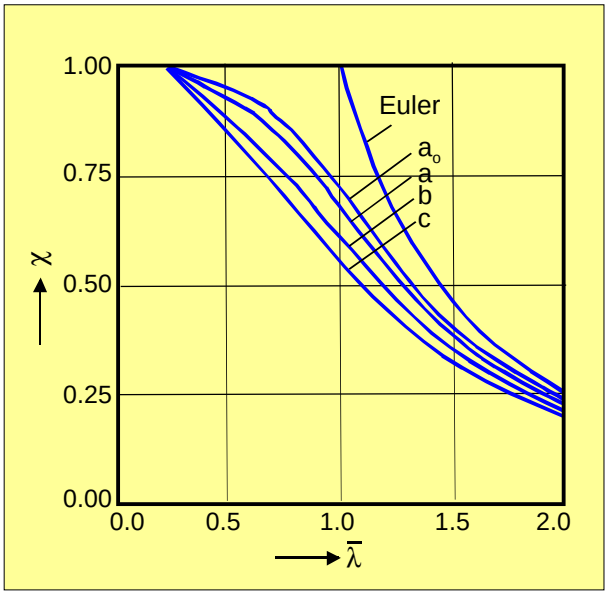

Fig. 2.3 European buckling curves

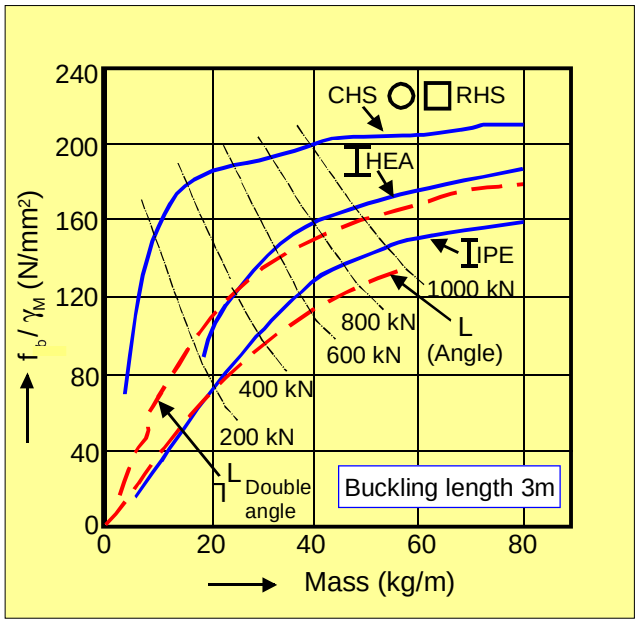

Fig. 2.4 Comparison of the masses of hollow and open sections under compression in relation to the loading

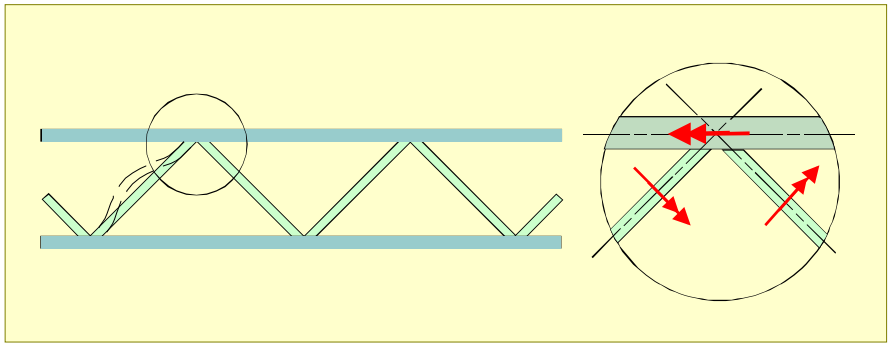

Fig. 2.5 Restraints for the buckling of a brace member

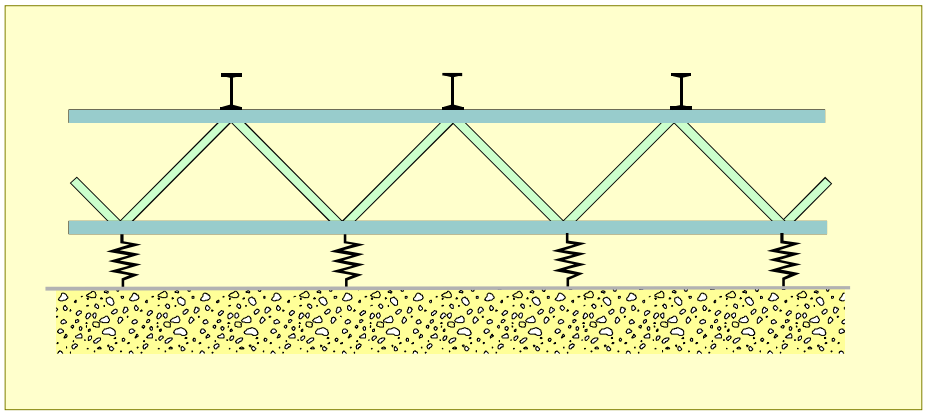

Fig. 2.6 Bottom chord laterally spring supported by the stiffness of the members, joints and purlins

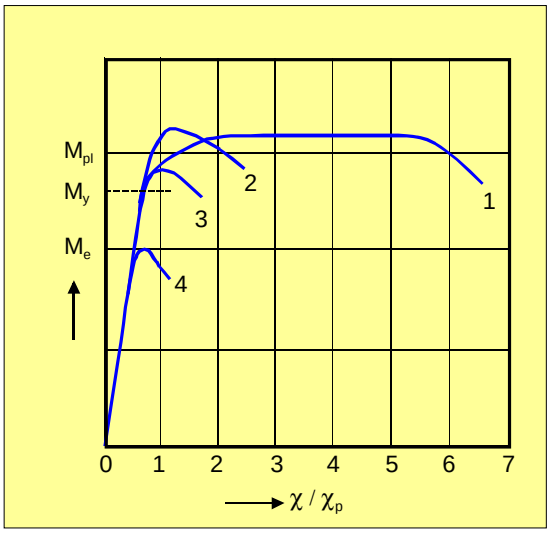

Fig. 2.7 Moment-rotation curves

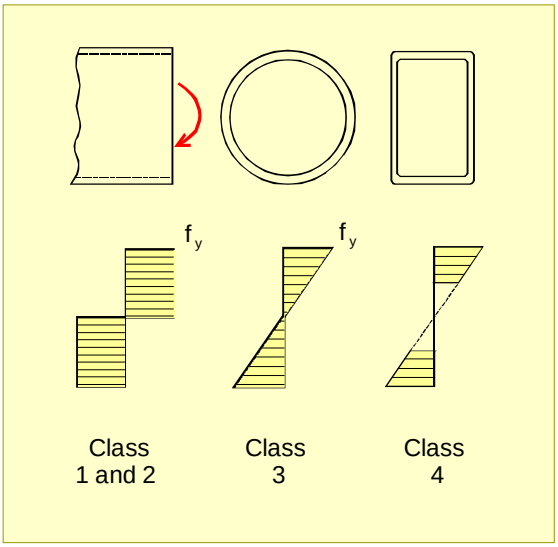

Fig. 2.8 Stress distribution for bending

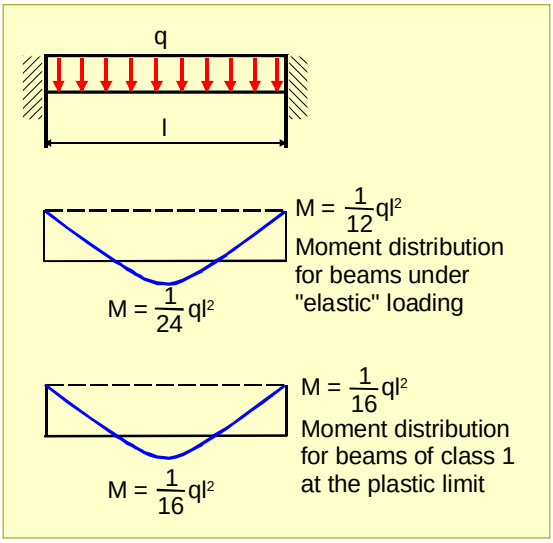

Fig. 2.9 Moment distribution in relation to cross section classification

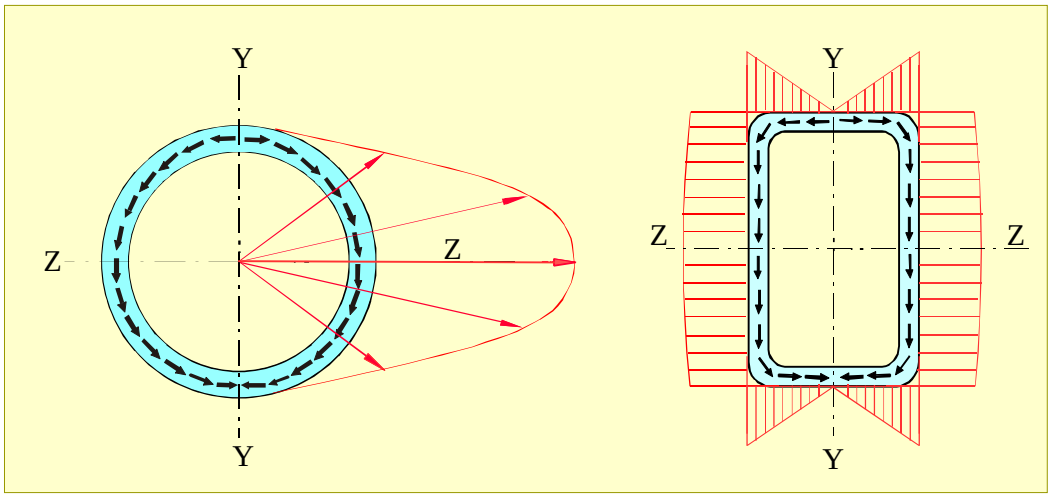

Fig. 2.10 Elastic shear stress distribution

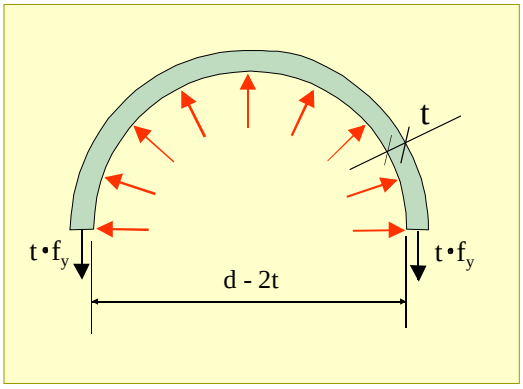

Fig. 2.11 Internal pressure

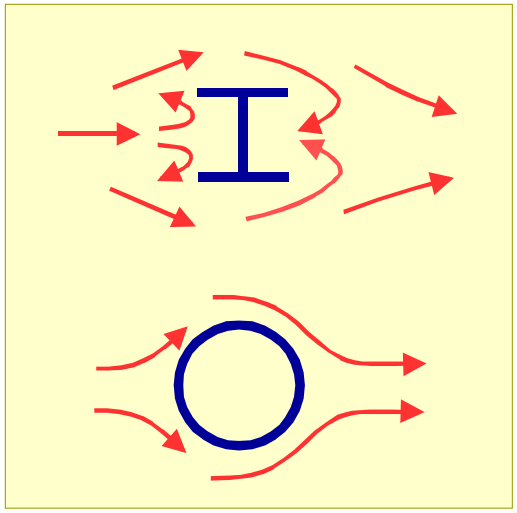
Fig. 2.12 Wind flow for open and circular hollow sections

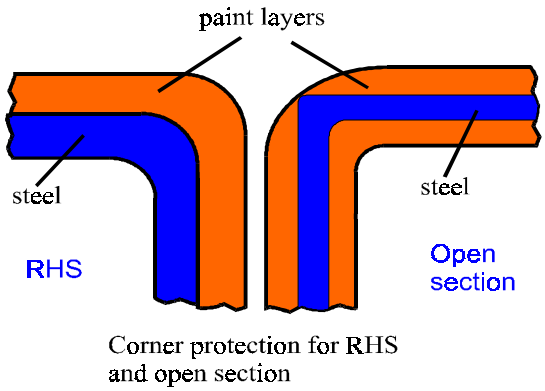

Fig. 2.13 Painted corners of RHS vs. Open sections

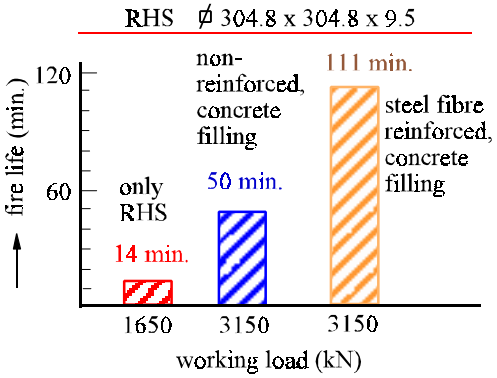

Fig. 2.14 Fire resistance of concrete-filled hollow sections

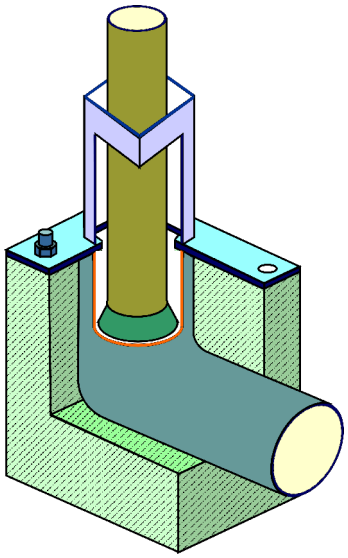

Fig. 2.15 Rain water down pipe through a hollow section column

Fig. 2.16a Aesthetically appealing tubular structures

Fig. 2.16b Aesthetically appealing tubular structures

3. APPLICATIONS

The applications of structural hollow sections nearly cover all fields. Sometimes hollow sections are used because of the beauty of their shape, to express a lightness or in other cases their geometrical properties determine their use. In this chapter, some examples will be given for the various fields and to show the possibilities [63,64,65].

3.1 BUILDINGS, HALLS, ETC.

In buildings and halls, hollow sections are mainly used for columns and lattice girders or space frames for roofs. In modern architecture they are also used for other structural or architectural reasons, e.g. facades.

Fig. 3.1 shows a 10-storey building in Karlsruhe, Germany with rectangular hollow section columns ⌀180x100 c.o.c. 1200 mm. Special aspects are that the columns are made of weathering steel and water filled to ensure the required fire protection

The columns are connected with water reservoirs to ensure circulation. Besides the fire protection, a further advantage is that due to the water circulation in the columns, the deformation of the building due to temperature differences by sunshine would be limited.

Fig. 3.2 shows a good example of lattice girder trusses used for a roof of an industrial building. For an optimal cost effective design it is essential that the truss connections are made without any stiffening plates.

Fig. 3.3 shows a very nice architectural application for the Bush Lane House in the city of London, UK. The external circular hollow section lattice transfers the facade loads and the loads on the floors to the main columns.

The hollow sections are filled with water for fire protection.

Fig. 3.4 shows the roof of the terminal of the Kansai international airport in Osaka, Japan with curved triangular girders of circular hollow sections.

An especially appealing application is given in Fig. 3.5, showing a tree type support of the airport departure hall in Stuttgart, Germany. For the connections, streamlined steel castings are used.

Nowadays, many examples of tubular structures are found in railway stations (Figs. 3.6 and 3.7) and (retractable) roofs of stadia and halls (Figs. 3.8 and 3.9). Indeed, as stated by one of the former CIDECT vice presidents at the Tubular Structures Symposium in Delft (1977) "The sky is the limit", whilst he showed beautiful applications of structural hollow sections. Figs. 3.10 - 3.12 show some more nice application examples.

3.2 BRIDGES

As mentioned in the introduction, the Firth of Forth Bridge is an excellent example of using the hollow section shape for structural applications in bridges. Nowadays, many examples exist. Figs. 3.13 to 3.16 show various examples of pedestrian bridges; the last two are movable bridges.

Fig. 3.17 shows a railway bridge near Rotterdam with a circular hollow section arch. A very nice example of a road-pedestrian bridge is shown in Fig. 3.18, being a composite steel-concrete bridge with hollow sections for the arch and braces and a concrete deck.

Circular hollow sections are sometimes also used for the flanges of plate girders, as shown in Fig. 3.13 for a triangular box girder.

3.3 BARRIERS

There are a few aspects which make hollow sections increasingly used for hydraulic structures, such as barriers. Due to environmental restrictions, the maintenance of hydraulic structures requires such precautions that it is expensive; therefore the durability is important. Structures of hollow sections are less susceptible to corrosion due to the rounded corners. Furthermore, especially circular hollow sections have lower drag coefficients, leading to lower forces due to wave loading. Fig. 3.19 shows a barrier with a support structure of circular hollow sections. Fig. 3.20 shows the storm surge barrier near Hook of Holland with triangular arms of circular hollow sections (length 250 m).

3.4 OFFSHORE STRUCTURES

Offshore, many application examples are available; most of them in circular hollow sections. For the support structure, the jacket or tower, not only is the wave loading important, but also other aspects are leading to the use of circular hollow sections. E.g. in jackets, the circular hollow section piles are often driven through the circular hollow section legs of the jacket, thus the pile is guided through the leg. Sometimes use is made of the internal void by using it for buoyancy. Further, the durability and easy maintenance in severe environments are extremely important.
Hollow section members are used for jackets, towers, the legs and diagonals in topside structures, cranes, microwave towers, flare supports, bridges, support structures of helicopter decks and further in various secondary structures, such as staircases, ladders, etc.

Figs. 3.21 to 3.23 show some examples.

3.5 TOWERS AND MASTS

Considering wind loading, corrosion protection and architectural appearance, there is no doubt that hollow sections are to be preferred. However, in many countries, electrical transmission towers are made of angle sections with simple bolted connections. Nowadays, architectural appearance becomes more important and due to the environmental restrictions, the protection and maintenance is more expensive. These factors stimulate designs made of hollow sections (Figs. 3.24 - 3.25).

3.6 SPECIAL APPLICATIONS

The special application field is large, e.g.: in transport sign gantries (Fig. 3.26), guard rails, parapets and sign posts. In mechanical engineering jibs (Fig. 3.27) and cranes (Fig. 3.28). In the agricultural field, glass houses (Fig. 3.29) and machinery (Fig. 3.30) are typical examples. Further, excellent application examples are in radiotelescopes (Fig. 3.31) and roller coasters (Fig. 3.32). Indeed, the sky is the limit.

Fig. 3.1 Facade of the Institute for Environment in Karlsruhe, Germany

Fig. 3.2 Roof with lattice girders

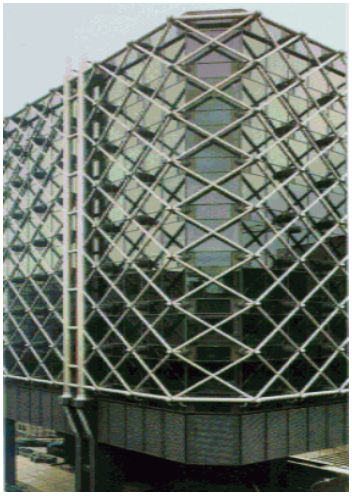

Fig. 3.3 Bush Lane House in London, UK

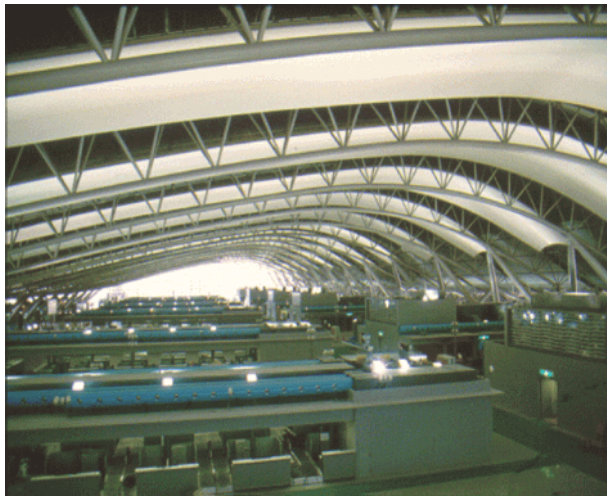

Fig. 3.4 Roof Kansai Airport, Osaka, Japan

Fig.3.5 Airport departure hall in Stuttgart,Germany

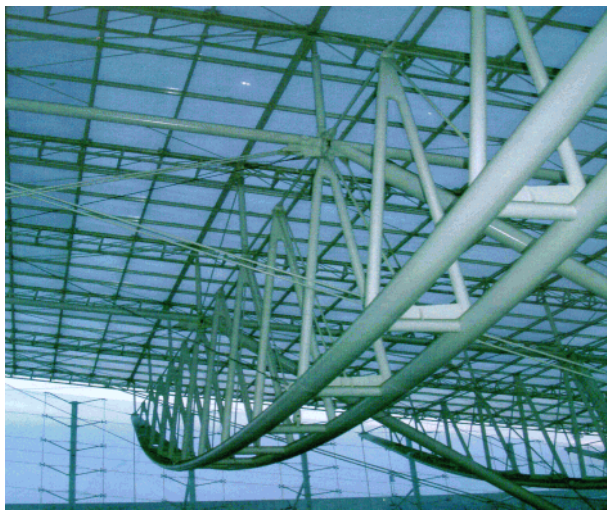

Fig. 3.6 TGV railway station at Charles de Gaulle Airport, France

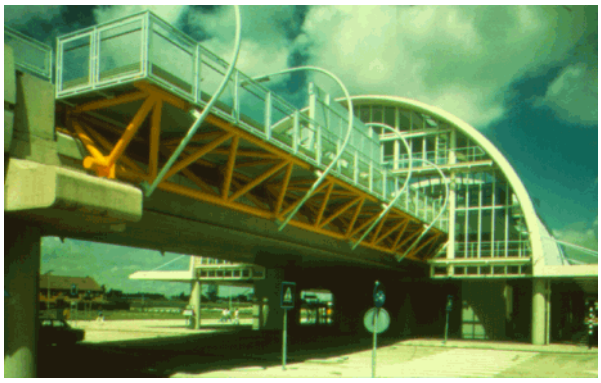

Fig. 3.7 Metro station, The Netherlands

Fig. 3.8 Retractable roof for the Ajax stadium in Amsterdam, The Netherlands

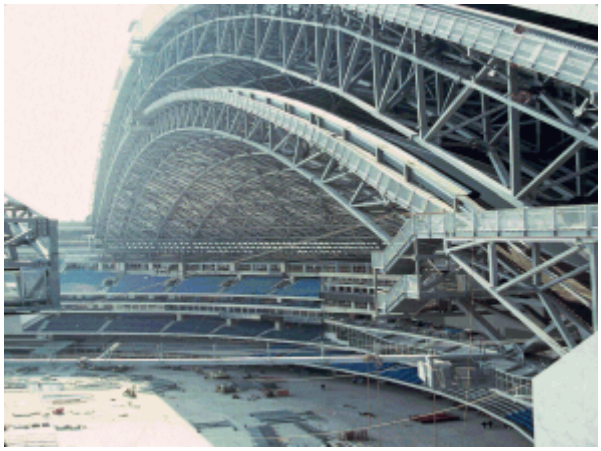

Fig. 3.9 Retractable roof for the Skydome in Toronto, Canada

Fig. 3.10 Glass facade with hollow section support structure

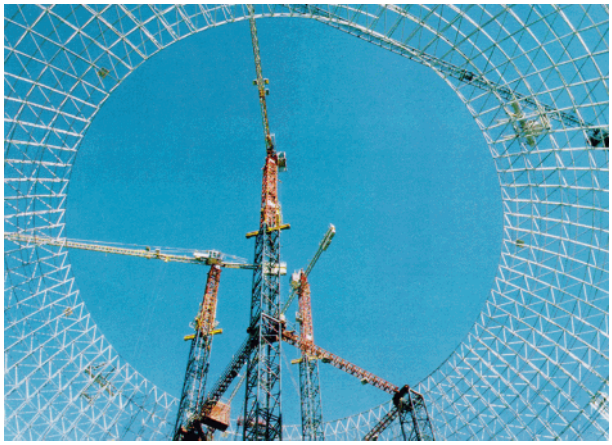

Fig. 3.11 Dome structure

Fig. 3.12 Barrel dome grid for the Trade Fair building in Leipzig, Germany

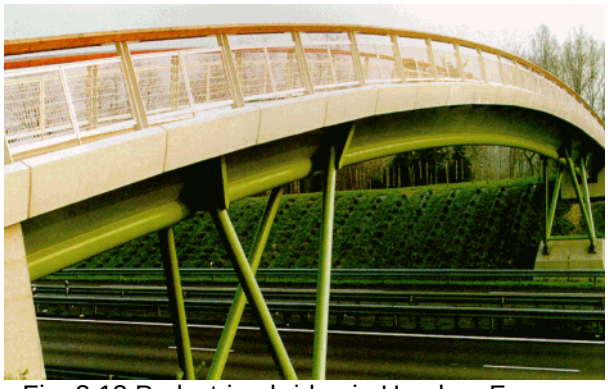

Fig. 3.13 Pedestrian bridge in Houdan, France

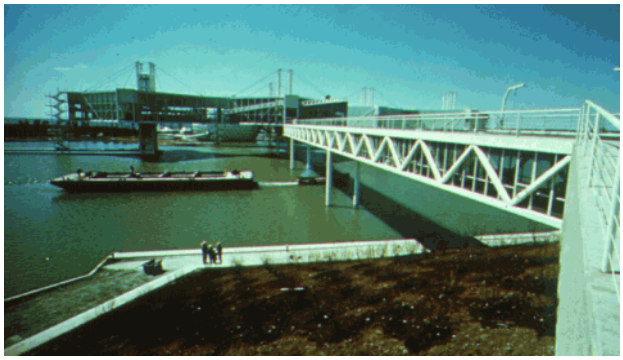

Fig. 3.14 Pedestrian bridge in Toronto, Canada

Fig. 3.15 Movable pedestrian bridge in RHS near Delft, The Netherlands

Fig. 3.16 Movable pedestrian bridge near Rotterdam, The Netherlands

Fig. 3.17 Railway bridge with a CHS arch

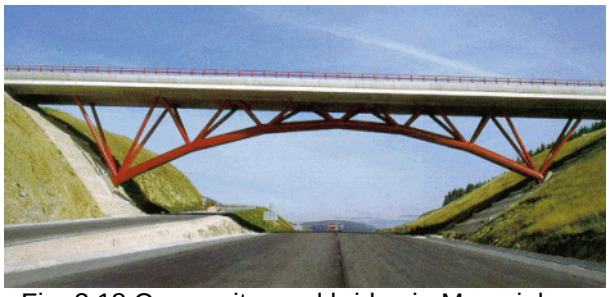

Fig. 3.18 Composite road bridge in Marvejols, France

Fig. 3.19 Eastern Scheldt barrier, The Netherlands

Fig. 3.20 Storm surge barrier near Hook of Holland, The Netherlands

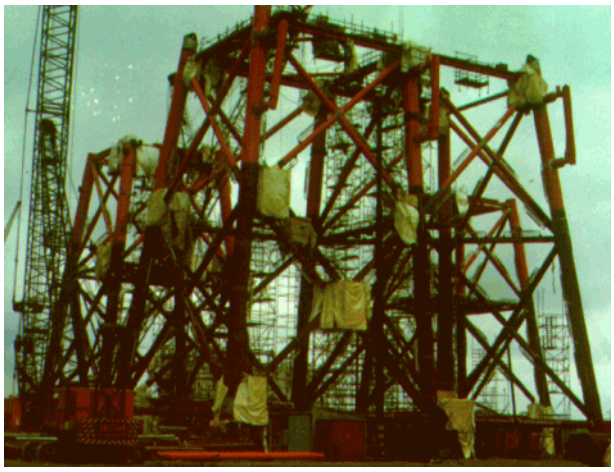

Fig. 3.21 Offshore jacket of hollow sections

Fig. 3.22 Offshore topside with various applications

Fig. 3.23 Offshore platform with jack-up

Fig. 3.24 Electricity transmission line tower

Fig. 3.25 Mast

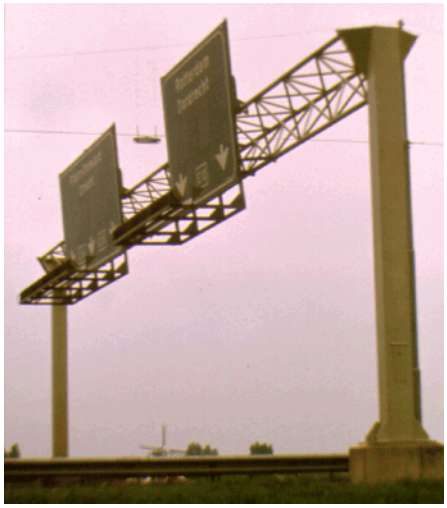

Fig. 3.26 Gantry

Fig. 3.27 Jib

Fig. 3.28 Crane

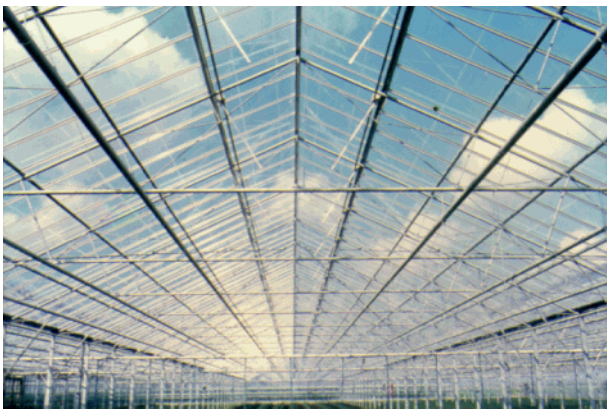

Fig. 3.29 Green House

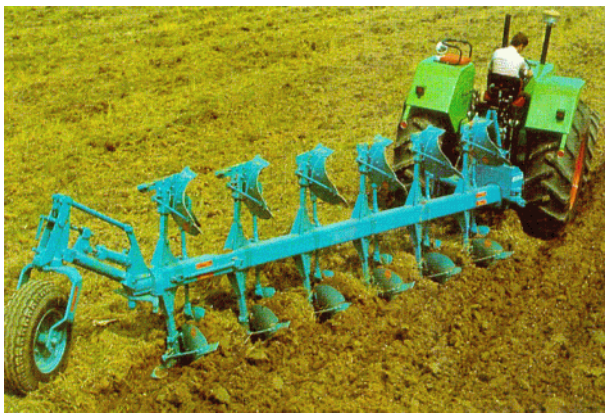

Fig. 3.30 Agricultural application

Fig. 3.31 Radiotelescope

Fig. 3.32 Roller coaster

4. COMPOSITE STRUCTURES

4.1 INTRODUCTION

Concrete filled hollow sections (Fig. 4.1) are mainly used for columns. The concrete filling gives a higher load bearing capacity without increasing the outer dimensions. The fire resistance can be considerably increased by concrete filling, in particular if proper reinforcement is used.
Due to the fact that the steel structure is visible, it allows a slender, architecturally-appealing design. The hollow section acts not only as the formwork for the concrete, but ensures that the assembly and erection in the building process is not delayed by the hardening process of the concrete.

CIDECT research on composite columns started already in the sixties, resulting in monographs and design rules, adopted by Eurocode 4 [13]. CIDECT design guide No. 5 [5] gives detailed information for the static design of concrete filled columns.
To a large extent, this chapter is based on this Design Guide No. 5.

4.2 DESIGN METHODS

In the last decades, several design methods have been developed, e.g. in Europe by Guiaux and Janss [66], Dowling and Virdi [67] and Roik, Wagenknecht, Bergmann and Bode [68], finally resulting in the design rules given in Eurocode 4. The design rules given in some other standards differ somewhat from those given in Eurocode 4.

In this chapter, the design method given is based on the simplified design method presented in Eurocode 4. The design of composite columns has to be carried out for the ultimate limit state, i.e. the effect of the most unfavourable combination of actions S_d should not exceed the resistance R_d of the composite member, or:

$S_d \leq R_d$

Proper load factors and partial safety factors have to be included. An exact calculation of the load bearing capacity considering the effect of imperfections and deflections (2nd order analysis), the effect of plastification of the section, cracking of the concrete, etc. can only be carried out by means of a computer program. With such a program, the resistance interaction curves as shown in Fig. 4.2, can be calculated. Based on these calculated capacities, simplified design methods have been developed.

4.3 SIMPLIFIED DESIGN METHOD FOR AXIALLY LOADED COLUMNS

Based on the work of Roik, Bergmann and Bode, a simplified design method is given, in which the design is approached in a similar way to that of steel columns, i.e.:

$$N_{Sd} \leq \chi \cdot N_{pl.Rd} \qquad (4.1)$$

where
N_{Sd} is the design normal force (including load factors)
χ is the reduction factor for the buckling curve "a" (see Fig. 2.3)
$N_{pl.Rd}$ is the resistance of the section against normal force according to eq. (4.2)

$$N_{pl.Rd} = A_a f_{yd} + A_c f_{cd} + A_s f_{sd} \qquad (4.2)$$

where

A_a, A_c and A_s are the cross sectional areas of the structural steel, the concrete and the reinforcement
f_{yd}, f_{cd} and f_{sd} are the design strengths of the materials, i.e.

$f_{yd} = f_y / \gamma_a$ for structural steel (4.3)

$f_{cd} = f_{ck} / \gamma_c$ for concrete (4.4)

$f_{sd} = f_{sk} / \gamma_s$ for reinforcement (4.5)

The safety factors in Eurocode 4 are boxed values, i.e. these values are recommended values which could be changed by national application documents (table 4.1).

The safety factors for the actions γ_F have to be chosen according to Eurocode 1 [10] or national codes respectively.
Table 4.2 shows the strength classes of concrete.

Classes higher than C50/60 should not be used without

further investigation. Classes lower than C20/25 are not allowed for composite construction.

In concrete filled hollow sections, the concrete is confined by the hollow section. Therefore, the normal concrete strength reduction factor of 0.85 for long term acting loads does not have to be used.

The χ reduction factor has to be determined for the relative slenderness $\overline{\lambda}$:

$$\overline{\lambda} = \sqrt{\frac{N_{pl.R}}{N_{cr}}} \qquad (4.6)$$

where

$N_{pl.R}$ is the resistance of the section to axial loads $N_{pl.Rd}$ acc. to (4.2) to (4.5).
However, with $\gamma_a = \gamma_c = \gamma_s = 1.0$ and

N_{cr} is the elastic buckling load of the member (Euler critical load)

$$N_{cr} = \frac{(EI) \cdot \pi^2}{\ell^2} \qquad (4.7)$$

where

ℓ is the buckling length of the column and

EI is the effective stiffness of the composite section.

The buckling (effective) length of the column can be determined by using the methods shown in literature or following the rules of Eurocode 3. For columns in non-sway systems, as a safe approximation, the column length may be taken as the buckling length.

$$EI = E_a I_a + 0.6 E_{cm} I_c + E_s I_s \qquad (4.8)$$

where

I_a, I_c and I_s are the moments of inertia of the cross sectional areas of the structural steel, the concrete (with the area in tension assumed to be uncracked) and the reinforcement, respectively.

E_a and E_s moduli of elasticity of the structural steel and the reinforcement and

$0.6 E_{cm} I_c$ is the effective stiffness of the concrete section with E_{cm} being the modulus of elasticity of concrete according to Table 4.2.

The simplified design method of Eurocode 4 has been developed with an effective stiffness modulus of the concrete of 600 f_{ck}. In order to have a similar basis like Eurocode 2, the secant modulus of concrete E_{cm} was chosen as a reference value. The transformation factor 0.6 in eq. 4.8 is incorporated to consider the effect of cracking of concrete under moment action due to the second order effects.

4.3.1 Limitations

The reinforcement to be included in the design calculations is limited to 4% of the concrete area. There is no minimum requirement. However, if the reinforcement is considered for the load bearing capacity, a minimum reinforcement of 0.3% of the concrete area is required.

The composite column is considered as "composite" if:

$$0.2 \le \delta \le 0.9 \qquad (4.9)$$

with

$$\delta = \frac{A_a \cdot f_{yd}}{N_{pl.Rd}} \qquad (4.10)$$

If the parameter δ is less than 0.2, the column shall be designed as a concrete column following Eurocode 2 [11]. On the other hand, when δ exceeds 0.9, the column shall be designed as a steel column according to Eurocode 3 [12].

To avoid local buckling, the following limits should be observed for bending and compression loading:

- for concrete filled rectangular hollow sections (h being the greater overall dimension of the section)
  $h/t \le 52\varepsilon$ (4.11)
- for concrete filled circular hollow sections
  $d/t \le 90\ \varepsilon^2$ (4.12)

The factor ϵ accounts for different yield limits.

$$\varepsilon = \sqrt{\frac{235}{f_y}} \qquad (4.13)$$

with f_y in N/mm^2.

The values given in Table 4.3 are based on a class 2 classification, thus for the analysis of the internal forces in a structure an elastic analysis should be used, but the plastic resistance of the section can be used.

4.3.2 Effect of long term loading

The influence of the long-term behaviour of the concrete on the load bearing capacity of the column is considered by a modification of the concrete modulus, since the load bearing capacity of the columns may be reduced by creep and shrinkage. For a loading which is fully permanent, the modulus of the concrete is half of the original value. For loads that are only partly permanent, an interpolation may be carried out:

$$E_c = 0.6\, E_{cm} \left(1 - 0.5\, \frac{N_{G.Sd}}{N_{Sd}} \right) \qquad (4.14)$$

where
N_{Sd} is the acting design normal force
$N_{G.Sd}$ is the permanent part of it

- This method leads to a redistribution of the stresses into the steel part, which is a good simulation of the reality.
- For short columns and/or high eccentricities of loads, creep and shrinkage do not need to be considered.
- If the eccentricity of the axial load exceeds twice the diameter or depth of the hollow section, the influence of the long-term effects may be neglected compared to the actual bending moments.
- Furthermore, the influence of creep and shrinkage is significant only for slender columns, i.e. the influence of long-term effects does not need to be taken into account if:

$$\overline{\lambda} \le \frac{0.8}{1-\delta} \text{ for braced and non-sway systems} \qquad (4.15)$$

$$\overline{\lambda} \le \frac{0.5}{1-\delta} \text{ for unbraced and sway systems} \qquad (4.16)$$

with δ according to eq. (4.10)

4.3.3 Effect of confinement

For concrete filled circular hollow section columns with a small relative slenderness $\overline{\lambda} < 0.2$ the bearing capacity is increased due to the impeded transverse strains. This results in radial compression in the concrete and a higher resistance for normal stresses, see Fig. 4.3. Above these values the effect is very small.
Detailed information can be found in [5].

4.4 RESISTANCE OF A SECTION TO BENDING

For the determination of the resistance of a section against bending moments, a full plastic stress distribution in the section is assumed (Fig. 4.4). The concrete in the tension zone of the section is assumed to be cracked and is therefore neglected. The internal bending moment resulting from the stresses and depending on the position of the neutral axis is the resistance of the section against bending moments $M_{pl.Rd}$.

4.5 RESISTANCE OF A SECTION TO BENDING AND COMPRESSION

The resistance of a cross section to bending and compression can be shown by the interaction curve between the normal force N_{Rd} and the internal bending moment M_{Rd}.
Figs. 4.5 to 4.8 show the interaction curves for RHS and CHS columns in relation to the cross section parameter δ. These curves have been determined without any reinforcement, but they may also be used for reinforced sections if the reinforcement is considered in the δ values and in $N_{pl,Rd}$ and $M_{pl.Rd}$ respectively.

The interaction curve has some significant points, shown in Fig. 4.9.
These points represent the stress distributions given in Fig. 4.10. The internal moments and axial loads belonging to these stress distributions can be easily calculated if effects of the corner radius are excluded.

Comparing the stress distribution of point B, where the normal force is zero, and that of point D (Fig. 4.10), the neutral axis moves over a distance h_n. So the normal force $N_{D.Rd}$ is determined by the additional compressed parts of the section. This determines the distance h_n, because the force $N_{D.Rd}$ is equal to $0.5\, A_c \cdot f_{cd} = 0.5 N_{p\ell.c.Rd}$.
Considering the stress distribution at point C (Fig. 4.10), the distance of the neutral axis to the centre line is again h_n. The moment $M_{C.Rd}$ is equal to the moment $M_{B.Rd}$, because the additional compressed sections do not increase the moment. The normal force is twice the value of that at point D, thus $N_{C.Rd} = N_{p\ell.c.Rd}$.

4.6 INFLUENCE OF SHEAR FORCES

The shear force of a composite column may either be assigned to the steel profile alone or be divided into a steel and a reinforced concrete component. The component for the structural steel can be considered by reducing the axial stresses in those parts of the steel profile which are effective for shear (Fig. 4.11).

The reduction of the axial stresses due to shear stresses may be carried out according to the Huber/Hencky/von Mises criterion or according to a more simple quadratic equation from Eurocode 4. For the determination of the cross-section interaction, it is easier to transform the reduction of the axial stresses into a reduction of the relevant cross sectional areas equal to that used for hollow sections without concrete filling:

$$\text{red } A_v = A_v \left[1 - \left(\frac{2V_{Sd}}{V_{pl.Rd}} - 1\right)^2\right] \qquad (4.17)$$

$$V_{pl.Rd} = A_v \cdot \frac{f_{yd}}{\sqrt{3}} \qquad (4.18)$$

The influence of the shear stresses on the normal stresses does not need to be considered if:

$$V_{Sd} \leq 0.5\, V_{pl.Rd} \qquad (4.19)$$

4.7 RESISTANCE OF A MEMBER TO BENDING AND COMPRESSION

4.7.1 Uniaxial bending and compression

Fig. 4.12 shows the method for the design of a member under combined compression and uniaxial bending using the cross-section interaction curve. Due to imperfections, the resistance of an axially loaded member is given by eq. 4.1 or χ on the vertical axis in Fig. 4.12.

The moment capacity factor μ_k at the level of χ is defined as the imperfection moment. Having reached the load bearing capacity for axial compression, the column cannot resist any additional bending moment. This imperfection moment is used to decrease the bearing capacity for additional bending moments at levels lower than χ (linearly to zero at the level of χ_n).

The value of χ_d resulting from the actual design normal force N_{Sd} ($\chi_d = N_{Sd}/N_{pl.Rd}$) gives the moment capacity factor μ_d for the capacity of the section. This factor μ_d is reduced by the relevant part of the imperfection moment to the value μ.

The influence of the imperfection on different bending moment distributions can be considered by means of the value χ_n. The value χ_n depends on the moment distribution in the columns. For end moments, χ_n may be taken as:

$$\chi_n = \chi \cdot \frac{1-r}{4} \qquad (4.20)$$

where
r is the ratio of the smaller to larger end moment, see Fig. 4.13, ($-1 \leq r \leq +1$).

The capacity for the combined compression and bending of the member can now be checked by:

$$M_{Sd} \leq 0.9 \cdot \mu \cdot M_{pl.Rd} \qquad (4.21)$$

where
M_{Sd} is the design bending moment of the column.

The additional reduction by the factor 0.9 covers the assumptions of this simplified design method:

- The interaction curve of the section is determined assuming full plastic behaviour of the materials with no strain limitation.
- The calculation of the design bending moment M_{Sd} is carried out with the effective stiffness, where the influence of cracking of the concrete on the stiffness is not covered for high bending moments.

Note: Interaction curves of the composite sections always show an increase in the bending capacity higher than $M_{pl.Rd}$. The bending resistance increases with an increasing normal force, because former regions in tension are compressed by the normal force. This positive effect may only be taken into account if it is ensured that the bending moment and the axial force always act together. If this is not ensured and the bending moment and the axial force result from different loading situations, the related moment capacity μ has to be limited to 1.0.

4.7.2 Biaxial bending and compression

The design of a member under biaxial bending and compression is based on its design under uniaxial bending and compression. In addition to 4.7.1, the interaction curve of the section and the moment factor μ have to be determined for both axes. The influence of the imperfection is only taken into account for the buckling axis which is most critical, resulting in χ_d.

The check can be expressed by the following condition:

$$\frac{M_{y.Sd}}{\mu_y \cdot M_{pl.y.Rd}} + \frac{M_{z.Sd}}{\mu_z \cdot M_{pl.z.Rd}} \leq 1.0 \qquad (4.22)$$

The values μ_y and μ_z are determined at the level of χ_d.

4.8 DETERMINATION OF BENDING MOMENTS

The critical moments and location depend on the loading of the column, e.g. end moments, lateral loading.
In principle, a second order analysis should be used to determine the exact bending moment.

The moment can also be determined by multiplying the first order bending moment by a factor k which depends on the moment distribution and the ratio between the design axial force N_{Sd} and the buckling load N_{cr}.

$$k = \frac{c}{1 - \frac{N_{Sd}}{N_{cr}}} \qquad (4.23)$$

with $c = 0.66 + 0.44r$ but $c \geq 0.44$.
For more detailed information, ref. [5] can be used.

4.9 LOAD INTRODUCTION

In the design of composite columns, a full composite action of the cross section is assumed. This means that in the bond area no significant slip can occur between the steel and the concrete. At locations of load introduction, e.g. at beam-column connections, this has to be verified.

The maximum bond stress based on friction is:

$\tau_{Rd} = 0.4$ N/mm^2

The shear load transfer can be increased considerably by shear connectors or steel components, see Fig. 4.14.

For concentrated loads, a load distribution according to Fig. 4.15 can be assumed

Table 4.1 Partial safety factors for resistances and material properties for fundamental combinations [13]

structural steel	concrete	reinforcement
$\gamma_a = 1.1$	$\gamma_c = 1.5$	$\gamma_s = 1.15$

Table 4.2 Strength classes of concrete, characteristic cylinder strength and modulus of elasticity for normal weight concrete

strength class of concrete $f_{ck.cyl}/f_{ck.cub}$	C20/25	C25/30	C30/37	C35/45	C40/50	C45/55	C50/60
cylinder strength f_{ck} [N/mm^2]	20	25	30	35	40	45	50
modulus of elasticity E_{cm} [N/mm^2]	29000	30500	32000	33500	35000	36000	37000

Table 4.3 Limit ratios of wall thickness for which local buckling is prevented under axial compression

steel grade		S235	S275	S355	S460
circular hollow sections	d/t	90	77	60	46
rectangular hollow sections	h/t	52	48	42	37

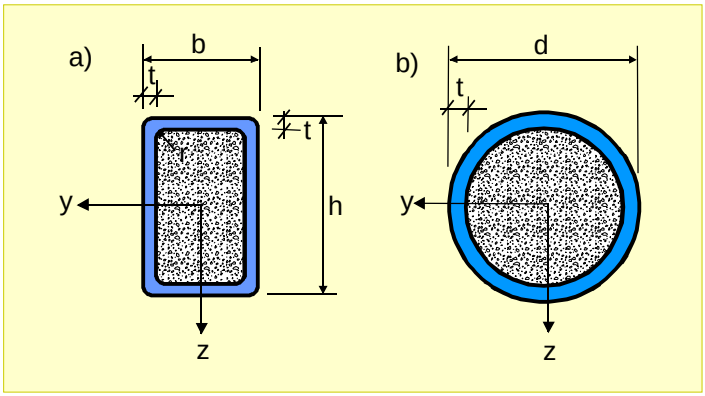

Fig. 4.1 Concrete filled hollow sections with notations

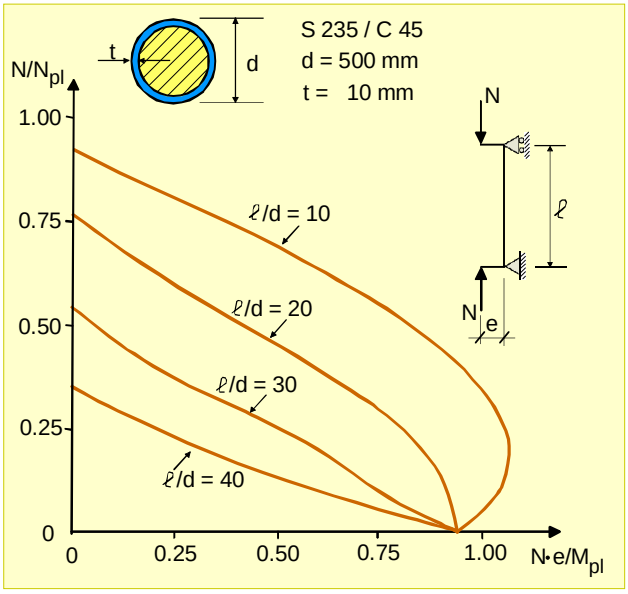

Fig. 4.2 Bearing capacity of a composite hollow section column

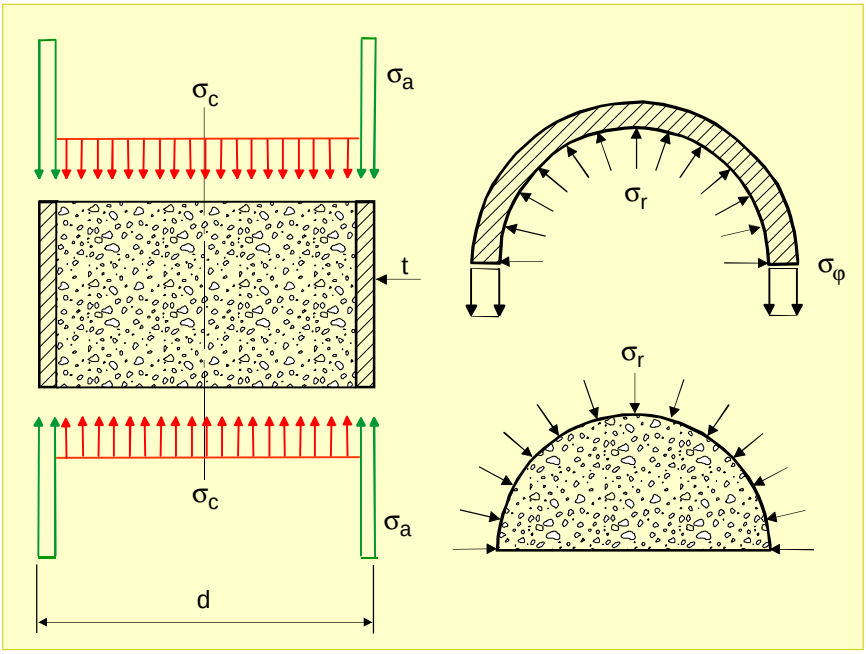

Fig. 4.3 Three dimensional effect in concrete filled hollow sections

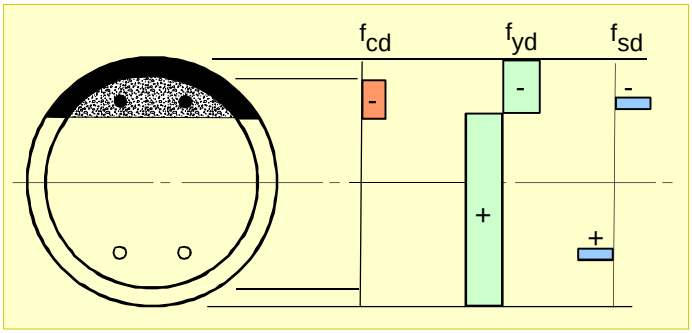

Fig. 4.4 Stress distribution for the bending resistance of a section

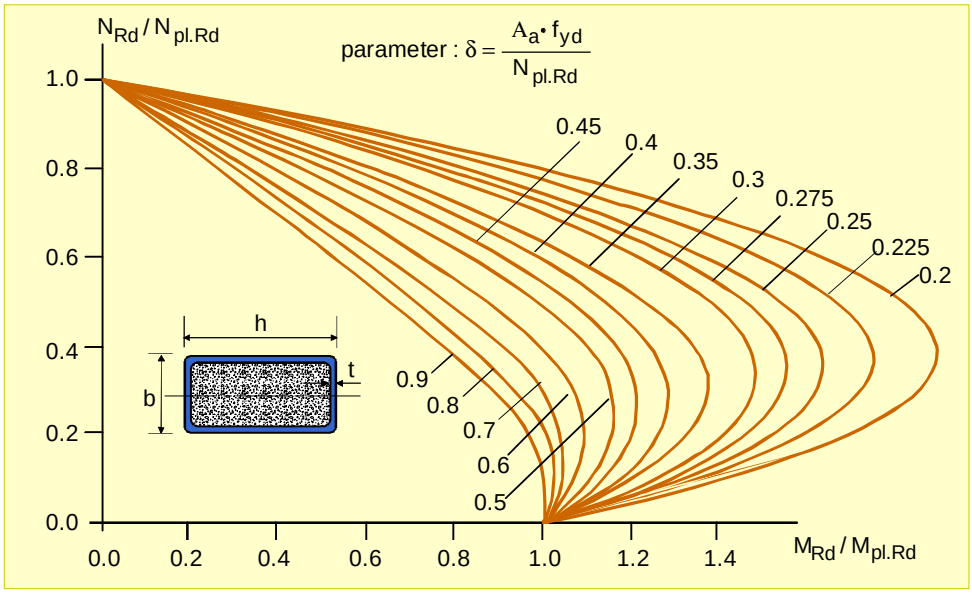

Fig. 4.5 Interaction curve for rectangular sections with bending over weak axis; b/h = 0.5

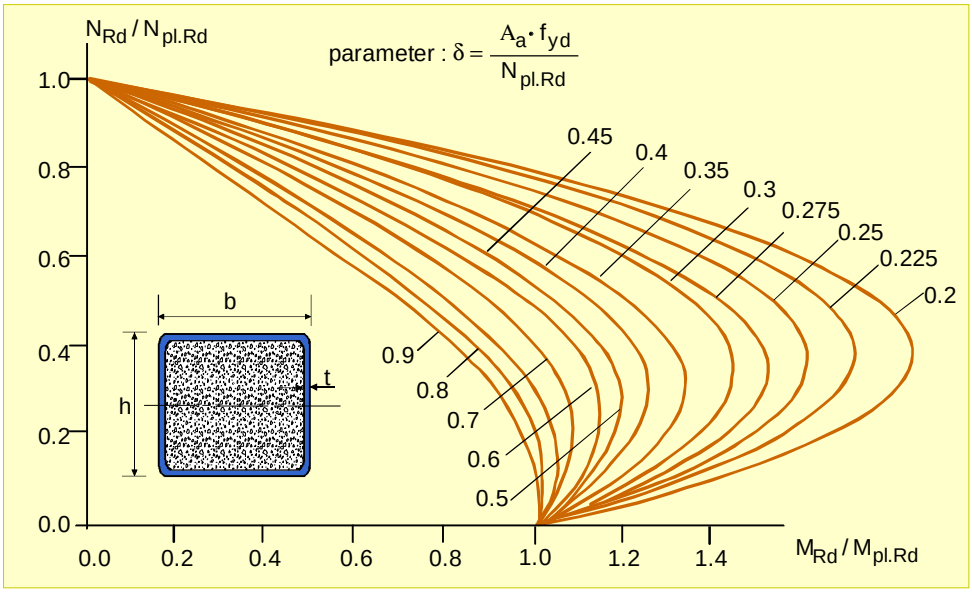

Fig. 4.6 Interaction curve for square sections with h/b = 1.0

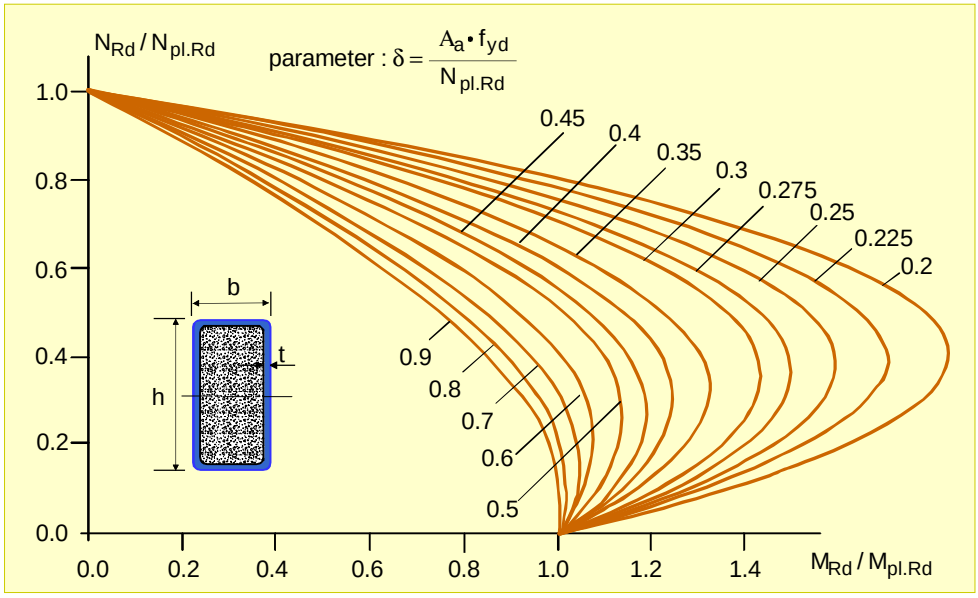

Fig. 4.7 Interaction curve for rectangular sections with h/b = 2.0

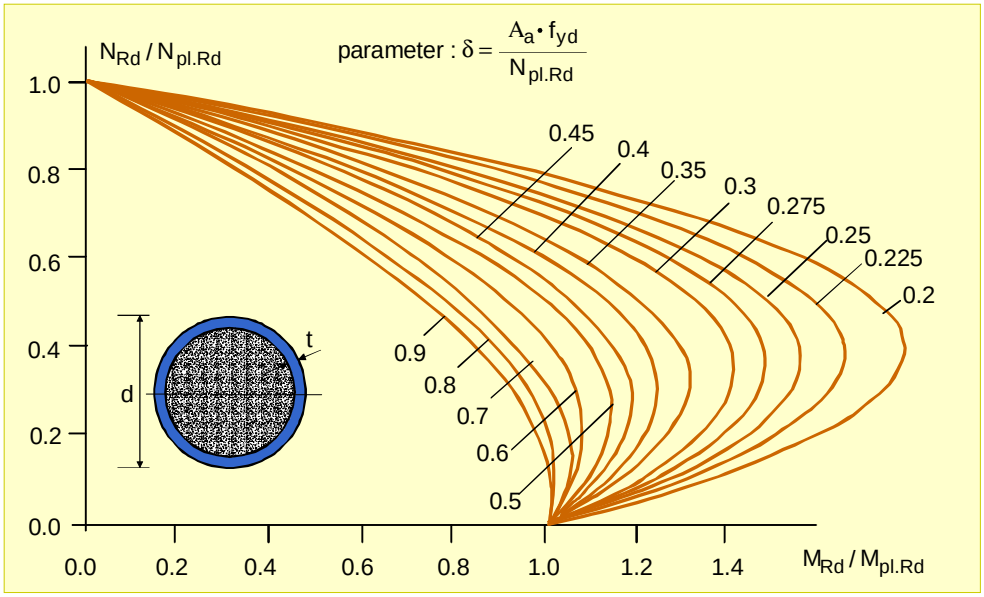

Fig. 4.8 Interaction curve for circular sections

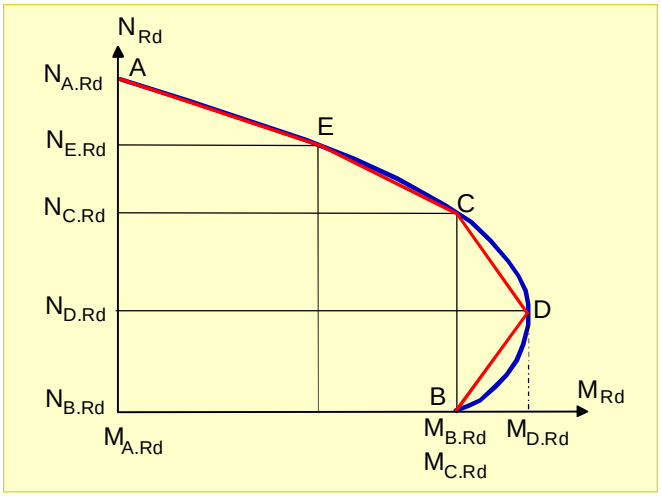

Fig. 4.9 Interaction curve approached by a polygonal connection of the points A to E

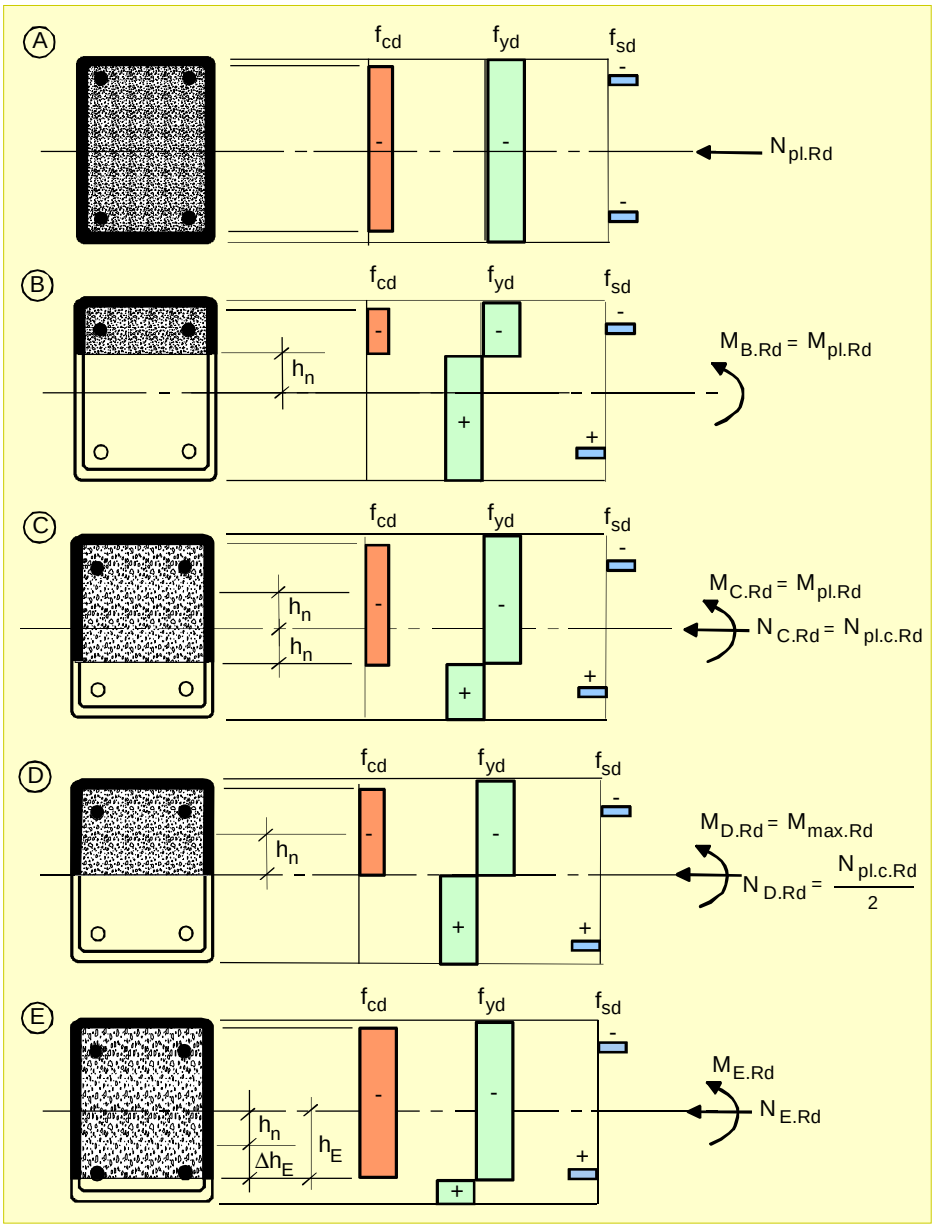

Fig. 4.10 Stress distributions of selected positions of the neutral axis (points A through E)

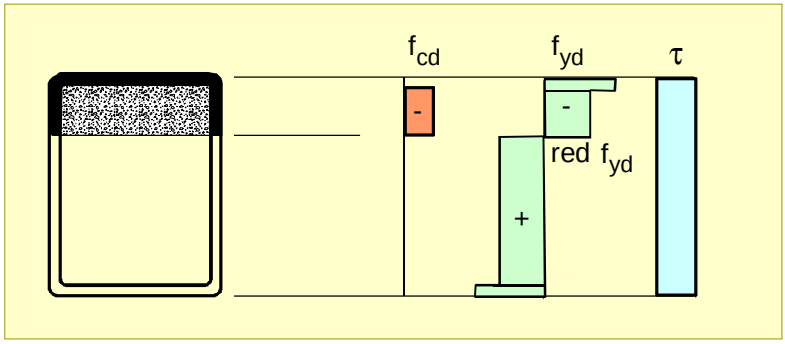

Fig. 4.11 Reduction of the normal stresses due to shear

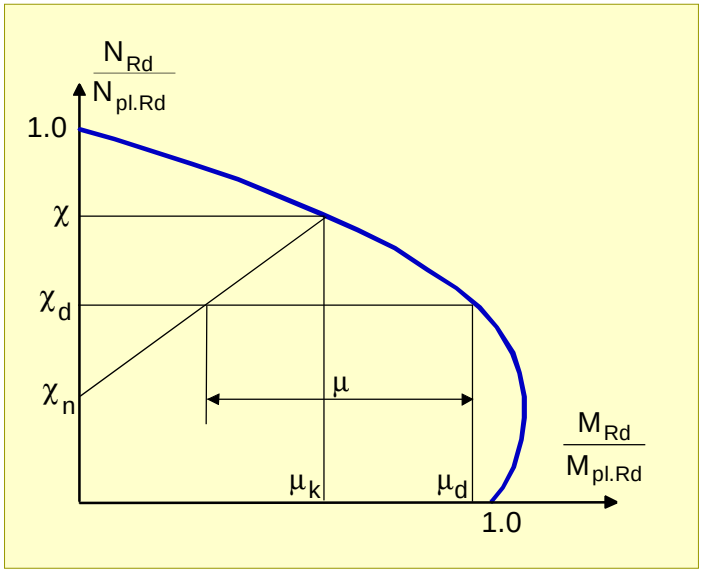

Fig. 4.12 Design for compression and uniaxial bending

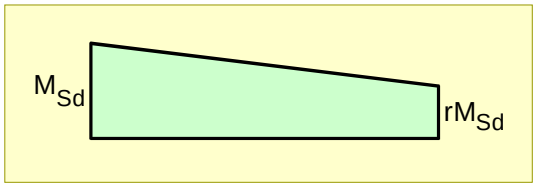

Fig. 4.13 Relation of the end moments ($-1 \leq r \leq +1$)

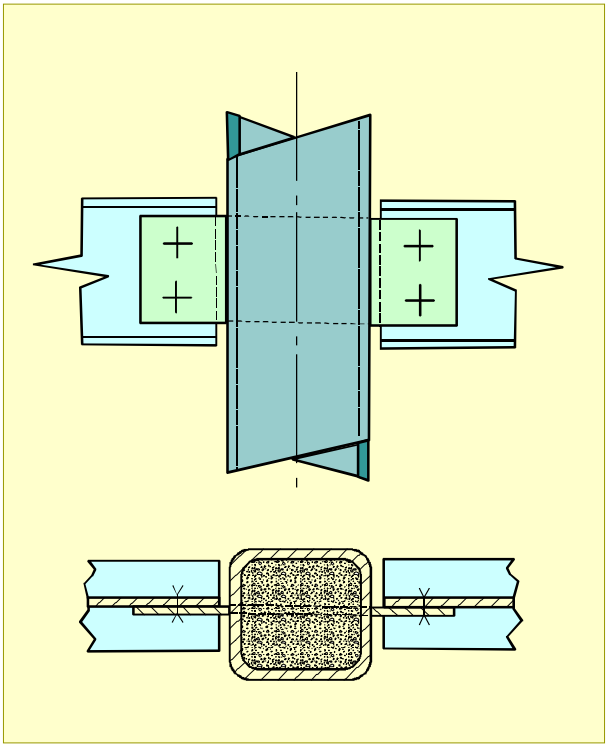

Fig. 4.14 Load introduction into hollow sections by inserted plates

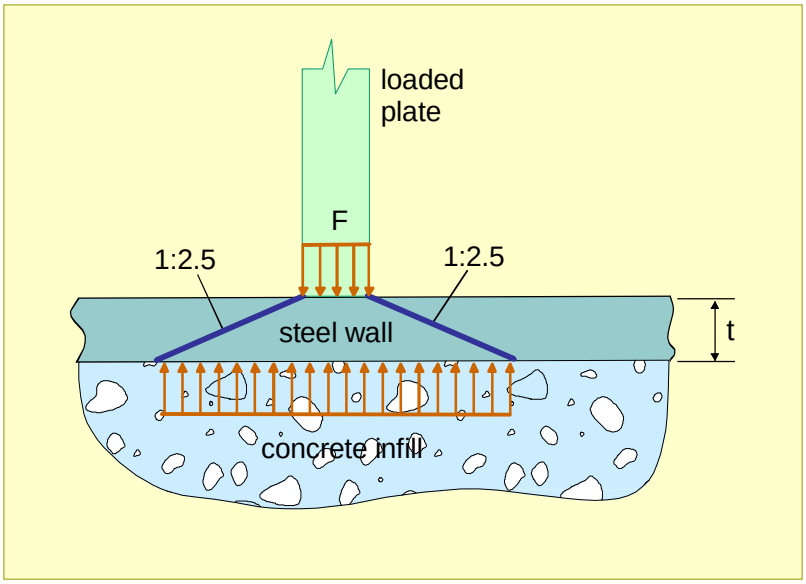

Fig. 4.15 Load introduction in composite column

5. FIRE RESISTANCE OF HOLLOW SECTION COLUMNS

5.1 INTRODUCTION

This chapter is a reduced version of the CIDECT Design Guide No 4 [4].

Unprotected structural hollow sections (SHS) have an inherent fire resistance of some 15 to 30 minutes. Traditionally, it has been assumed that unprotected steel members fail when they reach temperatures of about 450 to 550°C. However, the temperature at which a steel member reaches its ultimate limit state depends on the massivity of the section and the actual load level. If the service load level of a column is less than 50% of its resistance, the critical temperature rises to over 650°C, which, for bare steel, means an increase in failure time of more than 20%.
When hollow steel sections are required to withstand extended amounts of time in fire, additional measures have to be considered to delay the rise in steel temperature.

5.1.1 External insulation of the steel sections

This type of fire protection can be applied to all kinds of structural elements (columns, beams and trusses). The temperature development in a protected hollow steel section depends on the thermal properties of the insulation material (conductivity, on the thickness of the insulation material and on the shape factor (massivity) of the steel profile.
External fire protection materials can be grouped as follows:

- insulating boards (based mainly on gypsum or mineral fibre or lightweight aggregates such as perlite and vermiculite). If board protection is to be used on members carrying tensile loads, care must be taken to ensure the integrity of joints between the boards.
- spray coating or plaster (based mainly on mineral fibre or lightweight aggregates such as perlite and vermiculite);
- intumescent coatings (paint-like mixtures applied directly to the steel surface which, in case of fire, swell up to a multiple of their original thickness);
- suspended ceilings (protecting mainly roofs, trusses);
- heat radiation shielding (thin steel panels used for external structures)

In some countries, intumescent coatings are restricted to a fire resistance of 30 or 60 min., but this technology is rapidly developing.

5.1.2 Concrete filling of the section

Usually, this type of fire protection is applied to columns only. Filling hollow sections with concrete is a very simple and attractive way of enhancing fire resistance. The temperature in the unprotected outer steel shell increases rapidly. However, as the steel shell gradually loses strength and stiffness, the load is transferred to the concrete core.

Apart from the structural function, the hollow section also acts as a radiation shield to the concrete core. In combination with a steam layer between the steel and the concrete core, this leads to a lower temperature rise in the core compared to reinforced concrete structures. Depending on the fire resistance requirements, the concrete in the hollow section can be plain concrete (fire resistance up to 60 min.) or concrete with rebars or steel fibres. New research aimed at increasing the fire resistance of concrete filled hollow sections is focused on the use of high strength concrete.

5.1.3 Water cooling

This type of fire protection can be applied to all kinds of hollow sections, but has been mostly used for columns. The hollow section acts both as the load bearing structure and as the water container. The protection system is quite sophisticated; it needs a thorough design and proper hydraulic installations.

The cooling effect consists of the absorption of heat by water, the removal of heat by water circulation and its consumption in the vaporization of water. In practical applications, these effects are combined. A suitably designed water filled system will limit the average steel temperature to less than 200°C.

Two different systems can be used: permanently filled elements or elements filled only when a fire breaks out. In the latter case, protection depends on a fire detection system and a short water filling time. In unreplenished systems, the attainable fire resistance time depends on the total water content (including any reservoir tank)

and on the shape of the heated structure. In systems where the water is constantly renewed, the fire resistance is unlimited. Water cooling by natural flow is mainly used for vertical or inclined elements in order to ensure the circulation of the water.

5.2 FIRE RESISTANCE

5.2.1 Concept

Fire safety precautions are specified with the intent of avoiding any casualties and reducing economic fire damage to an acceptable level. As far as building construction is concerned, it is important that the construction elements can withstand a fire for a specified amount of time. In this respect, one should bear in mind that the strength and deformation properties of the commonly used building materials deteriorate significantly at the temperatures that may be expected under fire conditions. Moreover, the thermal expansion of most of the building materials appears to be considerable. As a result, the structural elements and assemblies may deform or even collapse when exposed to fire conditions.

The amount of time that a construction element can resist a fire depends largely on the anticipated temperature development of the fire itself. This temperature development depends, among other things, on the type and amount of combustible materials present, expressed in terms of kg of wood per m^2 floor surface and called the *fire load density*, and on the fire ventilation conditions, see Fig. 5.1.

In practical fire safety design, however, it is conventional to use a so-called "*standard fire curve*", defined in ISO 834 [22], which is more or less representative for post flash-over fires in buildings with relatively small compartments, such as apartment buildings and offices. Alternative standard fire curves, with differences from the ISO-curve, are in use in the USA and for maritime applications.

The amount of time a building component is able to withstand heat exposure according to the standard fire curve, is called the "*fire resistance*". In order to be able to determine the fire resistance of a building component, proper performance criteria have to be determined. These criteria are defined in relation to the anticipated function of the respective building element during fire. In general, there are three such performance criteria:
- stability
- insulation
- integrity

For details on the performance criteria, see [4].

For building components such as columns, with a load bearing function, the only relevant performance criterion is "stability".
As far as the determination of the fire resistance is concerned, there are basically two possibilities: an experimental approach and an analytical or fire engineering approach.
The experimental approach, i.e. the determination of the fire resistance of columns on the basis of standard fire tests, is the traditional approach. Although based on different national testing procedures, the concept of fire testing is by and large the same in the various countries.
The fire engineering approach is a relatively new development that has become possible by the recent development of computer technology. On an international level, calculation rules for the fire resistance of both steel and composite steel concrete columns, including concrete filled SHS columns, are available. There are significant advantages to the analytical approach, when compared with the experimental one. Important factors influencing the fire resistance of columns are:
- load level
- shape and size of the cross section
- buckling length

Bare steel columns (i.e. SHS columns without external protection or concrete filling) possess only a limited fire resistance. Depending on the load level and the shape factor (massivity), a fire resistance of 15 to 20 minutes is usually attainable. A 30 min. fire resistance can only be achieved in more exceptional cases. This situation may be dramatically improved by applying thermal insulation to the column. Depending on the type and thickness of the insulation material, fire resistances of many hours can be achieved, although most requirements today are limited to 120 minutes.

SHS columns filled with concrete have a much higher load bearing capacity and a higher fire resistance than unprotected empty SHS columns. Provided the concrete is of good quality (over, say, a crushing strength of 20 N/mm^2) and the cross sectional dimensions are not too small (not less than 150x150 mm), a fire resistance of at least 30 minutes will be achieved. Sections with larger dimensions will have a

higher fire resistance and by adding additional reinforcement to the concrete the fire resistance may be increased to over 120 minutes.

Infinite fire resistance can be achieved by water filling, provided an adequate water supply is available.

Improved fire performance of SHS columns can also be achieved by placing the columns outside the building envelope - an expedient often used for architectural purposes. By preventing direct flame impingement on the member, the need for additional fire protection measures can be significantly reduced or even become unnecessary.

Since fire safety requirements for columns are normally expressed solely in terms of the fire resistance to be attained, this emphasizes the need to consider the fire resistance requirements from the beginning in a structural design project.

5.2.2 Requirements

Fire safety in buildings is based on achieving two fundamental objectives:
- reducing the loss of life
- reducing the property or financial loss in or in the neighbourhood of a building fire.

In most countries, the responsibility for achieving these objectives is divided between the government or civic authorities who have the responsibility for life safety via building regulations, and the insurance companies dealing with property loss through their fire insurance policies.

The objectives of fire safety may be achieved in various ways. For example:
- by eliminating or protecting possible ignition sources (fire prevention)
- by installing an automatic extinguishing device, in order to prevent the fire from growing into a severe fire (operational or active measures, e.g. sprinklers).
- by providing adequate fire resistance to the building components using passive or structural measures to prevent fire spreading from one fire compartment to adjacent compartments.

Often a combination of the above measures is applied.

Requirements with regard to fire resistance clearly belong to the structural measures. To date, the use of a conventional fire scenario based on the ISO standard fire curve, is common practice in Europe and elsewhere. The standard fire test is not intended to reflect the temperatures and stresses that would be experienced in real fires, but provides a measure of the relative performance of elements of structures and materials within the capabilities and dimensions of the standard furnaces. In general, uncertainties about structural behaviour in real fires are taken into account by making conservative fire resistance requirements.

Required safety levels are specified in National Codes and normally depend on factors like:
- type of occupancy
- height and size of the building
- effectiveness of fire brigade action
- active measures, such as vents and sprinklers (but not in all countries)

An overview of fire resistance requirements as a function of the number of storeys and representative for many European countries is given in Table 5.1.

The following general features may be identified:
- no specified fire resistance requirements for buildings with limited fire load density (say: 15-20 kg/m^2) or where the consequences of collapse of the structure are acceptable
- fire resistance for a specified but limited amount of time, where the time requirement is mainly intended to allow for safe evacuation of the occupants and intervention by rescue teams
- extended fire resistance of the main structure to ensure that the structure can sustain a full burn out of combustible materials in the buildings or a specified part of it.

Sometimes unprotected steel may be sufficient, for example for situations where safety is satisfied by other means (e.g. sprinklers) and/or if requirements with respect to fire resistance are low (i.e. not over, say, 30 minutes).

A full fire engineering approach (Natural Fire Concept), in which compartment and steel temperature are calculated from a consideration of the combustible material present, compartment geometry and ventilation, is becoming more accepted and has shown considerable savings in fire protection costs in specific cases.

5.2.3 Performance criteria

The fundamental concept behind all methods designed to predict structural stability in fire is that construction materials gradually lose strength and stiffness at elevated temperatures. The reduction in the yield strength of structural steel and the compression strength of concrete with increasing temperature according to the Eurocodes is given in Fig. 5.2. It shows that there is not much difference in the relative reduction in strength of concrete and steel under high temperatures. The reason for the difference in the structural behaviour of steel and concrete elements under fire conditions is that heat propagates about 10 to 12 times faster in a steel structure than in a concrete structure of the same massivity, because the thermal conductivity of steel is higher than that of concrete.

Normally, the fire resistance design of structures is based on similar static boundary conditions to the design under ambient temperature. In a multi-storey braced frame, the buckling length of each column at room temperature is usually assumed to be the column length between floors. However, such structures are usually compartmented and any fire is likely to be limited to one storey. Therefore, any column affected by fire will lose its stiffness, while adjacent members will remain relatively cold. Accordingly, if the column is rigidly connected to the adjacent members, built-in end conditions can be assumed in the event of fire. Investigations have shown that *in fire* the buckling length of columns in *braced frames* is reduced to between 0.5 and 0.7 times the column length at room temperature, depending on the boundary conditions [69], see Fig. 5.3.

There is an increasing tendency toward assessing the fire resistance of individual members or sub-assembles by analytical fire engineering. The Eurocodes on structural fire design define three levels of assessments:
- level 1: Design Tables and Diagrams
- level 2: Simple Calculation Methods
- level 3: General Calculation Procedures

"General Calculation Procedures" is the most sophisticated level. Such calculation procedures include a complete thermal and mechanical analysis of the structure and use the values for the material properties given in the Eurocodes. General calculation methods enable real boundary conditions to be considered and take account of the influence of non-uniform temperature distribution over the section and therefore lead to more realistic failure times and, consequently, to the most competitive design. However, the handling of the necessary computer programs is quite time consuming and requires expert knowledge. For practising engineers and architects not accustomed to handling specialised computer programs, "Simple Calculation Methods" have been developed, which lead to a comprehensive design, but are limited in application range. They use conventional calculation procedures and normally provide adequate accuracy.

"Design Tables and Diagrams", which provide solutions on the safe side and allow fast design for restricted application ranges, form the lowest level of assessment.
In the following chapters, emphasis is put on the simple calculation procedures.

5.3 DESIGNING UNFILLED SHS COLUMNS FOR FIRE RESISTANCE

5.3.1 Basic principles

The calculation of the fire resistance of unfilled SHS columns comprises two steps:
- the determination of the temperature at which the column fails, the so called "critical steel temperature"; this is the mechanical response
- the determination of the temperature development in the bare or protected steel section; this is the thermal response.

Both assume a uniform temperature distribution across the cross section and along the length of the steel member. Combining the two calculation steps gives the number of minutes after which failure of the column would occur if exposed to standard fire conditions. This amount of time is the fire resistance of the column, see Fig. 5.4.

5.3.2 The mechanical response

The simple calculation rules for the critical temperature of steel columns discussed hereafter, hold for classes 1, 2 and 3 cross sections only (as defined in Eurocode 3, part 1-1 [12] and can be applied both to protected and unprotected columns. For columns with a class 4 cross section, a default value for the critical

temperature of 350°C is to be used.
The critical temperature of an axially loaded steel column depends on the ratio between the load which is present during a fire and the column minimum collapse load at room temperature. This ratio is called the *degree of utilisation* (μ). For an axially loaded column:

$$\mu = \frac{N_{fi}}{\chi_{min} \cdot N_{nc}} \qquad (5.1)$$

with:
N_{fi} : axial force in the fire situation
N_{nc} : compression resistance of gross cross section at room temperature
χ_{min} : minimum buckling coefficient

According to Eurocodes, in the fire situation generally the unfactored loads (being only about 60% of the design load for normal conditions of use) need to be taken into account. Also the partial safety factors, both for material properties and actions, are taken equal to unity.

The collapse load at room temperature is based on the column dimensions using the buckling curve "c" from Eurocode 3, irrespective of the type of SHS or its material.

The relation between the critical steel temperature and the modified degree of utilisation (c·μ) is represented by Fig. 5.5, where c is an adaptation factor used to correct model simplifications. Eurocode 3, Part 1.2 states that for columns under both axial and eccentric loading, c = 1.2. In theory, the modified degree of utilisation (c·μ) can vary between 1 and 0 and a high degree of utilisation corresponds to a low critical temperature. (Theoretically, c·μ = 1 implies that the column is about to fail under room temperature conditions.)

In the case of an eccentrically loaded column it is also possible to define an equivalent "degree of utilisation" using an interaction curve which describes the critical combinations of normal force and applied moment:

$$\mu = \frac{N_{fi}}{\chi_{min} \cdot N_{nc}} + \frac{k \cdot M_{fi}}{M_{p\ell}} \leq 1 \qquad (5.2)$$

with:
M_{fi} : the maximum applied end-moment in the fire situation
k : a reduction factor according to Eurocode 3, Part 1.1
$M_{p\ell}$: plastic moment capacity of cross section at room temperature

In effect, for the same degree of utilisation the combined effect of a normal force and a moment on the critical temperature of an eccentrically loaded steel column is equal to that of an equivalent axial force (N_{eq}):

$$N_{eq} = N_{fi} + \chi_{min} \cdot N_{nc} \cdot \frac{k \cdot M_{fi}}{M_{p\ell}} \qquad (5.3)$$

Provided that a column has been designed to satisfy the room temperature requirements of Eurocode 4, Part 1 [13], a minimum default value of 510°C can be taken as the critical temperature of a steel column without any further analysis.

5.3.3 The thermal response

For unprotected steel sections it can be shown that - for standard fire exposure - the temperature development of a steel section depends only on the relative geometry of the profile. This effect is taken into account by means of the shape sactor, A_m/V, where:

A_m = exposed surface area of the member per unit length [m^2/m]
V = volume of the member per unit length [m^3/m]

This is the same as the exposed steel perimeter/steel cross section

The curves presented in Fig. 5.6 illustrate the effect of the shape factor on the temperature development of an unprotected steel section when exposed to standard fire conditions. For commonly used I-sections, shape factors are within a range of, say, 50 to 400 m^{-1}. For SHS profiles exposed to heat from all sides, the shape factor may be approximated by:

A_m/V = Perimeter/(Perimeter x thickness) = 1/t m^{-1}

with: t = thickness of the steel hollow section.

For a practical range of the SHS thickness of 20 to 2.5 mm, this also leads to shape factors varying between 50 and 400 m^{-1}. However, for equivalent cross sections hollow sections have a A_m/V ratio which is about 60%

of that of comparable open sections.

For any given critical steel temperature θ_s, the fire resistance of an unprotected steel element - assuming standard fire conditions - depends only on its shape factor as illustrated in Fig. 5.7. In many practical situations, the critical temperature of a steel member will be approximately 550°C, so the time to reach 550°C may be taken as a reasonable approximation of its fire resistance. This figure shows that an unprotected steel member with a shape factor smaller than approximately 40 m^{-1} may have a fire resistance of 30 minutes or beyond.
If external fire insulation is provided, the steel temperature development depends not only on the shape factor, but also on the type and thickness of the insulation material. It is possible to construct charts which show how steel temperature varies with insulation thickness (d_i), shape factor (A_m/V) and time for a given insulation material. For more detailed information, see [4].

5.4 DESIGNING CONCRETE FILLED SHS COLUMNS FOR FIRE RESISTANCE

5.4.1 Unprotected columns - thermal and mechanical response

Because of their different locations in the cross section, the various components of a concrete filled SHS column will each have different time dependent strength reduction characteristics. The unprotected, directly exposed steel shell will be rapidly heated and will show a significant strength reduction within a short time.

The concrete core with its high massivity and low thermal conductivity will, for some time, maintain a significantly high proportion of its strength, mostly in the core area rather than near the surface.
Reinforcement, if used, is normally placed near the surface, but is protected by typically 20 - 50 mm of concrete, for this reason, it will have a retarded strength reduction. Fig. 5.8 demonstrates this characteristic behaviour and describes the fire performance of concrete filled SHS columns.

The load bearing capacity R of a cross section is the sum of the load bearing capacities of each of its components r_j. Under fire conditions, all component capacities are dependent on the fire endurance time t.

$$R(t) = \Sigma r_j(t) \qquad (5.4)$$

In room temperature design, the steel shell is likely to be the dominant load bearing component because of the high strength of the steel and the location of the profile. However, after a fire time t_1, only a small percentage of the original load bearing capacity of the steel shell can still be activated. This means that in case of fire the main part of the load carried by the steel section will be redistributed to the concrete core, which loses strength and stiffness more slowly than the steel section. Therefore:
- the load bearing capacity of the steel shell should be minimised, which means thin shell thickness and low steel grade;
- the load bearing capacity of the concrete core should be optimised, which means higher concrete strength and reinforcement.

Since the strength reduction of the components is directly affected by the relative heating characteristic of the cross section, a minimum column cross sectional dimension is often necessary to fulfil a required fire resistance.

With increasing temperature, strength and Young's modulus decrease. Thus, load bearing capacity of a structural member decreases with time, while its deformation increases. In practical fire design, the influence of the column slenderness also has to be taken into account.

5.4.2 Assessment methods for unprotected columns

Levels of assessment
As already explained in section 5.2.3, in the Eurocodes, assessment on three different levels is given. This chapter deals with design information on levels 1 and 2, i.e. tabulated data and simple calculation models. For more general calculation models, refer to [4].

Level 1 design tables and diagrams
Using Table 5.2, unprotected concrete filled hollow section columns may be classified according to:
- the degree of utilisation (μ)
- the minimum cross section size (b or d)
- the amount of reinforcement (%)
  ($p_s = [A_s/(A_c + A_s)] \cdot 100$)

- the minimum axis distance of the reinforcement bars (d_r)

The degree of utilisation μ is given by: (see section 5.3.2)

$\mu = N_{fi} / N_d$

with:
N_{fi} = axial force in the fire situation
N_d = the design resistance at room temperature

N_d is calculated according to the room temperature procedures of EC4, part 1. However, the following additional limitations apply:
- Irrespective of the actual steel grade, the yield strength of the SHS for calculations is limited to a maximum of 235 N/mm^2
- The wall thickness of the steel; is limited to a maximum of 1/25 of the main cross sectional dimension
- Reinforcement ratios higher than 3% are not taken into account.

Level 2: simple calculation methods
A level 2 modified computer program has been developed and verified by CIDECT to model the fire performance of concrete filled SHS columns [70,71,72]. This forms the basis of the Eurocode buckling curves for concrete filled SHS columns at elevated temperatures: design charts have been developed in which, for a standard fire exposure of 30, 60, 90 and 120 minutes, the collapse load $N_{cr,\theta}$ of concrete filled SHS columns is given as a function of the buckling length $L_{cr\theta}$. A typical chart is illustrated in Fig. 5.9 from which any combination of applied load and buckling length the relevant fire resistance class can be easily determined.

For a given buckling length and loading, the fire resistance of concrete filled SHS columns depends mainly on the cross sectional dimensions, the concrete quality and the reinforcement, if any. By a proper choice of these parameters, practically any fire resistance can be achieved. If no reinforcement is used and the column is under its maximum unfactored load at room temperature conditions, a fire resistance of 30 minutes can normally be achieved; 60 minutes, however, is not attainable unless the load level is significantly decreased. This is why the design charts focus on fire resistances of 60 minutes and more and only reinforced SHS columns are taken into account.

Small drain holes (10 to 15 mm dia.) are required in the walls of the SHS, usually in pairs. Such holes must be provided for each storey length at each floor level, with a maximum distance of 5.0 m. between pairs. They must be placed between 100 and 120 mm from each column end. Those holes are intended to prevent the bursting of the column under steam pressure from the heating of entrapped water in the enclosed concrete.
Besides the standard SHS cross sections, a variety of different cross section designs has also been developed in the past and successfully used for building projects. They are all based either on combinations of hollow sections (tube inside tube) or on combinations of hollow sections with other steel profiles. The advantages of such special cross section types are an increased load bearing capacity without the need to increase the outer cross sectional dimensions, or reduced dimensions for a given load capacity.
To fulfil architectural requirements, special steels, such as weathering steel, can also be used for the SHS of the columns.
Careful design of the top and bottom of a single column or at the joints of a continuous column is necessary to ensure that the loading is introduced into the composite cross section in a proper way.

5.4.3 Externally protected concrete filled SHS columns

If an extended fire resistance is desired, in combination with a high load level and/or a minimised column cross section, it may be necessary to apply conventional external protection to a concrete filled SHS column.

5.5 DESIGNING WATER FILLED SHS COLUMNS FOR FIRE RESISTANCE

5.5.1 Basic principles

Water filling using natural circulation provides a safe and reliable fire protection method for SHS columns, if two conditions are satisfied [73].
- the system is self activating in fire
- the system is self controlling.

In a properly designed system, the natural circulation will be activated when the columns are locally heated by a fire. The density of warm water is lower than that of cold water, which produces the pressure differentials

that activate the natural circulation. The effect will be intensified when localised boiling commences and steam is formed. As the fire develops, the rate of steam production will also increase, thus forcing the cooling effect obtained by naturally-activated circulation.
The following methods of permanent water filling are available:

Unreplenished columns
Simply filling a column with water, with no provision for replacing any water lost through steam production, will lead to an increased, but limited fire resistance compared to that of the empty column. In multi-storey columns, the fire resistance may be increased by externally protecting the top storey length and using it as a reservoir for the lower storeys. Heavy steam production may lead to an additional critical loss of water. Therefore, this column type should be used only for lower fire resistance requirements, up to, say, 60 minutes.

Columns with external pipe
This system has a connecting down pipe between the bottom and top of the columns. The lighter, upward flowing water-steam mixture must be separated at the top, so that the water can return down through the pipe to the bottom. In this manner, an external naturally forced circulation will be activated. In addition, the pipe can be connected with a water storage tank at the top of the building to replace the water lost from steam production and possibly act as a common water/steam separating chamber. A group of individual columns can be connected at their bottom to a shared connecting pipe as well as with a connecting pipe at the top. For such a group of columns, only one down pipe is necessary, connecting top and bottom of the whole group, see Fig. 5.10a.

Columns with internal pipe
In this system, an internal down tube is used within each column to provide a supply of cool water to the bottom of each column. This promotes the internal, naturally activated circulation of the upward flowing water-steam mixture and the down flowing water after steam separation. Thus, each column acts as an individual member without any connection to the other columns.

To minimise the number of water storage tanks, the tops of several columns can be connected by a common pipe leading to one storage tank for the whole group, see Fig. 5.10b.

Mixed systems
The above mentioned systems can be mixed within a building and they can be connected to act as a mixed integrated system. This can be advantageous for structures containing not only columns, but also water filled diagonals for bracing, etc.

In the naturally circulating systems described above, a minimum declination of about 45°is recommended.
It is not recommendable to use any electro-mechanical installation, such as pumps, acting against the naturally produced circulation. This may lead to a failure of the cooling system and thus to collapse of the water filled structure.

5.5.2 Assessment methods

A careful design is necessary to ensure the positive behaviour of a water filled SHS column system. Two main criteria must be fulfilled to ensure the cooling effect:

- natural circulation of the water is maintained
- water losses due to steam production are replaced.

The mass of the water cooled steel structure as well as the water within the system can be taken into account when calculating the time of commencement of boiling. The loss of water mass by evaporation has to be estimated only for the time difference between the start of boiling and the required fire resistance time. For the characteristic thermal behaviour, refer to Fig. 5.11.

The maximum temperature reached by the steel can be estimated from the boiling temperature of the water filling. The boiling temperature itself depends on the hydraulic water pressure, i.e. the static head. In addition, there will be a temperature gradient across the wall of the hollow section, which will lead to a slight increase of the temperature of the steel surface directly exposed to the fire. However, the maximum external steel surface temperature will normally not reach a value high enough to significantly affect the mechanical properties of the steel.

5.6 CONNECTIONS AND FIRE RESISTANCE

5.6.1 Unfilled SHS columns

Normally, the connections of both protected and unprotected steel structures have a lower local shape factor than the adjacent members and will therefore attain lower steel temperatures. Since neither in practice nor during fire tests has failure been initiated in a structure or a test element by the behaviour of connections, these can generally be designed using normal room temperature design codes. However, when bolted connections are used for insulated steel members, care must be taken to ensure that the bolt heads and nuts are as well protected as the cleat. Normally, this will lead to a local increase of insulation thickness.

5.6.2 Concrete filled SHS columns

Generally, concrete filled hollow section columns fulfil fire protection requirements without further precautions. For economic reasons this construction method needs easily erectable connections between the columns and beams, which preferably should correspond to those of pure steel construction. Suitably designed connections will be fire resistant and can even improve the fire performance of the whole structure. However, the loads have to be transferred from the beams to the columns in such a way that all structural components - structural steel, reinforcement and concrete - contribute to the load bearing capacity according to their strength.
A well constructed column/beam-connection should:

- enable simple installation
- optimise prefabrication of columns and beams
- ensure adequate fire resistance without disturbing any external protective cladding.

A typical example with a through plate is shown in Fig. 5.12.

Table 5.1 Variations in required fire resistance

Type of building	Requirements	Fire class
One storey	None or low	Possibly up to R30
2 or 3 storeys	None up to medium	Possibly up to R30
More than 3 storeys	Medium	R60 to R120
Tall buildings	High	R90 and more

Table 5.2 Minimum cross-sectional dimensions, reinforcement ratios and axis distances of the re-bars for fire resistance classification for various degrees of utilisation μ.

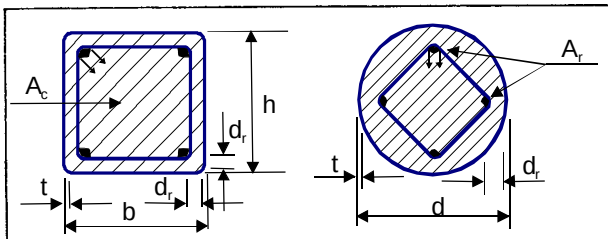

Steel section
b/t > 25
or
d/t > 25

	Fire Resistance Class				
	R30	R60	R90	R120	R180
Minimum cross-sectional dimensions for μ = **0.3**					
Minimum width (b) or diameter (d)	160	200	220	260	400
Minimum % of reinforcement (p_r)	0.0	1.5	3.0	6.0	6.0
Minimum depth of re-bar centre (d_r)	–	30	40	50	60
Minimum cross-sectional dimensions for μ = **0.5**					
Minimum width (b) or diameter (d)	260	260	400	450	500
Minimum % of reinforcement (p_r)	0.0	3.0	6.0	6.0	6.0
Minimum depth of re-bar centre (d_r)	–	30	40	50	60
Minimum cross sectional dimensions for μ = **0.7**					
Minimum width (b) or diameter (d)	260	450	500	–	–
Minimum % of reinforcement (p_r)	1.5	6.0	6.0	–	–
Minimum depth of re-bar centre (d_r)	25	30	40	–	–

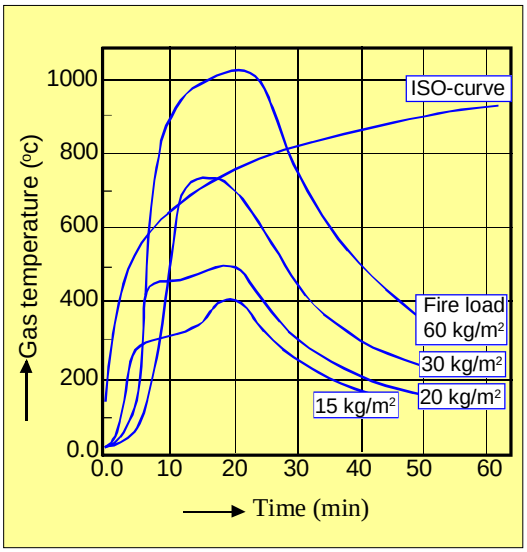

Fig. 5.1 Natural fire curves and ISO curve

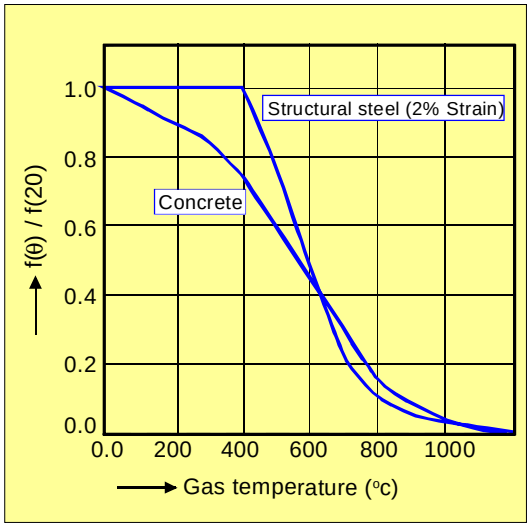

Fig. 5.2 Schematic material strength reduction for structural steel and concrete according to [11,12,13]

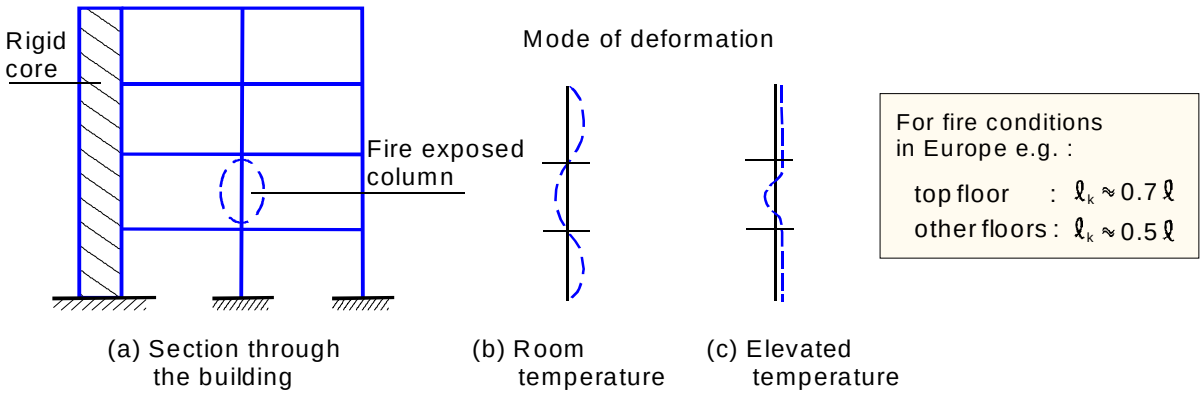

Fig. 5.3 Schematic structural behaviour of columns in braced frames

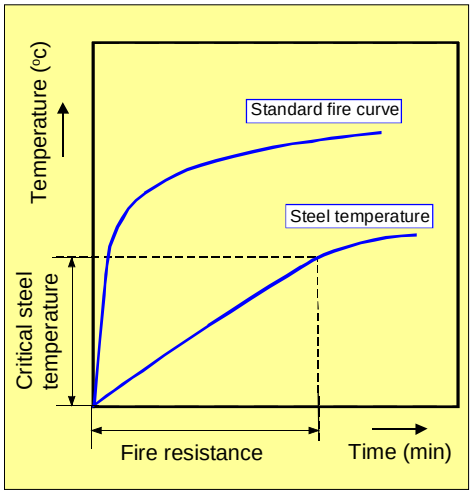

Fig. 5.4 Calculation scheme for the fire resistance of steel elements

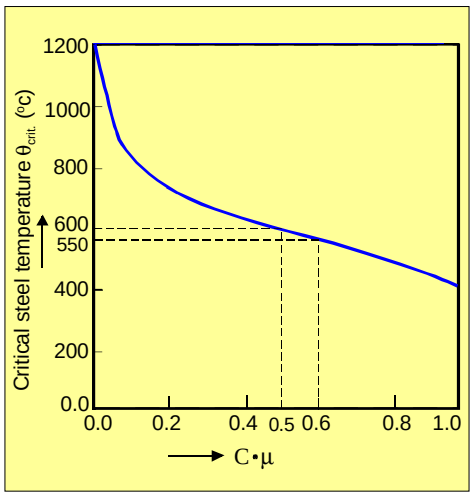

Fig. 5.5 Critical steel temperature as a function of the modified degree of utilisation (c·μ)

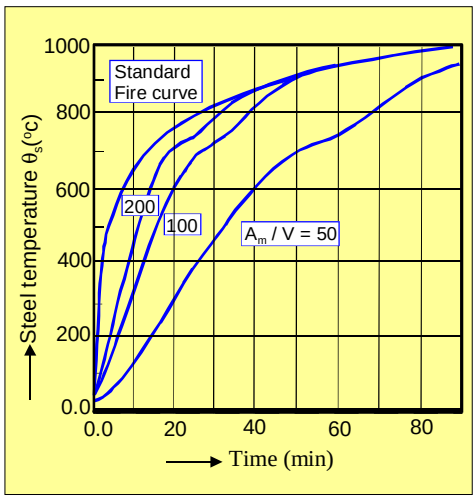

Fig. 5.6 Calculated temperature development in an unprotected steel section as a function of the shape factor

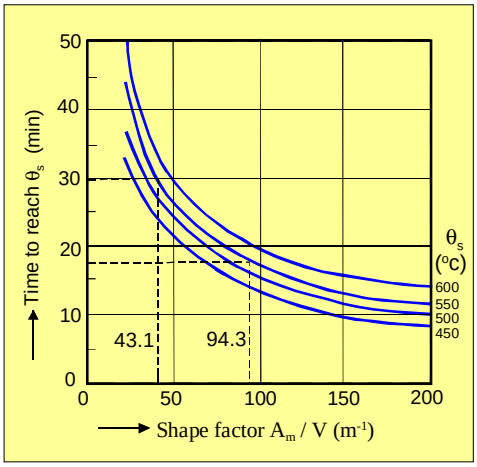

Fig. 5.7 Amount of time for an unprotected steel section to reach a given mean temperature under standard conditions as a function of the shape factor

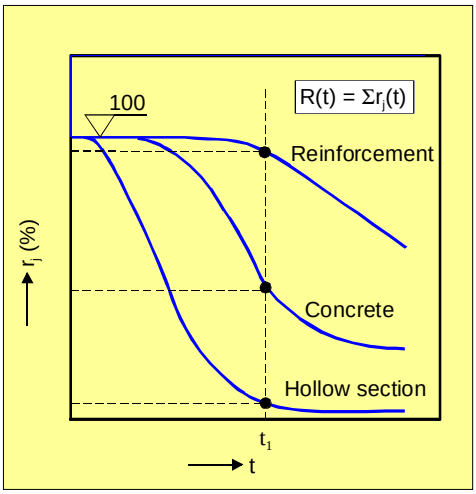

Fig. 5.8 Typical strength reduction characteristics of the various components of a concrete filled SHS column

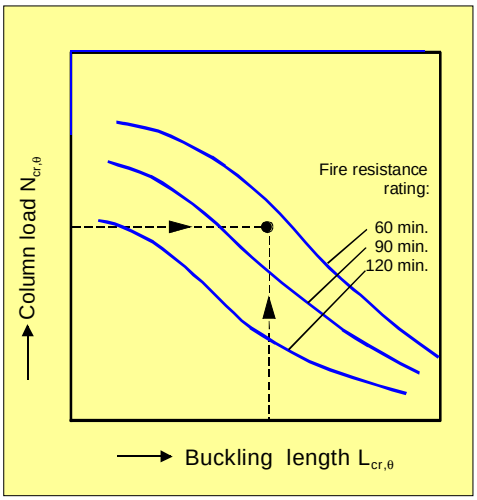

Fig. 5.9 Buckling curves for different fire resistance classes (qualitative)

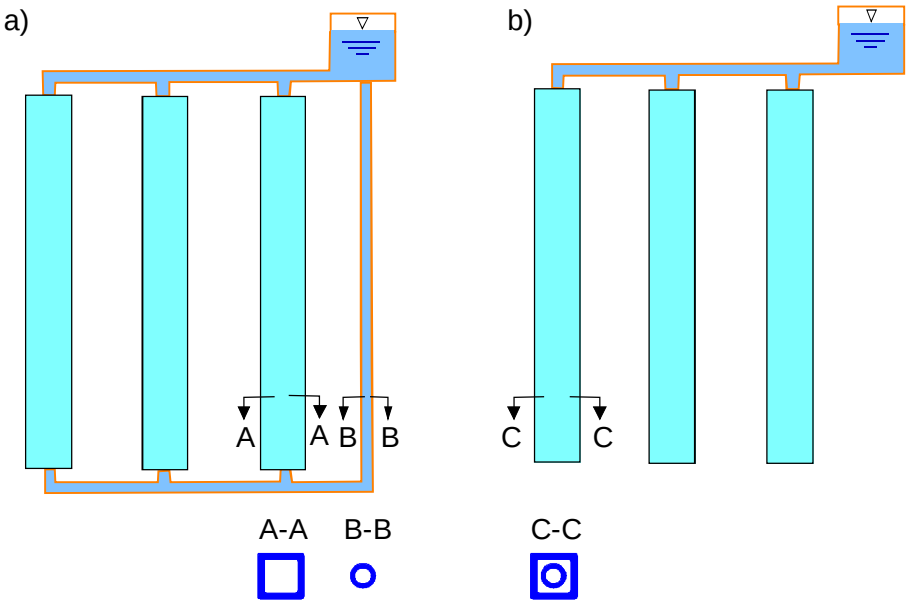

Fig. 5.10 Options for columns with external and internal pipes (CEP versus CIP)

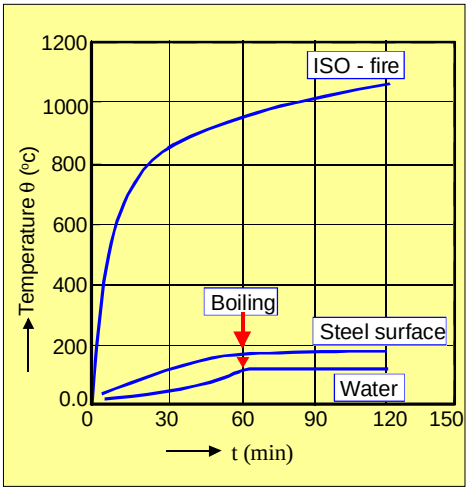

Fig. 5.11 Typical temperature development in a water filled SHS column, exposed to standard fire conditions

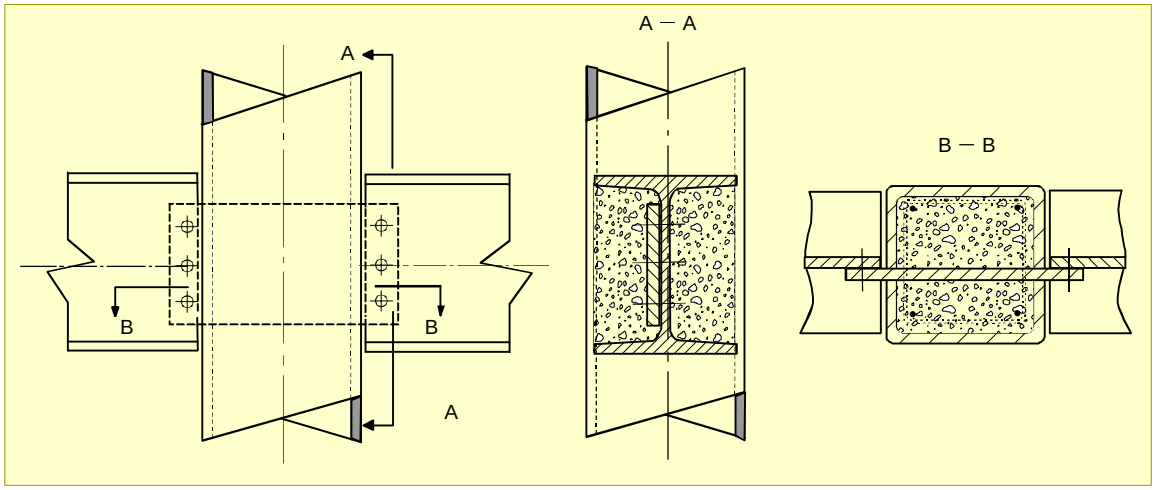

Fig. 5.12 Beam to column connection with a cleat passed through the column.

6. HOLLOW SECTION TRUSSES

Various types of trusses are used in practice, see Fig. 6.1. Trusses made of hollow sections should be designed in such a way that the number of joints and thus fabrication is minimised. This means that due to the lower number of joints a Warren type truss with K-joints (Fig. 6.1a) is preferred to a Pratt type truss with N-joints (Fig. 6.1b).

Vierendeel girders (Fig. 6.1c) are mainly used in those cases where architectural or functional requirements require that no diagonals are used.

The girders are characterised by their length ℓ, depth h, geometry and the distance between the joints.
The depth is normally related to the span, being about 1/10 to 1/16 ℓ. Considering total economy of a hall with all costs, a depth of 1/15 ℓ is a common choice. Whenever feasible, the joints are located at the load application points, e.g. at purlin locations.

Depending on the type of truss, various types of joints are used (Fig. 6.2), i.e. X, T, Y, N, K or KT.

Although here the designation X,T,Y, etc. is related to the configuration it is the loading which determines if a joint behaves like for example a T-joint. A K-joint with brace loadings acting in the same sense thus behaves as a T-joint and has therefore to be checked as a T-joint.

The symbols used for the parameters to formulate the geometry are shown in Fig. 6.3.

In designing hollow section trusses it is important that the designer considers the joint behaviour right from the beginning. Designing members of a truss based on member loads only may result in undesirable stiffening of joints afterwards. This does not mean that the joints have to be designed in detail in the conceptual design phase. It only means that chord and brace members have to be chosen in such a way that the main governing joint parameters provide an adequate joint strength and an economical fabrication.

Since the design is always a compromise between various requirements, such as static strength, stability, economy in fabrication and maintenance, which are sometimes in conflict with each other, the designer should be aware of the implications of a particular choice.

The following guidance is given to arrive at optimum design:

- Lattice structures can usually be designed assuming pin jointed members. Secondary bending moments due to the actual joint stiffness can be neglected for static design if the joints have sufficient rotation capacity. This can be achieved by limiting the wall slenderness of certain members, particularly the compression members, which is the basis for some of the geometric limits of validity. This will be the case if the joint parameters are within the range recommended in the IIW/CIDECT recommendations (which have also been adopted for Eurocode 3 [12]).

- It is common practice to design the members with the centre lines noding. However,for ease of fabrication it is sometimes required to have a certain noding eccentricity. If this eccentricity is kept within the limits indicated in Fig. 6.4, the resulting bending moments can be neglected for joint design and for chord members loaded in tension.
  Chord members loaded in compression, however, should always be checked for the bending effects of noding eccentricity (i.e. designed as beam-columns, with all of the moment due to noding eccentricity distributed to the chord sections).

- Gap joints (Fig. 6.5) are preferred to partial overlap joints, since the fabrication is easier with regard to end cutting, fitting and welding. However, fully overlapped joints (Fig. 6.4d) generally provide better joint strength than gap joints with similar fabrication.

  The gap g is defined as the distance measured along the length of the connecting face of the chord, between the toes of the adjacent brace members (ignoring welds). The percentage overlap O_v, defined in Fig. 6.5, is such that the dimension p pertains to the overlapping brace. In good designs a minimum gap should be provided such that $g \geq t_1 + t_2$, so that the welds do not overlap each other. On the other

hand, in overlap joints the overlap should be at least $O_v \geq 25\%$.

- In common lattice structures (e.g. trusses), about 50% of the material weight is used for the chords in compression, roughly 30% for the chord in tension and about 20% for the web members or braces. This means that with respect to material weight, the chords in compression should likely be optimised to result in thin walled sections. However, for corrosion protection (painting), the outer surface area should be minimised.

  Furthermore, joint strength increases with decreasing chord diameter or width to thickness ratio. As a result, the final diameter- (or width-) to-thickness ratio for the chord in compression will be a compromise between joint strength and buckling strength of the member and relatively stocky sections will usually be chosen. For the chord in tension, the diameter- or width-to-thickness ratio should be chosen to be as small as possible.

- Since the joint strength efficiency (i.e. joint strength divided by the brace yield load $A_i \cdot f_y$) increases with increasing chord to brace thickness t_o/t_i this ratio should be chosen to be as high as possible, preferably above 2. Furthermore, the weld volume required for a thin walled brace is smaller than that for a thick walled brace with the same cross section, if the welds are to develop the wall capacity of the connected member.

-Since the joint strength also depends on the yield stress ratio between chord and brace, the use of higher strength steel for chords (if available and practical) may offer economical possibilities. In principle, multiplanar trusses can be approached in a similar way as uniplanar trusses, although the depth can usually be smaller, between 1/15 and 1/18 ℓ.

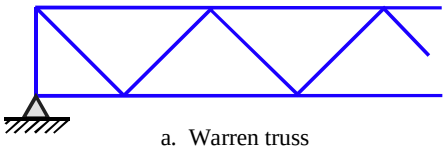

a. Warren truss

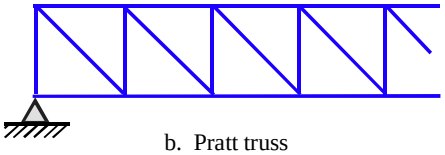

b. Pratt truss

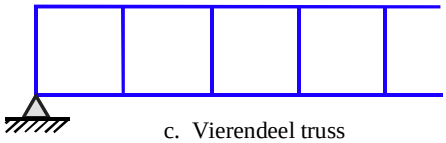

c. Vierendeel truss

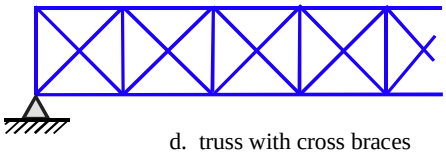

d. truss with cross braces

Fig. 6.1 Various types of trusses

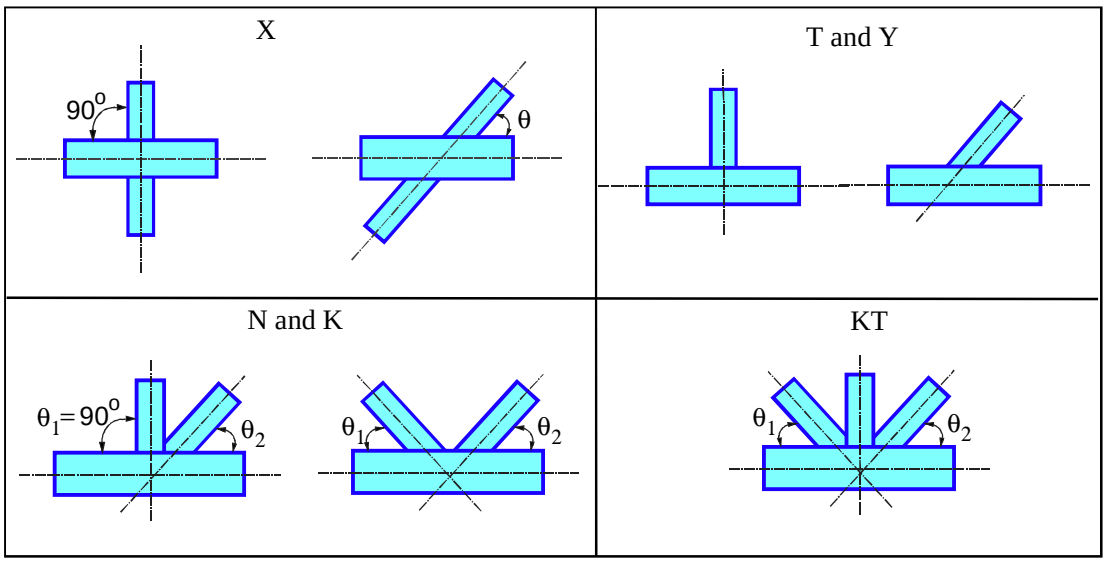

Fig. 6.2 Basic types of joints

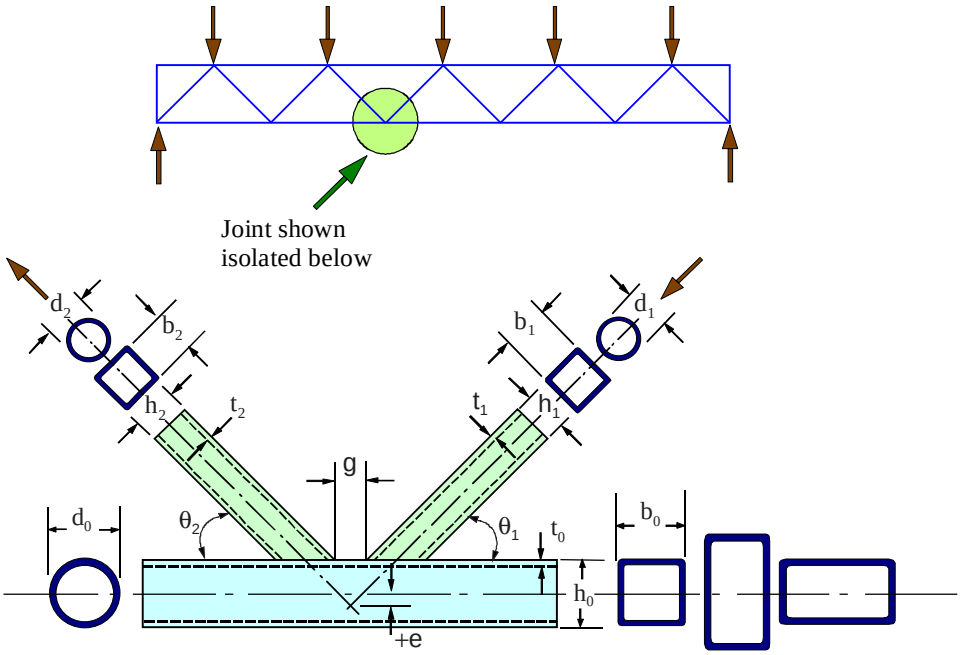

Fig 6.3 Symbols used for K gap joints

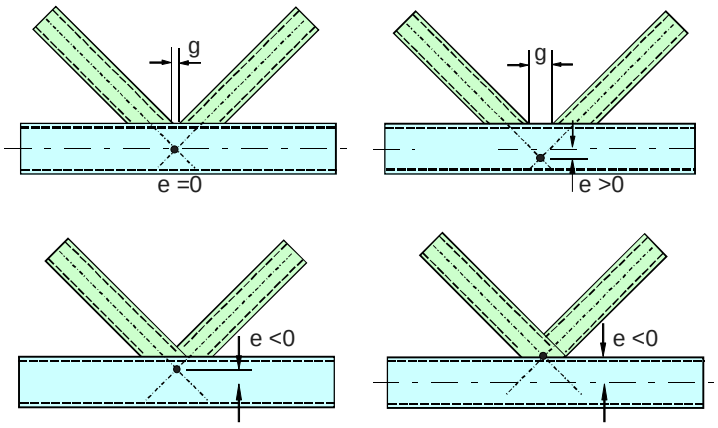

$$-0.55 \leq \frac{e}{h_0} \quad \text{or} \quad \frac{e}{d_0} \leq 0.25$$

Fig 6.4 Noding eccentricity

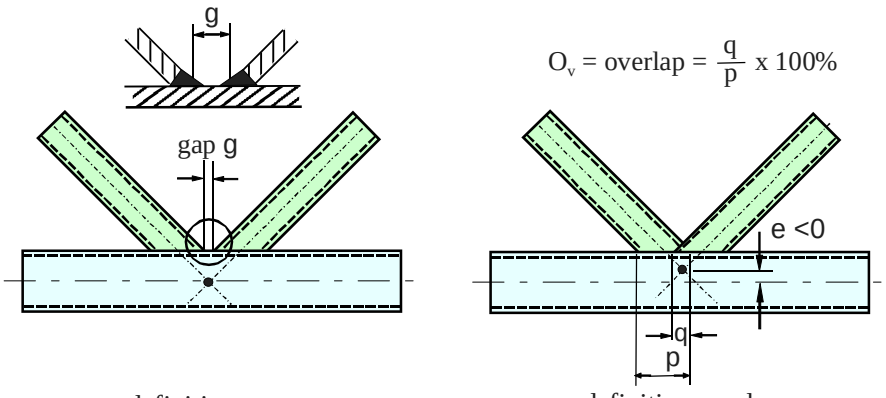

Fig 6.5 Gap and overlap

7. BEHAVIOUR OF CONNECTIONS

For a proper understanding of the behaviour of tubular joints or welded connections between hollow sections it is important to consider the load path, the internal stiffness distribution in a connection and the material properties.

7.1 GENERAL INTRODUCTION

7.1.1 Load path

The load path shows what parts the loads have to pass and where failure may occur. For example, Fig. 7.1 shows a welded connection between plates and a hollow section. The load has to pass the following parts:

- plate
- weld
- hollow section face (through thickness)
- hollow section side wall

Thus, in principle failures can occur in these parts. If the width of the plate b_1 is small compared to b_o, several types of failure can occur in the chord face. This will be discussed later.

7.1.2 Internal stiffness distribution

The stiffness distribution in the joint determines the elastic stress distribution. Here, the plate to RHS chord connection of Fig. 7.1 will be considered again.

Consider the stiffness of the plate and the connected face of the hollow section.

a. *Plate*
The plate end remains straight if loaded by a uniform loading q per unit length. The deformation is determined by the plate stiffness for axial stresses, which is high.

b. *Hollow section face*
First consider a unit load q_1 at a small unit length at the plate sides (Fig. 7.2b).

Here, the load q_1 can flow directly into the hollow section side wall. Thus, here the deformation is determined by the stiffness of the hollow section side wall for axial stresses.

Now consider a unit load q_2 at the centre of the hollow section face (Fig.7.2c). The load has to be transmitted to the side walls by bending. Thus, the deformation is determined by the bending stiffness of the top face of the hollow section and the axial stiffness of the hollow section side walls.

Consequently, the stiffness for a q_2 load is considerably smaller than for a q_1 load.
This is graphically shown in Fig. 7.3.
For loads on the top face at locations between q_1 and q_2 the behaviour is in between that for q_1 and q_2.

The resulting elastic stress pattern in the plate can now be determined in two ways.

1. *Consider the deformations under a uniform stress:*
For a uniform stress, the plate and hollow section faces do not have the same deformed shape. To ensure that the plate and the hollow section face have the same deformation, the stresses at the centre should be lower and at the sides higher. Thus, additional stresses have to be added, as shown in Fig. 7.4b, which increase the stresses at the sides and reduce the stresses at the plate centre. Thus the highest stresses occur at the stiff parts.

As shown in Fig. 7.4b, the plate remains almost straight due to the much higher axial stiffness of the plate than the bending stiffness of the top face, thus the plate could have been assumed as being nearly rigid compared with the stiffness of the hollow section top face.

2. *Assume rigid plate*
If the plate is assumed to be rigid, the stress pattern can be directly determined with Fig. 7.3. For a deformation δ_1, the stress for q_1 is much higher than for q_2, resulting in the stress pattern of Fig. 7.4c.

From this evaluation it is clear that the non-uniformity largely depends on the b_o/t_o ratio. If b_o/t_o is very small, approaching a solid profile, the stress distribution is uniform if contraction is not considered. If b_o/t_o is large, it may even be that the stress at the centre has the opposite sign of that at the sides.

7.1.3 Effect of material properties

In Fig. 7.5 the σ-ε diagram of two materials is given:
a: steel with a yield strength f_y and a strain hardening part with an ultimate tensile strength f_u.
b: A fictitious steel with no deformation capacity at all, i.e.: it fails immediately after reaching the maximum stress $f_{u,b}$.

Suppose that failure of the plate to RHS connection is governed by the failure of the plate just before the weld. This means that the stress pattern in the plate (Fig. 7.4c) has to be considered in relation with the material behaviour.
The stress pattern in Fig. 7.4c is based on an elastic material behaviour, thus equivalent to material b. As soon as the maximum stress at the side (1) reaches the ultimate stress $f_{u,b}$, the material will start cracking.

If the material "a" of Fig. 7.5 had been used, the maximum stress would first reach the yield stress f_y. With increasing load the material at location (1) yields i.e. the stress remains constant f_y and the strain ε increases. With increasing load, the material just besides location (1) in Fig. 7.4c will yield, etc. At a certain strain, the material at location (1) will reach the strain hardening part in the σ-ε diagram of Fig. 7.5. After further increase of the loading, the stress will increase until the ultimate stress f_u, after which the "actual stress" will still increase, although the "engineering stress", based on the original cross section will decrease. At a certain strain ε_u cracking will occur at location (1).

Sometimes cracking occurs at the very stiff locations and still the loading can be increased due to a more uniform stress distribution in the remaining cross section.

The above shows the importance of yielding for the load capacity of hollow section joints.

Another aspect which is also extremely important for static design is the deformation capacity. Similar to members, the deformation capacity determines if secondary moments can be redistributed in structures.

For example in a truss, secondary bending moments exist due to the joint stiffness of the welded connections. However, these moments are not necessary for the load transfer. If the truss is loaded up to failure and the connection strength is governing compared to the member strength, yielding occurs at a certain moment due to the combination of axial loading and the (secondary) bending moments. If the deformation capacity is sufficient, the axial forces in the members will increase with a decrease of the (secondary) bending moments due to plastic rotation of the connection. In the failure stage, the secondary bending moments may have totally disappeared.

7.1.4 Failure modes

Following the load path (see 7.1.1) shows the possible failure locations, whereas the stiffness distribution (7.1.2) in combination with the material behaviour (7.1.3) determines the failure mode for the various locations. The lowest failure load for all these failure modes gives the governing strength. Now the possible failure modes for the plate to RHS connection of Fig. 7.1 will be considered.

1. *Plate*
Fig. 7.6a shows the possible stress distribution in the plate after yielding and after reaching the ultimate strain at the sides (location 1). If the chord width-to-thickness ratio b_o/t_o is low and the material has sufficient ductility, the yield capacity of the plate can be reached. In most cases the capacity is lower.

2. *Welds*
If the strength of the fillet welds (Fig. 7.6b) is lower than that of the plate, the welds may fail. If the plastic deformation occurs in the welds only, the total deformation for the joint is small, resulting in a connection with no deformation capacity (generally not allowed).
Therefore it is recommended that the welds should preferably be designed to be stronger than the connected elements.
Only for very low loaded structures, e.g. where members have been selected based on aesthetical aspects, are smaller welds allowed provided the secondary effects and the effective perimeter is considered [37,74].

3. *Chord face*
The loading and thus the stresses have to pass via the top face to the side walls. Especially for thick material, cracking can occur due to Mn.S inclusions, called lamellar tearing (Fig. 7.6c). To avoid this material problem, material with good Through Thickness Properties (TTP) should be used, i.e. steels with low sulphur contents.

If $b_1 < b_o$, other failure modes can be obtained for the chord, i.e.: top face plastification or chord punching shear.
For the connection with $b_1 = b_o$ the top face is held in position by the plate and the stiff connection to the side wall. Therefore, top face yielding with a yield line pattern can only occur after excessive yielding of the plate at the sides and/or excessive yielding of the hollow section side walls under the plate.

Punching shear of the hollow section face can only occur if the plate width b_1 is smaller than b_o-2t_o (see Fig. 7.6d).

4. *Chord side wall*
All the stresses have to be transmitted through the side walls over a limited width, thus this may be a critical failure mode (chord side wall yielding shown in Fig. 7.6e).
If the loading is compression instead of tension, the stability of the side wall may be critical.

7.2 GENERAL FAILURE CRITERIA

In general, the static strength can be characterized by various criteria, i.e.:

- ultimate load resistance
- deformation limit
- (visually observed) crack initiation

The ultimate load capacity is well defined for those joints which show a maximum in the load deformation diagram, e.g. for some joints loaded in compression. Other joints show an increasing load capacity with increasing deformation such that the maximum is obtained at excessive deformation.

To avoid two checks having to be made, i.e. one for ultimate strength and one for serviceability, in recent work a deformation limit has been defined for the ultimate load capacity. This limit being, $0.03d_o$ or $0.03b_o$, as shown in Fig. 7.7, has been based on the fact that the deformation at serviceability load should not be governing and that crack initiation should not occur at serviceability either [75]. This deformation is taken as the local indentation of the chord wall at the connection of the brace to the chord.

Thus, the ultimate load capacity is defined by the criterion that is first met, i.e. the maximum capacity or the deformation limit for ultimate loading.

For serviceability an arbitrary limit of $0.01\ d_o$ or $0.01\ b_o$ is used. This 1% limit is the same as the out-of-roundness limit and has shown to give not unacceptable deformations.
However, it must be mentioned that most formulae in the codes have been developed based on ultimate load or end of test data and later on checked for the 1% d_0 or b_0 rule for serviceability.

7.3 GENERAL FAILURE MODES

For the plate to hollow section chord in Fig. 7.1 it has been shown that various failure modes can occur. Hollow section joints also show, depending on the loading, joint type and geometrical parameters, various modes of failure.
As an example, in Fig. 7.8 various failure modes are shown for a K-joint of rectangular hollow sections, i.e.:

a) plastification of the chord face
b) chord punching shear
c) brace failure (effective width)
d) chord shear failure
e) local buckling of the compression brace
f) local buckling of the chord

If the welds are not strong enough, weld failure can also occur or if the material does not have sufficient through thickness properties (TTP) lamellar tearing is possible.

The failure modes and associated analytical models for determination of the strength formulae are described in detail in the following chapters.

7.4 JOINT PARAMETERS

The geometry of a particular joint is generally defined by the dimensions given in Fig. 6.3 and by the joint parameters α, β, γ, τ and g' shown in Fig. 7.9. Originally the parameters were related to the radius of a section; nowadays the diameter, width or depth is used which explains the α and γ ratio. To avoid confusion with older codes the same values are used for α and γ as previously.

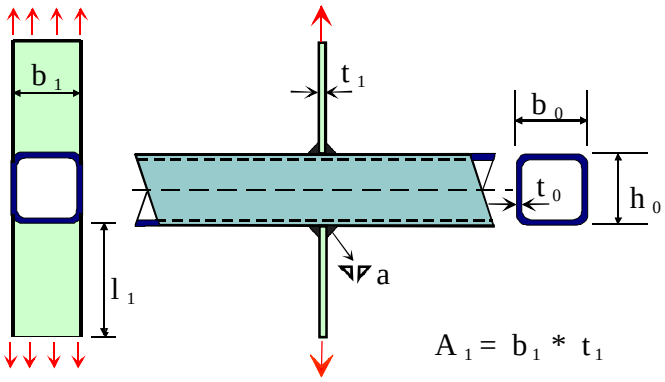

Fig. 7.1 Plate to RHS connection

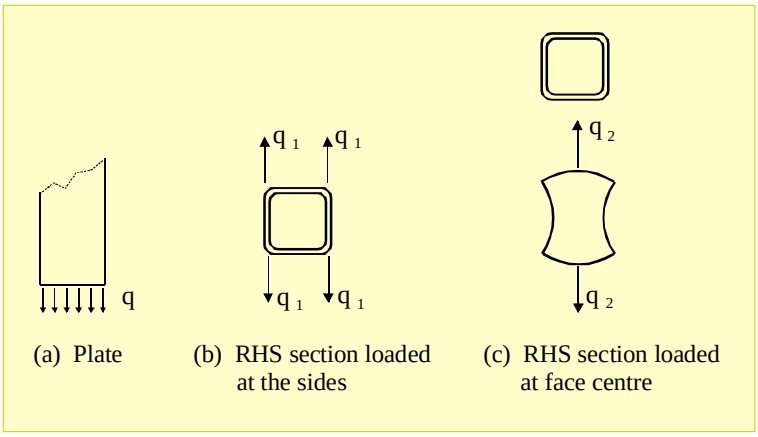

Fig. 7.2 Plate to RHS chord connection

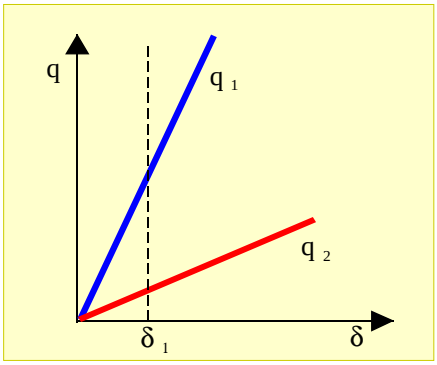

Fig. 7.3 Load-deformation diagram

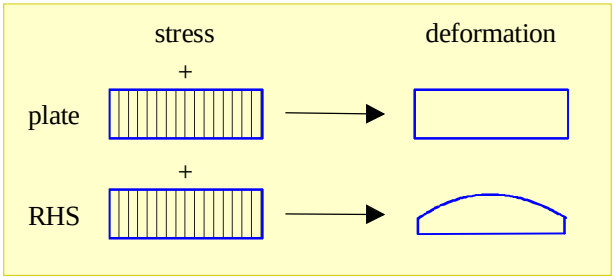

Fig. 7.4a Stress and resulting deformation

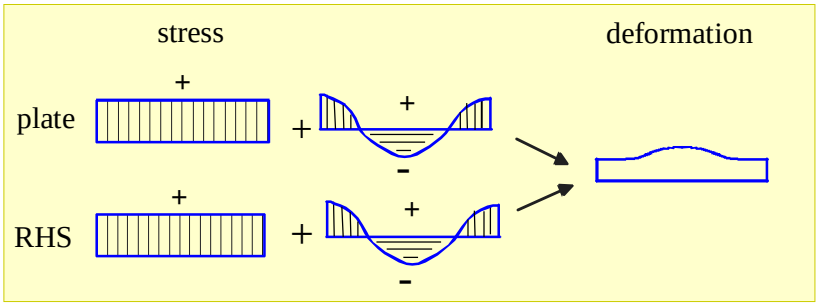

Fig. 7.4b Compatibility

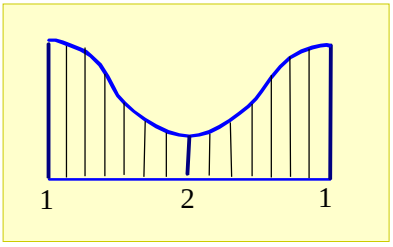

Fig. 7.4c Resulting stress pattern in the plate

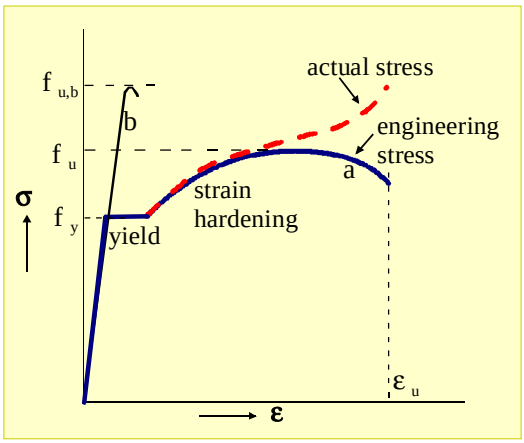

Fig. 7.5 σ-ε diagram

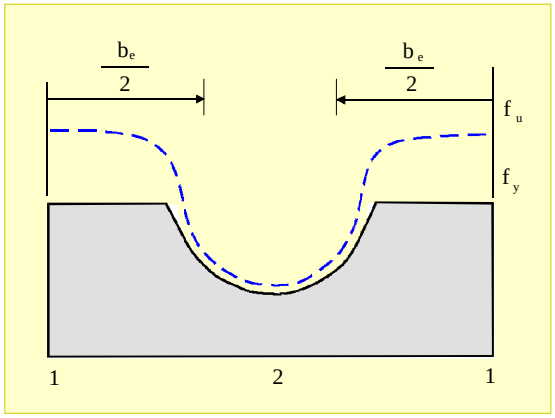

Fig. 7.6a Plastic stress pattern and ultimate condition at failure

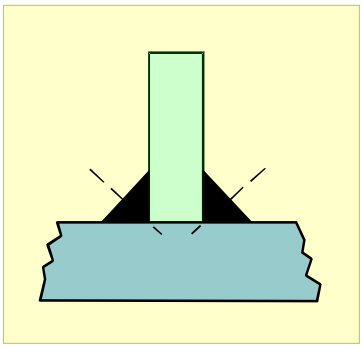
Fig. 7.6b Weld failure

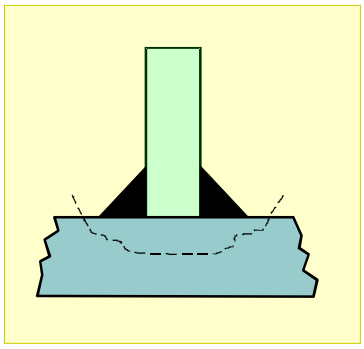
Fig. 7.6c Lamellar tearing

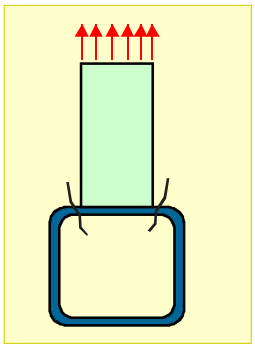
Fig. 7.6d Punching shear

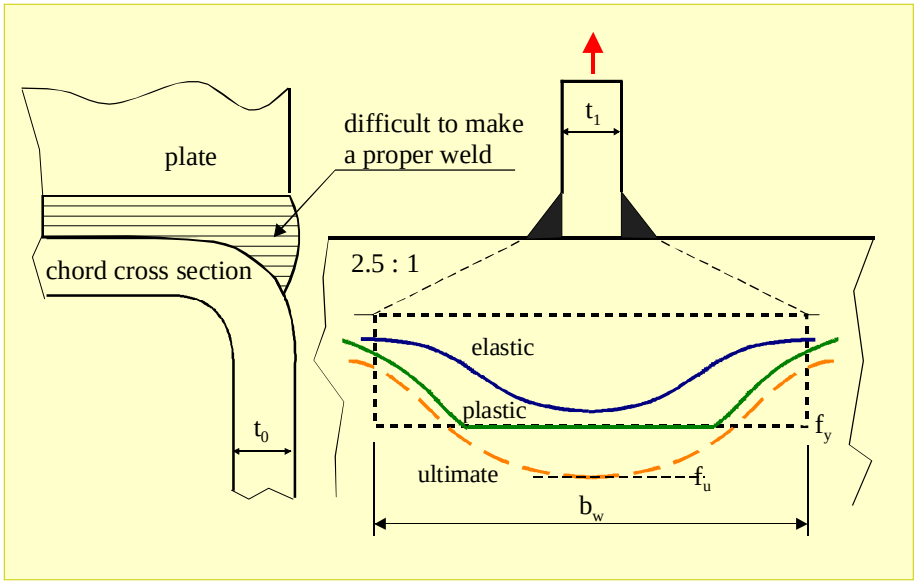

Fig. 7.6e Chord side wall failure

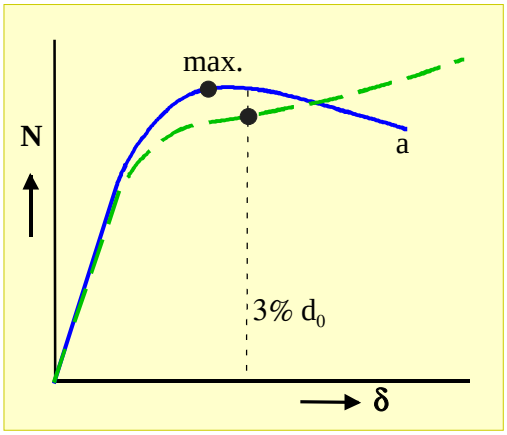

Fig. 7.7 Deformation limit

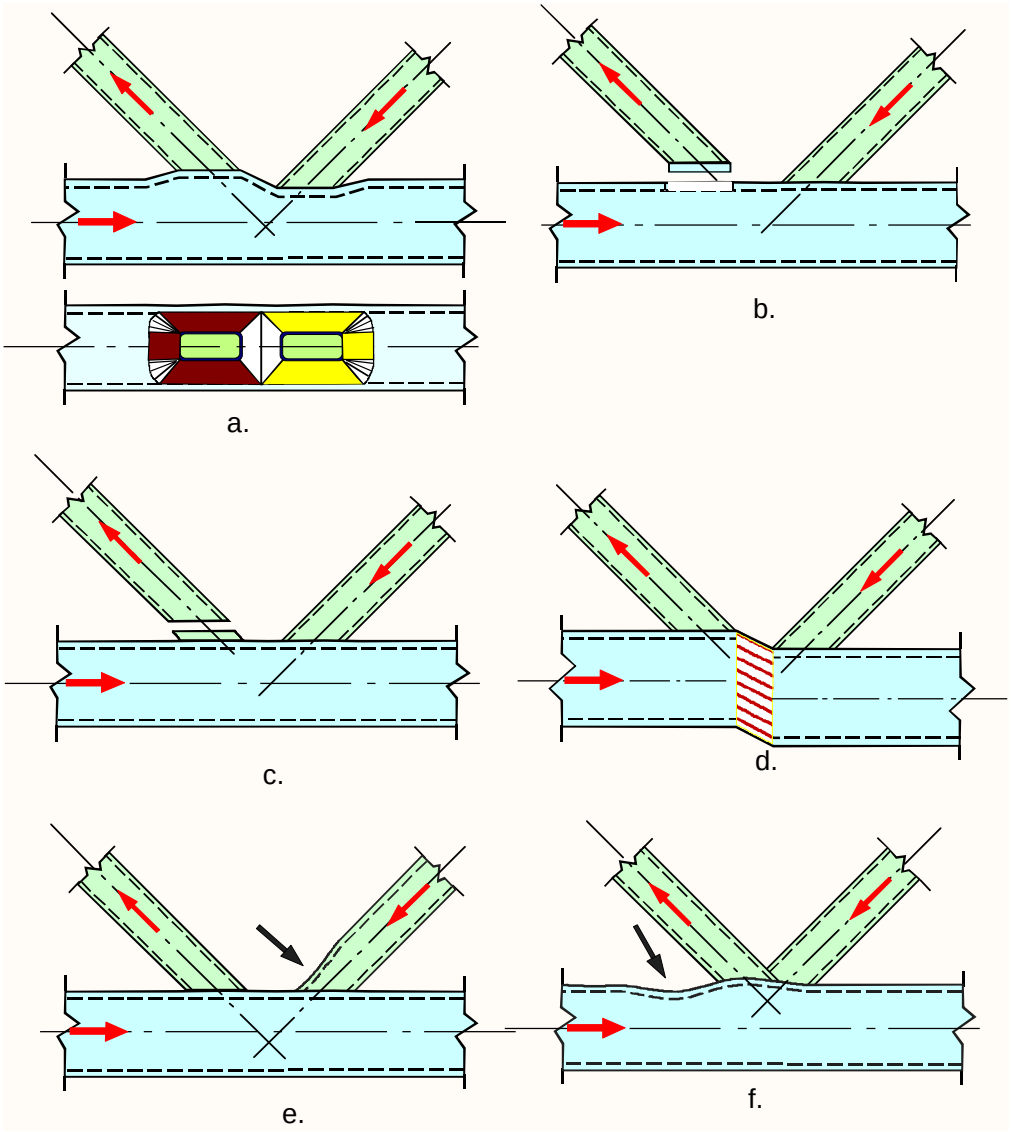

Fig. 7.8 Failure modes for a K-joint of rectangular hollow sections

$$\alpha = \frac{2\ell}{d_o} \quad \text{or} \quad \frac{2\ell}{h_o}$$ for T-,Y-,and X-joints

$$\beta = \frac{d_1}{d_o} \quad \text{or} \quad \frac{d_1}{b_o} \quad \text{or} \quad \frac{b_1}{b_o}$$ for T-, Y- and X-joints

$$\beta = \frac{d_1 + d_2}{2d_o} \quad \text{or} \quad \beta = \frac{d_1 + d_2}{2b_o} \quad \text{or} \quad \beta = \frac{b_1 + b_2 + h_1 + h_2}{4b_o}$$ for K- and N-joints

$$\beta = \frac{d_1 + d_2 + d_3}{3d_o} \quad \text{or} \quad \beta = \frac{d_1 + d_2 + d_3}{3b_o} \quad \text{or} \quad \beta = \frac{b_1 + b_2 + b_3 + h_1 + h_2 + h_3}{6b_o}$$ for KT-joints

$$\gamma = \frac{d}{2t_o} \quad \text{or} \quad \frac{b}{2t_o}$$

$$\tau = \frac{t_i}{t_o}$$

$$g' = \frac{g}{t_o}$$

$$n = \frac{\sigma_o}{f_{yo}}$$

$$n' = \frac{\sigma_{op}}{f_{yo}}$$

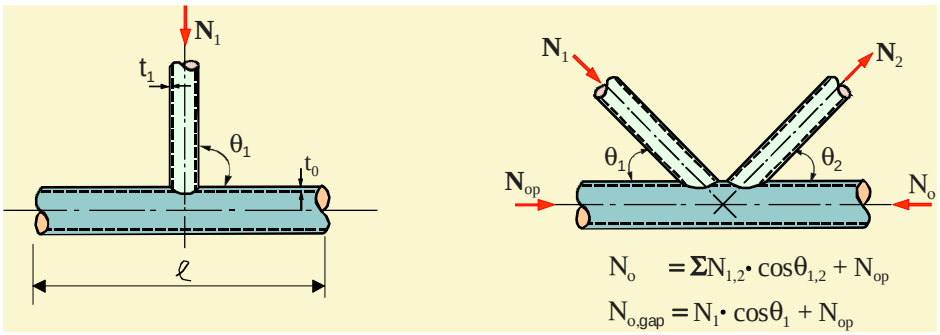

Fig. 7.9 Symbols used for defining the joint geometry

8. WELDED CONNECTIONS BETWEEN CIRCULAR HOLLOW SECTIONS

8.1 INTRODUCTION

Circular hollow sections can be connected in various ways, i e.:
- with special prefabricated connectors (Fig. 8.1)
- with end pieces which allow a bolted connection (Fig. 8.2)
- welded to a plate (Fig. 8.3)
- welded directly to the through member (chord)
  For transport or erection it may be that bolted connections are preferred or required, whereas for space structures prefabricated connectors are generally used. However, the simplest solution is to profile the ends of the members which have to be connected to the through member (chord) and weld the members directly to each other. Nowadays, end profiling does not give any problem and the end profiling can be combined with the required bevelling for the welds.

  Although the direct welded connection (Fig. 8.4) is the simplest and cleanest solution, the load transfer is rather complex due to the non-linear stiffness distribution along the perimeter of the connected braces. The design rules have been based on simplified analytical models in combination with experimental evidence, resulting in semi-empirical design formulae.

8.2 MODES OF FAILURE

In chapter 7 it was already indicated that the ultimate load capacity is based on the maximum in the load deformation diagram (if the chord deformation is smaller than 0.03 d_o) or the load at a chord deformation of 0.03 d_o.

Following the procedure described in chapter 7, i.e. following the loads, various possible failure modes (Fig. 8.5) can be expected, i.e.
- brace failure (yielding, local buckling)
- weld failure
- lamellar tearing
- chord plastification (face/wall, or cross section)
- chord punching shear failure
- chord local buckling
- chord shear failure

As indicated in chapter 7, to avoid weld failure it is recommended to design the welds to be stronger than the connected members, i.e. according to Eurocode 3 the throat thickness "a" of a fillet weld should satisfy the following requirements:
$a \geq 0.84\ t$ for S 235
$a \geq 0.91\ t$ for S 275
$a \geq 1.05\ t$ for S 355

Only for very lightly loaded structures smaller welds are allowed provided care has been taken of the effective perimeter [37,74].

Prequalified full penetration welds can be considered to be always stronger than the connected members.

The material should not be susceptible to lamellar tearing, i.e. for the larger thicknesses the sulphur content should be low (TTP quality).

Furthermore, in the current design recommendations, the d/t ratios have been limited to avoid local buckling. Limiting the d/t ratio also has the effect that the effective width criterion for the brace is not a governing failure criterion anymore.
Furthermore, within the range of validity of the design recommendations, it has been shown that the chord shear criterion can be covered by the formula for chord plastification.

As a result, the governing modes of failure to be considered have been reduced to:
- chord plastification
- chord punching shear.

8.3 ANALYTICAL MODELS

For the determination of the influencing joint parameters, three models are used, i.e.:
- ring model (for chord plastification)
- punching shear model (for chord punching shear)
- chord shear model

8.3.1 Ring model

The ring model, originally developed by Togo [47], is based on the assumption that for example in an X-joint most of the loading is transferred at the saddles of the brace, since the chord behaves most stiffly at that part of the connection perimeter, see the elastic stress

distribution in Fig. 8.6.
Consequently, the load N_1 in the brace can be divided into two loads of $0.5\ N_1 \cdot \sin\theta_1$ perpendicular to the chord at a distance $c_1 \cdot d_1$ at the saddles of the brace ($c_1 < 1.0$). These loads will be transferred by an effective length B_e of the chord. In the model, the load $0.5\ N_1 \cdot \sin\theta_1$ is now considered as a line load over the length B_e, see Fig. 8.7.
At failure, the plastic yield capacity will be reached at the locations A and B (in Fig. 8.8).

Neglecting the influence of axial and shear stresses on the plastic moment per unit length m_p results in:

$$m_p = \frac{1}{4} \cdot t_o^2 \cdot f_{yo} \qquad (8.1)$$

Assuming $d_o - t_o \approx d_o$ gives for the equilibrium:

$$2 \cdot M_p \cdot B_e = \frac{N_1 \cdot \sin\theta_1}{2} \cdot \left(\frac{d_o}{2} - \frac{c_1 d_1}{2} \right) \qquad (8.2)$$

$$N_1 = \frac{2 \cdot B_e / d_o}{(1 - c_1 \cdot \beta)} \cdot \frac{t_o^2 \cdot f_{yo}}{\sin\theta_1} \qquad (8.3)$$

Initially, the effective width B_e was determined experimentally and depends on the β ratio, e.g. for $\beta = 1.0$ the width B_e is smaller than for $\beta = 0.5$ due to the direct load transfer through the chord. An average value is: $B_e = 2.5\ d_o$ to $3.0 d_o$.

This ring model only considers the chord plastification which is caused by the brace load components perpendicular to the chord. It may be clear that the loads in the chord also have an influence on the load capacity of the connection and this is given by a function f(n'), which is determined experimentally.
As a result, the strength equation has the form:

$$N_1 = \frac{c_o}{(1 - c_1 \beta)} \cdot \frac{t_o^2 \cdot f_{yo}}{\sin\theta_1} \cdot f(n') \qquad (8.4)$$

where c_o, c_1 and f(n') are based on experiments; see 8.4. For X-joints, this model gives an excellent agreement with the test results, but the formula needs more modifications for the more complicated joints, such as K- and N-joints.

8.3.2 Punching shear model

The punching shear failure mode is also caused by the brace load component perpendicular to the chord, i.e. $N_1 \cdot \sin\theta_1$. The joint resistance is based on the effective punching shear area multiplied by the punching shear resistance (Fig. 8.9). Due to the unequal stiffness distribution, the stress distribution will be non uniform, even after yielding. However, tests have shown that within the range of validity given, the full perimeter can be considered to be effective.

For joints with $\theta = 90°$ the punching shear area will be $\pi \cdot d_1 \cdot t_o$ and the limiting value for the punching shear stress will be $f_y / \sqrt{3}$. Thus the punching shear capacity is given by:

$$N_1 = \pi \cdot d_1 \cdot t_o \cdot \frac{f_{yo}}{\sqrt{3}} \qquad (8.5)$$

For angles $\theta < 90°$ the component perpendicular to the chord has to be considered and the joint perimeter will increase. Projecting the connection perimeter to a flat surface through the chord crown gives an ellipse and the ratio between the perimeter of this ellipse and the circle for $\theta = 90°$ is given by $\frac{1 + \sin\theta_1}{2 \cdot \sin\theta_1}$, resulting in:

$$N_1 = 0.58 \cdot \pi \cdot d_1 \cdot t_o \cdot f_{yo} \cdot \frac{1 + \sin\theta_1}{2 \cdot \sin^2\theta_1} \qquad (8.6)$$

Since it is expected that the chord stresses have a small effect, the chord prestress function f(n') has not been included, which has been confirmed by tests.

Note:
In modern codes, criteria for failure modes with fracture are related to the ultimate stress with additional partial strength factors. Thus, for consistency, the yield stress f_{yo} could have been replaced by the ultimate stress f_{uo}, divided by an additional partial safety factor γ_M.

8.3.3 Chord shear model

In T-joints the failure is governed by a combination of the local failure of the chord cross section due to the brace load component perpendicular to the chord and chord failure due to shear, bending and, if present, the

axial loading of the chord. This has been worked out in detail by van der Vegte [76].

K-joints with a large β value may fail by a shear failure in the gap location, Fig. 8.10. The failure mode is a chord cross section plastification due to shear load, axial load and, if present, bending.
For compact chords it can be shown with plastic analysis (see section 2.3.5) that the chord shear capacity is given by:

$$V_{p\ell} = A_v \cdot \frac{f_{yo}}{\sqrt{3}}$$

$$= \frac{2}{\pi} \cdot A_o \cdot (0.58 \cdot f_{yo}) \qquad (8.7)$$

The axial load capacity is given by:

$$N_{p\ell} = A_o \cdot f_{yo} = \pi\,(d_o - t_o) \cdot t_o \cdot f_{yo} \qquad (8.8)$$

If the bending moments are small, only the interaction between axial load and shear load has to be considered, i.e.:

$$\left[\frac{N_i \cdot \sin\theta_i}{V_{p\ell}}\right]^2 + \left[\frac{N_{o,gap}}{N_{p\ell}}\right]^2 \le 1.0 \qquad (8.9)$$

or

$$N_{o,gap} \le A_o \cdot f_{yo} - A_o \cdot f_{yo} \sqrt{1 - \left(\frac{N_i \cdot \sin\theta_i}{0.58 \cdot f_{yo} \cdot A_v}\right)^2} \qquad (8.10)$$

If the chord is only loaded by the brace load components, i.e. $N_{op} = 0$, the value of
$N_{o,gap} = N_i \cdot \cos\theta_i$, which is shown in Fig. 8.11.

8.4 EXPERIMENTAL AND NUMERICAL VERIFICATION

Nowadays, not only a lot of experimental evidence exists, but also many results based on numerical analyses are available. Ref. [77] gives a good survey of the available data.

The experimental work has been mainly carried out in Germany, Japan, U.S.A., The Netherlands, U.K and Norway. The joints have been tested in various testing set-ups (Fig. 8.12), on mainly isolated joints. Only a few tests have been carried out on joints in complete frames. For the experimental tests it is important to consider the support and loading conditions to avoid constraint effects [78].

For numerical results it is important that the models used have been calibrated with experimental data. The elements and the mesh should be considered properly (see Fig. 8.13); details are given in [76].

8.5 BASIC JOINT STRENGTH FORMULAE

The analytical ring model has been used as a basis for the determination of the joint strength formulae.
Based on the available test results for X-joints and using eq. (8.4), the values for c_o and c_1 have been determined to obtain the function for the mean strength, see Fig. 8.14.

Due to the fact that for T, Y, K and N joints the load transfer is more complicated, functions for β and γ have been determined experimentally as well as the functions for the gap g resulting in a general presentation:

$$N_1 = f(\beta) \cdot f(\gamma) \cdot f(g') \cdot \frac{f_{yo} \cdot t_o^2}{\sin\theta_1} \cdot f(n') \qquad (8.11)$$

In the comparison of the test results with the resulting formulae it was shown that within the range of validity given the results can be described by a basic joint strength function for chord plastification with a check for punching shear. The chord shear criterion did not have to be checked separately.

The chord prestress function f(n') has been investigated separately [1,34,42,47]. Initially, separate functions existed for X and K joints. In the evaluation to design rules by the international committees of IIW-XV-E and the CIDECT Projects Group, this has been simplified to one function based on the chord stress σ_{op} caused by the prestressing load N_{op}. Since this function is still based on the prestress which is in contradiction with the function for joints with square hollow sections, which is based on the maximum chord stress, this item is still under investigation.

8.6 EVALUATION TO DESIGN RULES

In the analysis for the basic joint strength formulae, functions for predicting the mean strength with the lowest coefficient of variation have been determined.

Considering the scatter in test results, typical tolerances in dimensions and workmanship and the variation in yield stress, characteristic joint strength formulae have been determined [34,42] with a 5% probability of lower strength.

These characteristic formulae have been divided by a partial safety factor γ_M = 1.1 and somewhat simplified to derive the design resistance formulae given in the IIW recommendations [18], the CIDECT design guide [1] and Eurocode 3 [12].

These formulae have now been adopted in many national recommendations. The American API [15] and AWS [16] recommendations are an exception in this case [16,79,80].

Table 8.1 shows the design resistance formulae. As shown, the chord plastification criterion and the general punching shear criterion have to be checked. It is also noted that the formula for X-joints fully agrees with eq (8.4) based on the ring model.

Fig. 8.15 shows that a compression stress σ_{op} in the chord gives a reduction of the joint resistance, whereas for tension no influence is given. This influence is fully based on experimental evidence. Theoretically there should also be a reduction of the joint resistance for high tensile loads in the chord, although the tests did not show a reduction for chord loads up to about 80 to 90% of the chord yield capacity [42].

Fig. 8.16 shows that overlapping of the braces has a beneficial effect on the joint resistance, especially in the case of high $2\gamma = d_o/t_o$ ratios. For very low 2γ ratios the influence is marginal.
It should be noted that the actual joint resistance for high 2γ values is lower than for low 2γ values, since the influence of t_o^2 overrules the effect in the $f(\gamma,g')$ factor.

8.7 OTHER TYPES OF JOINTS

8.7.1 Related types of joints

The joint design resistance for the types of joints shown in table 8.2 can be directly related to that for the basic type of joints in table 8.1.
The first and third joints in the table 8.2 have a similar loading effect as for an X-joint and the design resistance is therefore related to that for X-joints.
The second and fourth joints have a loading comparable to that for a K-joint and the design resistance is therefore related to that for K-joints.
In all cases the brace load components perpendicular to the chord have to be considered, since these affect the chord plastification.

It will also be clear that in the latter case the shear of the chord will be higher than for a K-joint and has to be considered separately.

8.7.2 Plate to CHS connections

Table 8.3 shows some joints with a circular hollow section chord and various configurations for the brace. In general, the design resistance for these types of joints can be related to each other by a general strength function [1,82]:

$$N_1 = f(\beta) \cdot f(\eta) \cdot f_{yo} \cdot t_o^2 \cdot f(n') \qquad (8.12)$$

$$\text{with } f(\beta) = \frac{5}{1-0.81\beta} \qquad (8.13)$$

$$f(\eta) = 1 + 0.25\,\eta \quad \text{(lower bound value)} \qquad (8.14)$$

8.7.3. Multiplanar joints

In multiplanar joints, two additional effects influence the joint capacity compared to that for uniplanar joints, i.e.:
- the geometrical effects (stiffening by the multiplanar joints)
- the loading effects

For example, consider the XX joint in table 8.4. If the out of plane braces are very small in diameter, and unloaded, they will have hardly any effect on the deformation of the chord. However, if the diameter increases (e.g. β = 0.6), the chord cross section will be stiffened considerably. As a consequence, the

geometrical effect on the joint capacity will be minor for small β values and high for larger β values.
Note that for equal braces the maximum $\beta = 0.7$ if no overlapping braces are used.

The deformation capacity will decrease for high β ratios since the deformation is concentrated at the gap locations between the braces.
For the load effects in XX joints it will be clear that loads in the brace planes in the opposite sense will decrease the joint capacity, whereas loads in the same sense will increase the joint capacity.
Although the effects depend on the joint parameters [76] the influence function in table 8.4 for XX joints can be considered to be an approximate measure of the effect.

For KK-joints the effect especially depends on the out of plane gap parameter. In [86] Yamada et al. give detailed recommendations in relation to the out of plane gap and the loading, including asymmetric loading in the braces for which the loading influence is larger.

8.7.4 Joints loaded by bending moments

In principle, the design resistance formulae for joints loaded by in plane or out of plane bending moments have been determined in a similar way as for axially loaded joints, also resulting in two strength criteria, i.e.: chord plastification and chord punching shear. The design resistance formulae can be found in [1,12,33,36,37,38,42]. In the case of Vierendeel girders it is recommended to choose joints with $\beta = 1.0$ to provide sufficient stiffness and strength.

8.8 DESIGN CHARTS

In the design process it is important that the designer knows how to design and that he or she can check quickly if a particular design will be appropriate. That is why design graphs have been established [1] in which the joint resistance has been expressed as an efficiency, i.e.: the joint resistance is given as a fraction of the yield capacity $A_i \cdot f_{yi}$ of the connected brace. This results in the following efficiency formula:

$$\text{eff} = \frac{N_i^*}{A_i \cdot f_{yi}} = C_e \cdot \frac{f_{yo} \cdot t_o}{f_{yi} \cdot t_i} \cdot \frac{f(n')}{\sin\theta_i} \qquad (8.15)$$

The efficiency parameter C_e (C_T for T-joints, C_X for X-joints and C_K for K-joints), see Figs 8.17 to 8.20, gives the efficiency for a joint with:

$\theta_i = 90°$
$f_{yo} \cdot t_o = f_{yi} \cdot t_i$, (identical thickness and yield stress for brace and chord).
$f(n') = 1.0$, i.e. chord in tension.

As an example using Fig. 8.19 shows that for a K-joint with $g = 2t_o$, $2\gamma \approx 25$, $\beta \approx 0.5$
gives a value $C_k \approx 0.4$.

Thus, for an angle $\theta = 45°$, a 100% efficiency can be obtained if

$$\frac{f_{yo} \cdot t_o}{f_{yi} \cdot t_i} \geq 1.77$$

Thus, for a 100% efficiency, $f_{yo} \cdot t_o$ should always be considerably larger than $f_{yi} \cdot t_i$.

The chord prestress function f(n') is given as a function of the parameter $n' = \frac{\sigma_{op}}{f_{yo}}$. For simply supported lattice girders the influence of the prestressing function near the supports is small (small chord loads), whereas it has a large influence at the centre of the girder where the chord loads are high, but generally the brace loads are small. The prestressing function is especially important in the case of continuous or cantilevered lattice girders.

8.9 CONCLUDING REMARKS

For more detailed information about joints loaded by bending moments, interaction between axial load and bending moments as well as special types of joints such as cropped end joints, flattened end joints, etc., reference is made to the appropriate literature, see [1,33,34,37,42,85,90,91].

Table 8.1 Design resistance of welded joints between circular hollow sections

Type of joint	Design strength (i = 1, 2)
T- and Y-joints	chord plastification
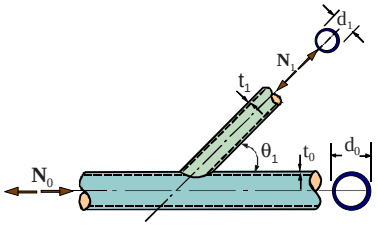	$N_1^* = \frac{f_{yo} \cdot t_o^2}{\sin\theta_1} \cdot (2.8 + 14.2\beta^2) \cdot \gamma^{0.2} \cdot f(n')$ (eq. 4.2.1)
X-joints	chord plastification
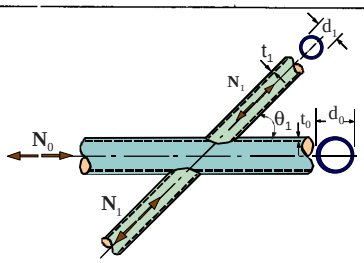	$N_1^* = \frac{f_{yo} \cdot t_o^2}{\sin\theta_1} \cdot \left[\frac{5.2}{1 - 0.81\beta}\right] \cdot f(n')$
K and N gap or overlap joints	chord plastification
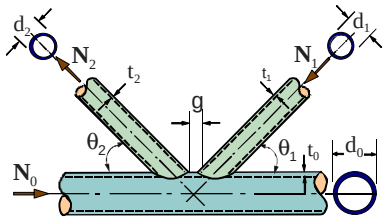	$N_1^* = \frac{f_{yo} \cdot t_o^2}{\sin\theta_1} \cdot \left(1.8 + 10.2\frac{d_1}{d_o}\right) \cdot f(\gamma, g') \cdot f(n')$ $N_2^* = N_1^* \cdot \frac{\sin\theta_1}{\sin\theta_2}$
general	punching shear
punching shear check for T,Y,X and K,N,KT joints with gap	$N_i^* = \frac{f_{yo}}{\sqrt{3}} \cdot t_o \pi d_i \cdot \frac{1 + \sin\theta_i}{2\sin^2\theta_i}$
functions	
$f(n') = 1.0$ for $n' \geq 0$ $\quad n' = \frac{f_{op}}{f_{yo}}$ (tension) $f(n') = 1 + 0.3n' - 0.3n'^2$ for $n' < 0$ (compression)	$f(\gamma, g') = \gamma^{0.2} \cdot \left[1 + \frac{0.024\gamma^{1.2}}{\exp(0.5g' - 1.33) + 1}\right]$
validity ranges	

$0.2 < \frac{d_i}{d_0} \leq 1.0$	$\frac{d_i}{2t_i} \leq 25$ and see table 8.1a	$30^o \leq \theta_i \leq 90^o$ $-0.55 \leq \frac{e}{d_o} < 0.25$	$\gamma \leq 25$ $\gamma \leq 20$ (X-joints)	$Ov \geq 25\%$ $g \geq t_1 + t_2$

Table 8.1a d_1/t_1 limits for the compression brace or limits for efficiency [1] to avoid local buckling of the compression brace

d_1/t_1 limits for which the joint efficiencies derived from Figs. 8.17 to 8.20 can always be used		efficiency limit * for compression brace					
		f_{y1}	d_1/t_1				
yield stress	d_1/t_1 limit		30	35	40	45	50
f_y = 235 N/mm^2	$d_1/t_1 \le 43$	235	1	1	1	1	0.9
f_y = 275 N/mm^2	$d_1/t_1 \le 37$	275	1	1	1	0.9	0.9
f_y = 355 N/mm^2	$d_1/t_1 \le 28$	355	1	0.9	0.9	0.8	0.8

* $\dfrac{N_i^*}{A_i \cdot f_{yi}} \le$ values given in the table

Considering member buckling the above mentioned limitations will not frequently be critical.

Table 8.2 Design resistance of related types of joints

Type of joint	Design strength formulae (in relation to table 8.1)
a 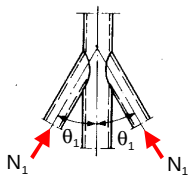	$N_1 \le N_1^*$ N_1^* from X-joint
b 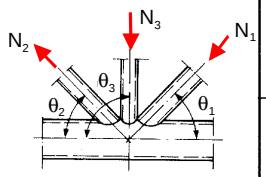	$N_1 \cdot \sin\theta_1 + N_3 \cdot \sin\theta_3 \le N_1^* \cdot \sin\theta_1$ (N_1^* from K-joint) $N_2 \cdot \sin\theta_2 \le N_1^* \cdot \sin\theta_1$
	replace $\dfrac{d_1}{d_o}$ by $\dfrac{d_1 + d_2 + d_3}{3\,d_o}$ in K-joint strength formula
c 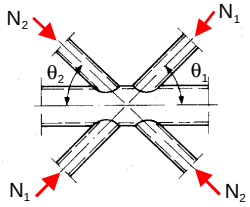	$N_1 \cdot \sin\theta_1 + N_2 \cdot \sin\theta_2 \le N_i^* \cdot \sin\theta_i$ (N_1 from X-joint) where $N_i^* \cdot \sin\theta_i$ is the larger of $N_1^* \cdot \sin\theta_1$ and $N_2^* \cdot \sin\theta_2$
d 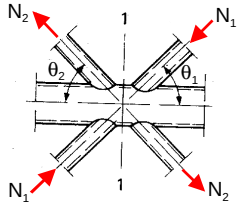	$N_1 \le N_1^*$ (K-joint) $N_2 \le N_2^*$ (K-joint) check cross section 1-1 for plastic shear capacity; see chapter 8.3 (gap joints only)

Table 8.3 Design resistance of welded CHS joints with gusset plates or open sections

type of joint	axial loading $N^* = f(\beta) \cdot f(\eta) \cdot f(n') \cdot f_{yo} \cdot t_o^2$			
	$f(\beta)$	$f(\eta)$	$f(n')$	$f_{yo} \cdot t_o^2$
XP-1/TP-1 XP-3/TP-3 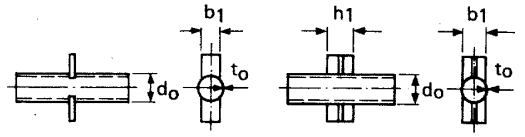	$\frac{5.0}{1 - 0.81\,\beta}$	1	$f(n')$	$f_{yo} \cdot t_o^2$
XP-2/TP-2 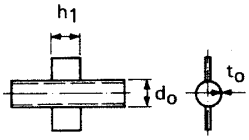	5.0	$(1 + 0.25\,\eta)$ $\eta \leq 4$	$f(n')$	$f_{yo} \cdot t_o^2$
XP-4/TP-4 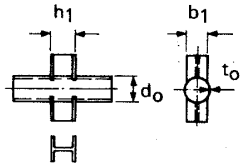	$\frac{5.0}{1 - 0.81\,\beta}$	$(1 + 0.25\,\eta)$ $\eta \leq 4$	$f(n')$	$f_{yo} \cdot t_o^2$
XP-5/TP-5 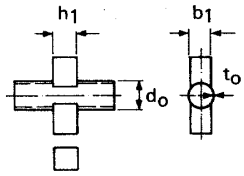	$\frac{5.0}{1 - 0.81\,\beta}$	$(1 + 0.25\,\eta)$ $\eta \leq 2$	$f(n')$	$f_{yo} \cdot t_o^2$

Note : These formulae may also be used for connections with a plate at one side i.e. the TP connections although the formulae may give in most cases a somewhat conservative strength, see [1,82].

Table 8.4 Correction factors for the design resistance of multiplanar joints

Type of joint	Correction factor to uniplanar joint $60^o \leq \phi \leq 90^o$
TT 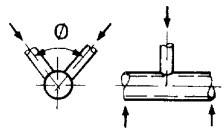	1.0
XX 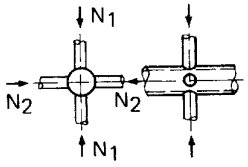	$1 + 0.33 \frac{N_2}{N_1}$ Note: take account of the sign of N_2 and N_1 ($N_1 \geq N_2$)
KK 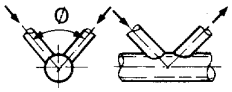	0.9 (symmetrical or asymmetrical loading)

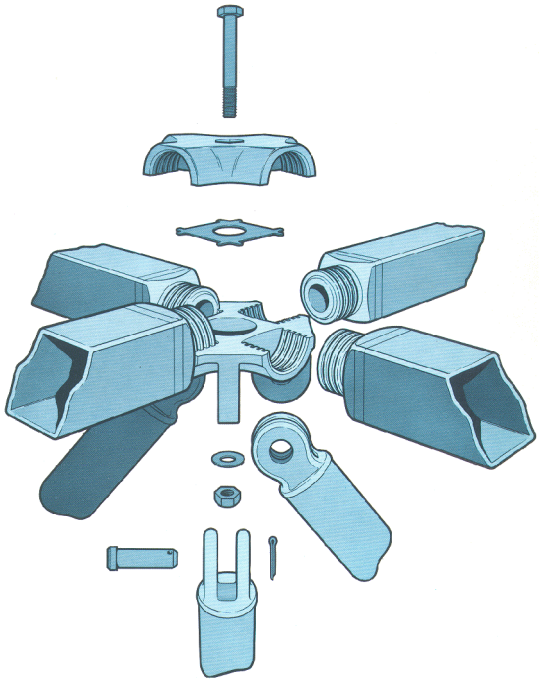

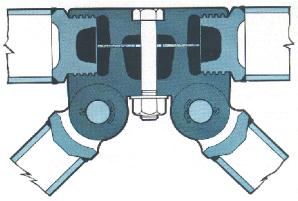

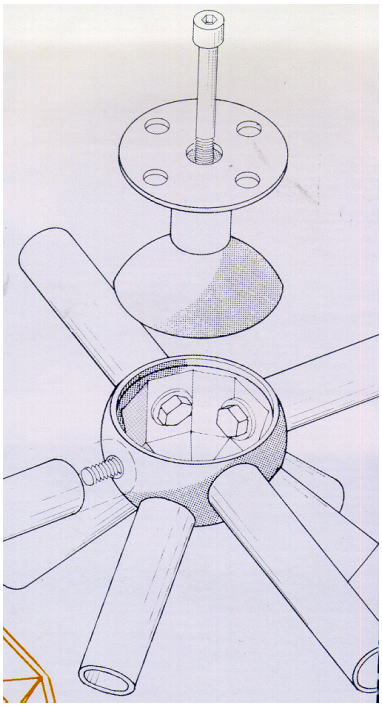

Fig. 8.1 Joints with prefabricated connectors

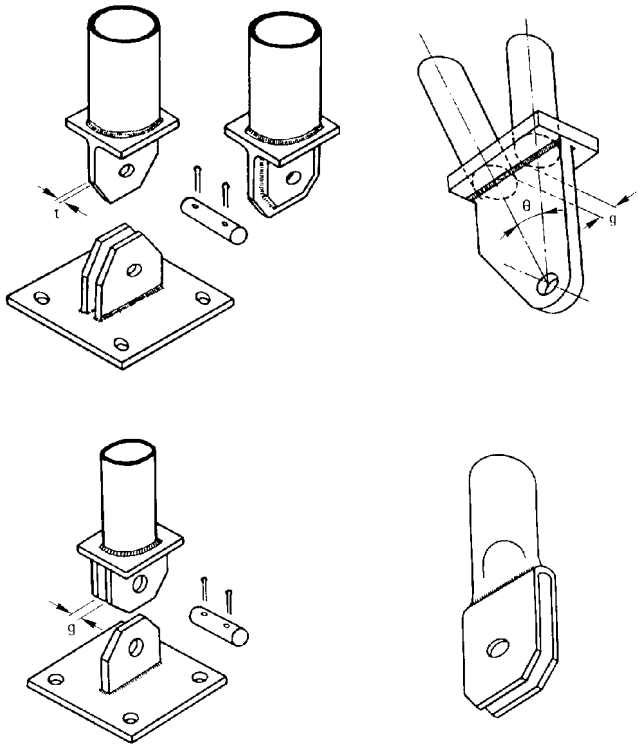

Fig. 8.2 Joints with end pieces for bolted connections

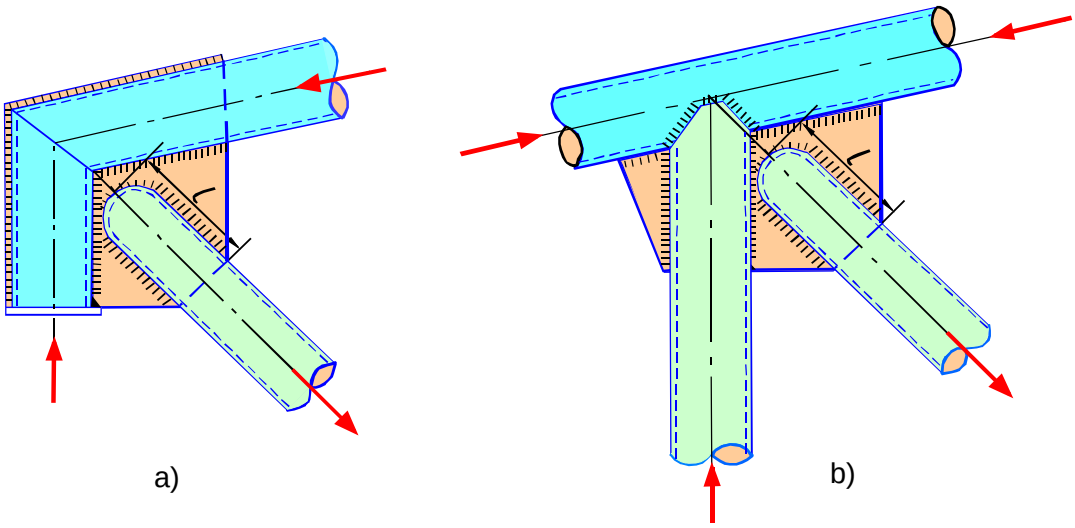

Fig. 8.3 Welded gusset plated connections (expensive and old fashioned)

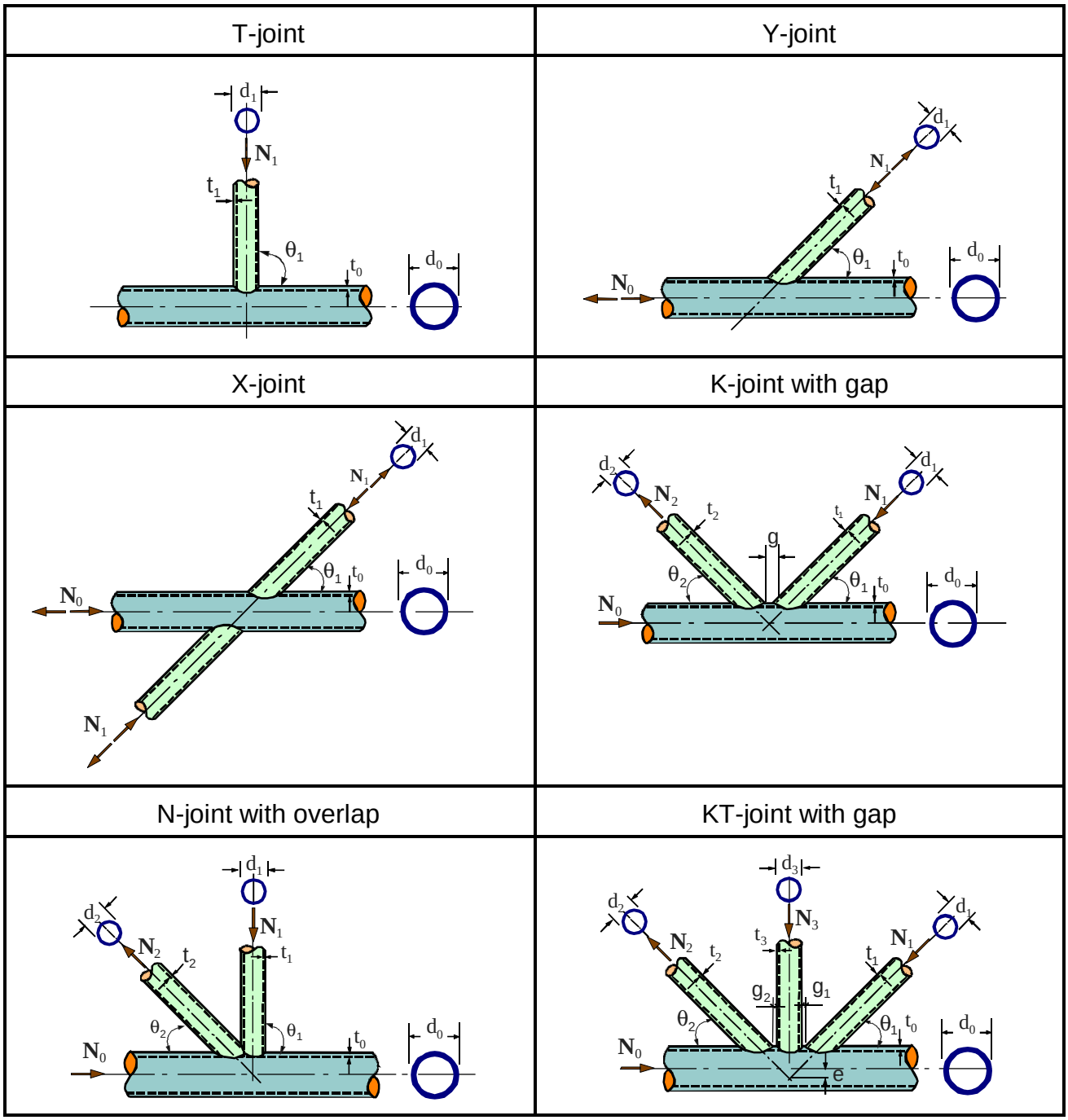

Fig. 8.4 Welded CHS joints

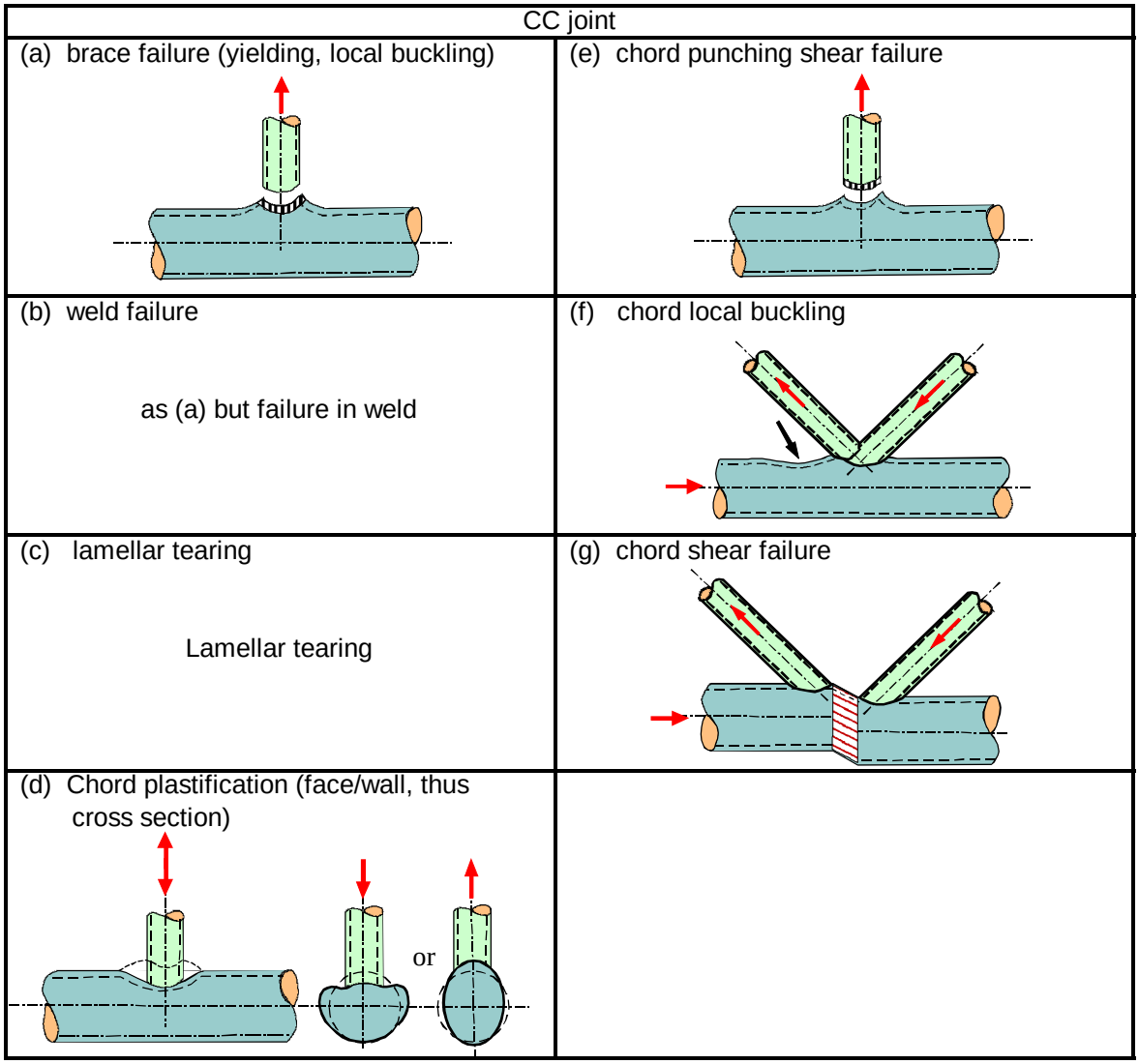

Fig. 8.5 Failure modes for joints between circular hollow sections

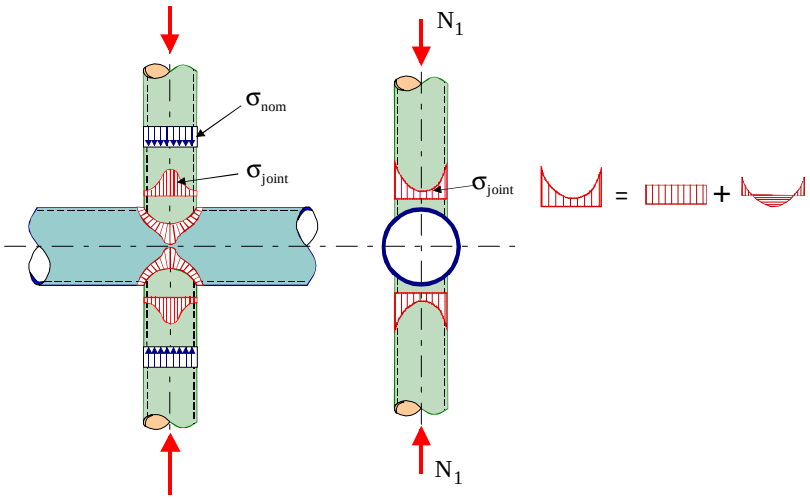

Fig. 8.6 Elastic stress distribution in an X-joint

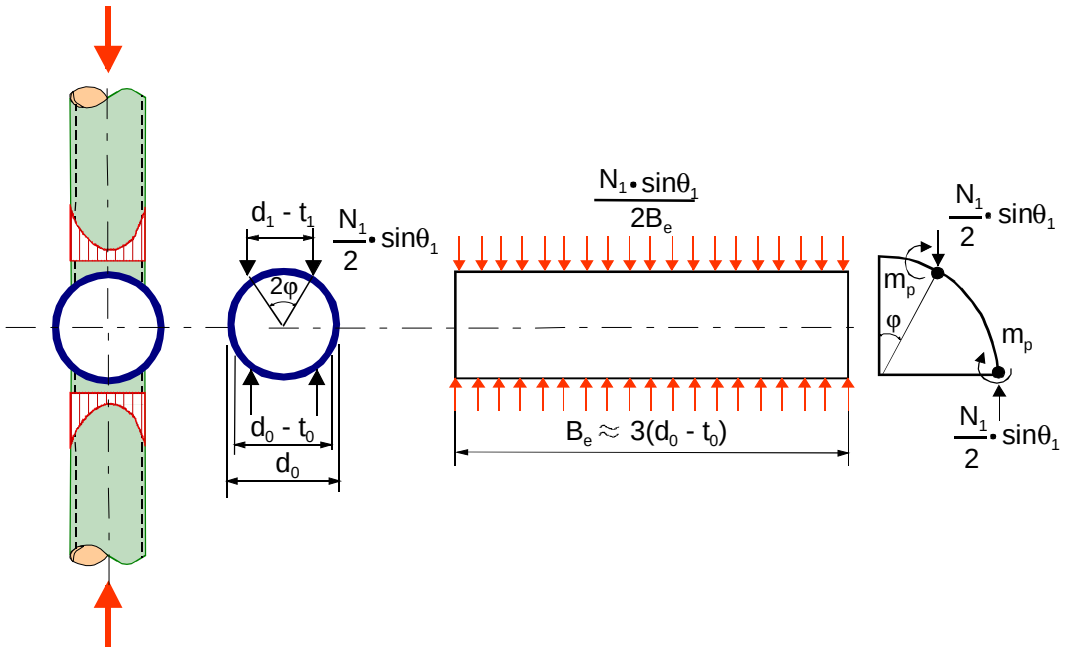

Fig. 8.7 Ring model

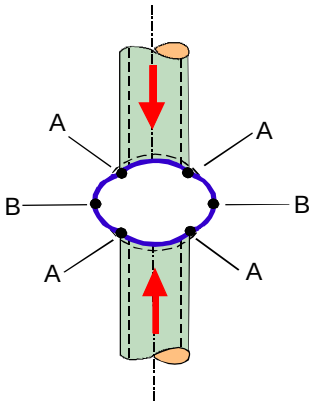

Fig. 8.8 Plastic hinges in the Ring model at failure

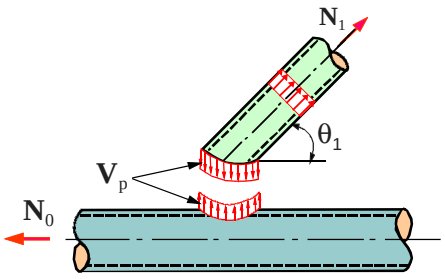

Fig. 8.9 Punching shear model

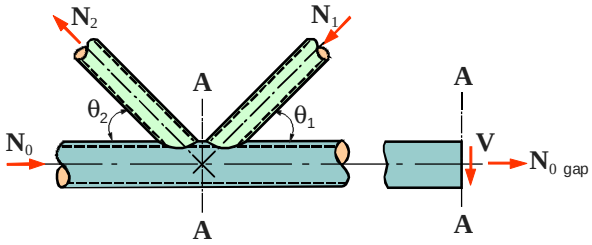

Fig. 8.10 Chord shear model

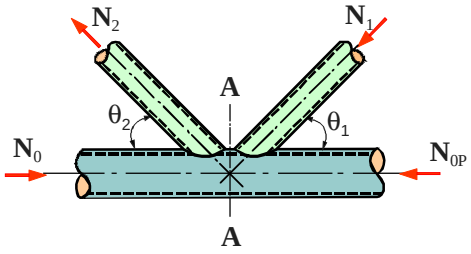

$$N_0 = \Sigma N_{1,2} \cdot \cos\theta_{1,2} + N_{0P}$$

$$N_{0,gap} = N_1 \cdot \cos\theta_1 + N_{0P}$$

Fig. 8.11 Chord preload N_{op}

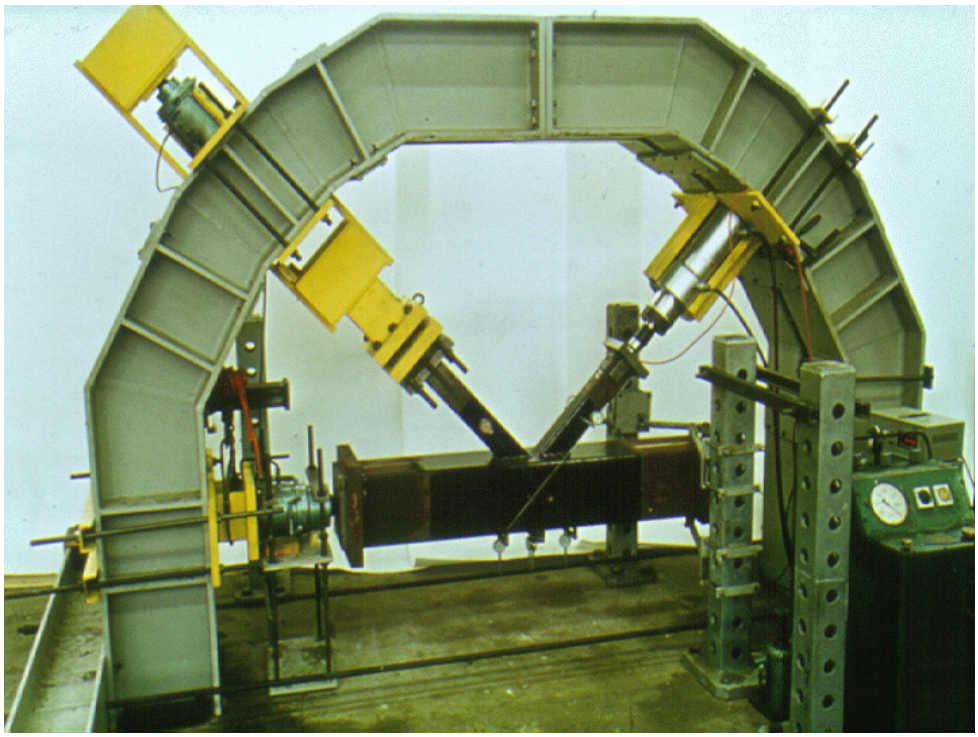

Fig. 8.12 Test rig for isolated joint tests

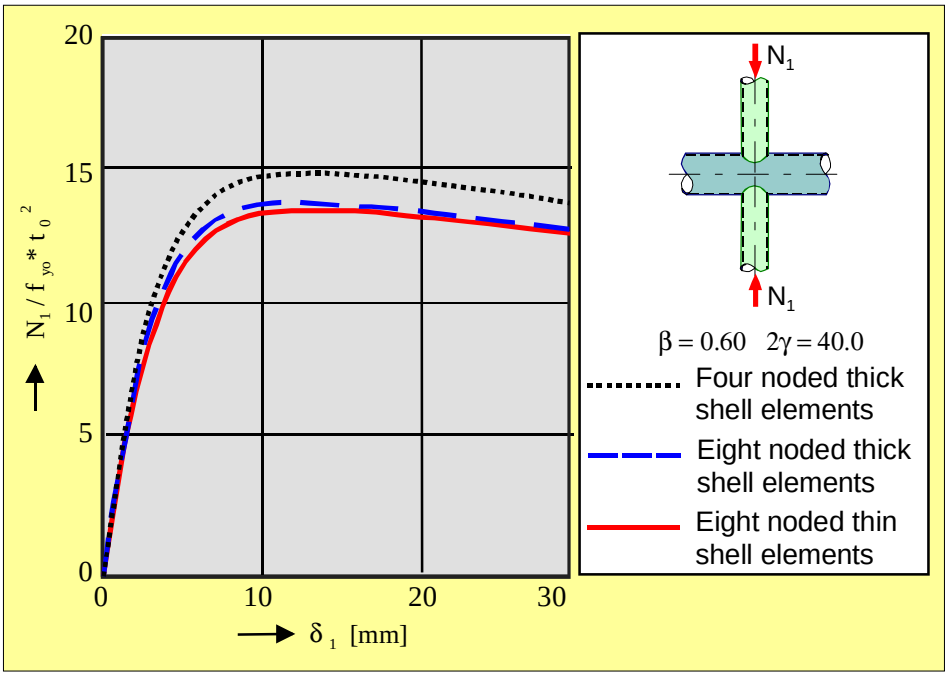

Fig. 8.13 The effect of element type on numerical results

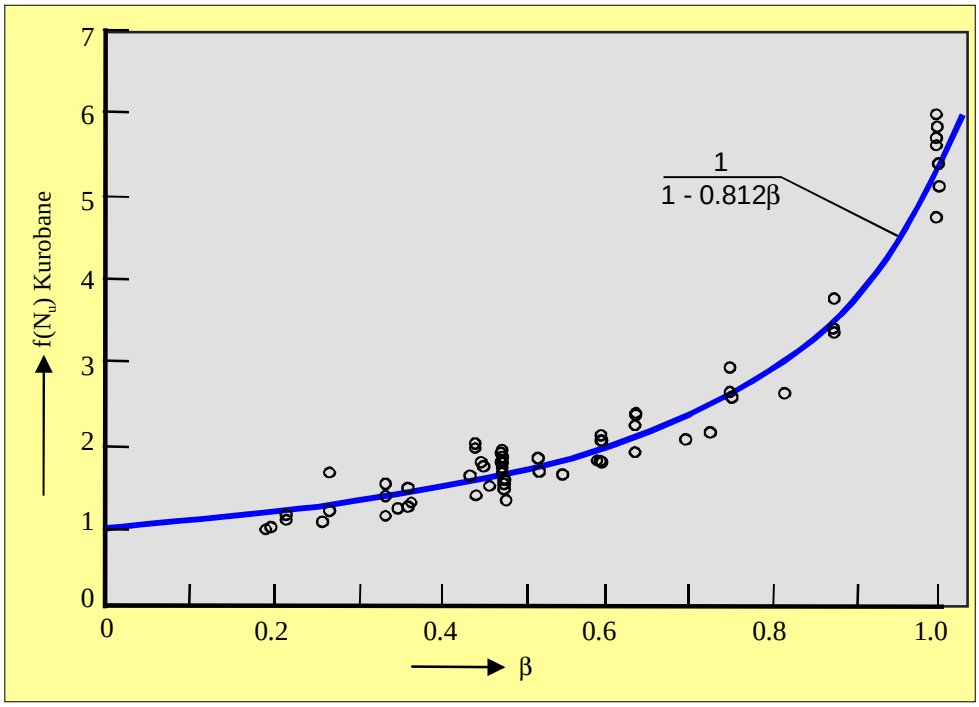

Fig. 8.14 Comparison of experiments with the mean joint resistance function (X-joints)

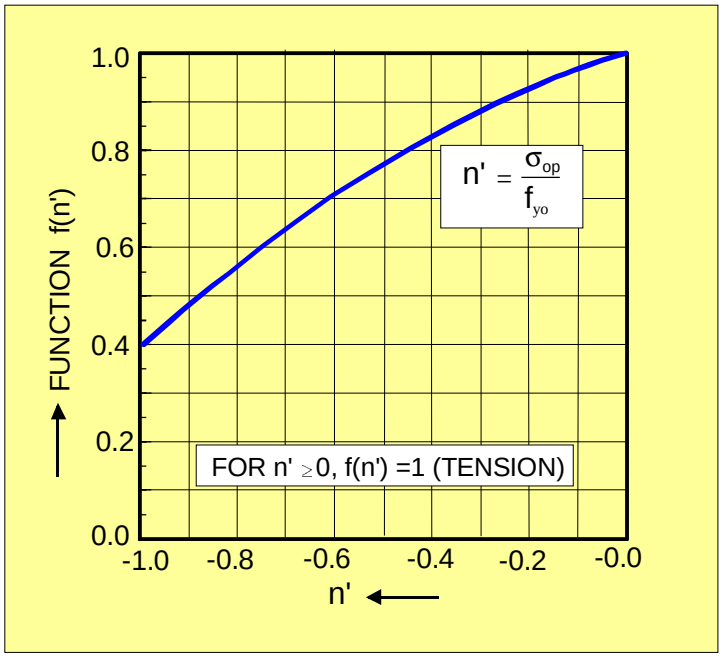

Fig. 8.15 Chord prestressing function f(n')

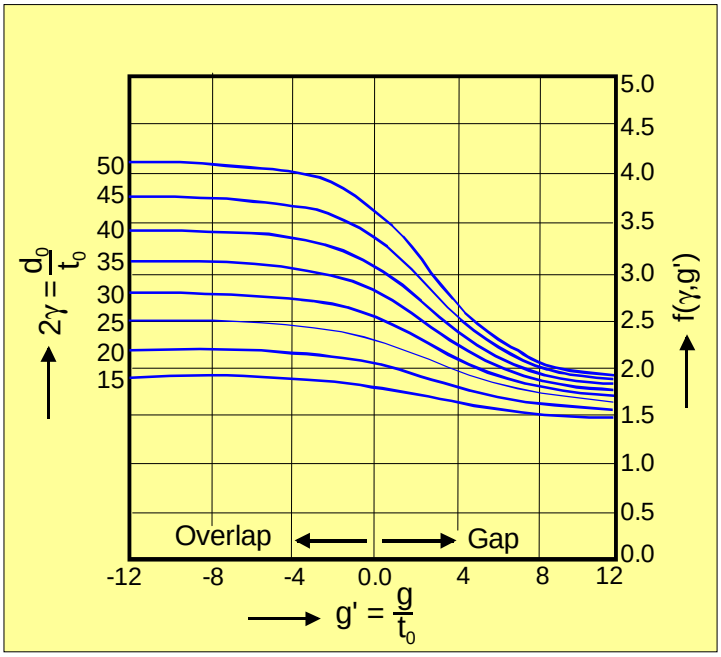

Fig. 8.16 Influence function f(γ,g') for the gap in K-joints

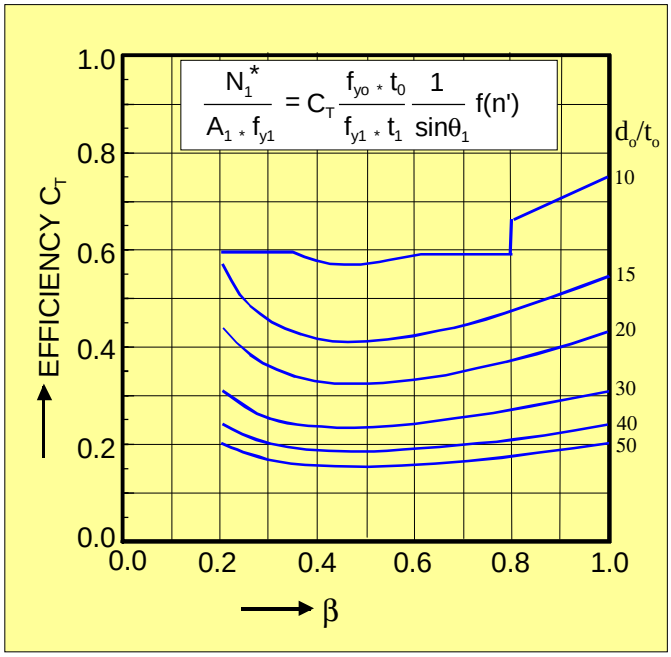

Fig. 8.17 Design charts for T- and Y-joints of circular hollow sections

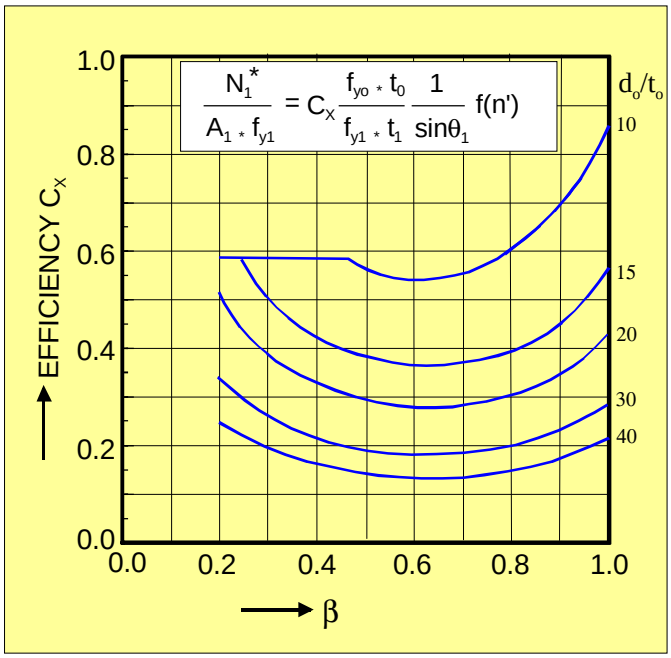

Fig. 8.18 Design charts for X-joints of circular hollow sections

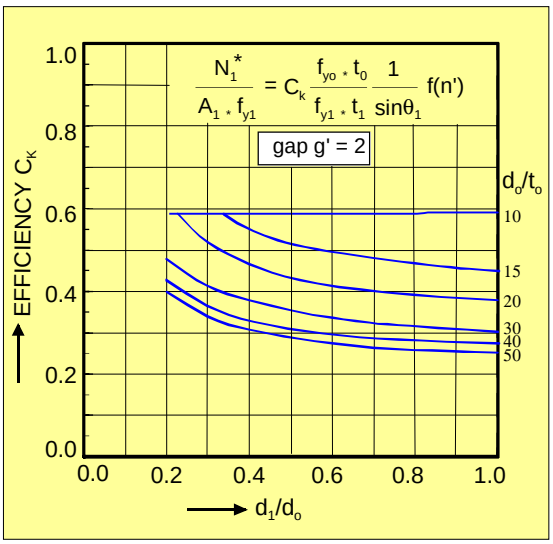

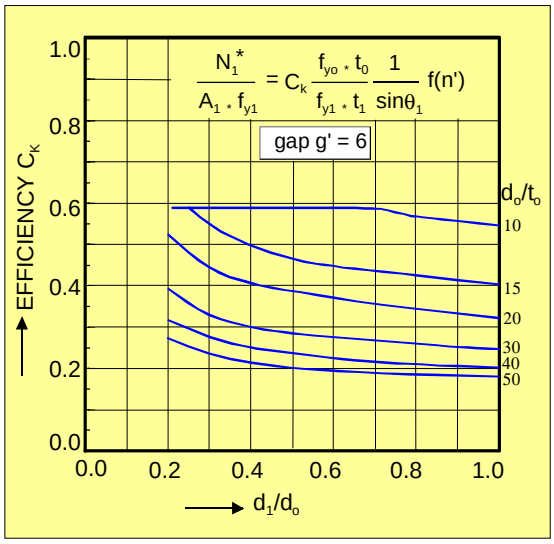

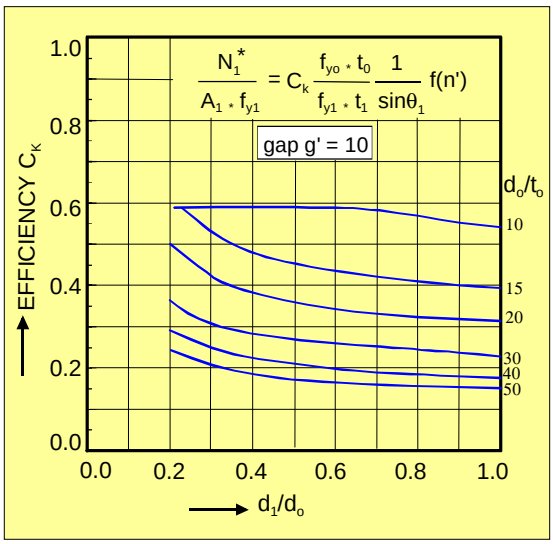

Fig. 8.19 Design charts for circular hollow section K-joints with gap

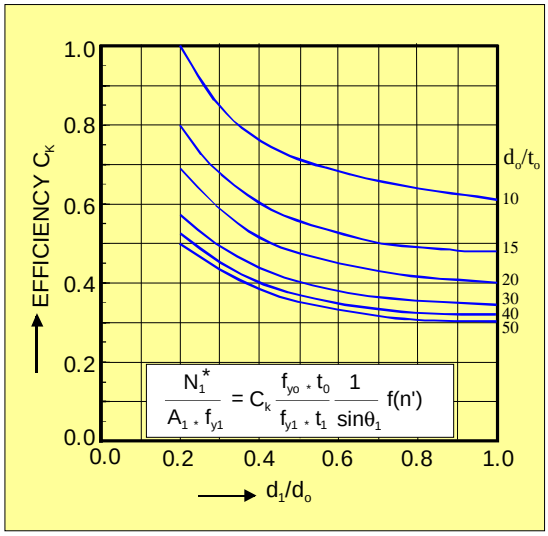

Fig. 8.20 Design charts for circular hollow section K-joints with overlap

9. WELDED CONNECTIONS BETWEEN RECTANGULAR HOLLOW SECTIONS

9.1 INTRODUCTION

The most economical and common way to connect rectangular hollow sections is by direct connection without any intersecting plates or gussets, as shown in Fig. 9.1. This also gives the most efficient way for protection and maintenance.

The connections between rectangular hollow sections can be easily made, since the connecting members have to be provided with straight end cuts only.

Although the fabrication is simple, the load transfer is more complex due to the non-uniform stiffness distribution in the connections. Due to the flat sides, the difference in stiffness at a corner and at the centre of a face is even greater than for circular hollow sections.

The general philosophy to identify the various failure modes and to observe the load transfer has been described in chapter 7, but will be described here in more detail for the connections between rectangular and square hollow sections.
Most failure modes can be related to analytical models to study the impact of the various influencing parameters. Based on the analytical models and the tests carried out, design rules have been established.

9.2 MODES OF FAILURE

Similar to circular hollow section joints, the ultimate load capacity is based on the maximum in the load deformation diagram (if the chord deformation is less than 0.03 b_o) or the load at a deformation of 0.03 b_o of the chord.
As already indicated in chapter 7 and shown in Fig. 9.2, the following modes of failure can occur:

- brace failure (brace effective width: partial failure or buckling)
- weld failure
- lamellar tearing
- chord face plastification
- chord punching shear failure
- chord side wall yielding or buckling
- chord local buckling
- chord shear failure

Similar to connections between circular hollow sections to avoid weld failure, the welds should be stronger than the connected members and the throat thickness should satisfy the same requirements as given in 8.2. Prequalified full penetration welds can always be considered to be stronger than the connected members.

Also here, for very thick walled members (t > 25 mm), a TTP quality with a low sulphur content should be used for the chords to avoid lamellar tearing.

Similar to connections for circular hollow sections, the width to wall thickness ratios b/t have been limited in the current design recommendations to avoid local buckling and/or to limit the deformations.

As a result, the following failure modes still have to be considered in design:

- brace failure (effective width)
- chord face plastification
- chord punching shear
- chord side wall failure
- chord shear failure

Due to the fact that rectangular hollow sections can be connected with various orientations and in various combinations, several failure modes have to be considered, which makes the checking procedure more complicated.
In case of connections between square hollow sections and within a smaller validity range, the modes to be checked can be limited to one or two.

Brace (effective width) failure generally occurs for joints with relatively thin walled braces and is a general failure mode for overlap joints.

Chord face plastification is the most common type of failure for T, Y, X and K and N gap joints with width ratios $\beta < 0.85$.

Chord punching shear may occur for joints with relatively low or high β ratios, however,
$b_i < b_o - 2\,t_o - 2(1.4a)$ to allow shear of the chord face, where a is the weld throat thickness.

Chord side wall failure is a common failure mode for T, Y and X-joints with a β ratio close or equal to 1.0.

Chord shear may occur for K-gap joints with a high β ratio or K gap joints with chords with a low h_o/b_o ratio.

9.3 ANALYTICAL MODELS

Similar to circular hollow section joints, the analytical models are used to describe the joint behaviour and to determine the governing parameters for the joint strength. Sometimes the joint behaviour will be too complicated to cover all influencing parameters and in combination with the test results semi-empirical formulae have been developed to describe the joint strength.

9.3.1 Yield line model

The yield line model, originally developed by the Danish researcher Johansen for plates, is widely used for joints between rectangular hollow sections. For joints with medium β ratios the yield line model gives a good estimate of the chord face plastification capacity [92,93,94,95]. For very small β ratios the deformation to realise the yield line pattern may be too high. For high β ratios the model predicts infinite strengths and other failure modes will be governing, e.g. punching shear or side wall failure.

In principle, the yield line method is an upper bound approach; therefore, various yield line patterns have to be examined in order to obtain the lowest capacity. However, the difference in capacity between the various yield line patterns is relatively small. Furthermore, local strain hardening effects and membrane action is ignored. Therefore, the simplified yield line pattern shown in Fig. 9.3 (model a) is generally used for T, Y and X joints instead of the more complicated pattern shown in Fig. 9.3 (model b).

The principle of the yield line method is based on equating the external energy by the external force N_1 over a deflection δ and the internal energy by the plastic hinge system with yield lines length ℓ_i and rotation angles φ_i.

$$N_1 \cdot \sin\theta_1 \cdot \delta = \Sigma \ell_i \cdot \varphi_i \cdot m_p \qquad (9.1)$$

$$m_p = \frac{1}{4} \cdot t_o^2 \cdot f_{yo} \text{ per unit length} \qquad (9.2)$$

The energy dissipated in the various yield lines is also indicated in Fig. 9.3. Equating the sum to the external work gives:

$$N_1 \cdot \sin\theta = \frac{2 f_{yo} \cdot t_o^2}{1-\beta} \left(\tan\alpha + \frac{(1-\beta)}{\tan\alpha} + \frac{\eta}{\sin\theta_1} \right) \qquad (9.3)$$

This is a minimum for:

$$\frac{dN_1}{d\alpha} = 0 \quad \text{or} \qquad (9.4)$$

$$\tan\alpha = \sqrt{1-\beta} \qquad (9.5)$$

Substitution of eq. (9.5) in (9.3) gives the capacity:

$$N_1 = \frac{f_{yo} \cdot t_o^2}{(1-\beta)} \left(\frac{2\eta}{\sin\theta_1} + 4\sqrt{1-\beta} \right) \frac{1}{\sin\theta_1} \qquad (9.6)$$

In this model some simplifications have been incorporated, i.e. the thickness of the sections has been neglected (b_o-$2t_o \approx b_o$). The same applies to the weld sizes, which have not been incorporated.

For K-joints, also yield line models can be used. However, the load transfer becomes more complicated since in the gap area the stress situation in the yield hinge is largely influenced by membrane stresses, shear stresses and work hardening. These effects complicate the models in such a way that semi-empirical formulae are used for design.

9.3.2 Punching shear model

Similar to connections between circular hollow sections, the brace can be pulled away from the chord, resulting in cracking in the chord by shear around the brace connection perimeter. Since the stiffness along the perimeter is non uniform, the deformation capacity of certain parts may not be sufficient to obtain a full effective perimeter for punching shear, i.e. only certain parts can be assumed to be effective for resisting the punching shear. For example, for a T or Y joint (Fig. 9.4) the sides along the chord walls are the stiffest part. Depending on the b_o/t_o ratio of the chord, a larger or smaller part along the cross walls will be effective, designated as b_{ep}.

Punching shear is caused by the brace load component perpendicular to the chord face, thus the punching shear criterion is given by:

$$N_1 = \frac{f_{yo}}{\sqrt{3}} \cdot t_o \left(\frac{2h_1}{\sin\theta_1} + 2b_{ep} \right) \cdot \frac{1}{\sin\theta_1} \qquad (9.7)$$

It will be clear that b_{ep} will be a function of b_o/t_o. The smaller b_o/t_o, the larger b_{ep}. The value for b_{ep} is determined experimentally.

For K-gap joints the gap size is extremely important for the effective punching shear length. For example, if the gap size is close to zero and the β value is low to medium (Fig. 9.5a), the gap part is relatively too stiff compared to the other perimeter parts, resulting in

$$N_2 \cdot \sin_2 = \frac{f_{yo}}{\sqrt{3}} \cdot t_o \left(b_2 + 2c \cdot \frac{h_2}{\sin\theta_2} \right) \text{ with } c << 1 \qquad (9.8)$$

For a large gap (Fig. 9.5c) a similar situation occurs as for T, Y and X-joints, thus

$$N_2 \cdot \sin\theta = \frac{f_{yo}}{\sqrt{3}} \cdot t_o \left(\frac{2h_2}{\sin\theta_2} + 2b_{ep} \right) \qquad (9.9)$$

For a gap where the stiffness is about the same as at the sides of the braces (Fig. 9.5b), the punching shear criterion becomes:

$$N_2 \sin\theta_2 = \frac{f_{yo}}{\sqrt{3}} \cdot t_o \left(\frac{2h_2}{\sin\theta_2} + b_2 + b_{ep} \right) \qquad (9.10)$$

Neglecting the thickness and the weld sizes, the gap value here has to satisfy [42]:

$$\frac{g}{2} \approx \frac{b_o - b_i}{2} \text{ or } \frac{g}{b_o} \approx 1 - \beta$$

Due to the deformation capacity of the material, which has been proved experimentally, the limit can be extended to

$$0.5\,(1-\beta) \le \frac{g}{b_o} \le 1.5\,(1-\beta) \qquad (9.11)$$

For larger β values these limits are impractical and a minimum gap $g = t_1 + t_2$ for welding is required.

9.3.3 Brace effective width model

The brace effective width model has a certain relationship with the punching shear model. Due to the non uniform stiffness along the connection perimeter, both have an effective part, although due to the different deformation capacity for failure in the brace and chord punching shear, the values for b_e and b_{ep} are different.
Furthermore, punching shear is caused by the brace load component perpendicular to the chord, whereas for the brace effective width criterion the brace load is taken. The effect of the angle θ has not yet been defined clearly and has been conservatively excluded up to now.

For a T, Y and X joint, the effective width criterion can thus be given by:

$$N_1 = f_{y1} \cdot t_1 \,(2h_1 + 2\,b_e - 4t_1) \qquad (9.12)$$

The term $4t_1$ has to be included to avoid the corners being counted twice. Similar to the punching shear criterion, the effective width b_e is determined experimentally and becomes larger if b_o/t_o decreases.

For K-joints with gap the same applies as for the punching shear criterion, i.e. the gap size should satisfy eq. (9.11) for having a full effective cross wall of the brace at the gap, i.e.:

$$N_2 = f_{y2} \cdot t_2 \,(2h_2 + b_2 + b_e - 4t_1) \qquad (9.13)$$

This criterion is also directly applicable to overlap joints for the overlapping brace, see Fig. 9.7.

9.3.4 Chord side wall bearing or buckling model

T, Y and X joints with a high β ratio generally fail by yielding or buckling of the chord side walls, shown in Fig. 9.8. The model used is similar to that used for beam to column connections between I-sections [42]. For joints with β = 1.0 the capacity can be easily determined by:

$$N_1 = 2f_{yo} \cdot t_o \left(\frac{h_1}{\sin\theta_1} + 5t_o \right) \cdot \frac{1}{\sin\theta_1} \qquad (9.14)$$

For slender walls the yield stress f_{yo} is replaced by a buckling stress f_k which depends on the chord web slenderness h_o/t_o.

A model which is in better agreement with the test results is based on the "4 hinge yield line" mechanism, shown in Fig. 9.9 and further elaborated by Yu [94]. In case of compression, Yu also used a buckling stress, but for a buckling length $(h_o - 2t_o)/2$.

9.3.5 Chord shear model

Similar to circular hollow section joints, this model, shown in Fig. 9.10, is based on the basic formulae for plastic design. The plastic shear load capacity is given by:

$$V_{pl} = \frac{f_{yo}}{\sqrt{3}} \cdot A_v \qquad (9.15)$$

In principle, the webs are effective for shear, but if the gap is small, a part of the top flange may also be effective, thus:

$$A_v = (2\, h_o + \alpha \cdot b_o)\, t_o \qquad (9.16)$$

The coefficient α depends on the g/t_o ratio and can be easily determined based on plastic analysis [42].
The remaining cross section has to transmit the axial force. Based on the Huber Hencky-Von Mises criterion, the following interaction formula can be determined:

$$N_{o,gap} \le (A_o - A_v) \cdot f_{yo} + A_v \cdot f_{yo} \sqrt{1 - \left(\frac{V_{Sd}}{V_{pl}} \right)^2} \qquad (9.17)$$

This formula is comparable with that for circular hollow section joints, eq. (8.10).

9.4 EXPERIMENTAL AND NUMERICAL VERIFICATION

Initially, based on the models and test evidence, either analytical or semi-empirical formulae were developed. For example, for T, Y and X joints, the yield line model is used as a lower bound for the test results and also incorporated in the recommendations [3,13,18,37,42], whereas for K joints with gap a semi-empirical formula is used. Fig. 9.11 shows a comparison between the formula for the strength of K-gap joints and the experiments [42].

In the last 10 years, the results of many numerical investigations became available [94], which may result in a reanalysis of all data and the presentation of a revision of the recommendations.

9.5 BASIC JOINT STRENGTH FORMULAE

For T, Y and X joints up to β = 0.85, the yield line model for chord face plastification is used as a basic lower bound formula for the joint resistance (Fig. 9.12). Above β = 0.85, the joint resistance is governed either by side wall failure, brace effective width or for $b_1 < b_o - 2\, t_o - 2(1.4a)$ by punching shear.

For K gap joints, a semi-empirical formula [42] based on chord face plastification is used as the basic criterion. Depending on the joint parameters, various other criteria may become critical, e.g. brace effective width, chord punching shear or chord shear.

Due to the fact that in joints of rectangular hollow sections the sections can have different orientations and depth to width ratios, many configurations are possible, resulting in many failure modes and thus many strength formulae.

For K-joints with overlap, the basic joint strength criterion is based on brace effective width. If the b/t values are restricted, other failure modes will not be critical.

9.6 EVALUATION TO DESIGN RULES

In principle, the evaluation to design rules, e.g. for K-joints with gap, is similar as described for joints between circular hollow sections.

Since for T, Y and X joints for chord face plastification a lower bound yield line criterion is used, no statistical evaluation has been carried out. In more recent analyses based on numerical results, also a deformation limit is used for the ultimate strength [75] and a full statistical treatment of the results has been carried out.

Table 9.1 shows the design resistance formulae for rectangular hollow section joints with the range of validity given in table 9.2.

It is shown that many criteria exist. However, with a smaller range of validity, the design formulae for joints between square hollow sections can be reduced such that only one check has to be carried out, see tables 9.3 and 9.4.

9.7 OTHER TYPES OF JOINTS OR OTHER LOAD CONDITIONS

9.7.1 Joints between circular braces and a rectangular chord

As far as chord face plastification concerns the joint

strength of a joint with a circular hollow section brace with diameter d_i is about $\frac{\pi}{4}$ times that of a joint with a square hollow section brace with a width $b_i = d_i$, see Fig. 9.13. This means that the same formulae can be used as for square hollow section joints, but they have to be multiplied by $\frac{\pi}{4}$ [42].

This also means that the joints have the same efficiency, i.e.: the joint strength divided by the squash load of the brace.

9.7.2 Joints between plates or I sections and RHS chords

These connections are approached in a similar manner as the rectangular hollow section joints and the same modes of failure have to be considered.

Within the scope of this book they will not be further discussed in this chapter, but reference is made to [3,12] and chapter 12.

9.7.3 Multiplanar Joints

Similar to circular hollow section joints, compared to uniplanar joints, multiplanar joints have a geometrical effect and a loading effect to be considered.

It is logical that a multiplanar brace has a geometrical influence only if the β value is large, because then the chord side wall is stiffened, see e.g. Fig. 9.14 for an XX joint.

The tendency of the loading effect is similar but less compared to joints of circular hollow sections, see Fig. 9.15.

For K joints (Fig. 9.16), the first investigations carried out by Bauer and Redwood [98] showed that the strength of multiplanar K joints can be considered to be the same as that for uniplanar joints. Later work in the U.K. and The Netherlands showed that especially for joints with high b_o/t_o ratios somewhat lower results could be obtained. Currently, similar to CHS connections, a reduction factor of 0.9 is used. Multiplanar K-connections with gap are also being investigated in more detail.

It should be noted that for a similar connection the chord preload in a multiplanar joint may be twice that of a uniplanar joint, resulting in a larger chord loading reduction effect.

9.7.4 Joints loaded by bending moments

The design resistances are derived in a similar way as for the axially loaded joints. To simplify the design, also here limitations are given for the range of validity to limit the criteria to be checked.
For Vierendeel girders it is recommended to choose joints with $\beta = 1.0$ to provide sufficient stiffness and strength.

9.8 DESIGN CHARTS

In a similar way as for circular hollow section joints, in Figs 9.17 and 9.18 the joint resistances have been expressed as an efficiency, i.e the joint resistance is given as a fraction of the yield capacity $A_i \cdot f_{yi}$ of the connected brace. This resulted in the following efficiency formula:

$$\text{eff} = \frac{N_i^*}{A_i \cdot f_{yi}} = C_e \cdot \frac{f_{yo} \cdot t_o}{f_{yi} \cdot t_i} \cdot \frac{f(n)}{\sin\theta_i} \qquad (9.18)$$

For detailed explanation, see chapter 8.8.
Using the charts of Fig. 9.19 shows that e.g. a K-gap joint with $2\gamma \approx 25$ and $b_1 = b_2$ gives a $C_k \approx 0.33$.

Thus, for an angle $\theta = 45^\circ$ a 100% efficiency can be obtained if:

$$\frac{f_{yo} \cdot t_o}{f_{yi} \cdot t_i} \geq 2.15, \text{ provided } f(n) \geq 1.0.$$

Fig. 9.18 shows the chord load function. It is noted that in contradiction to joints between circular hollow sections, the function f(n) is given as a function of the parameter $n = \sigma_o/f_{yo}$, thus the maximum compression stress in the chord is used.

9.9 CONCLUDING REMARKS

For more detailed information about joints loaded by bending moments, interaction between axial loads and bending moments as well as special types of joints, reference is made to the appropriate literature, see [3,33,37,41,42,95,96,99,100].

Table 9.1: Design resistance of welded joints between rectangular hollow sections

type of joints	factored joint resistane (i = 1,2)	
T-, Y- and X-connections	$\beta \le 0.85$	basis: chord face yielding
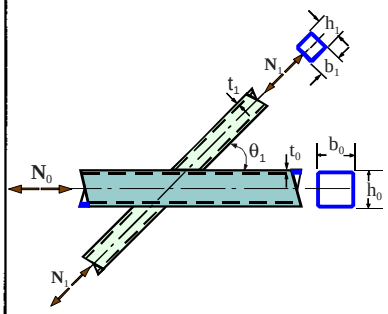	$N_1^* = \frac{f_{y0} \cdot t_0^2}{(1-\beta)\sin\theta_1} \cdot \left[\frac{2\eta}{\sin\theta_1} + 4(1-\beta)^{0.5}\right] \cdot f(n)$	
	$\beta = 1.0$ chord side wall failure[1]	for $0.85 < \beta \le 1.0$ use linear interpolation of chord face yielding and chord side wall criteria
	$N_1^* = \frac{f_k \cdot t_0}{\sin\theta_1} \cdot \left[\frac{2h_1}{\sin\theta_1} + 10\,t_0\right]$	
	$\beta > 0.85$	basis: effective width
	$N_1^* = f_{y1} \cdot t_1 [2h_1 - 4t_1 + 2b_e]$	
	$0.85 \le \beta \le 1 - 1/\gamma$	basis: punching shear
	$N_1^* = \frac{f_{y0} \cdot t_0}{\sqrt{3}\sin\theta_1} \cdot \left[\frac{2h_1}{\sin\theta_1} + 2b_{ep}\right]$	
K- and N-gap connections		basis: chord face yielding
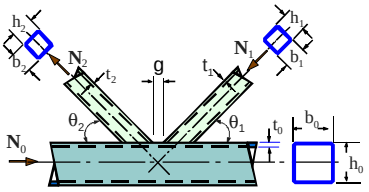	$N_i^* = 8.9 \cdot \frac{f_{y0} \cdot t_0^2}{\sin\theta_i} \cdot \left[\frac{b_1 + b_2 + h_1 + h_2}{4b_0}\right] \cdot \gamma^{0.5} \cdot f(n) \quad (i = 1,2)$	
		basis: chord shear
	$N_i^* = \frac{f_{y0} \cdot A_V}{\sqrt{3} \cdot \sin\theta_i}$ Also, $N_{0(\text{in gap})}^* \le (A_0 - A_V) f_{y0} + A_V \cdot f_{y0} [1 - (V/V_{p0})^2]^{0.5}$	
		basis: effective width
	$N_i^* = f_{yi} \cdot t_i [2h_i - 4t_i + b_i + b_e]$	
	$\beta \le 1 - 1/\gamma$	basis: punching shear
	$N_i^* = \frac{f_{yo} \cdot t_0}{\sqrt{3}\sin\theta_i} \cdot \left[\frac{2h_i}{\sin\theta_i} + b_i + b_{ep}\right]$	
K- and N-overlap joints	similar to joints of square hollow sections (Table 9.3)	
circular braces	multiply formulae by $\pi/4$ and replace $b_{1,2}$ and $h_{1,2}$ by $d_{1,2}$	

functions

tension: $f_k = f_{y0}$ compression: $f_k = f_{kn}$ (T-, Y-joints) $f_k = 0.8 \sin\theta_1 \cdot f_{kn}$ (X-joints)

f_{kn} = buckling stress, using a column slenderness ratio of $3.46(h_0/t_0 - 2)(1/\sin\theta_1)^{0.5}$

$f(n) = 1.0$ for $n \ge 0$ (tension) $f(n) = 1.3 + \frac{0.4}{\beta} \cdot n$ for $n < 0$ but ≤ 1.0 (compression)	$V_p = \frac{f_{y0} \cdot A_V}{\sqrt{3}}$ $\alpha = \left(\frac{1}{1 + \frac{4g^2}{3t_0^2}}\right)^{0.5}$ For square and rectangular braces, $A_v = (2h_0 + \alpha \cdot b_0) \cdot t_0$ For circular braces, $A_v = 2h_0 \cdot t_0$	
$b_e = \frac{10}{b_0/t_0} \cdot \frac{f_{y0} \cdot t_0}{f_{yi} \cdot t_i} \cdot b_i$ $\le b_i$	$b_{ep} = \frac{10}{b_0/t_0} \cdot b_i$ $\le b_i$	$b_{e(ov)} = \frac{10}{b_j/t_j} \cdot \frac{f_{yj} \cdot t_j}{f_{yi} \cdot t_i} \cdot b_i$ $\le b_i$

Note[1]: For X-connections with angles $\theta < 90°$, the chord side walls must be checked for shear

Table 9.2 Range of validity for welded joints between rectangular hollow sections

type of joints	joint parameters (i = 1 or 2, j = overlapped brace)						
	b_i/b_0 h_i/b_0	b_i/t_i, h_i/t_i, d_i/t_i compression	tension	h_i/b_i	b_0/t_0 h_0/t_0	gap/overlap b_i/b_j t_i/t_j	eccentricity
T, Y, X	≥ 0.25	$\leq 1.25\sqrt{\frac{E}{f_{y1}}}$	≤ 35	$0.5 \leq \frac{h_i}{b_i} \leq 2$	≤ 35		
K, N gap	$\geq 0.1 + 0.01\frac{b_o}{t_0}$ $\beta \geq 0.35$	≤ 35	≤ 35		≤ 35	$0.5(1-\beta) \leq \frac{g}{b_0} \leq 1.5(1-\beta)$ [b] $g \geq t_i + t_2$	$-0.55 \leq \frac{e}{h_0} \leq 0.25$
K, N overlap	≥ 0.25	$\leq 1.1\sqrt{\frac{E}{f_{y1}}}$			≤ 40	$25\% \leq O_v \leq 100\%$ $\frac{t_i}{t_j} \leq 1.0$, $\frac{b_i}{b_j} \geq 0.75$	
for circular braces (web members)	$0.4 \leq \frac{d_i}{b_0} \leq 0.8$	$\leq 1.5\sqrt{\frac{E}{f_{y1}}}$	≤ 50	limitations as above for $d_i = b_i$			

Note: [a] f_{yi}, $f_{yj} \leq 355$ N/mm², f_{yi} (or f_{yj})/$f_{ui} \leq 0.8$

[b] if g > the larger of $1.5(1-\beta)\cdot b_o$ and (t_1+t_2), treat the effective width and punching shear acc.to table 9.1, as for a T- or Y-joint

Table 9.3 Design resistance of welded joints between square hollow sections

type of joints	factored joint resistane (i = 1,2)
T-, Y- and X-joints	$\beta \le 0.85$ basis: chord face yielding
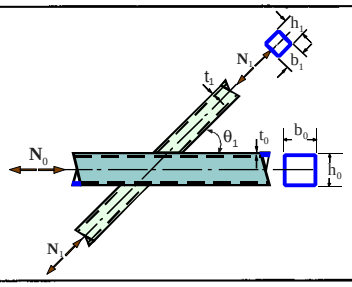	$N_1^* = \frac{f_{y0} \cdot t_0^2}{(1-\beta)\sin\theta_1} \cdot \left[\frac{2\beta}{\sin\theta_1} + 4(1-\beta)^{0.5}\right] \cdot f(n)$
K- and N-gap joints	$\beta \le 1.0$ basis: chord face plastification
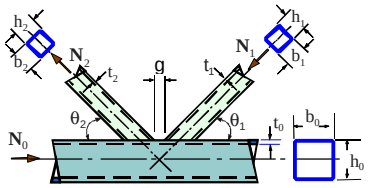	$N_i^* = 8.9 \cdot \frac{f_{y0} \cdot t_0^2}{\sin\theta_i} \cdot \left[\frac{b_1 + b_2}{2 b_0}\right] \cdot \gamma^{0.5} \cdot f(n)$ $(i = 1,2)$
K- and N-overlap joints[1]	$25\% \le O_v < 50\%$ basis: effective width
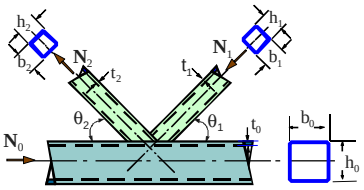	$N_i^* = f_{yi} \cdot t_i \left[\left(\frac{O_v}{50}\right)(2h_i - 4t_i) + b_e + b_{e(ov)}\right]$
	$50\% \le O_v < 80\%$ basis: effective width
	$N_i^* = f_{yi} \cdot t_i \,[2h_i - 4t_i + b_e + b_{e(ov)}]$
	$O_v \ge 80\%$ basis: effective width
	$N_i^* = f_{yi} \cdot t_i \,[2h_i - 4t_i + b_i + b_{e(ov)}]$
circular braces	multiply formulae by $\pi/4$ and replace $b_{1,2}$ and $h_{1,2}$ by $d_{1,2}$
functions	
$f(n) = 1.0$ for $n \ge 0$ (tension)	$f(n) = 1.3 + \frac{0.4}{\beta} \cdot n$ for $n < 0$ (compression) but ≤ 1.0
$b_e = \frac{10}{b_0/t_0} \cdot \frac{f_{y0} \cdot t_0}{f_{yi} \cdot t_i} \cdot b_i$ $\le b_i$	$b_{e(ov)} = \frac{10}{b_j/t_j} \cdot \frac{f_{yj} \cdot t_j}{f_{yi} \cdot t_i} \cdot b_i$ $\le b_i$

Note [1]: Effective width computations need only be done for the overlapping brace member. However the efficiency (the joint resistance divided by the full yield capacity of the brace member), of the overlapped brace member is not to be taken higher than that of the overlapping brace member.

Table 9.4 Range of validity for welded joints between square hollow sections

type of joints	joint parameters (i = 1 or 2, j = overlapped brace)						
	b_i/b_0	b_i/t_i compression	b_i/t_i tension	b_0/t_0	$(b_1 + b_2)/2b_i$ b_i/b_j t_i/t_j	gap/overlap	eccentricity
T, Y, X	$0.25 \le \frac{b_i}{b_0} \le 0.85$ [a]	$\le 1.25\sqrt{\frac{E}{f_{y1}}}$	$\frac{b_2}{t_2} \le 35$	$10 \le \frac{b_0}{t_0} \le 35$ [a]			
K, N gap	$\ge 0.1 + 0.01\frac{b_0}{t_0}$ $\frac{b_i}{b_0} \ge 0.35$	≤ 35		$15 \le \frac{b_0}{t_0} \le 35$ [a]	$0.6 \le \frac{b_1 + b_2}{2b_i} \le 1.3$ [a] i = 1 or 2	$0.5(1-\beta) \le \frac{g}{b_0} \le 1.5(1-\beta)$, but $g \ge t_i + t_2$	$-0.55 \le \frac{e}{h_0} \le 0.25$
K, N overlap	≥ 0.25	$\le 1.1\sqrt{\frac{E}{f_{y1}}}$		$\frac{b_0}{t_0} \le 40$	$\frac{t_i}{t_j} \le 1.0$ $\frac{b_i}{b_j} \ge 0.75$	$25\% \le O_v \le 100\%$	
for circular bracings (web members)	$0.4 \le \frac{d_i}{b_0} \le 0.8$	$\frac{d_i}{t_i} \le 1.5\sqrt{\frac{E}{f_{y1}}}$	$\frac{d_2}{t_2} \le 50$	limitations as above for $d_i = b_i$			

Note: [a] Outside this range of validity other failure criteria may be governing; e.g., punching shear, effective width, side wall failure, chord shear or local buckling. If these particular limits of validity are violated the connection may still be checked as one having a rectangular chord using Table 9.1, provide the limits of validity in Table 9.2 are still met.

T-joint	Y-joint
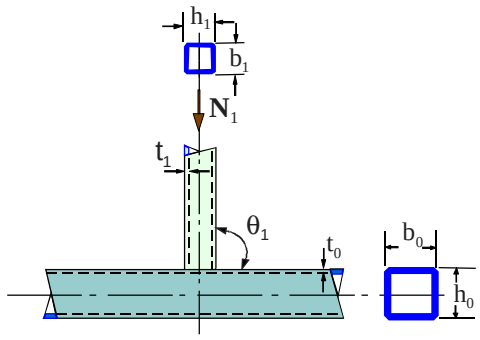	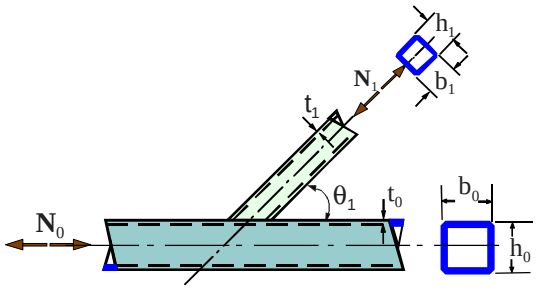
X-joint	**K-joint with gap**
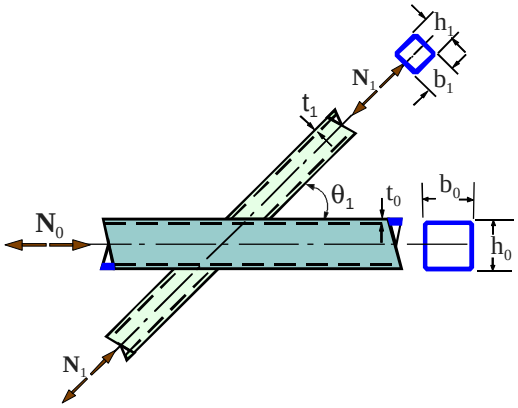	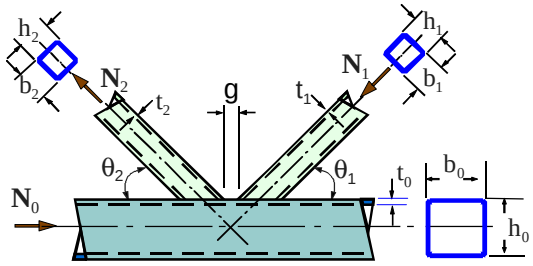
N-joint with overlap	**KT-joint with gap**
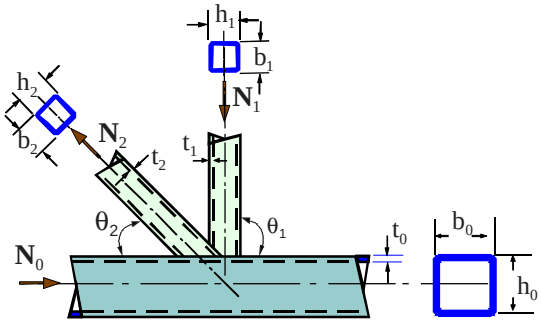	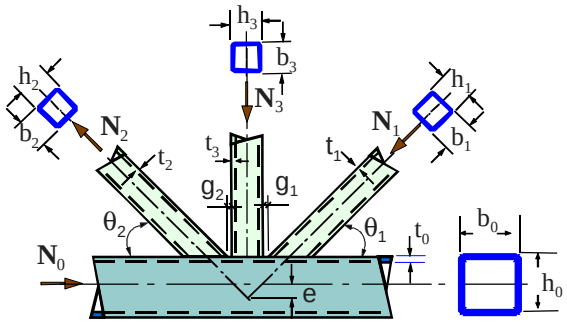

Fig. 9.1 Welded RHS connections

(a) Brace failure

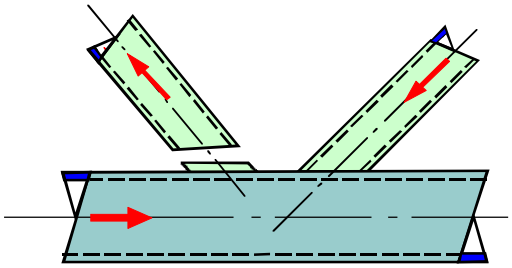

(e) Chord punching shear failure

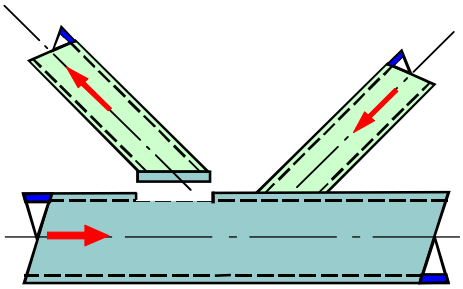

(b) Weld failure

as (a) but failure in weld

(f) Chord side wall yielding or buckling

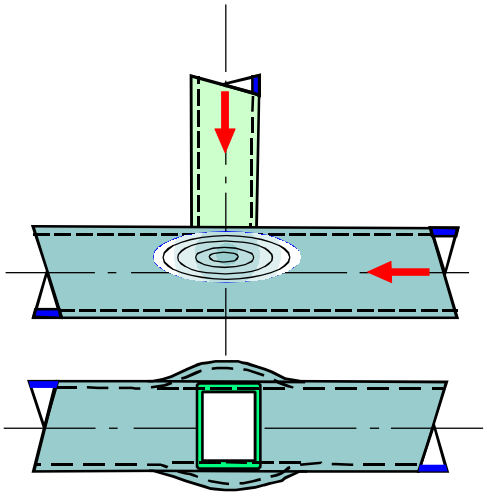

(c) Lamellar tearing

see e.g. Fig. 7.6c

(g) Chord local buckling

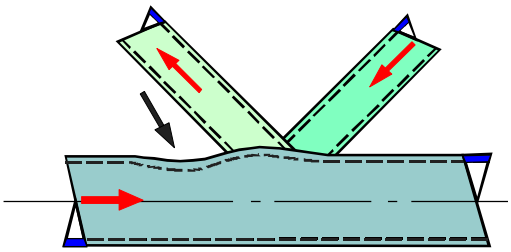

(d) Chord face plastification

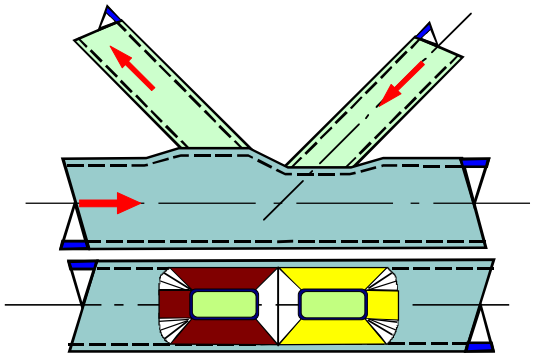

(h) Chord shear failure

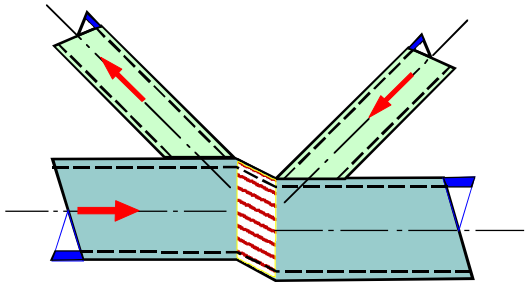

Fig. 9.2 Failure modes for welded RHS connections

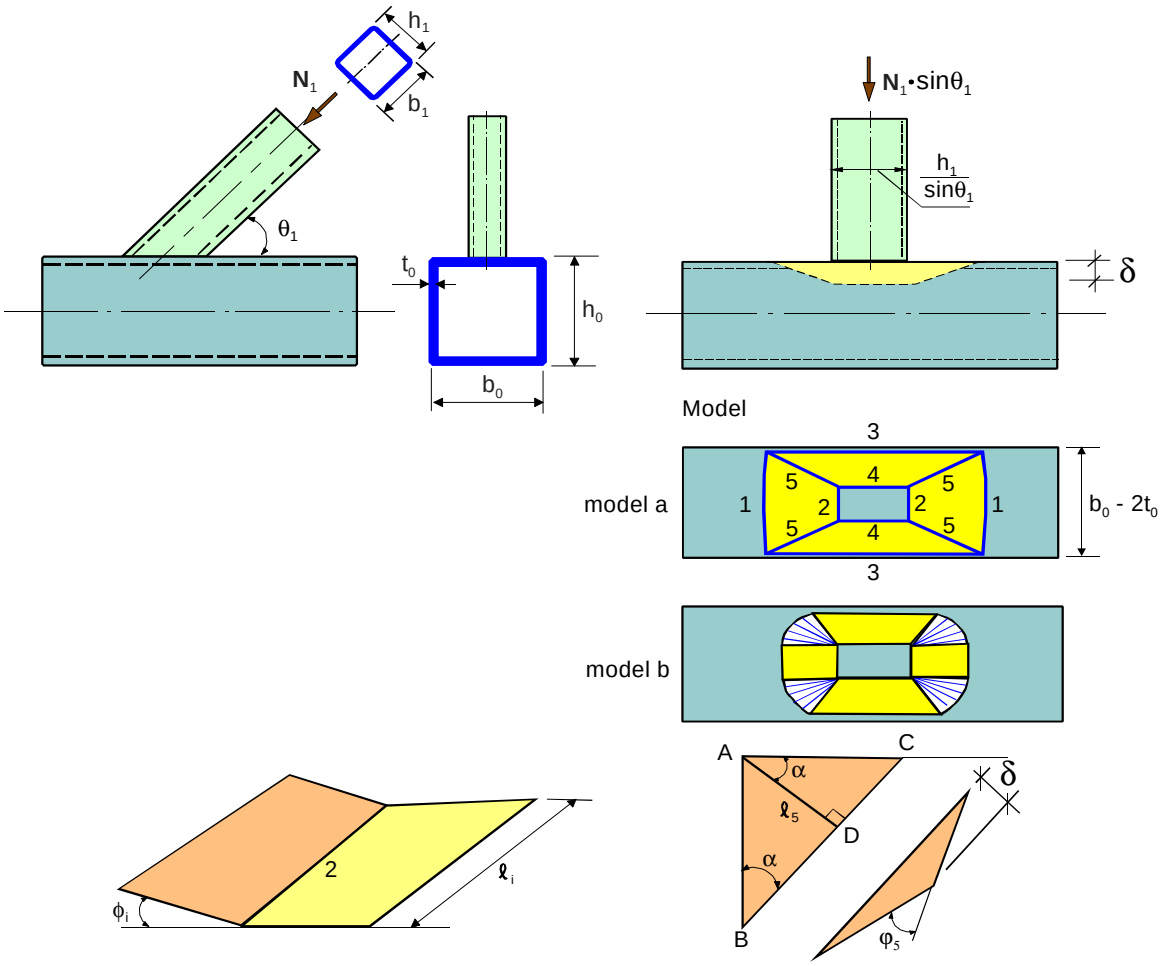

The total energy dissipated in the yield lines 1 to 5 is as follows:

yield lines 1 : $2b_0 \dfrac{2\delta}{(b_0 - b_1)\cot\alpha} \cdot m_p = \dfrac{4\tan\alpha}{1-\beta} \cdot \delta \cdot m_p$

yield lines 2 : $2b_1 \cdot \dfrac{2\delta}{(b_0 - b_1)\cot\alpha} \cdot m_p = \dfrac{4\tan\alpha}{1-\beta} \cdot \delta \cdot m_p$

yield lines 3 : $2\left(\dfrac{h_1}{\sin\theta_1} + 2\,\dfrac{b_0 - b_1}{2}\cot\alpha\right)\dfrac{2\delta}{b_0 - b_1} \cdot m_p = \left\{\dfrac{4\eta}{(1-\beta)\sin\theta_1} + 4\cot\alpha\right\} \cdot \delta \cdot m_p$

yield lines 4 : $2\,\dfrac{h_1}{\sin\theta_1} \cdot \dfrac{2\delta}{b_0 - b_1} \cdot m_p = \dfrac{4\eta}{(1-\beta)\sin\theta_1} \cdot \delta \cdot m_p$

yield lines 5 : $4\ell_5\left(\dfrac{\delta}{\ell_5 \cdot \tan\alpha} + \dfrac{\delta}{\ell_5 \cdot \cot\alpha}\right) \cdot m_p = 4(\tan\alpha + \cot\alpha) \cdot \delta \cdot m_p$

with $m_p = \dfrac{f_{yo} \cdot t_0^{\,2}}{4}$

Total energy $E_d = \dfrac{8 \cdot m_p \cdot \delta}{(1-\beta)}\left\{\tan\alpha + \dfrac{(1-\beta)}{\tan\alpha} + \dfrac{\eta}{\sin\theta_1}\right\}$

Fig. 9.3 Yield line model for a T, Y and X joint

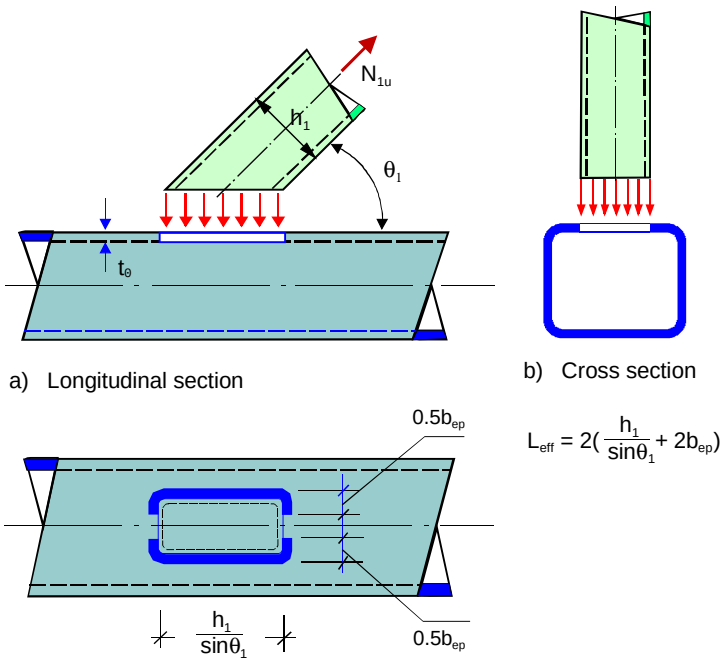

$$L_{eff} = 2\left(\frac{h_1}{\sin\theta_1} + 2b_{ep}\right)$$

Fig. 9.4 Chord punching shear model for a T, Y and X joint

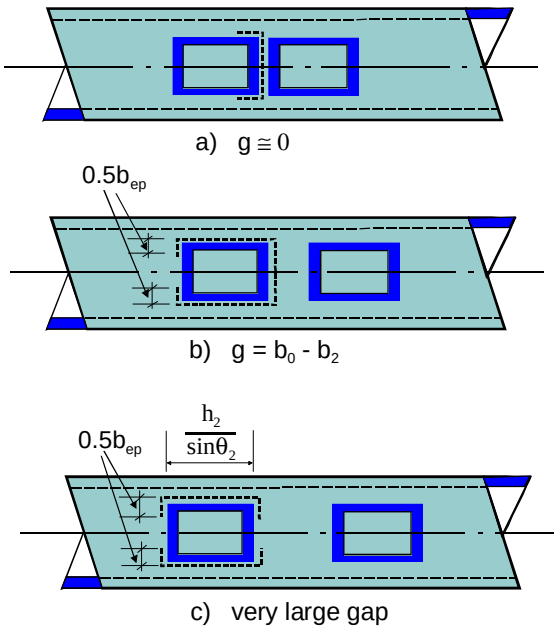

Fig. 9.5 Chord punching shear model for a K-gap joint (chord face)

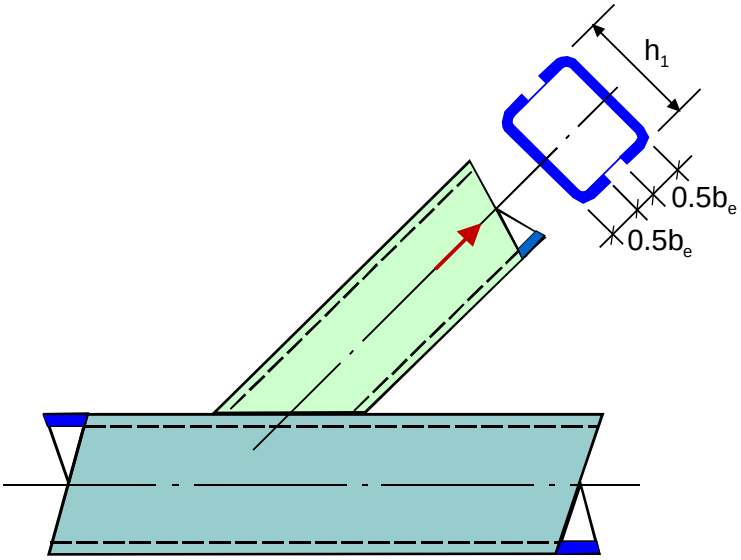

Fig. 9.6 Brace effective width criterion for T, Y and X joints

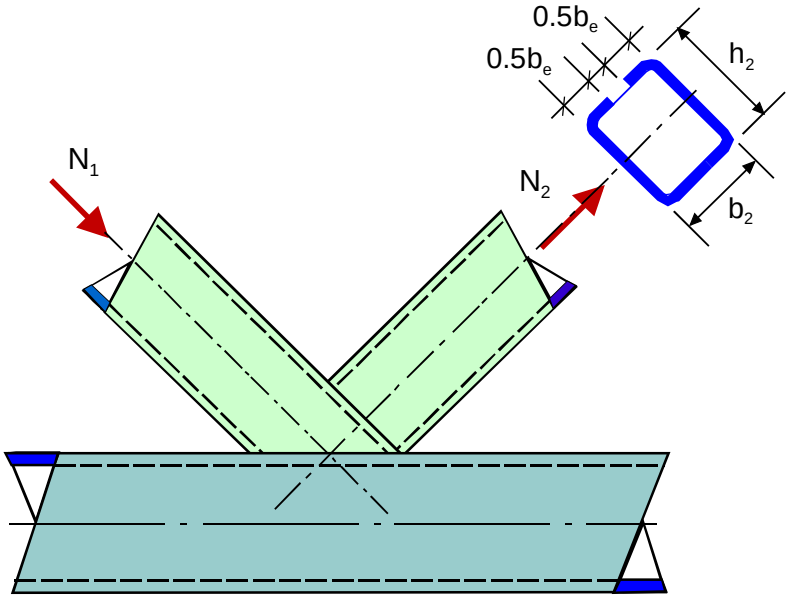

Fig. 9.7 Brace effective width criterion for overlap joints

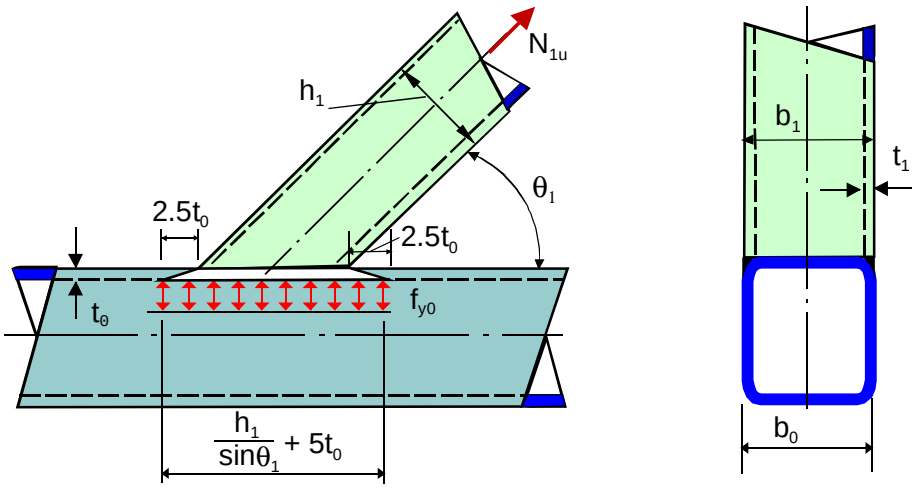

a) Elevation b) Cross-section

Fig. 9.8 Chord side wall failure model

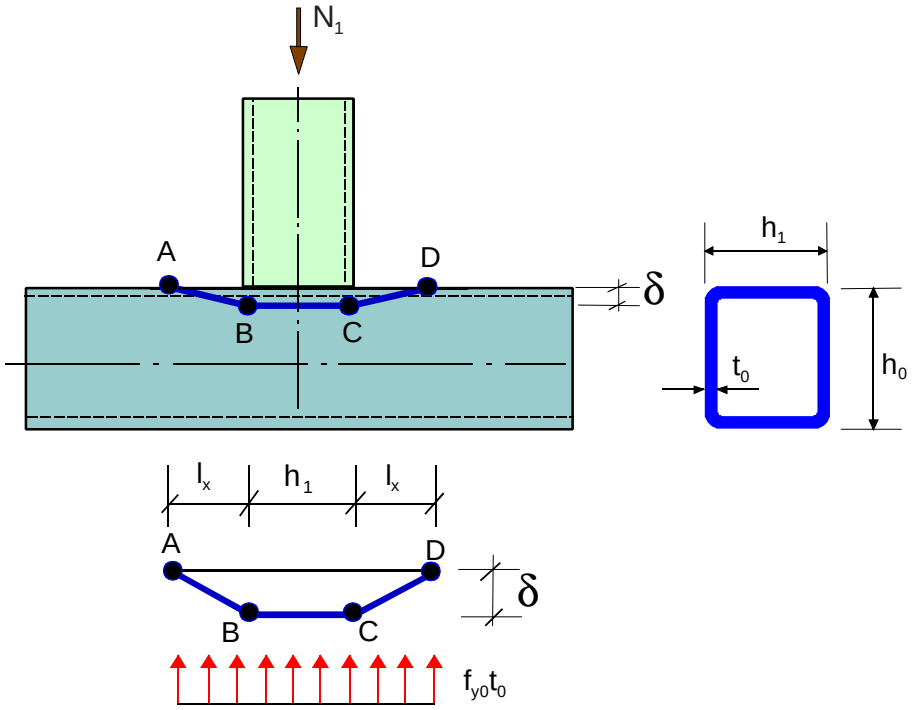

Fig. 9.9 4 hinge yield line model

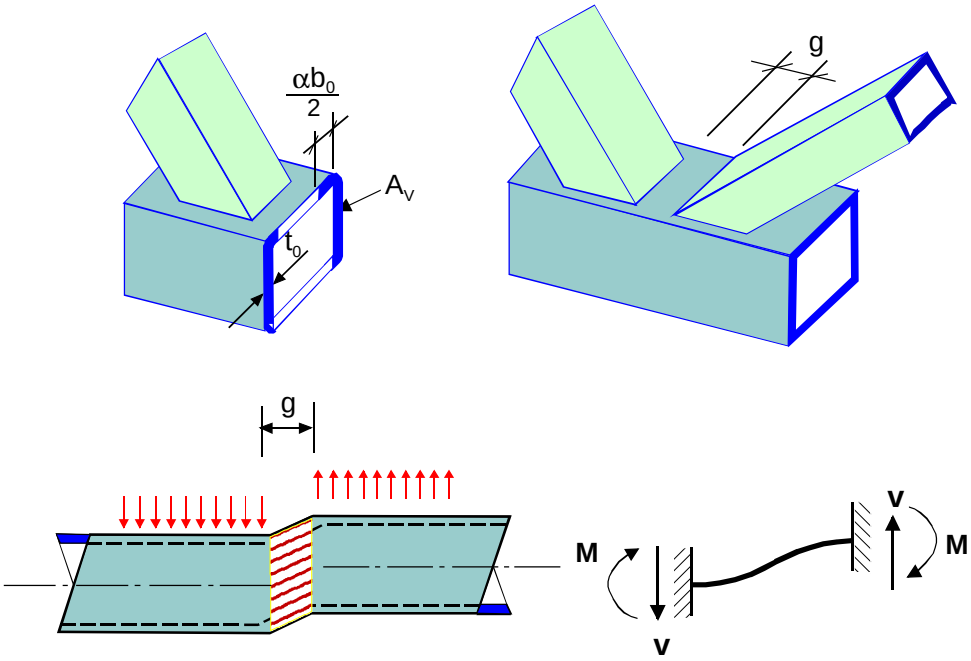

Fig. 9.10 Chord shear failure model

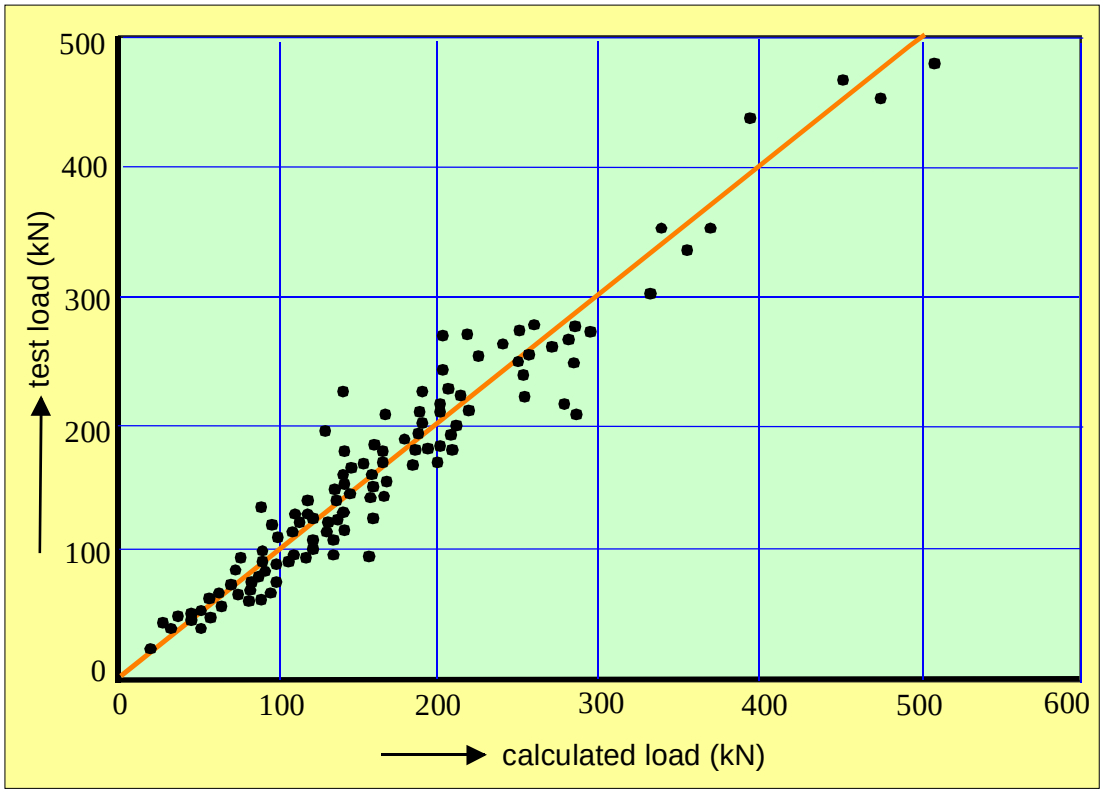

Fig. 9.11 Comparison between experiments and the mean joint strength equation for K-joints with gap [42]

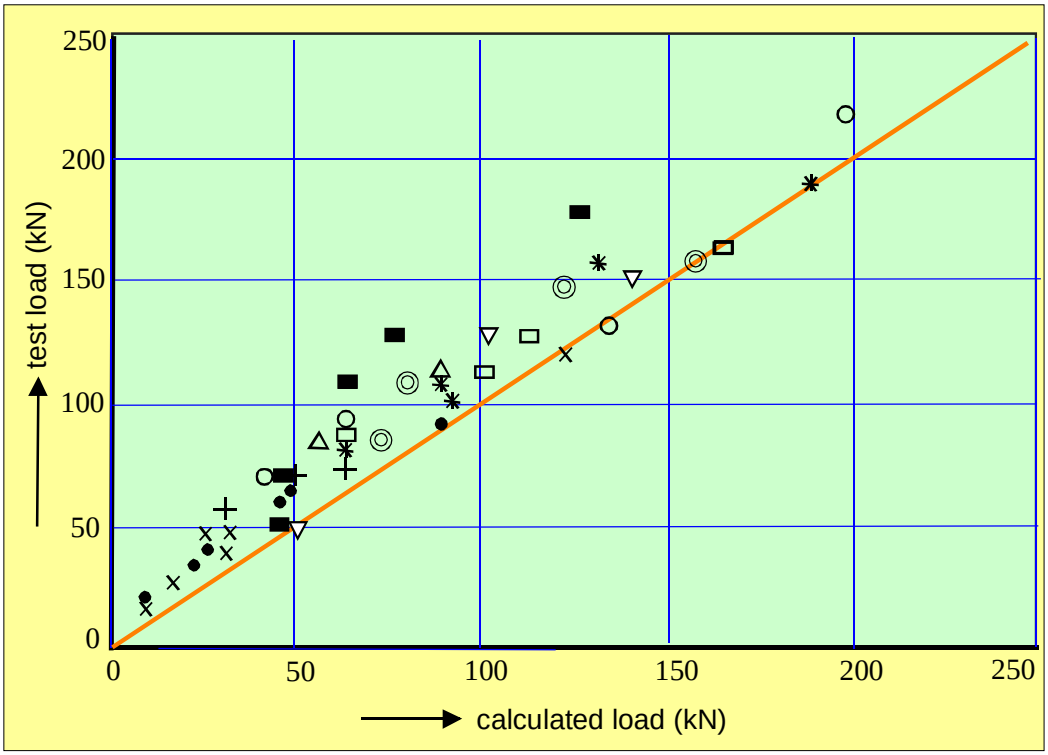

Fig. 9.12 Evaluation of the chord plastification criterion for T, Y and X joints based on the yield line model [42]

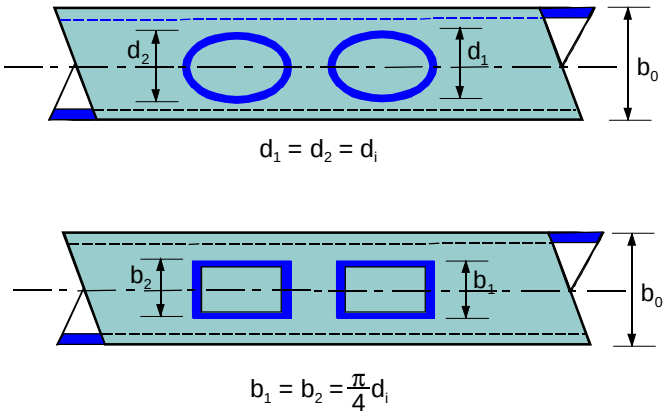

Fig. 9.13 Comparison of a K-joint with a circular brace and an equivalent joint with a square brace (chord face)

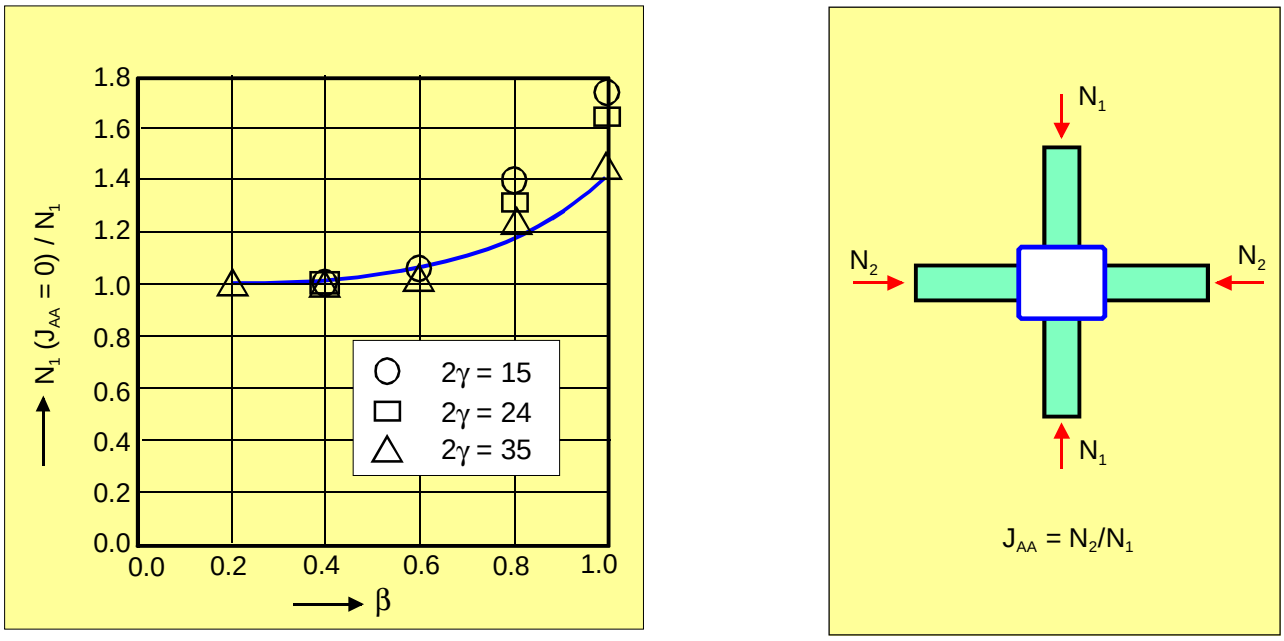

Fig. 9.14 Multiplanar geometry effect for an XX joint of square hollow sections [94]

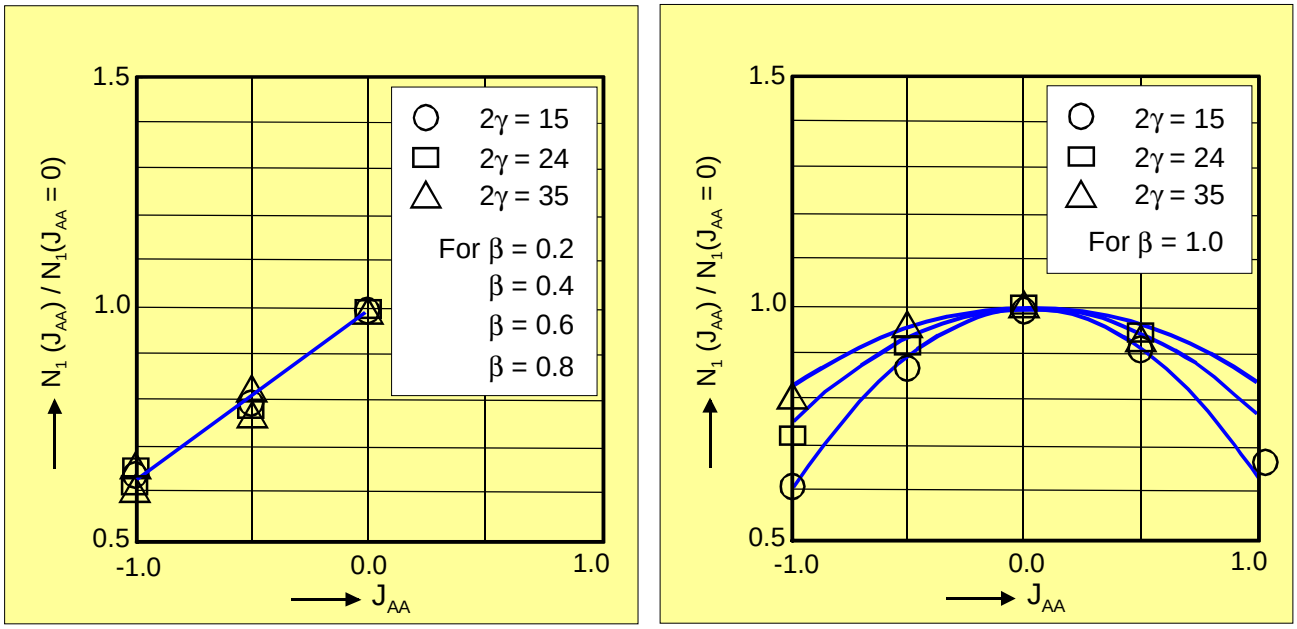

Fig. 9.15 Multiplanar loading effect for an XX joint of square hollow sections [94]

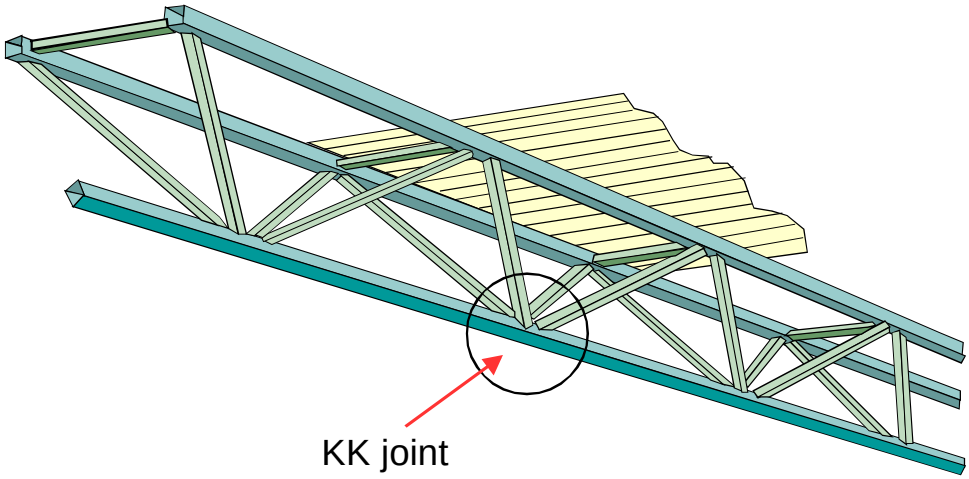

Fig. 9.16 Multiplanar K joint of square hollow sections

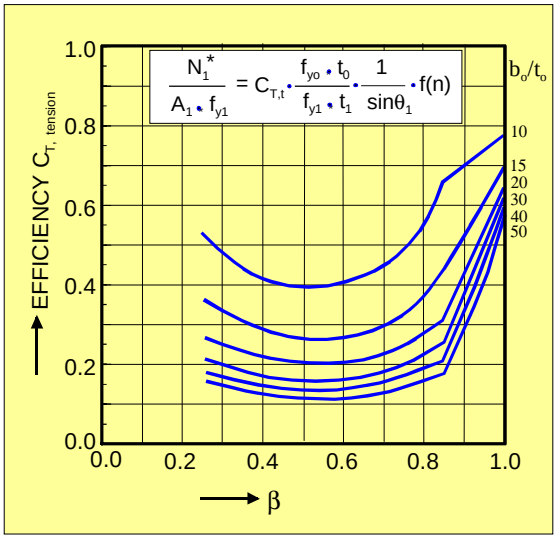

Fig. 9.17 Efficiency for T, Y and X joints of square hollow sections

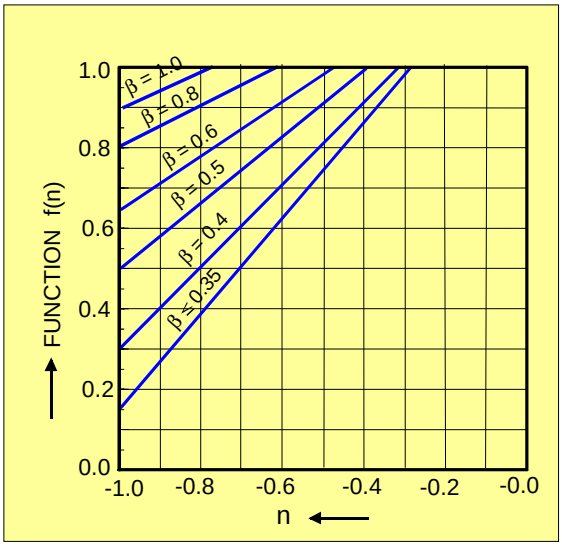

Fig. 9.18 Chord load function for square hollow section joints

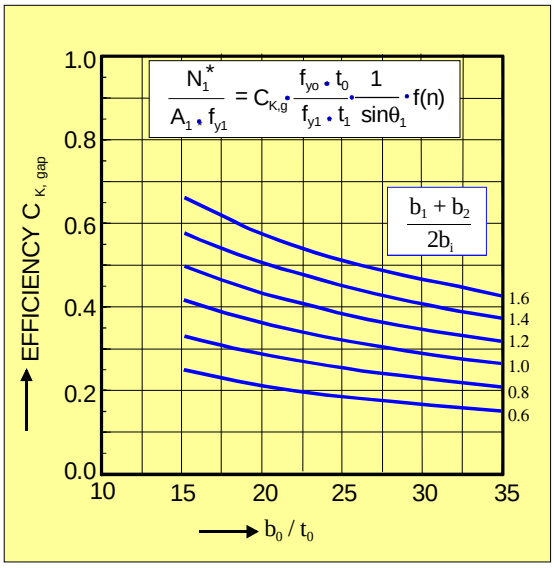

Fig. 9.19 Efficiency for K-gap joints between square hollow sections

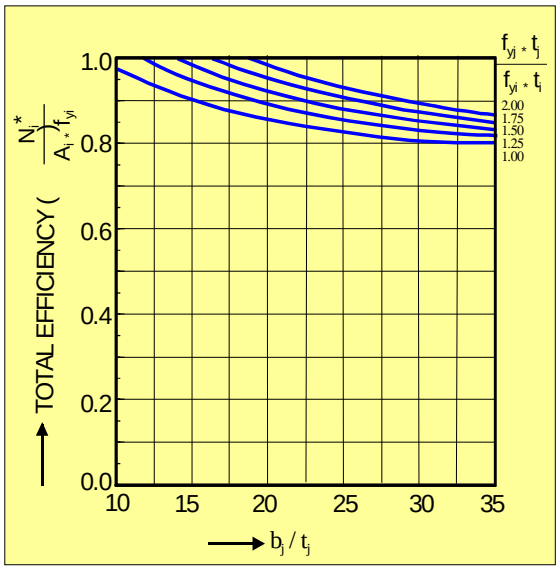

Fig. 9.20 Efficiency for K-overlap joints (100% overlap) between square hollow sections

10. WELDED CONNECTIONS BETWEEN HOLLOW SECTIONS AND OPEN SECTIONS

10.1 INTRODUCTION

Hollow sections and open sections are used in various ways, for example:
- hollow section braces and open section chords as shown in Figs. 10.1 and 10.2(a).
- open section braces and rectangular hollow section chords, shown in Fig. 10.2(b).
- I-section beams connected to hollow section columns, dealt with in chapter 12.

Other combinations, but with bolted connections, are considered in chapter 11.

In this chapter it will be shown that in many respects the behaviour of connections between open sections and hollow sections is comparable to that of connections between rectangular hollow sections.

10.2 MODES OF FAILURE

Following the same procedure as described in chapter 7, the following failure modes (Fig. 10.3) can be expected and observed for connections between hollow section braces and I-section chords:
- brace failure (yielding, local buckling)
- weld failure
- lamellar tearing
- chord web failure (yielding, local buckling)
- chord shear failure
- chord local buckling

Chord face plastification will not occur, since this can only take place after excessive yielding of the chord web. As indicated before, the welds should be stronger than the connected members, assuming the latter are loaded to their limit, thus the welds should satisfy certain requirements, see 8.2.

Similar to the other connections, lamellar tearing should be avoided by choosing proper material. Local buckling of the members can be avoided by choosing proper diameter, width and depth-to-thickness ratios, thus by limiting the range of validity.

As a result, the governing failure modes to be considered are:
- brace failure (effective width)
- chord web failure
- chord shear failure

For connections between hollow section braces and channel section chords it can be easily shown that with the same limitations as discussed above, the failure modes (Fig. 10.4) to be considered in more detail are:
- brace effective width
- chord face plastification
- chord punching shear failure
- chord side wall failure
- chord shear failure

Since hot rolled channel sections (UNP) have thick flanges, which act as walls here, chord side wall failure will not be critical for these particular sections.
In principle, the other failure modes can be approached in a similar way as for connections between rectangular hollow sections [42,102,103]. If chords of cold formed channel sections are used, the situation will be different, since the side walls will deform when the top face deforms, resulting in lower strengths.
For detailed information about connections with channel section chords, reference can be made to [42].

The connections of Fig. 10.2 with welded angles or channels at the sides of a rectangular hollow section are not different from other connections in open sections. Besides weld failure, chord side wall failure (generally not critical) and chord shear failure have to be considered.

10.3 ANALYTICAL MODELS

10.3.1 Brace effective width

The most effective part of the brace will be located at the crossing with the chord web, shown in Fig. 10.5. Here, the same model can be used as for beam to column connections of open sections, i.e. for a T, Y or X-joint:

$$N_1 = 2\, b_e \cdot t_1 \cdot f_{y1} \qquad (10.1)$$

$$\text{with } b_e = t_w + 2r_o + (c \cdot \frac{f_{yo}}{f_{y1}} \cdot t_o \qquad (10.2)$$

If $b_e > b_1$, it is conservatively proposed to use the approach shown in Fig. 10.5, which has been verified with experiments.

Similar to joints of rectangular hollow sections, the effective width criterion is also used for overlap joints.

10.3.2 Chord web failure model

The load from the brace has to be transferred by an effective area of the chord web, see Fig. 10.6. The effective areas are located underneath at the location where the brace walls cross the chord web. Similar to the formulae used for beam-to-column connections of open sections:

$$N_1 \cdot \sin\theta_1 = b_m \cdot t_w \cdot f_{yo} \qquad (10.3)$$

with

$$b_m = 2\,\{t_1 + c\,(t_o + r_o)\} \qquad (10.4)$$

$$b_m \le \frac{h_1}{\sin\theta_1} + c\,(t_o + r_o) \qquad (10.5)$$

For beam-to-column connections c = 5 is used, which was shown to be also valid for these connections [42].

10.3.3 Chord shear model

Similar to connections with a rectangular hollow section chord, an interaction formula can be determined for the combined effect of shear and axial load at the gap location in the chord, see Fig. 10.7.
By equilibrium, the moment in flange is:

$$M_f = \frac{V_f \cdot g}{2} \qquad (10.6)$$

The interaction formula for a rectangular cross section, assuming the web yields, is:

$$\left(\frac{M_f}{M_{p\ell,f}}\right)^2 + \left(\frac{V_f}{V_{p\ell,f}}\right)^2 = 1 \qquad (10.7)$$

$$M_{p\ell,f} = \frac{b_o \cdot t_o^2}{4} \cdot f_{yo} \qquad (10.8)$$

$$V_{p\ell,f} = b_o \cdot t_o \cdot \frac{f_{yo}}{\sqrt{3}} \qquad (10.9)$$

Combination of (10.6), (10.8) and (10.9) results in:

$$\frac{M_f}{M_{p\ell,f}} = \frac{V_f}{V_{p\ell,f}} \cdot \frac{2g}{t_o\sqrt{3}} \qquad (10.10)$$

or

$$\frac{V_f}{V_{p\ell,f}} = \sqrt{\frac{1}{1 + \frac{4g^2}{3t_o^2}}} \qquad (10.11)$$

Thus, for a specified section the active part of the flange can be specified as:

$$\alpha \cdot b_o \cdot t_o \qquad (10.11)$$

with

$$\alpha = \sqrt{\frac{1}{1 + \frac{4g^2}{3t_o^2}}} \qquad (10.12)$$

For high sections the effectiveness of the bottom flange will be considerably lower than that for the top flange and the following effective shear area is proposed for connections with RHS braces:

$$A_v = (A_o - 2\,b_o \cdot t_o) + \alpha \cdot b_o \cdot t_o + (t_w + 2r_o)t_o \qquad (10.13)$$

If circular hollow section braces are used, the chord flange is less stiffened at the gap location; consequently, α is lower. Based on tests, here $\alpha = 0$ is proposed.

For the interaction between the axial load and the shear load at the gap location, based on the Huber-Hencky-Von Mises criterion, the following formula now applies (see 9.3.5):

$$N_o = (A_o - A_v)\,f_{yo} + A_v \cdot f_{yo}\sqrt{1 - \left(\frac{V}{V_{p\ell}}\right)^2} \qquad (10.14)$$

with

$$V_{p\ell} = A_v \cdot \frac{f_{yo}}{\sqrt{3}} \qquad (10.15)$$

10.4 EXPERIMENTAL VERIFICATION

The formulae developed in 10.3 for joints with an I-section chord have been verified by experiments [42,102], see e.g. Fig. 10.8. Later on, some small modifications to the original equation have been adopted for brace effective width to make it more in line with the flange effective width equation used for beam- to-column connections.

Generally, chord web failure and chord shear failures show more deformation capacity than brace effective width failures.

The experiments further showed that within certain parameter limits the brace effective width criterion does not have to be checked, since the other criteria are governing.

The design criteria for joints with a hot formed channel chord section have also been checked by tests. It was shown that for medium to high width ratios, β, chord shear failure was the most common failure mode for the K-gap joints and chord punching shear or chord face plastification was governing for low β values. For 100% overlap joints only the brace effective width has to be checked.

10.5 EVALUATION TO DESIGN CRITERIA

In principle, the same approach has been used as for the connections discussed in chapters 8 and 9. However, due to the limited number of tests, no thorough statistical analysis was carried out. Due to the lower deformation capacity, a higher γ_M factor (1.25) or a higher margin between test results and design formulae was taken for the brace effective width criterion compared to the analytical yield criteria, e.g. for chord shear failure.

10.6 JOINTS PREDOMINANTLY LOADED BY BENDING MOMENTS

Here, only the beam-to-column connections with a hollow section brace and an I-section column are of practical interest.
The design strength here is governed by the beam effective width failure with formulae based on eqs. 10.1 and 10.2 (see Fig. 10.9) and column web failure based on eqs. 10.3 to 10.5 (see Fig. 10.10).

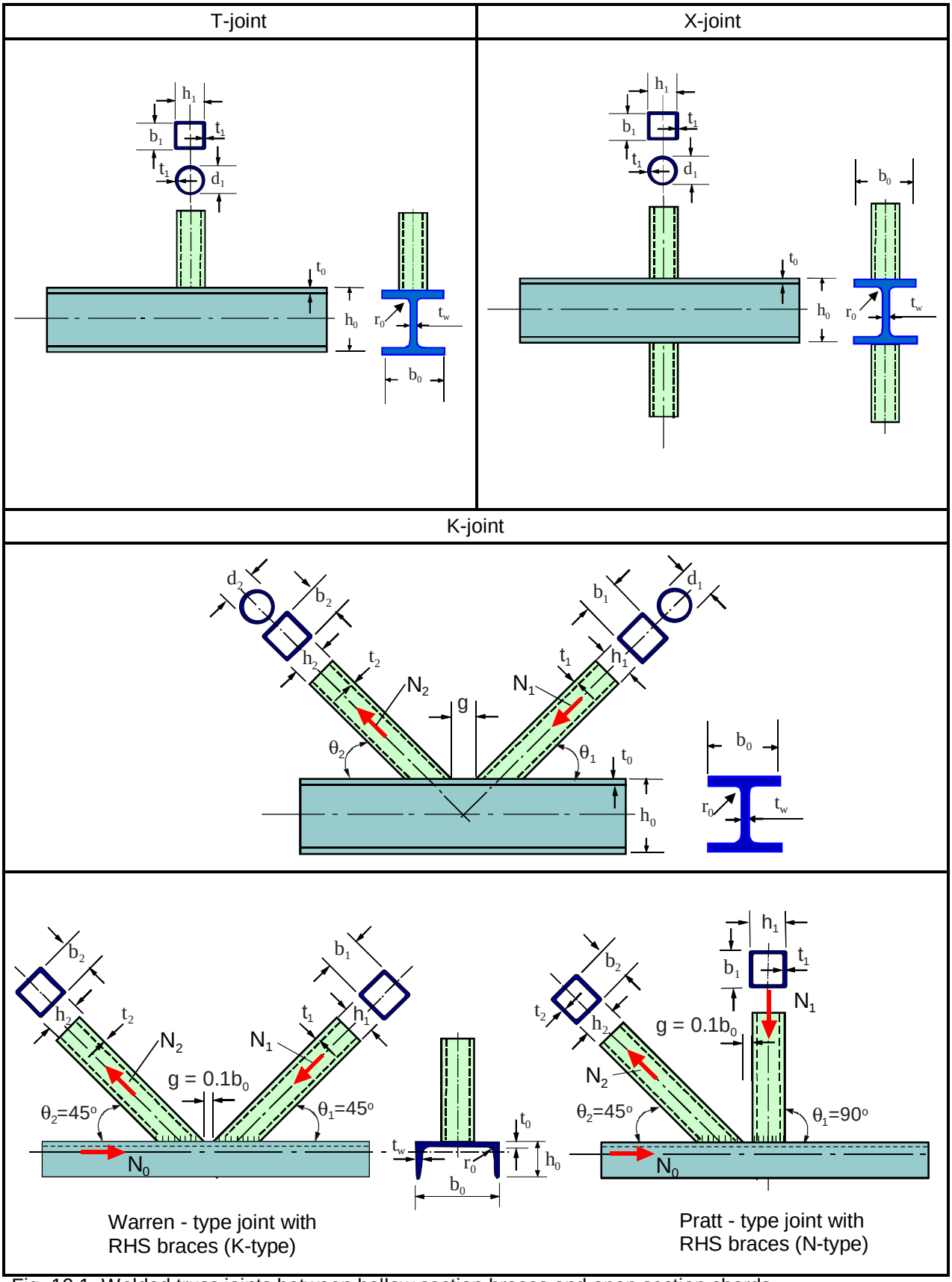

Fig. 10.1 Welded truss joints between hollow section braces and open section chords

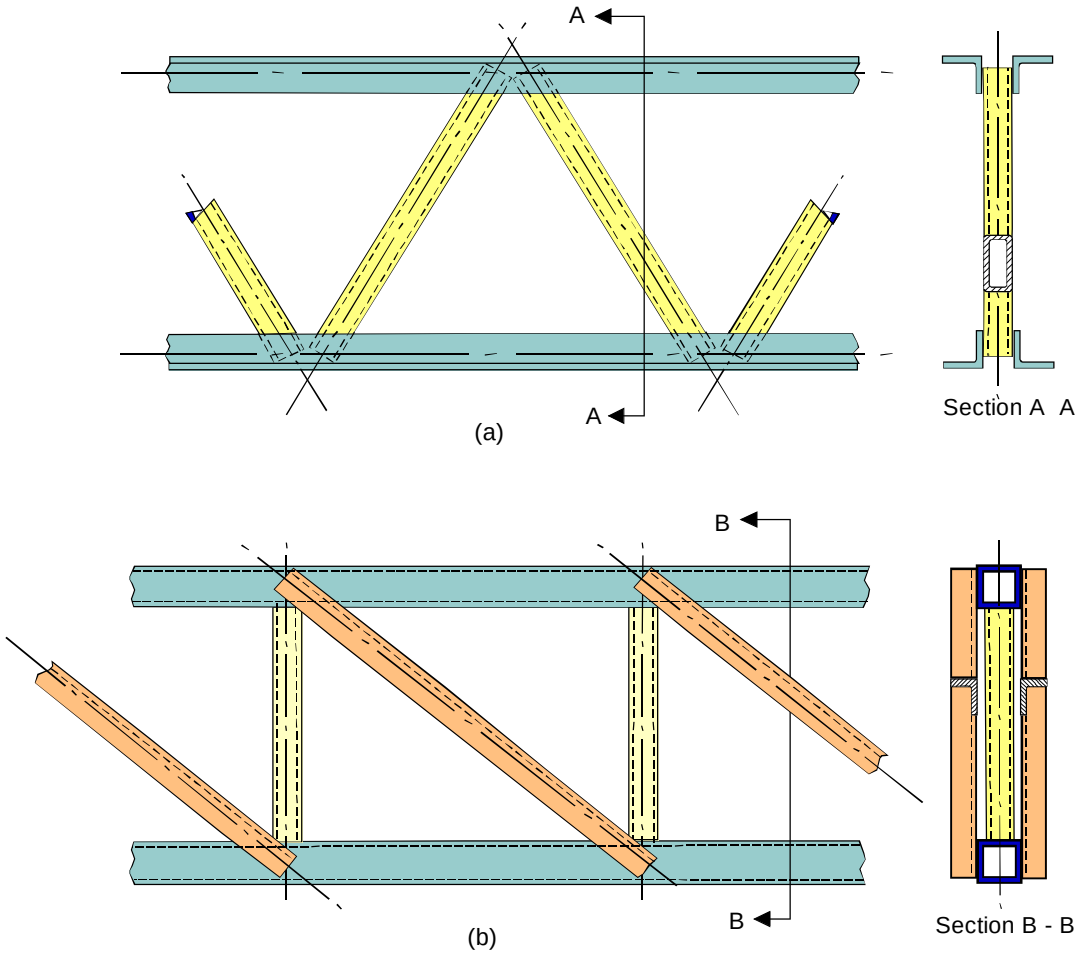

Fig. 10.2 Welded truss connections between open sections and hollow sections [37]

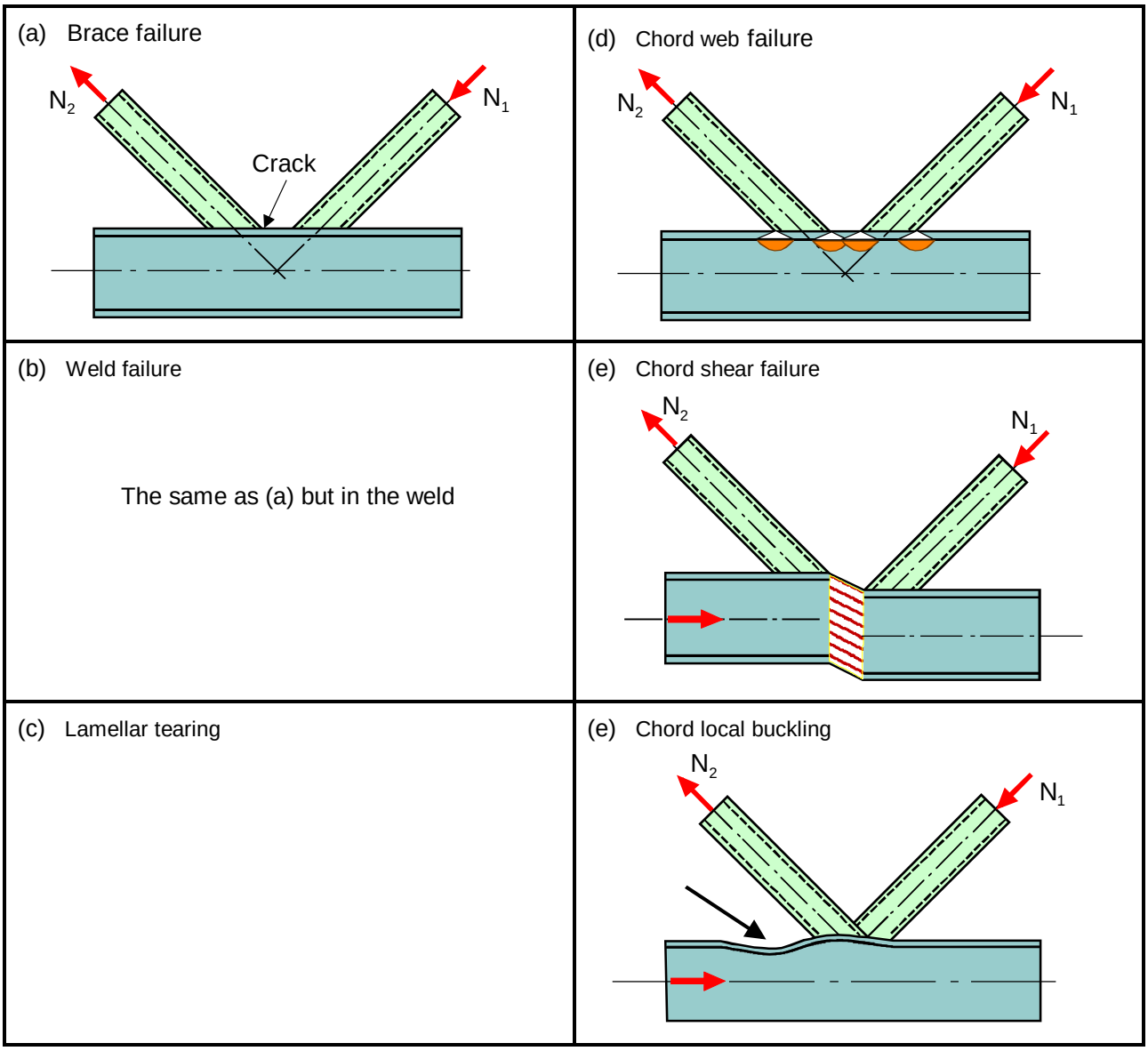

Fig. 10.3 Governing failure modes of joints between hollow section braces and I-section chords

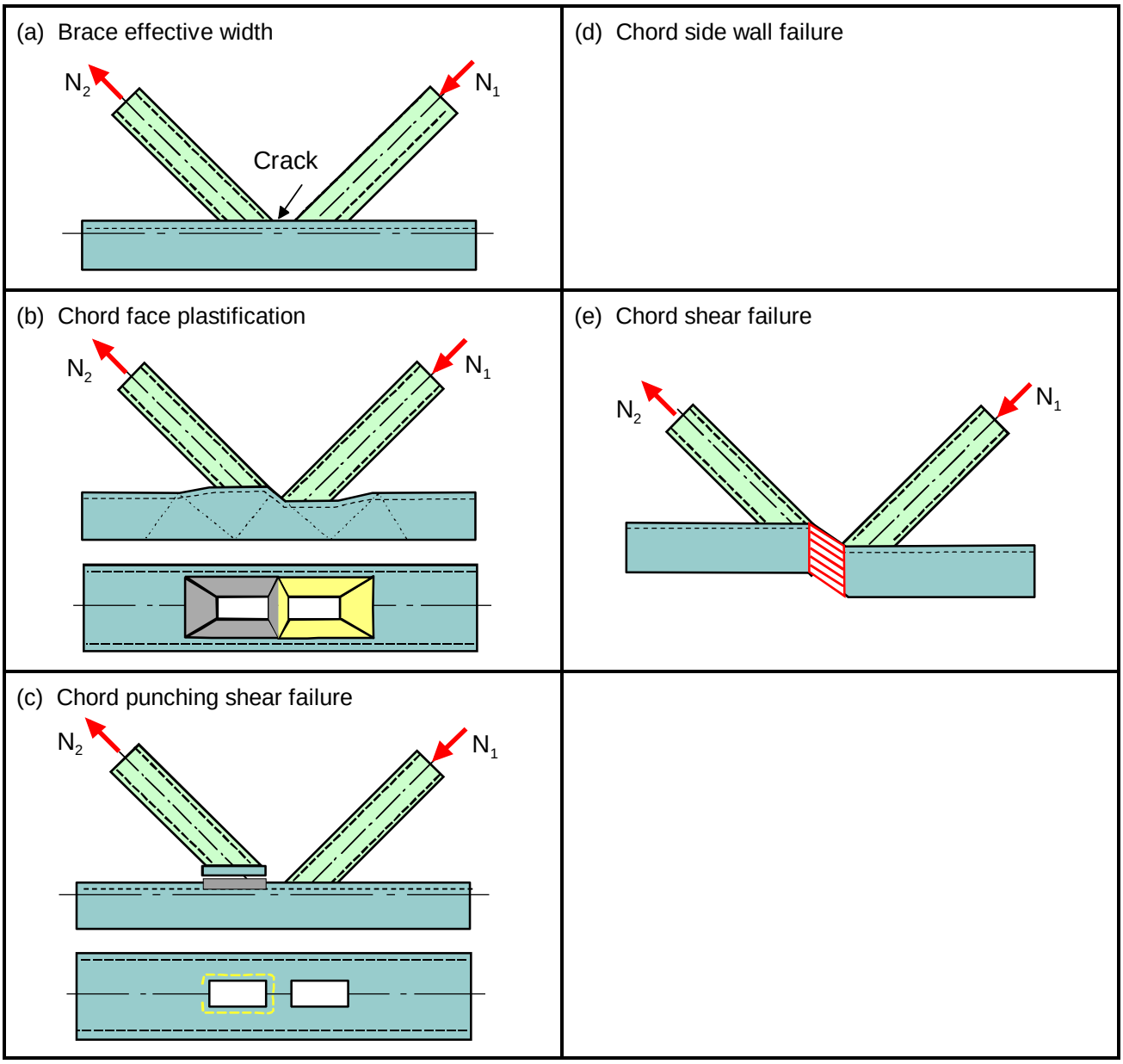

Fig. 10.4 Governing failure modes of joints between hollow section braces and a channel section chord

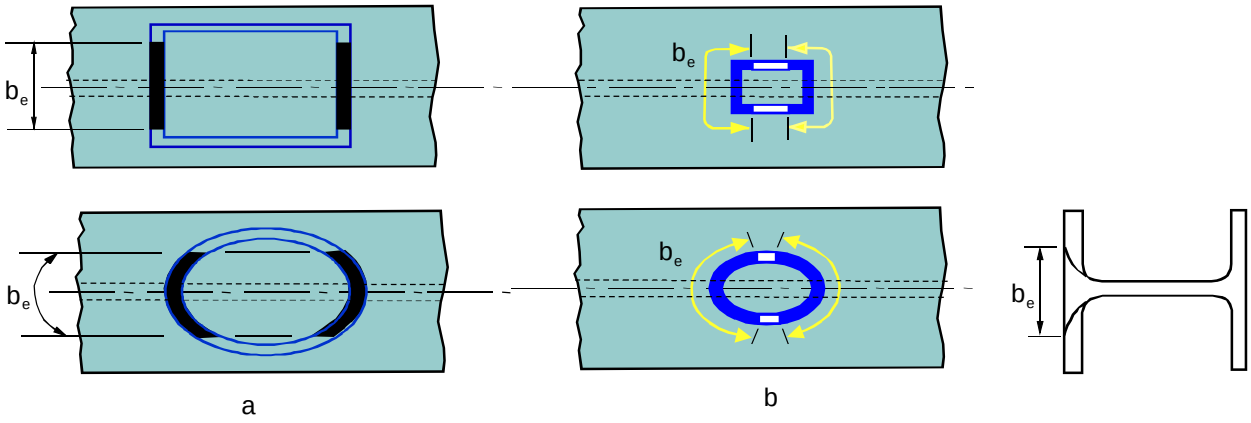

Fig. 10.5 Brace effective width model

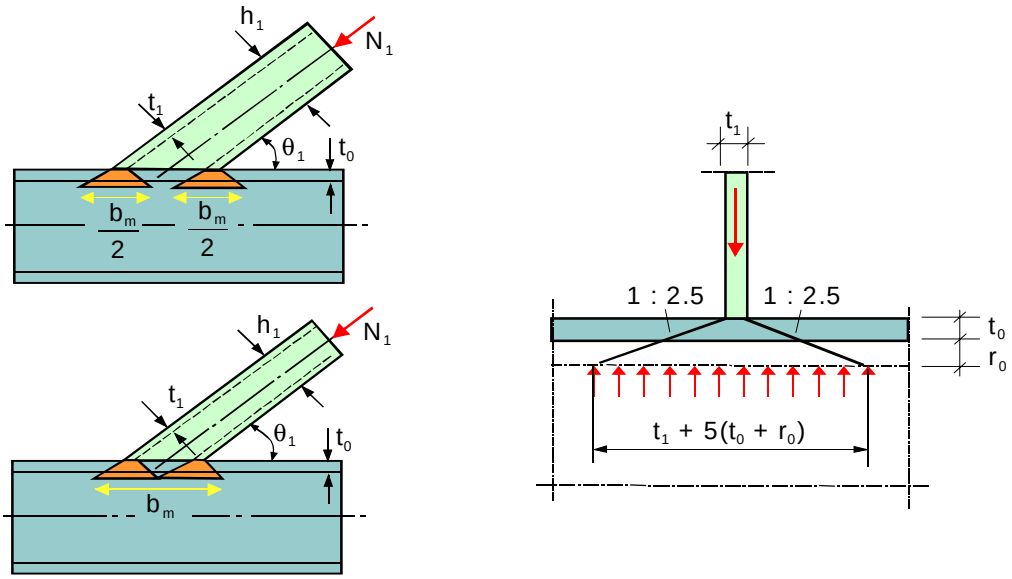

Fig. 10.6 Model for chord web failure

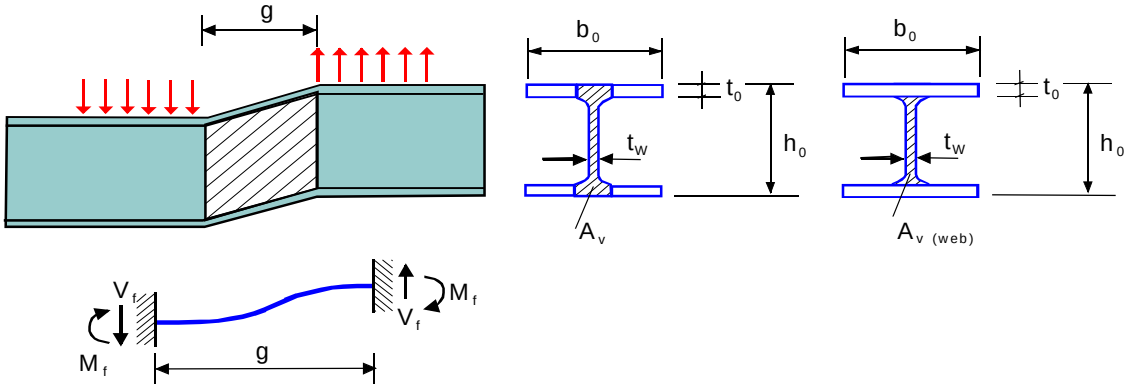

Fig. 10.7 Chord shear model

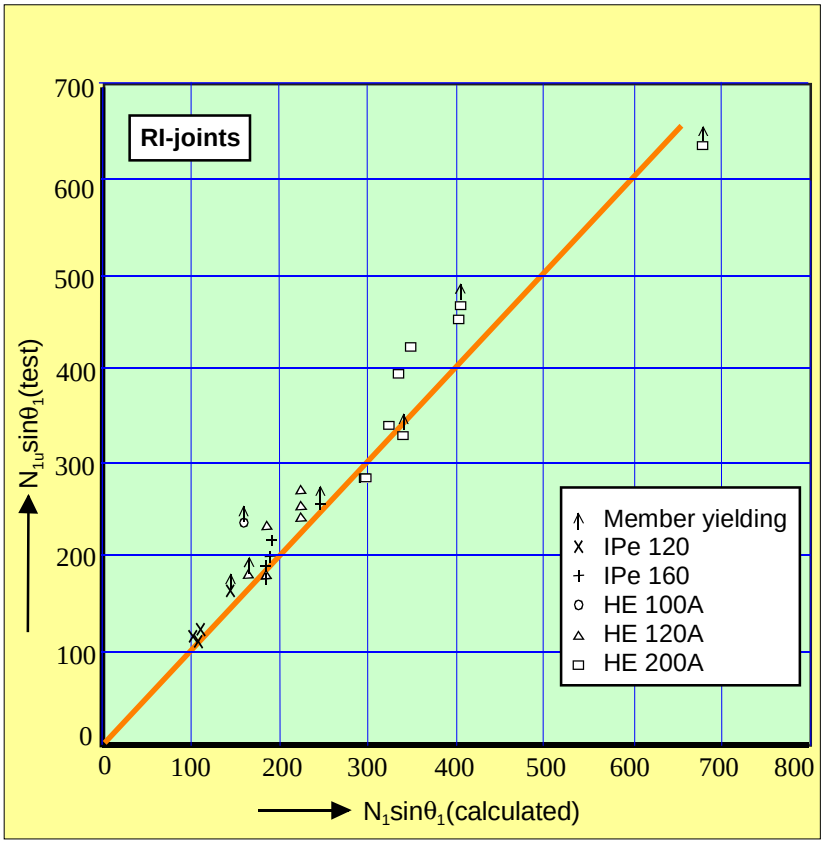

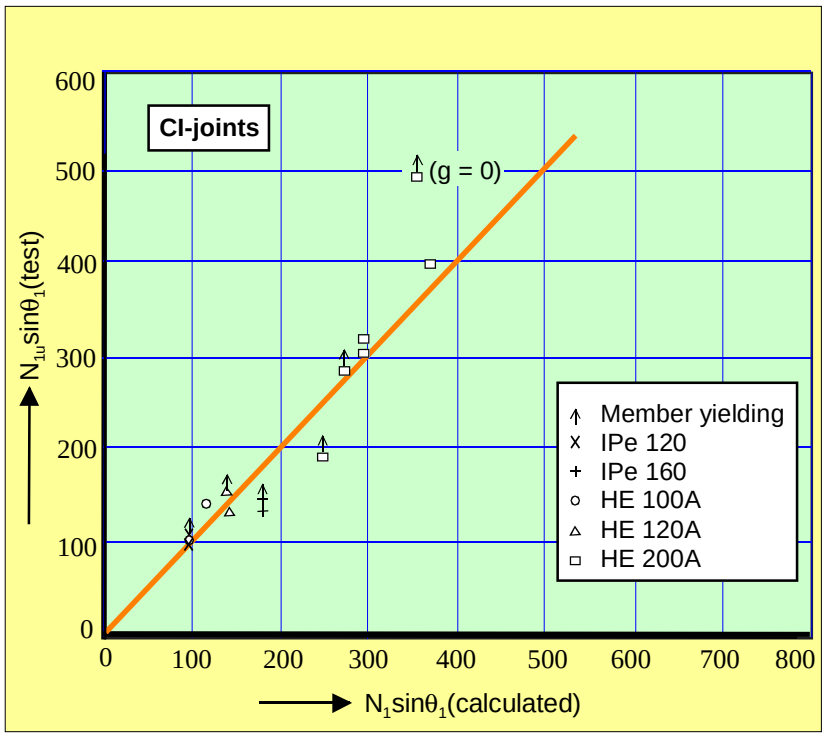

Fig. 10.8 Comparison between test results and eq. 10.14 for joints between hollow section braces and an I-section chord [42]

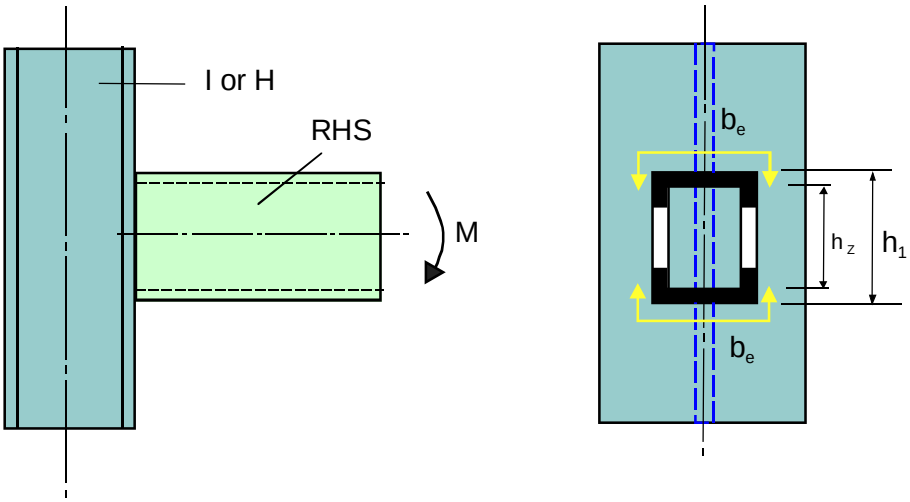

Fig. 10.9 Effective width criterion for moment loading of RHS beam to I-column connection

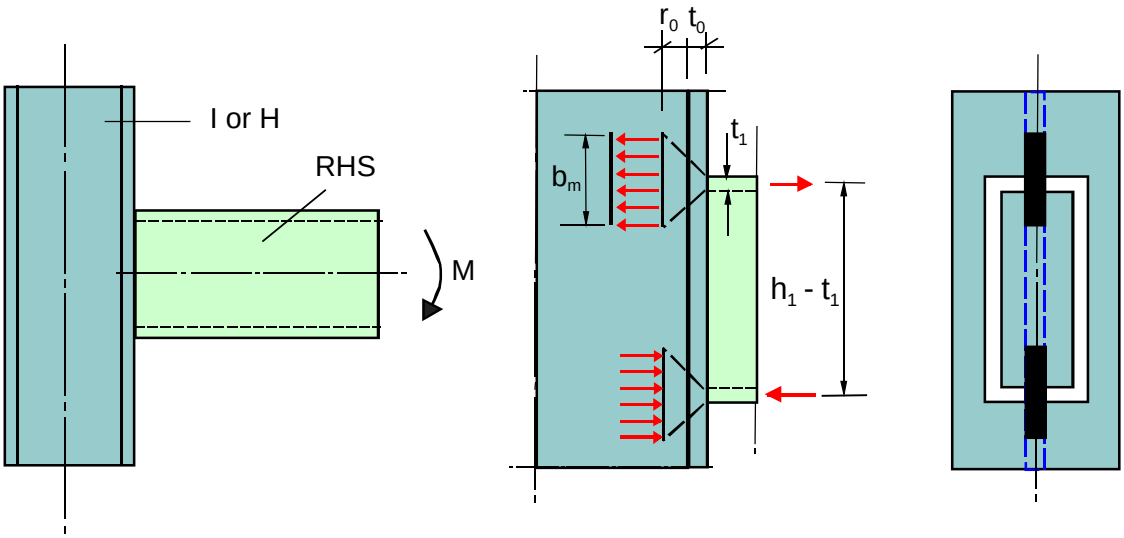

Fig. 10.10 Column web failure criterion for moment loading

11. WELDED I-BEAM TO CHS OR RHS COLUMN MOMENT CONNECTIONS

11.1 INTRODUCTION

Beam-to-column connections can be welded or bolted. In the case of bolted connections, in most cases plates or stubs welded to the column or beams are used to provide a possibility for bolting. Examples of bolted connections are shown in chapter 12. This chapter will focus mainly on unstiffened welded connections between CHS or RHS columns and I-section beams, as shown in Fig. 11.1. Examples of some stiffened connections especially used in earthquake prone regions, e.g. Japan, are shown in Fig. 11.2.

In chapters 8 and 9 it has been already stated that the design formulae for hollow section joints loaded by bending moments can be determined in a similar way to axially loaded joints. Thus, where the joints act as beam-to-column connections, the same applies. For more detailed information, reference can be made to [12, 33, 37,104,105,106].

11.2 MODES OF FAILURE

In a similar way as described in chapter 7, the various modes of failure (Fig. 11.3) can be determined by following the loads:

a. beam failure (effective width: yielding, local buckling)
b. weld failure
c. lamellar tearing
d. column plastification (face, wall or cross section)
e. column punching shear
f. column local buckling
g. column shear failure

As indicated in chapter 7, several modes of failure can be avoided, e.g.:

- weld failures by making the welds stronger than the connected beam, i.e. for **double** fillet welds the throat thickness "a" should meet at least 0.5 times the value given in 8.2
- lamellar tearing can be avoided by choosing material which is not susceptible to lamellar tearing (TTP quality)
- local buckling can be avoided by limiting the width-to-thickness and/or the diameter-to-thickness ratio.

As a result, the following modes of failure have to be considered for design:

- beam failure (effective width)
- column plastification (face, wall or cross section)
- column punching shear
- column shear failure

11.3 MODELS

11.3.1 Effective width

The effective width for the beam shown in Fig. 11.4 can be determined from the plate-to-CHS and/or the plate-to-RHS connections (see 8.7.2 and 9.7.2 with more detailed information in 9.3) because the flange connections are governing.
The moment capacity can be given by:

$$M_1 = N_1 \cdot (h_1 - t_1) \qquad (11.1)$$

where N_1 is the flange capacity for axial loading based on the effective width criterion similarly determined as for the joints between hollow sections. For plate-to-CHS column connections tests have shown that within the range of validity of the formulae the effective width was not critical compared to the other criteria.
For plate-to-RHS column connections the capacity according to the effective width criterion is given by:

$$M_1 = f_{y1} \cdot t_1 \cdot b_e \cdot (h_1 - t_1) \qquad (11.2)$$

with b_e similar to that for joints between rectangular hollow sections, see table 9.1.

11.3.2 Column plastification

The plastification of the I-beam to CHS or RHS column connection is not only determined by the connection of the flanges but also by the column depth, since the I-beam web forces the chord face of an RHS column into a different yield line pattern than that which would be observed by two flanges at a certain distance apart, see Fig. 11.5.

If the web was **not** present, the capacity of the flange could be given according to eq. 11.1 with N_1 being the flange capacity based on the plastification criterion. For example for an RHS column eq. 9.6 would apply with $\theta = 90°$ and $\eta = t_1/b_o$, which is very small, thus:

$$M_1 \approx f_{yo} \cdot t_o^2 \cdot \left(\frac{4}{\sqrt{1-\beta}}\right) \cdot (h_1 - t_1) \qquad (11.3)$$

If the influence of the web is incorporated, the equation becomes considerably more complicated and reference can be made to [106].

For the chord side wall plastification criterion, similar rules can be used as for beam-to-column connections between I-sections and those used for RHS connections with $\beta = 1.0$, i.e.:

$$M_1 = 2 \cdot f_{yo} \cdot t_o \cdot b_m \cdot (h_1 - t_1) \qquad (11.4)$$

with $b_m = t_1 + 5\, t_o$ (11.5)

$$\leq \frac{h_1 + 5\, t_o}{2}$$

For I-beam to CHS column connections the strength for the flange plate connection can be based on the ring model (see chapter 8). However, for moment loading with the beam web included, the formulae become rather complicated and have to be calibrated with test results, resulting in semi-empirical formulae [105].

11.3.3 Column punching shear

The column punching shear strength can be directly determined from the plate-to-CHS or RHS connections (see [3] and for more detailed information [42]). Here, similar to the effective width criterion, the flanges are governing because the webs are located at the softest part of the column face and are generally not effective.

As shown in Fig. 11.6, the capacity is given by:

$$M_1 = \frac{f_{yo}}{\sqrt{3}} \cdot t_o \cdot (2\, b_{ep} + 2\, t_1) \cdot (h_1 - t_1) \qquad (11.6)$$

For plate-to-CHS column connections it was shown that, within the range of application given in table 8.1, b_{ep} can be taken as b_1.

For plate-to-RHS column connections the same b_{ep} can be taken as given in tables 9.1 and 9.3.

11.3.4 Column shear failure

If the beam-to-column connections only have a moment loaded beam on one side, or alternatively the beam moments on either side of the connection do not balance each other, shear forces will act in the column, which may cause a shear failure of the column. Here the cross section of the column has to be checked for the combined actions of axial load, shear load and bending moment. For class 1 and class 2 sections, the interaction can be based on the Huber-Hencky-Von Mises criterion [42] or a suitable possible stress distribution can be assumed as e.g. shown in Fig. 11.7.b. Based on the Huber-Hencky-Von Mises criterion the following can be derived for a side wall of an RHS column:

$$f_y^2 = \sigma^2 + 3\tau^2 \qquad (11.7)$$

or

$$1 = \left(\frac{\sigma}{f_y}\right)^2 + \left(\frac{\tau}{f_{y/\sqrt{3}}}\right)^2 \qquad (11.7a)$$

or

$$\left(\frac{M}{M_p}\right)^2 + \left(\frac{V}{V_p}\right)^2 = 1 \qquad (11.7.b)$$

$$\left(\frac{N}{N_p}\right)^2 + \left(\frac{V}{V_p}\right)^2 = 1 \qquad (11.7.c)$$

or

$$M = M_p \sqrt{1 - \left(\frac{V}{V_p}\right)^2} \qquad (11.8)$$

$$N = N_p \sqrt{1 - \left(\frac{V}{V_p}\right)^2} \qquad (11.9)$$

Adding the flanges and assuming that the effective shear area is $2\, h_m \cdot t_o$ results in:

$$M_{p,Q} = b_m \cdot h_m \cdot t_o\, f_{yo} + 0.5\, h_m^2\, t_o \cdot f_{yo} \sqrt{1 - \left(\frac{V}{V_p}\right)^2} \qquad (11.10)$$

$$N_{p,Q} = 2 b_m \cdot t_o \cdot f_{yo} + 2 h_m \cdot t_o \cdot f_{yo} \sqrt{1 - \left(\frac{V}{V_p}\right)^2} \qquad (11.11)$$

The formulae 11.10 and 11.11 show the plastic capacities for axial loading and moment, reduced by the effect of shear.

In a similar way, the interaction between axial load and bending moment can be determined [42]. By introducing $N_{p,Q}$ and $M_{p,Q}$ instead of N_p and M_p, the full interaction can be obtained. In the standards [12], these formulae have been approximated by simpler formulae. Also the effect of small shear loads has been neglected, e.g. for $V \leq 0.5\ V_p$.

11.4 EXPERIMENTAL AND NUMERICAL VERIFICATION

Most initial tests on plate-to-CHS and I-beam-to-CHS connections have been carried out in Japan [82, 104]. A good survey of all existing evidence on beam to CHS column connections, including many tests on stiffened connections, is given by Kamba [104]. Later work by De Winkel [105] concentrated on a numerical parameter study with experiments carried out for validation of the numerical models. This study not only dealt with simple unstiffened connections, but also with I-beam-to-CHS column connections in which the column was filled with concrete and/or combined with a composite steel-concrete floor.
A similar investigation to that carried out by De Winkel has also been done by Lu for plate and I-beam to RHS column connections [106].
Stiffened connections with strips welded at the sides of the flanges have been investigated by Shanmugan [107]; i.e. the cross section of the flange at the connection with the RHS column has also an I shape.

11.5 BASIC JOINT STRENGTH FORMULAE

In the studies mentioned in 11.4 [105, 106] on unstiffened connections, strength formulae have been determined using analytical models as a basis. These formulae have been modified to fit the numerical data. Since the strength data have been based on a deformation criterion of 3% of the chord width, the resulting formulae for plate-to-RHS column connections give, for low β ratios, lower strengths than those given in the CIDECT Design Guide [3, 75, 106].

At present, only strength functions are available for uniplanar and multiplanar joints and no formulae are available for the stiffness, although the stiffness is extremely important for the determination of the moment distribution in unbraced frames. However, many moment rotation diagrams are available for many parameter variations. From these moment rotation diagrams indications can be obtained for the stiffness.

The effect of the connection stiffness on the elastic moment distribution is represented in Figs. 11.8 and 11.9. It is shown that with semi-rigid connections the elastic moment distribution can be influenced considerably.

If a rigid-plastic analysis is used, the moment resistance of the connections is of primary importance. Furthermore, the rotation capacity is important. For example, if the stiffness of the connections of the beam in Fig. 11.8 is very low, the plastic moment capacity of the beam at mid-span $M_{p\ell,Rd}$ will be reached first. The moment capacity of the end connections $M_{j,Rd}$ can only be reached if the beam has sufficient rotation capacity at the location of the plastic moment. In the case of connections with a very low stiffness this might not be the case, e.g. see "e" in Fig. 11.10.

If the stiffness of the connection is high, the (partial) strength capacity of the end connections (e.g. "b" in Fig. 11.10) may be reached first. Now these connections should have sufficient deformation capacity to develop the plastic moment capacity of the beam at mid-span.

Thus, for a proper analysis of frames with semi-rigid connections, a description of the moment-rotation behaviour is required. Therefore, evidence is required regarding:
- stiffness (serviceability and at the ultimate limit state)
- strength (ultimate limit state)
- rotation capacity

However, all this information is not yet generally available for beam-to-tubular column connections. Other options are that the stiffness is such that the connections can be classified as (nearly) rigid or (nearly) pinned. For both cases, limits can be given. However, the deflections can only be determined properly if the joint stiffnesses are available (Fig. 11.11).

In Eurocode 3 Annex J stiffness classifications are given, see Fig. 11.12.
A possible joint modelling approach is given in Fig. 11.13.
For I-beam-to-tubular column connections the factors c_1 and c_2 still have to be defined. Another complication is that the axial loads and moments in the column do not only influence the strength, but also the stiffness, as shown by the dashed line in Fig. 11.13.

11.6 CONCLUDING REMARKS

The design recommendations, e.g. given in Eurocode 3 and the CIDECT Design Guides, give strength functions related to the strength of the plate-to-CHS or RHS column connection. As mentioned, for low β ratios the deformations may exceed the 3% diameter (or width) criterion. The formulae proposed in the later studies [105, 106] have not yet been simplified in such a way that they can already be incorporated in a code or standard.
This chapter intends to give students basic background information without going too much into detail in the resulting design formulae. The design of frames with semi-rigid connections is not typical for tubular structures and therefore not described in detail.

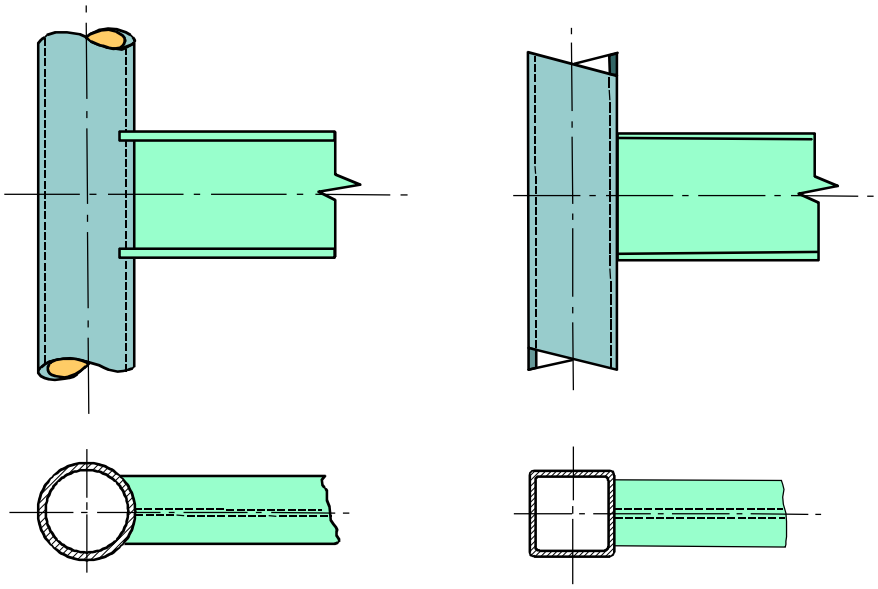

Fig. 11.1 Unstiffened I-beam-to-CHS or RHS column connections

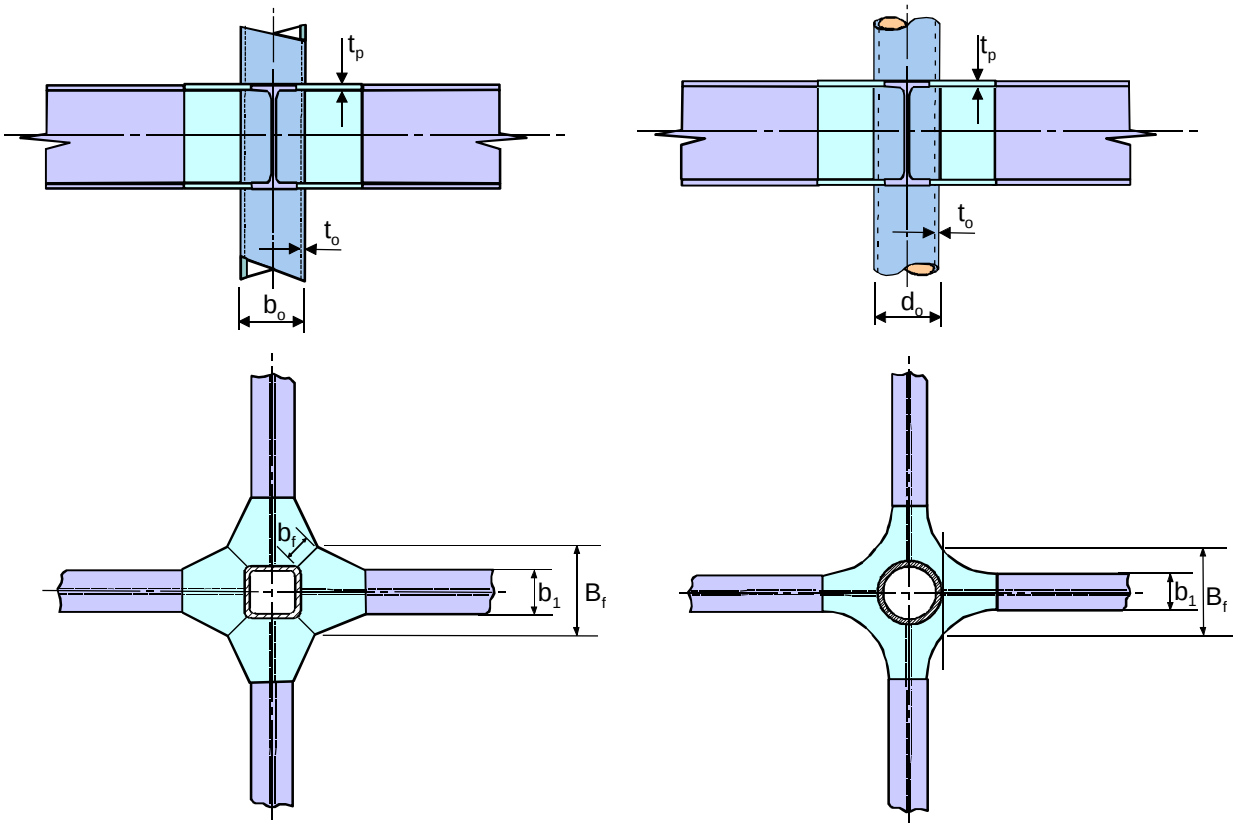

Fig. 11.2 Flange diaphragm I-beam-to-CHS or RHS column connections

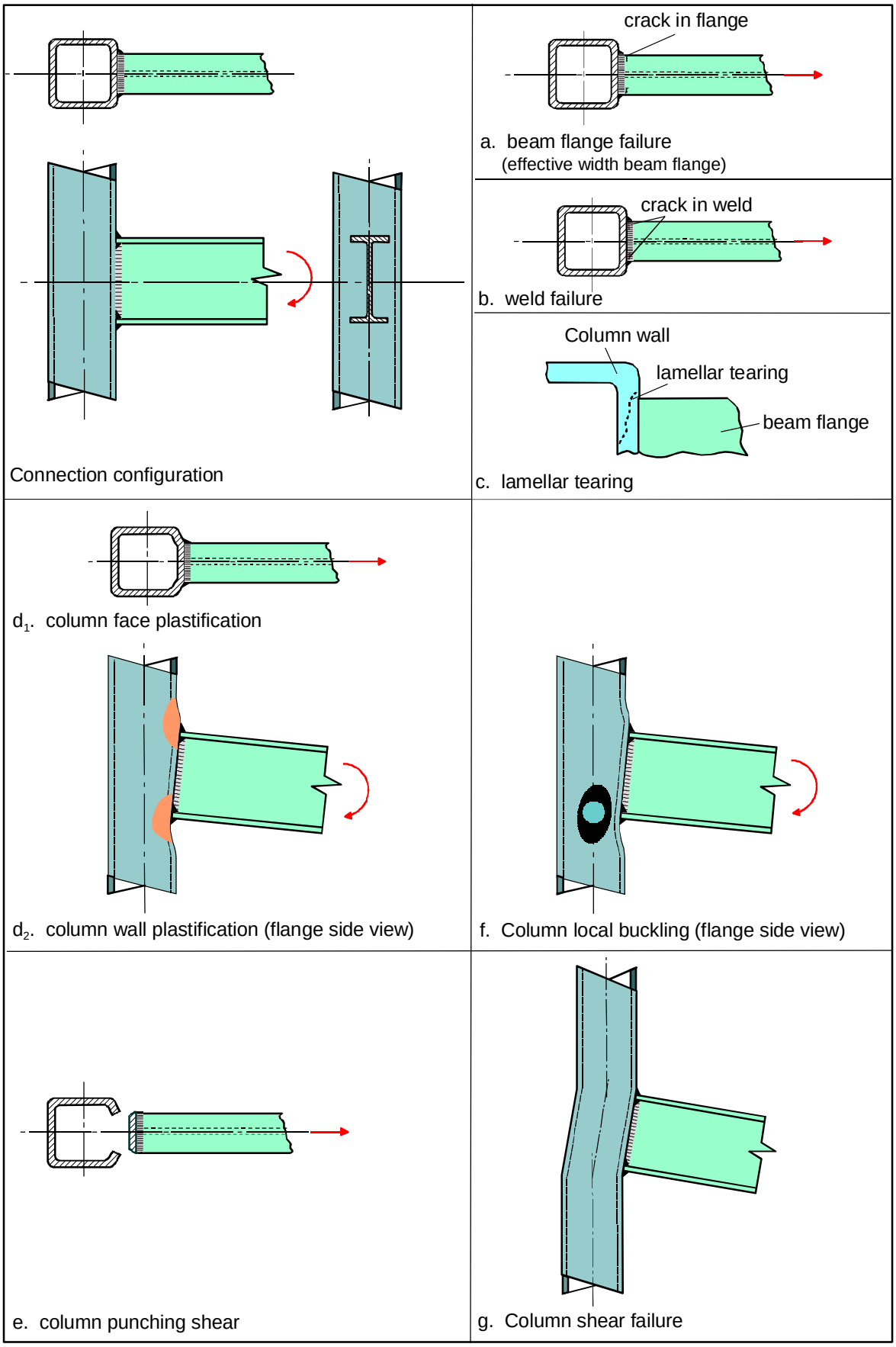

Fig. 11.3 Modes of failure for I-beam-to-RHS column connections

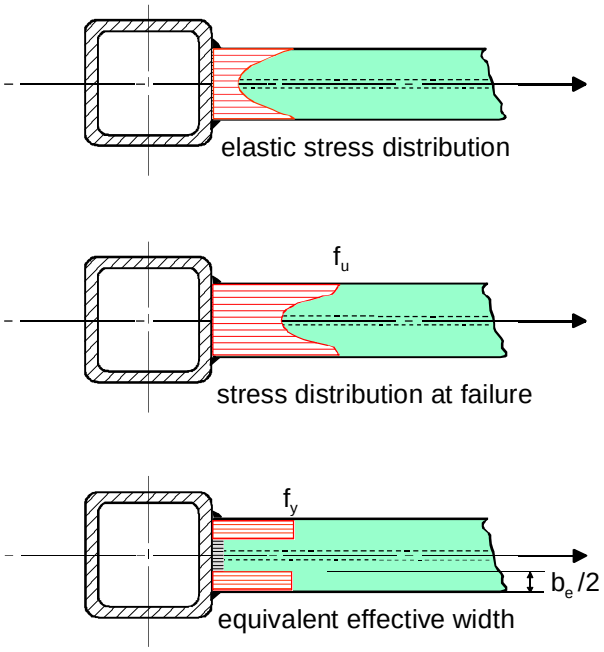

Fig. 11.4 Effective width

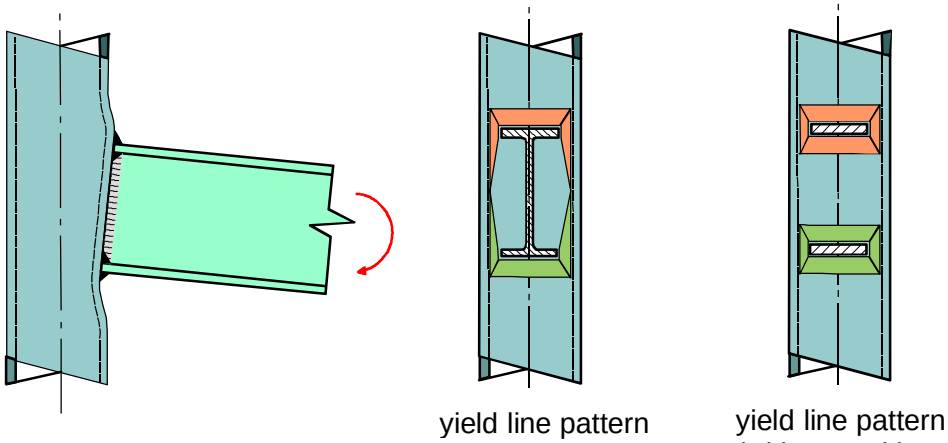

Fig. 11.5 RHS column face plastification

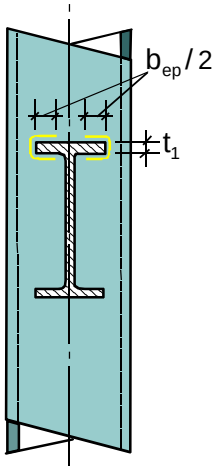

Fig. 11.6 RHS column punching shear

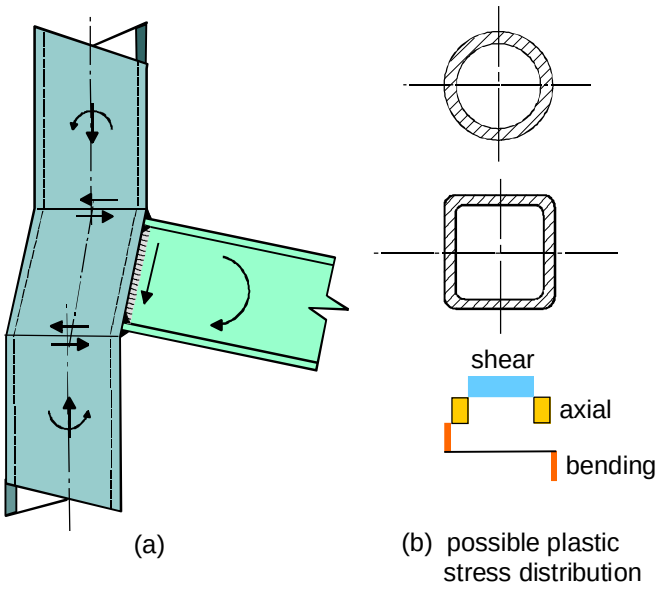

Fig. 11.7 Column shear failure

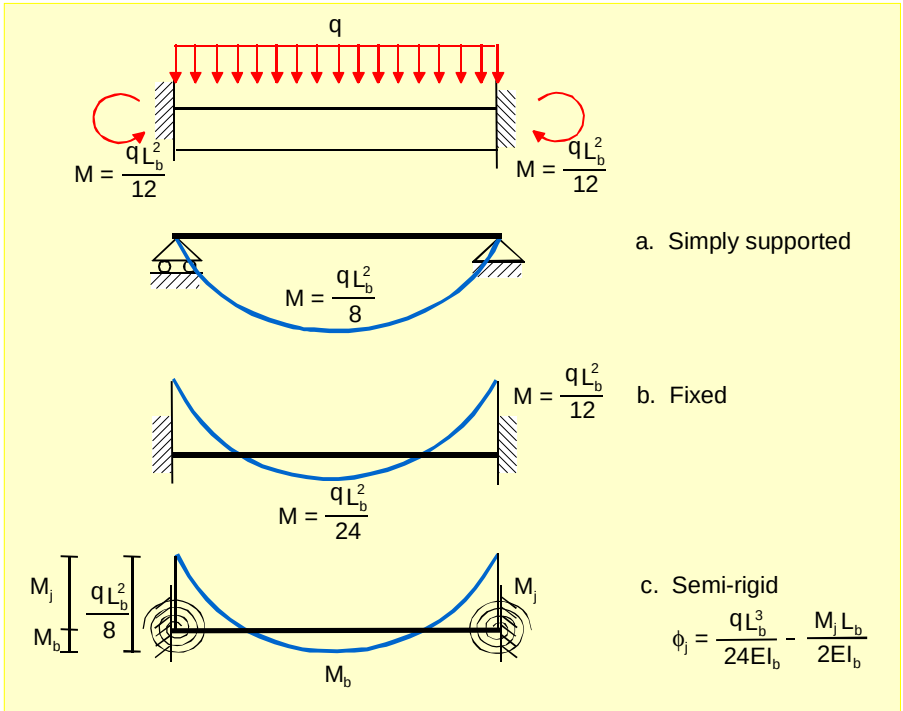

Fig. 11.8 Beam with various end conditions

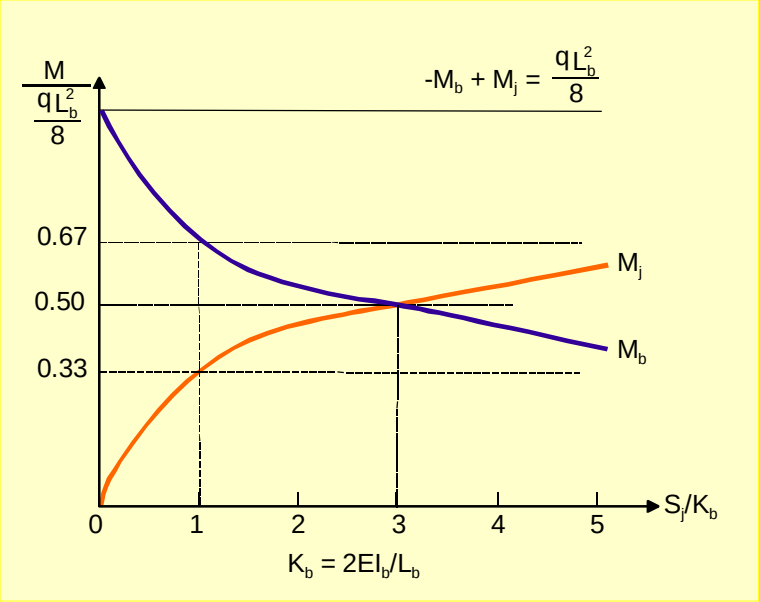

Fig. 11.9 Variation of elastic moment distribution with connection stiffness

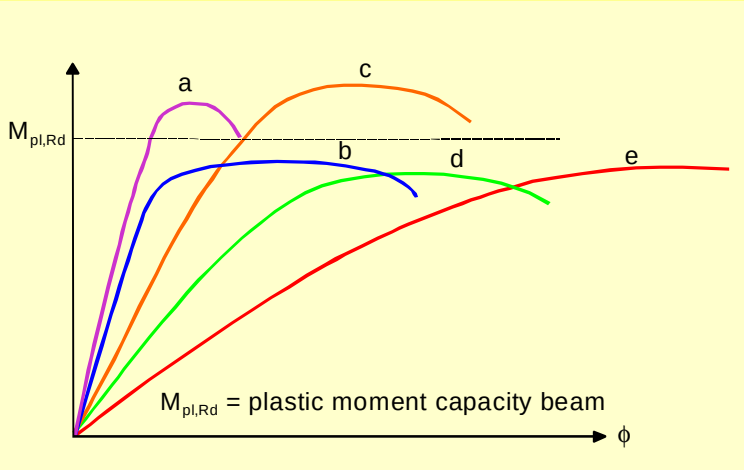

Fig. 11.10 Various M-ϕ characteristics

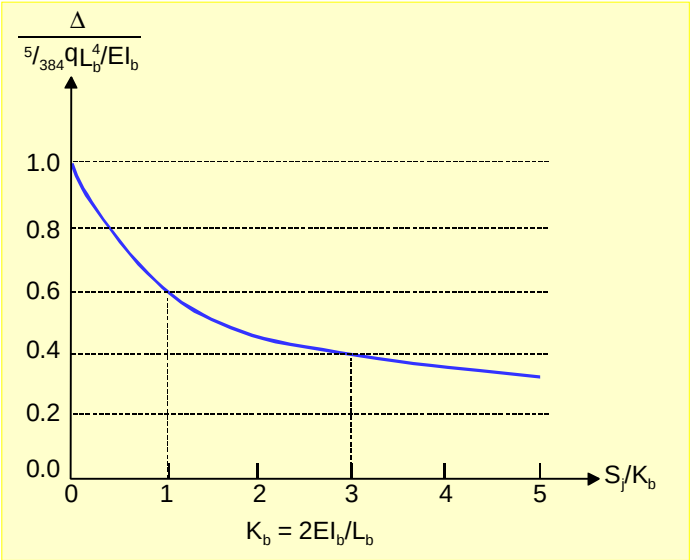

Fig. 11.11 Variation of midspan deflection with connection stiffness

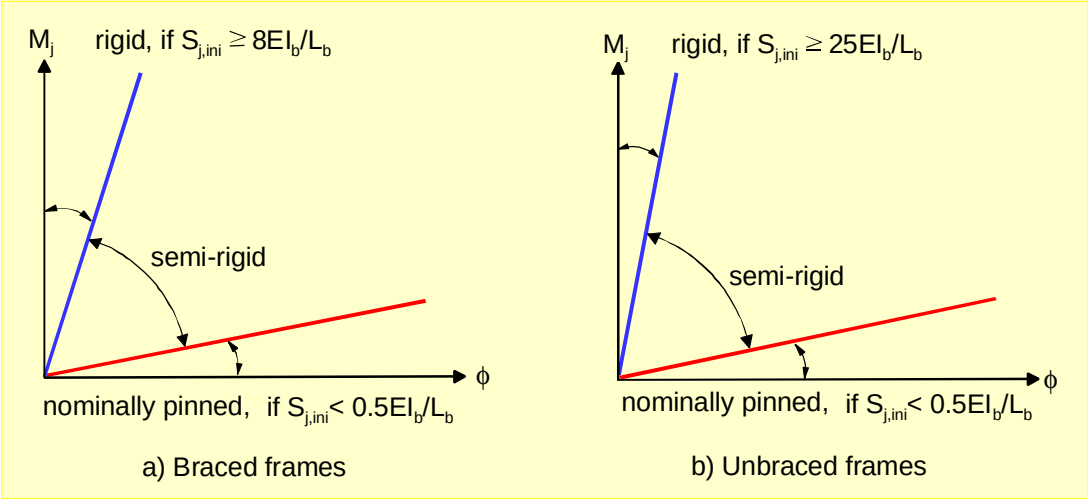

Fig. 11.12 Boundaries for stiffness classification of beam-to-column joints according to Eurocode 3

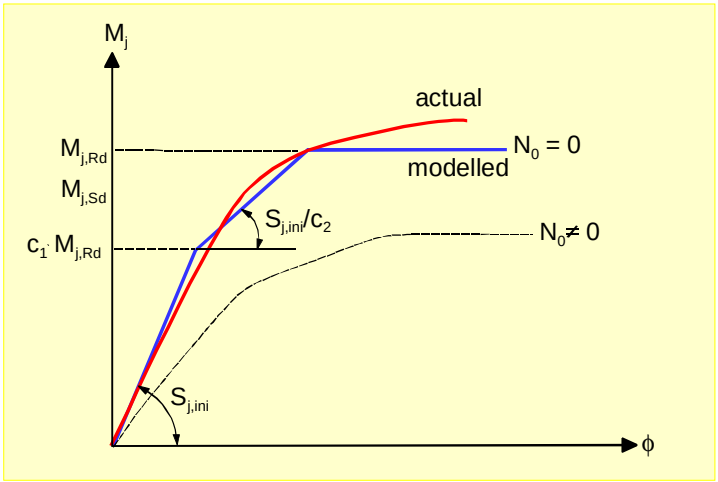

Fig. 11.13 M-Φ modelling

12. BOLTED CONNECTIONS

The calculation methods used for bolted connections between or to hollow sections are basically not different from those used for any other type of connection in conventional steel construction.
Most details given in this chapter are presented without (detailed) design formulae.

12.1 FLANGE PLATE CONNECTIONS

12.1.1 Flange plate connections to circular hollow sections

For the flange plate connections shown in Fig. 12.1, various investigations have been carried out. [37,43,108,109] Economical structural tension connections can be obtained if prying force is permitted at the ultimate limit state, with the connection proportioned on the basis of a yielding failure mechanism of the flange plates. In the CIDECT Design Guide No. 1 [1], formulae and tables are given based on the work of Igarashi et al. [109] In the context of this lecture book, only the failure modes are presented (Fig. 12.2). Primary structural connections are preferably to be designed on the basis of the yield resistance of the circular hollow section.

12.1.2 Flange plate connections to rectangular hollow sections

Research by Packer et al. [110] on bolted RHS flange plate connections with bolts on two sides only, see Fig. 12.3, showed that in principle the strength of these connections can be analysed on the basis of the traditional prying model developed for T stubs by Struik and de Back [111,112], provided that the location of the plastic hinge lines is adjusted, i.e. the distance b in Fig. 12.4 is adjusted to b' with:

$$b' = b - \frac{d}{2} + t_i \qquad (12.1)$$

Furthermore, since the RHS member tends to yield adjacent to the plastic hinge, it participates in the failure mechanism. Detailed formulae are given in [37,110].
Many tests have been carried out on RHS flange plate connections with bolts on 4 sides, as shown in Fig. 12.3. Further, many analytical failure mechanisms have been evaluated. However, up to now, the models do not sufficiently fit the test results and further research is still going on.

12.2 END CONNECTIONS

Some bolted end connections are shown in Fig. 12.5. The flange of the tee in Fig. 12.5d, as well as the other flange plates perpendicular to the CHS or RHS section, must be sufficiently thick to effectively distribute the load to the cross section [2,6,37,41].

12.3 GUSSET PLATE CONNECTIONS

Fig. 12.6 shows some examples of bolted gusset plate connections. It must be borne in mind that fitting of these connections is very sensitive with regard to dimensional tolerances and to deformations of the welded gusset due to weld-induced distortions. Thus, care has to be taken to ensure fitting at site.
For bolted connections the design can be based on the various possible failure modes, e.g. for a tension member:
- yielding of the cross section
- rupture of the effective net area or
  rupture of the effective net area reduced for shear lag.

Similar to other bolted connections, the effective net area is the sum of individual net areas along a potential critical section of a member, see Fig. 12.7. If such a critical section comprises net areas, loaded in tension and segments loaded in shear, the shear segments should be multiplied by the shear strength and the tension areas by the ultimate strength, see Fig. 12.7.

When a member is connected by some, but not all parts of its cross section elements and if the net section includes elements which are not connected, the net area perpendicular to the load has to be multiplied by a shear lag factor which depends on the shape of the section, the number of connected faces and the number of transverse rows of fasteners.
In the CIDECT Design Guide [3], shear lag factors between 0.75 and 0.90 are recommended.
The effective net area reduced for shear lag also applies to **welded connections** if a member is not welded all around its cross-section. An example is given in Fig. 12.6 (b), where bolting plates are welded to the sides of the brace member. For welds parallel to

the direction of the load (as in Fig. 12.6 (b), along the corners of the RHS), the shear lag factor is a function of the weld lengths and the distance between them. The distance between such welds would be b_i. The shear lag factor to be applied is [3] :

1.00 when the weld lengths (L) along the RHS corners are $\geq 2b_i$
0.87 when the weld lengths (L) along the RHS corners are $1.5\ b_i \leq L < 2b_i$
0.75 when the weld lengths (L) along the RHS corners are $b_i \leq L < 1.5\ b_i$.

The minimum length of welds (L) is the distance between them.

A failure mode of the gusset plate which must be checked is yielding across an effective dispersion width of the plate, which can be calculated using the Whitmore [37] effective width concept illustrated in Fig. 12.8. For this failure mode (for two gusset plates) the strength is given by:

$$N_i^* = 2 f_{yp}\ t_p\ (g + 1.15 \Sigma p) \cdot \frac{1}{\gamma_m} \text{ with } \gamma_m = 1.1 \quad (12.2)$$

If the member is in compression, buckling of the gusset plate must also be prevented. The term Σp represents the sum of the bolt pitches in a bolted connection or the length of the weld in a welded connection.

12.4 SPLICE CONNECTIONS

Fig. 12.9 shows a splice connection for circular hollow sections. This type of connection can, for example, be executed with four, six or eight strips welded longitudinally on the periphery of the hollow sections and connected by double lap plates, one on each side. Lightly loaded splice connections can be made as shown in Fig. 12.10 and for architectural appearance the bolts can be hidden. Using one plate at each side instead of the solution in Fig. 12.10 provides a more fabrication-friendly solution. Such a joint, however, has little stiffness and resistance to out of plane loading, thus the designer should be confident that such a condition cannot arise.

12.5 BOLTED SUBASSEMBLIES

Lattice structures are often connected to columns by bolted flanges, plates or Tee profiles. Some examples are shown in Fig. 12.11.

12.6 BEAM TO COLUMN CONNECTIONS

Bolted beam to column connections can be designed in various ways, mainly depending on the type of load that has to be transmitted.
In general, shear connections are simpler to fabricate than moment connections. Typical connections are given in Figs. 12.12 to 12.16 without detailed description.

12.7 BRACKET CONNECTIONS

Typical connections for lightly loaded beams are shown in Fig. 12.17.

12.8 PURLIN CONNECTIONS

Fig. 12.18 shows some examples of purlin connections for trusses with CHS or RHS chords.

12.9 BLIND BOLTING SYSTEMS

Due to the closed nature of hollow sections, in many cases additional welded plates are used for bolted connections. However, then solutions are not aesthetically appealing. In recent years, systems have been developed for direct connections for one side only.

Special types of bolts and systems allow to bolt from one side of a hollow section. A number of patented blind bolting systems is available, e.g. Huck "Ultra Twist Blind Bolt" and Lindapter "HolloFast" and "HolloBolt". The latter, which uses a special insert and a standard bolt, has been investigated by CIDECT [113] with regard to its axial, shear and bending capacity (see Fig. 12.19).
The systems are based on the principle that after bringing them in from one side the bolts are torqued and a “bolt head” forms on the inside of the connected plies.

The design rules for blind bolting systems are based on typical failure modes, i.e.

- punching shear of the fastener through the column face
- yielding of the column face (yield line pattern around the bolts)
- bolt failure in shear, tension or a combination of both.

12.9.1 Flowdrill

The flowdrill system is a special patented method for extruded holes [114]. CIDECT has carried out extensive tests to prove the load bearing capacity of this type of joint using this method in structural hollow sections [114], see Fig. 12.20.

Flowdrilling is a thermal drilling process (Fig. 12.21) to make a hole through the wall of a hollow section by bringing a tungsten carbide bit into contact with the hollow section wall and generating sufficient heat by friction to soften the steel. As the bit moves through the wall, the metal flows to form an internal bush. In the subsequent step, the bush is threaded using a roll tap.

At the present stage of investigation, the bolting of hollow sections with wall thicknesses up to 12.5 mm can be recommended by using the flowdrill method. Recommendations are given in [114].

12.10 NAILED CONNECTIONS

As an alternative to bolting or welding, steel Circular Hollow Sections (CHS) can be nailed together to form reliable structural connections. Up to now, this method of connection has only been verified for splice connections between two co-axial tubes (see Fig. 12.22). In such a connection, one tube can fit snugly inside the other, in such a way that the outside diameter of the smaller equals the inside diameter of the larger. Nails are then shot fired and driven through the two wall thicknesses and arranged symmetrically around the tube perimeter.
As an alternative, two tubes of the same outside diameter can be joined to each other by means of a tubular collar over both tube ends; in this case nails are again inserted by driving them through the two tube walls.
Research to date has covered a range of tube sizes with various diameter to thickness ratios, tube wall thickness and lack of fit [115,116,117]. The observed failure modes were nail shear failure, tube bearing failure, and net section fracture of the tube. These failure modes have been identified for both static and fatigue loading. Simple design formulae, derived from bolted and riveted connections, have been verified for both these load cases.

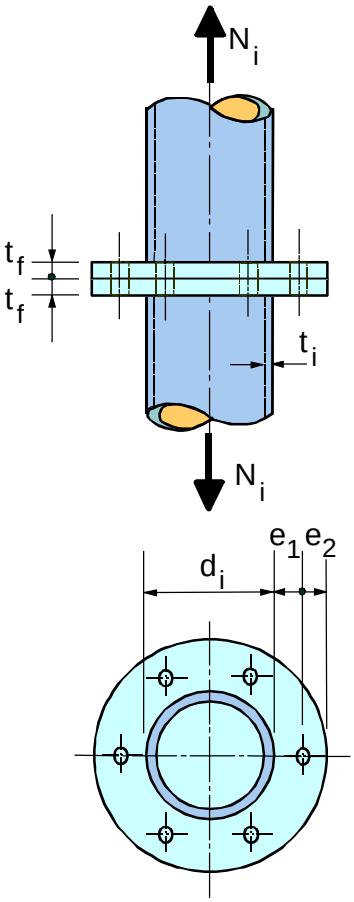

Fig. 12.1 Bolted CHS flange plate connection

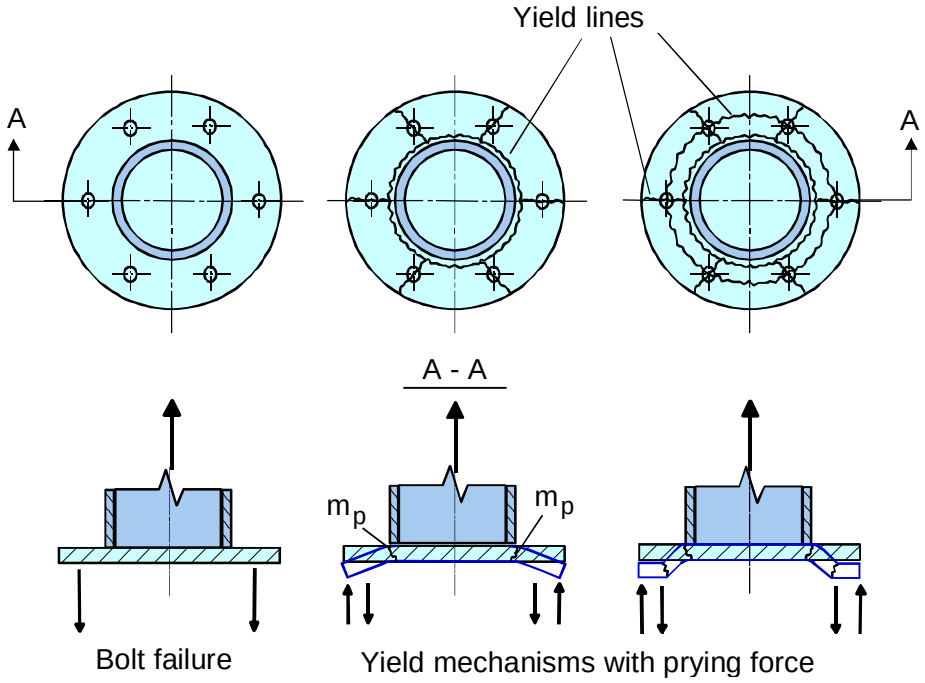

Fig. 12.2 Failure modes for bolted CHS flange plate connections

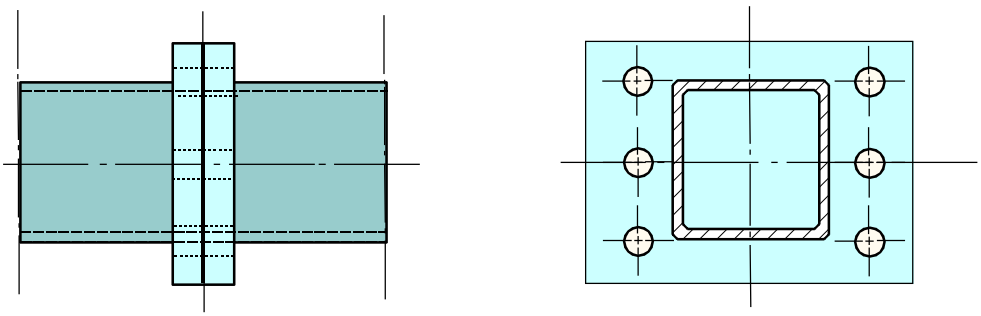

Bolts on two sides only

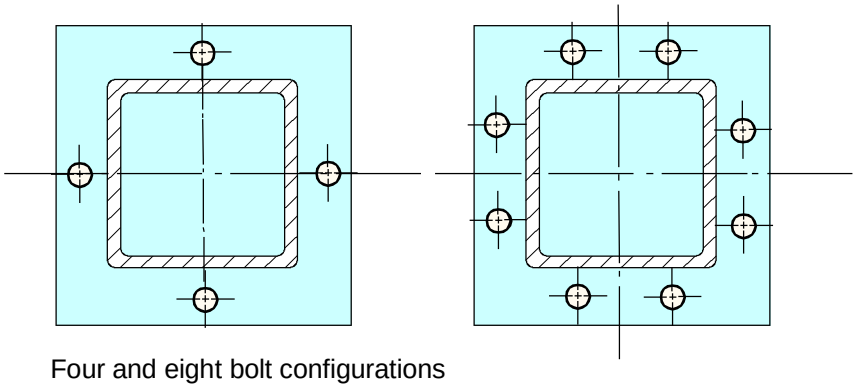

Four and eight bolt configurations

Fig. 12.3 Bolted RHS flange plate connections

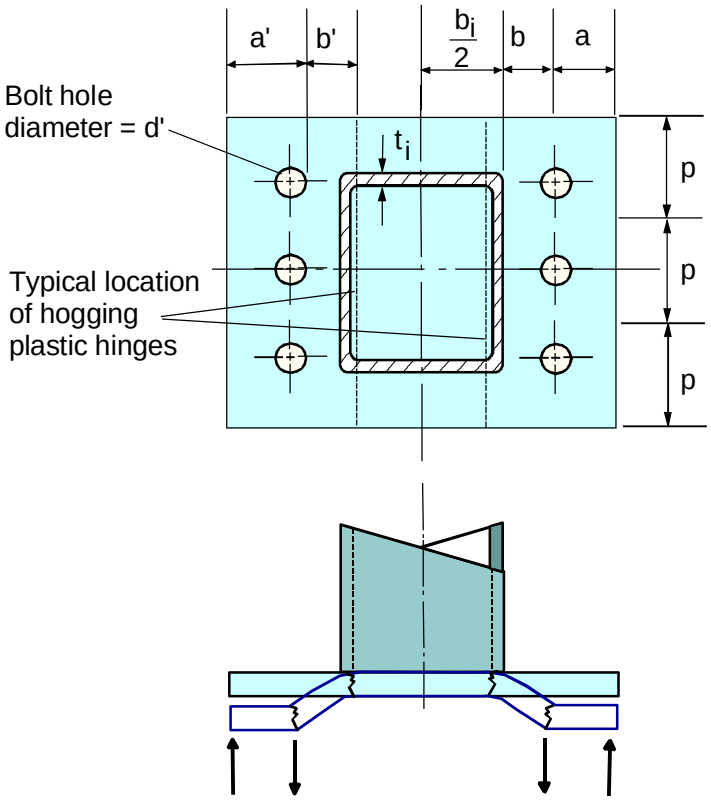

Fig. 12.4 RHS flange plate connection with bolts at two sides

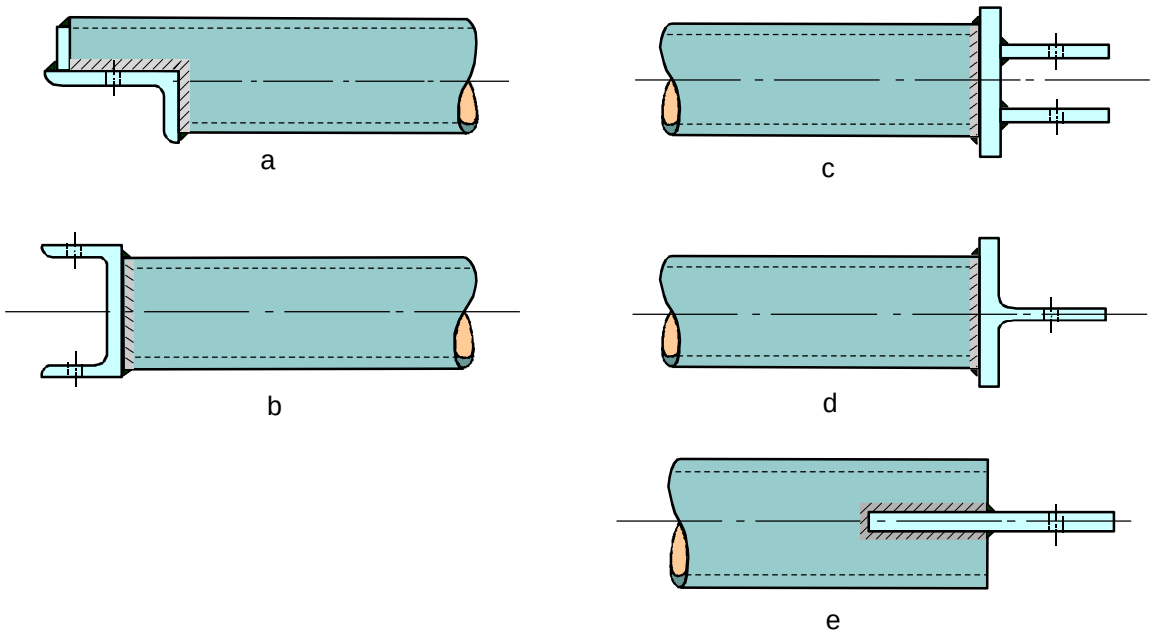

Fig. 12.5 Bolted shear end connections

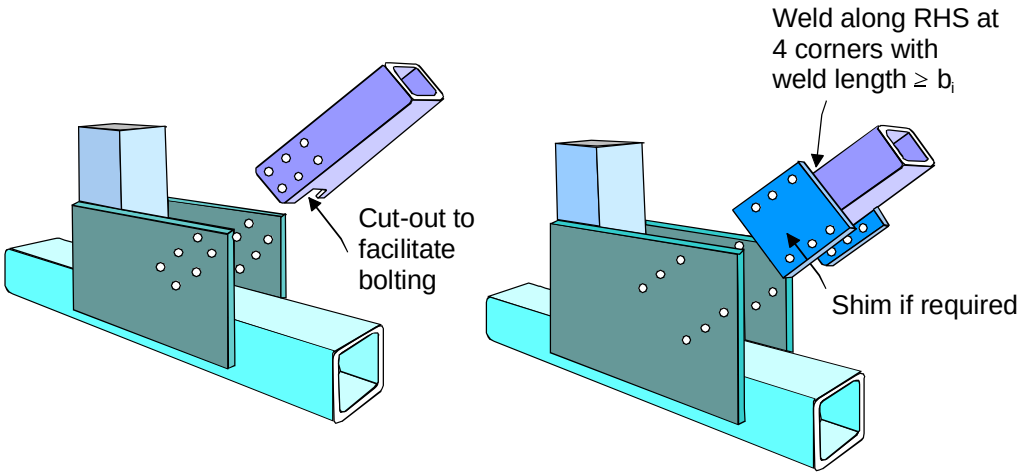

a) Simple shear splice

b) Modified shear splice

Fig. 12.6 Some examples of bolted gusset plate connections

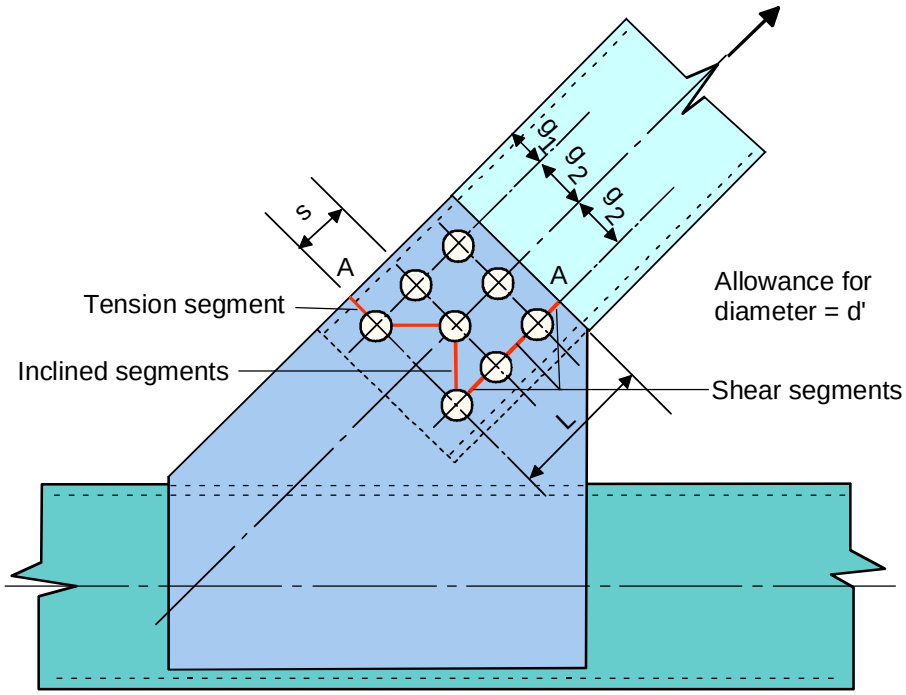

Effective net area for critical section A-A is the sum of the individual segments :

for tension segment	:	$(g_1 - d'/2)t$
for shear segments	:	$0.6(L - 2.5d')t$
for each inclined segment	:	$(g_2 - d')t + \{(\frac{s^2}{4g_2})\}t$

Fig. 12.7 Calculation of effective net area for a gusset plate

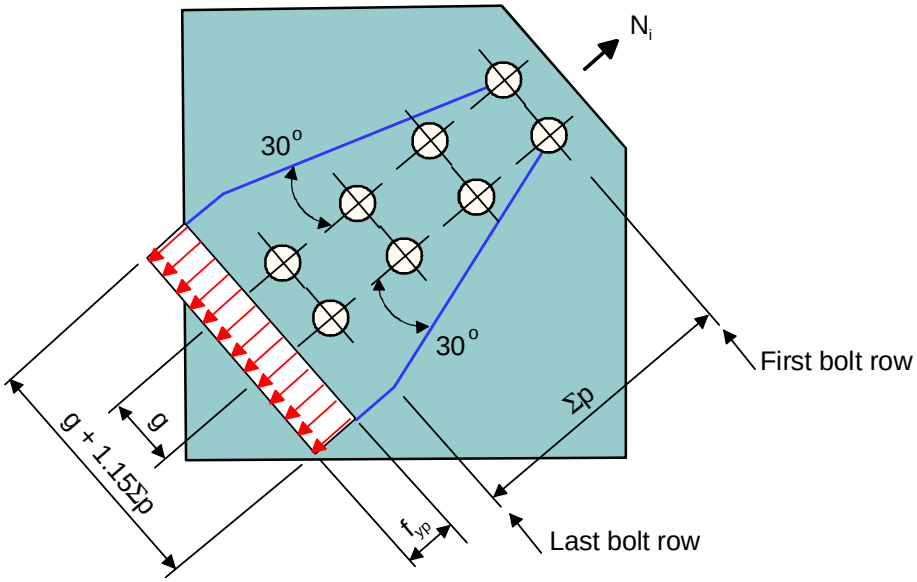

Fig. 12.8 Whitmore criterion for gusset-plate yielding

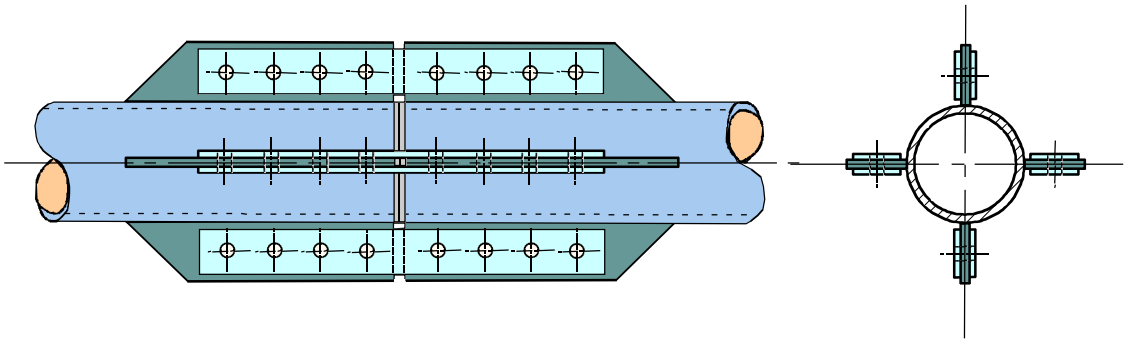

Fig. 12.9 Bolted splice connection for CHS

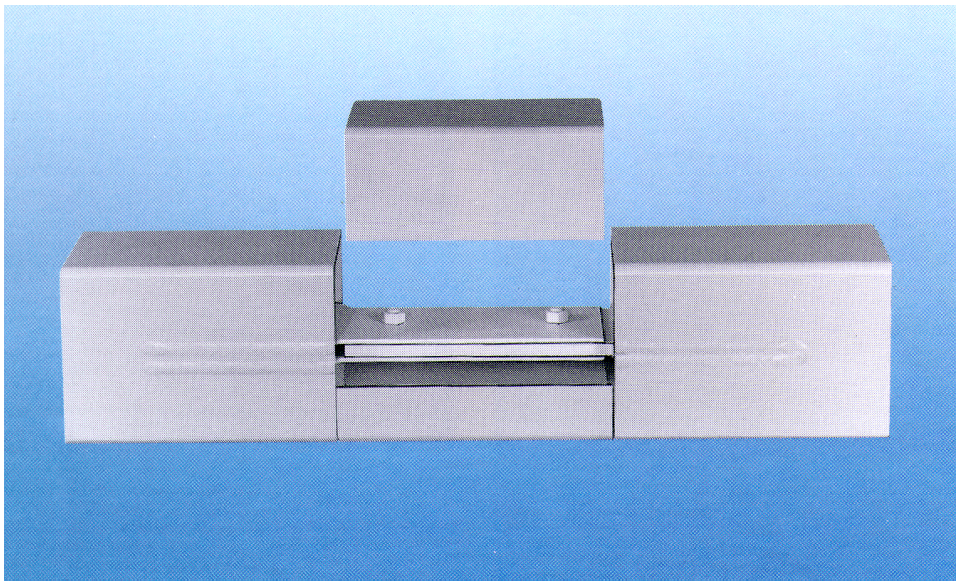

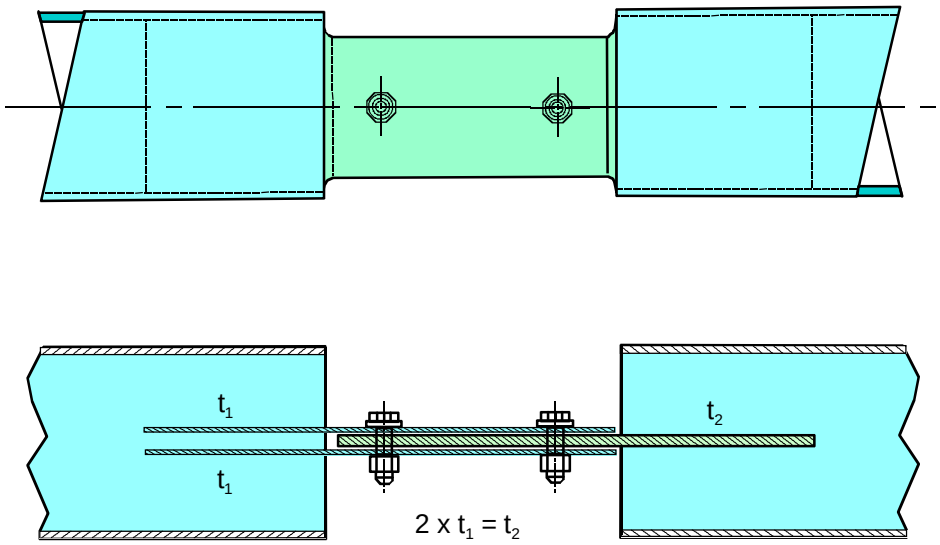

Fig. 12.10 Hidden bolted splice connection

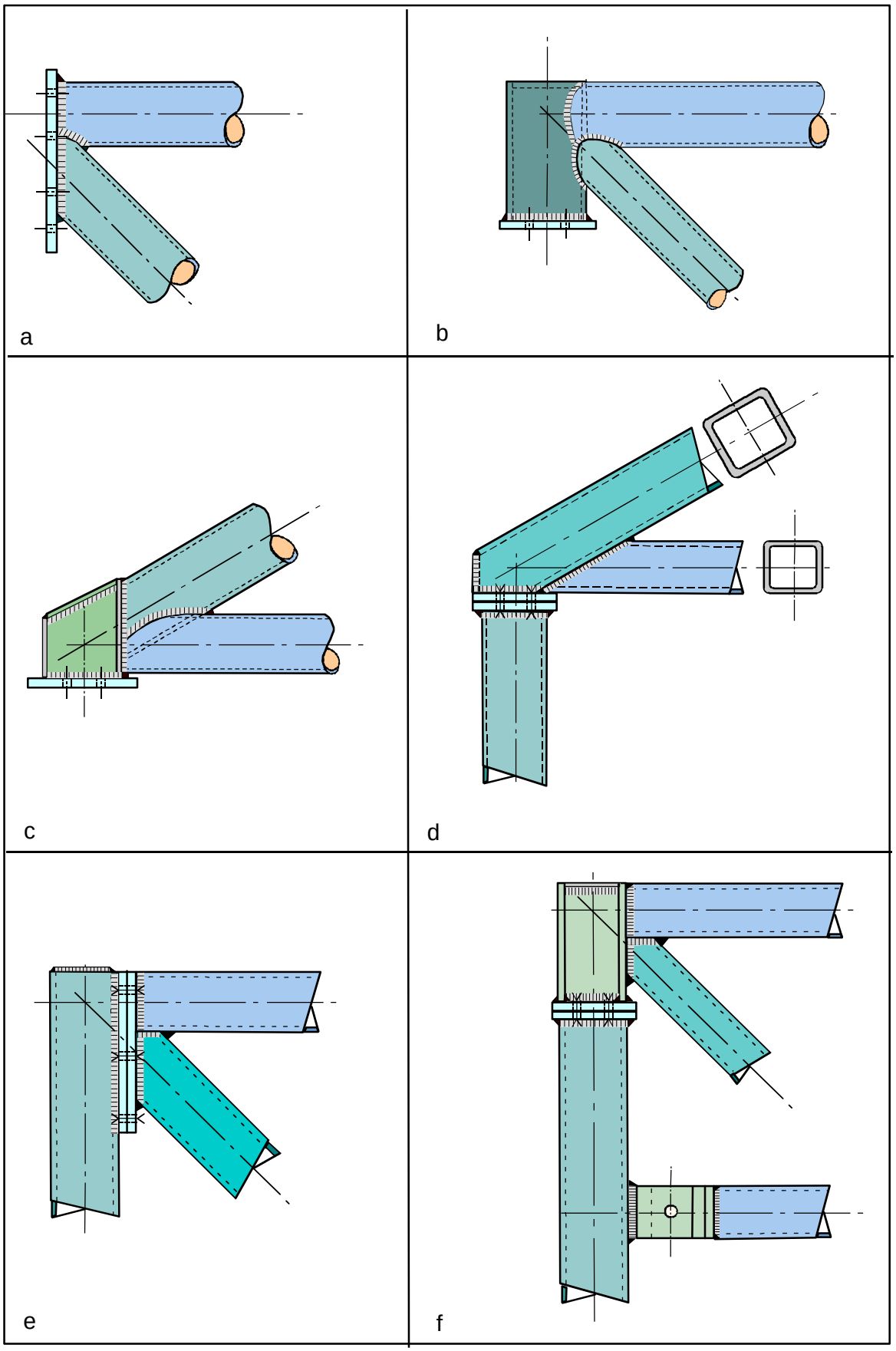

Fig. 12.11 Bolted connections for lattice girder supports

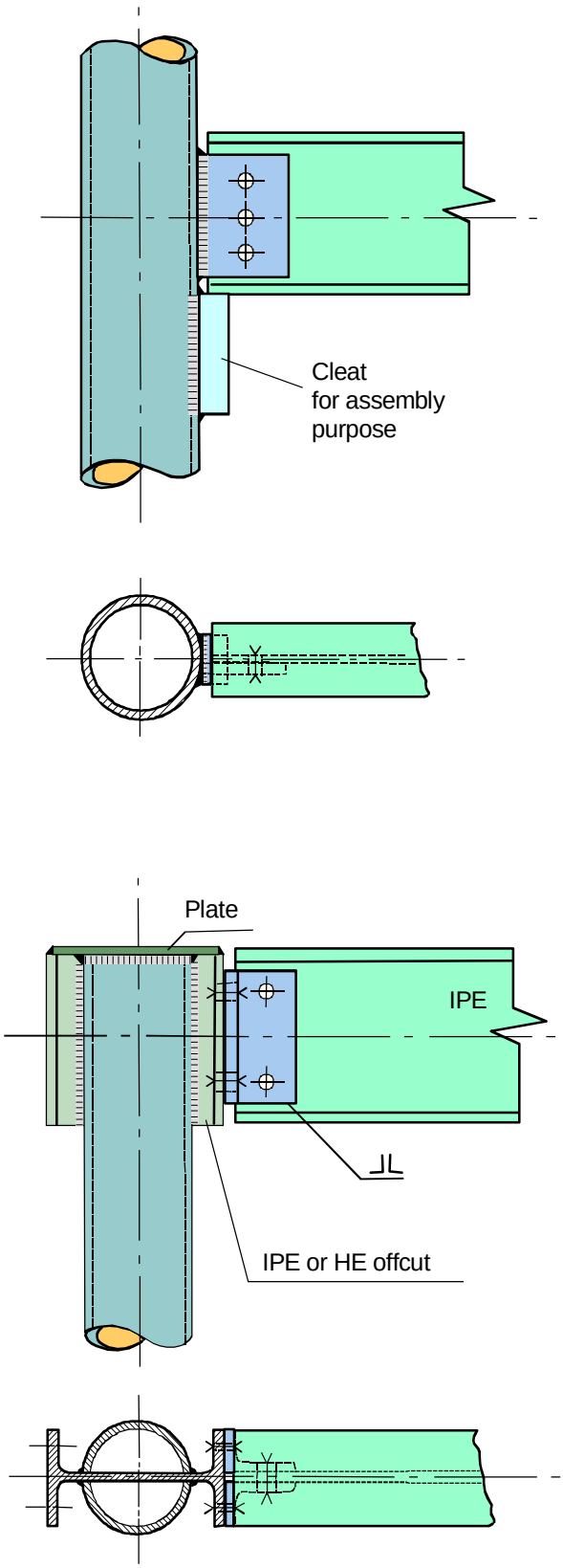

Fig. 12.12 I-section beam to CHS-column connections

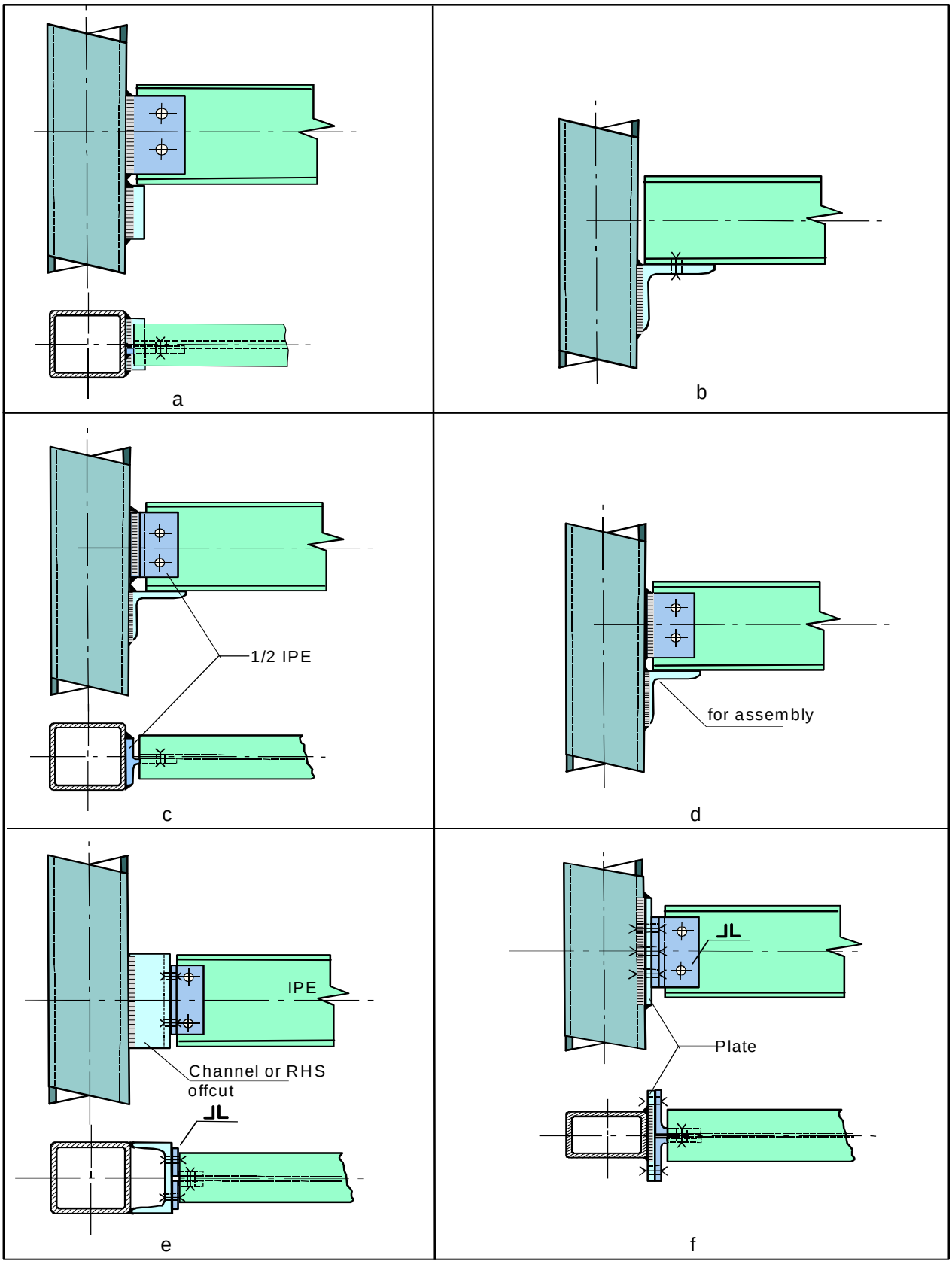

Fig. 12.13 I-section beam to RHS column simple shear connections

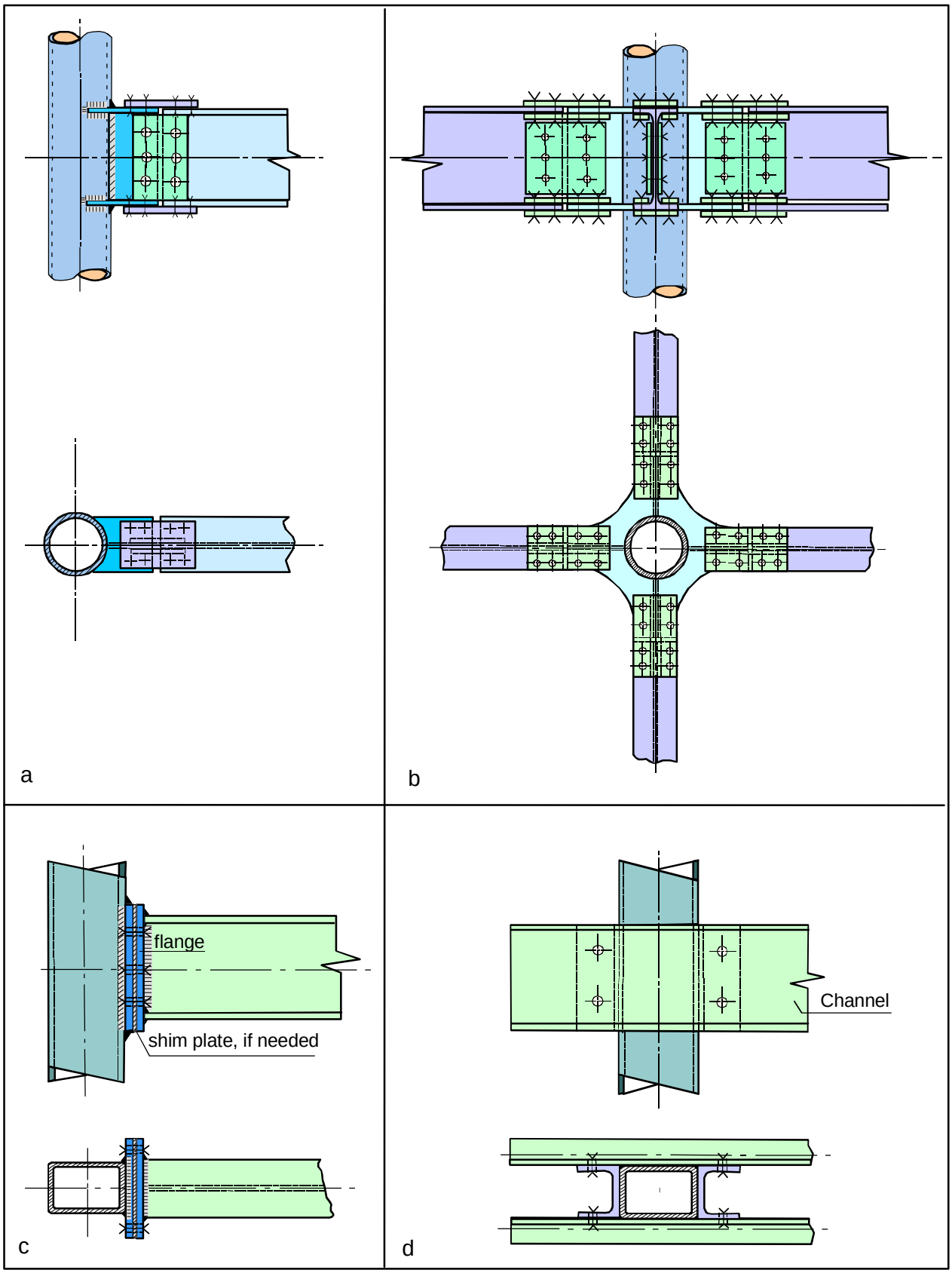

Fig. 12.14 Moment connections between open section beams and CHS or RHS columns

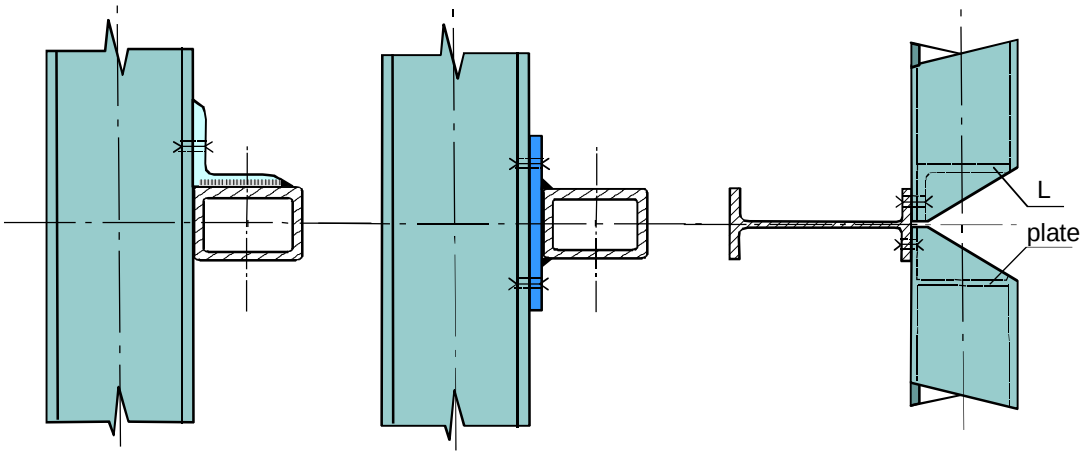

Fig. 12.15 Hollow section cross members connected to I-section columns

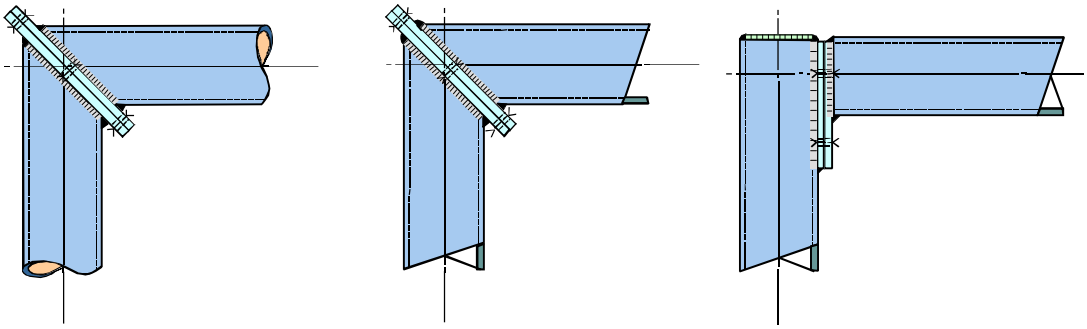

Fig. 12.16 Knee joint assemblies for portal frames

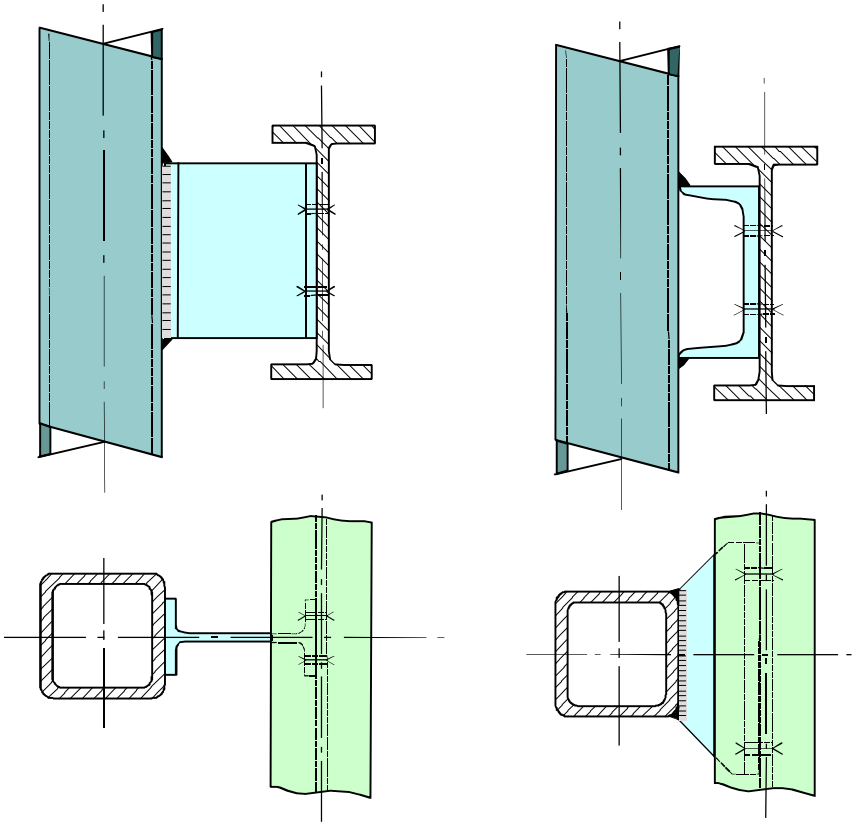

a b

Fig. 12.17 Bracket connections

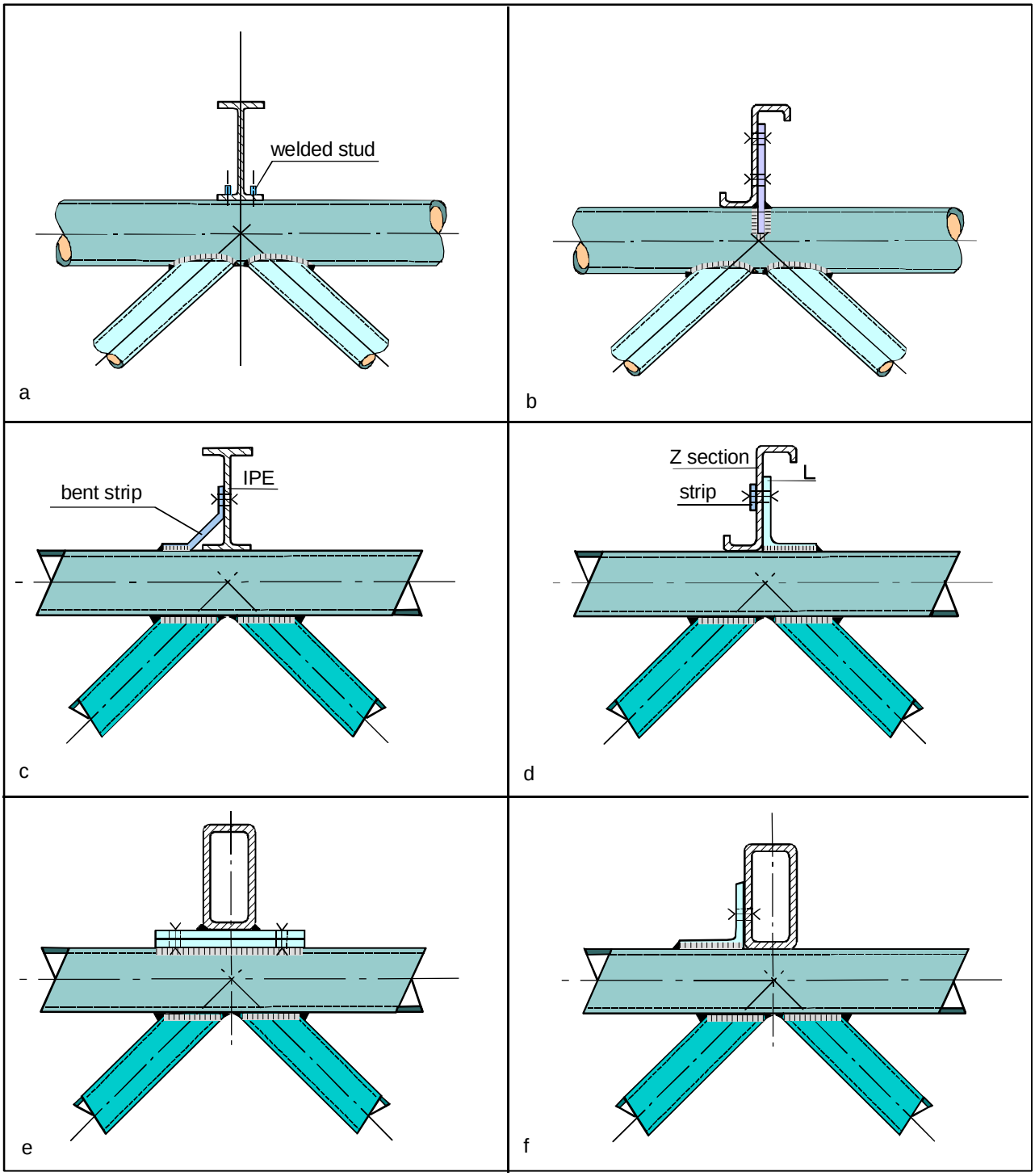

Fig. 12.18 Purlin connections

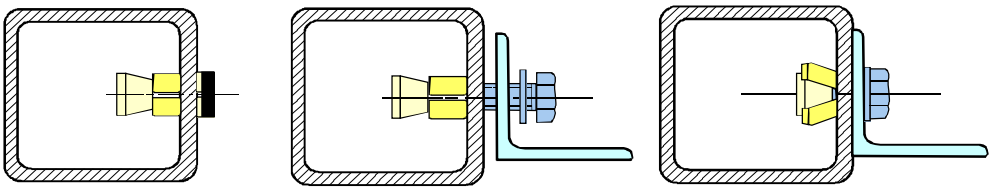

Fig. 12.19 Lindapter "HolloFast"

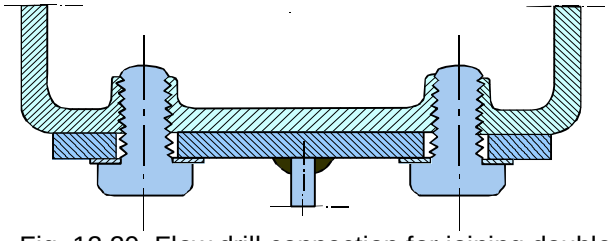

Fig. 12.20 Flow drill connection for joining double angle web cleats or flexible end plates to RHS

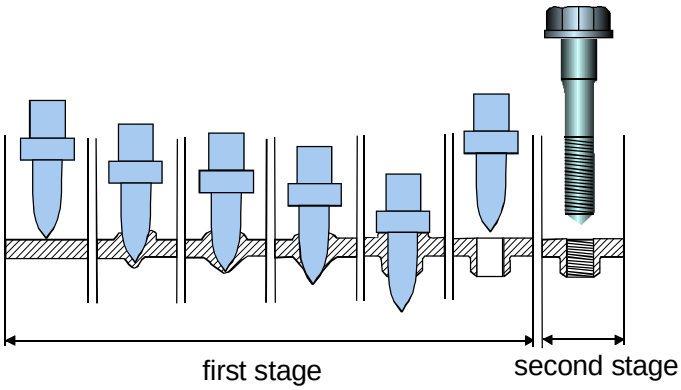

Fig. 12.21 Flowdrill process

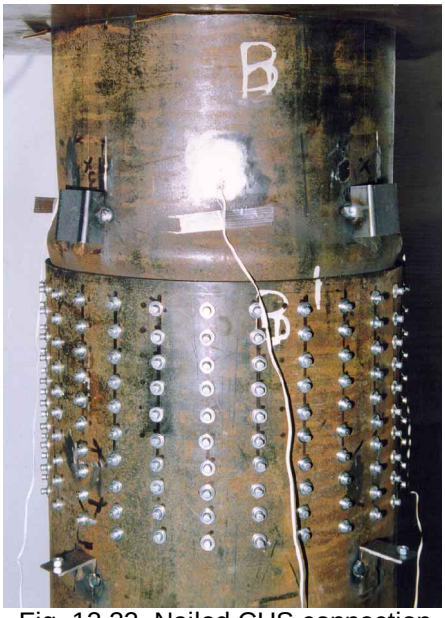

Fig. 12.22 Nailed CHS connection

13. FATIGUE BEHAVIOUR OF HOLLOW SECTION JOINTS

Fatigue is a mechanism whereby cracks grow in a structure under fluctuating stress. Final failure generally occurs when the reduced cross section becomes insufficient to carry the load without rupture. Generally the fatigue cracks start at locations with high stress peaks.
High stress peaks may occur at local notches, e.g. at welds (Fig. 13.1). However, geometric peak stresses may also occur due to the geometry, e.g. at holes or in hollow section joints due to the non-uniform stiffness distribution at the perimeter of the connection (Fig. 13.2).

Thus the fatigue behaviour is largely influenced by the loading and the way the members are connected. Hollow sections without any connections or attachments are rarely prone to fatigue. Thus the effect of the attachments or the connections is generally governing for the fatigue behaviour.

In a fatigue analysis the loading and the loading effects should be carefully evaluated and compared with the fatigue resistance.

Sometimes it is difficult to determine the loading effects accurately, e.g. the secondary bending moments in lattice girders. In such cases simplified approaches can be used.

13.1 DEFINITIONS

Stress range $\Delta\sigma$
The stress range $\Delta\sigma$ (shown in Fig. 13.3) is the difference between the maximum and minimum stress in a constant amplitude loading regime.

Stress ratio R
The stress ratio R is defined as the ratio between the minimum stress and the maximum stress in a stress cycle of constant amplitude loading (Fig. 13.3).

Fatigue Strength
The fatigue strength of a welded component is defined as a stress range $\Delta\sigma$, which causes failure of the component after a specified number of cycles N.

Fatigue life
The number of cycles N to a defined failure is known as the endurance or fatigue life.

Fatigue limit
The stress range below which it is assumed that no fatigue failure occurs for a constant amplitude loading, is known as the fatigue limit. For Eurocode 3 [12] and the IIW recommendations [19], for example, this occurs at $N = 5 \times 10^6$ cycles.

Cut off limit
The stress range below which it is assumed that the stress ranges of a variable amplitude loading do not contribute to the fatigue damage, is known as the cut off limit. For Eurocode 3, for example, this occurs at $N = 10^8$ cycles (see Fig. 13.6).

Geometric stress
The geometric stress, also called hot spot stress, is defined as the extrapolated principal stress at a specified location at the weld toe. The extrapolation must be carried out from the region outside the influence of the effects of the weld geometry and discontinuities at the weld toe, but close enough to fall inside the zone of the stress gradient caused by the global geometrical effects of the joint. The extrapolation is to be carried out on the brace side and the chord side of each weld (see Fig. 13.7). Generally the geometric stress (or the hot spot stress) can be determined by considering the stress normal to the weld toe since the orientation of the maximum principal stress is normal or almost normal to the weld toe.

Stress concentration factor
The stress concentration factor (SCF) is the ratio between the geometric peak stress, or hot spot stress, excluding local effects, at a particular location in a joint and the nominal stress in the member due to a basic member load which causes this geometric stress.

13.2 INFLUENCING FACTORS

The fatigue behaviour can be determined either by $\Delta\sigma$-N methods or with a fracture mechanics approach. The various $\Delta\sigma$-N methods are based on experiments resulting in $\Delta\sigma$-N graphs (Fig. 13.4) with a defined stress range $\Delta\sigma$ on the vertical axis and the number of cycles N to a specified failure criterion on the horizontal axis.

The relation between the number of cycles fo failure N and the stress range $\Delta\sigma$ can be given by:

$$N = C \cdot \Delta\sigma^{-m} \qquad (13.1)$$

or

$$\log N = \log C - m \log(\Delta\sigma) \qquad (13.2)$$

On a log - log scale this gives a straight line with a slope (-m), see Fig. 13.4.

The fracture mechanics approach is based on a fatigue crack growth model and will not be further discussed in the context of this book. Due to the appearance of residual stresses, the stress ratio $R = \sigma_{min}/\sigma_{max}$ (see Fig. 13.3) is not taken into account in modern fatigue design. Only if the structure is fully stress relieved, might it be advantageous to take the stress ratio into account.
The influence of residual stresses is shown in the example in Fig. 13.5 for f_y = 240 N/mm^2.
A nominal $\Delta\sigma_{nom}$ = 120 N/mm^2 is applied on the plate, resulting in a nominal average $\Delta\sigma_{nom} = \frac{80 \times 120}{60} = 160$ N/mm^2 at the nett cross section at the hole.

With a geometric stress concentration factor SCF = 3, this results in a theoretical geometric
$\Delta\sigma_{geom}$ = SCF. $\Delta\sigma_{nom}$ = 3 x 160 = 480 N/mm^2.
However, at 240 N/mm^2 the material is yielding, resulting in the stress pattern "b".
Unloading to zero means that the elastic stress pattern "a" has to be subtracted from "b" resulting in the residual stress pattern "c". The next cycle will thus fluctuate between the pattern "c" and "b", thus starting from a residual stress equal to the yield stress.

In welded structures, residual stresses and discontinuities exist at welds too. That is why it is assumed that locally the stress will fluctuate between the yield stress and a lower limit f_y - $\Delta\sigma_{geom}$.

The example in Fig. 13.5 with a tensile loading resulted in a compressive residual stress at the hole, which is favourable. However, it also shows that a compressive loading would have resulted in a tensile residual stress at the hole, which is unfavourable. In this latter case, it would result in fatigue failure under an external compression stress range $\Delta\sigma$.

In practical situations, various stress ranges occur and the residual stress ranges are not known. That is why generally no difference is made between tensile and compressive loading.
For general details, e.g. butt-welded, end-to-end connections, cover plates, attachments, etc., $\Delta\sigma$-N lines can be determined. These $\Delta\sigma$-N lines (Figs. 13.4 and 13.6) already take the effect of the welds and the geometry of the connection into account.

For more complicated geometries, such as the directly-welded connections between hollow sections, the peak stresses and thus the peak stress ranges depend on the geometrical parameters. This means that for every connection a separate $\Delta\sigma$-N line exists. This is why in modern design the fatigue behaviour of hollow section connections is related to basic $\Delta\sigma$-N curves, in which $\Delta\sigma$ represents a geometrical or hot spot stress range taking into account the effect of the geometry of the connection. This geometrical stress range can also be calculated by multiplying the nominal stress range with a relevant stress concentration factor (SCF). As a consequence of this method, stress concentration factors should be available for connections with various geometries. The effect of the weld is included in the basic $\Delta\sigma$-N lines. As will be shown later, the thickness of the sections is also an influencing parameter. The fatigue loading is seldom critical for the members compared to the connections.

13.3 LOADING EFFECTS

As stated before, the stress range $\Delta\sigma$ is a governing parameter for fatigue. For constant amplitude loading, the $\Delta\sigma$-N line is generally cut off between N = 2 x 10^6 to 10^7 cycles depending on the code. Eurocode 3 [12] and IIW [19] use 5 x 10^6 (see Figs. 13.4 and 13.6).

For random loading, also called spectrum loading, the smaller cycles also have an effect and the cut off is taken at 10^8 to 2 x 10^8, depending on the code. EC3 uses a cut off at N = 10^8. Between 5 x 10^6 to 10^8 a $\Delta\sigma$-N line is used with a shallower slope of m = -5. Although the sequence of the stress ranges affects the damage, the simplest and best rule available up to now to determine the cumulative damage is the Palmgren-Miner linear damage rule, i.e.

$$\Sigma \frac{n_i}{N_i} \leq 1.0 \qquad (13.3)$$

in which n_i is the number of cycles of a particular stress range $\Delta\sigma_i$ and N_i is the number of cycles to failure for that particular stress range. If vibration of the members occurs, the nominal stress ranges may be considerably increased. This will be the case if the natural frequency of a structural element is close to the frequency of the loading. It is therefore essential to avoid this.
For very high stress ranges and consequently a low

number of cycles, low cycle fatigue may occur. In this case, no $\Delta\sigma$-N curves are given in the codes, since the fatigue is mainly governed by the strains. In [120], it is shown that the various $\Delta\sigma$-N curves can be used if translated into strain, i.e. $\Delta\epsilon$-N curves. In this case the loading should be evaluated based on the resulting strain range $\Delta\epsilon$. However, such high strain ranges may finally result in brittle fracture after a fatigue crack is initiated.

13.4 FATIGUE STRENGTH

The fatigue strength for members with butt welded or fillet welded end-to-end connections, with plates or members with attachments, etc. is given as the stress range at 2×10^6 cycles in EC3. This classification is in line with the classifications given for other members such as I-sections, etc. Some classifications according to EC3 are given in Table 13.1.
It is shown that the classification of 160 or 140 N/mm^2 in Table 13.1 for a plain section without attachments or connections is much higher than the classification for details.
It is also clear that a butt welded end-to-end connection shows a better fatigue behaviour than a fillet welded end-to-end connection with an intersecting plate.

The classification is independent of the steel grade. Higher strength steels are more sensitive to notches, which reduces the favourable effect of higher strength. However, recent investigations have shown that, especially for thin walled sections and in particular if improved welding methods are used or post weld improvements (grinding, TIG or plasma dressing, etc.) are carried out to give a smooth transition from parent material to weld, higher fatigue strengths can be obtained for high strength steels (e.g. for S 460).

13.5 PARTIAL SAFETY FACTORS

In using the fatigue strengths it should be noted that the stress ranges produced by the (unfactored) loading have to be multiplied, according to EC3, by a partial safety factor which depends on the type of structure (fail safe or non fail safe) and the possibility for inspection and maintenance. The partial safety factors according to Eurocode 3 are given in Table 13.2.

For example a γ_M=1.25 for a slope of m = -3 results in a factor $(1.25)^{-3} \approx 0.5$ on fatigue life (i.e. half the value of N).

13.6 FATIGUE CAPACITY OF WELDED CONNECTIONS

In 13.4 the basic parameters influencing the strength of members with attachments or with end-to-end connections are discussed. It has already been stated that in welded connections between hollow sections the stiffness around the intersection is not uniform, resulting in a geometrical non-uniform stress distribution as shown in Fig. 13.2 for an X-joint of circular hollow sections. This non-uniform stress distribution depends on the type of loading (axial, bending in plane, bending out of plane), the connection types and geometry. This is the reason why the fatigue behaviour of hollow section joints is generally treated in a different way than, for example, that for welded connections between plates.

13.6.1 Geometrical stress approach

Since peak stresses determine the fatigue behaviour, in modern design methods the fatigue design is related to the geometrical stress range of a connection. This geometrical stress range includes the geometrical influences but excludes the effects related to fabrication such as the configuration of the weld (flat, convex, concave) and the local condition at the weld toe (radius of weld toe, undercut, etc.). The fatigue behaviour of fillet welded connections is sometimes related by factors to that for butt welded connections. Since the geometrical peak stress (also called hot spot stress) can only be determined with finite element methods or by measurements on actual specimens, stress concentration factors have been developed for the basic types of joints and basic loadings. These stress concentration factors are defined as the ratio between the geometrical (peak) stress and the nominal stress causing the geometrical stress, for example for an axially loaded X-joint without chord loading:

$$SCF_{i,j,k} = \frac{\text{geometrical stress}_{i,j,k}}{\text{nominal stress in the brace}} \qquad (13.4)$$

with:
i = chord or brace
j = location, e.g. crown, saddle or in between for CHS joints
k = type of loading

Thus, several SCFs have to be determined for various locations which are the likely critical positions (Fig. 13.7). The maximum SCF and the location depend on

the geometry and loading. This is particularly important for combined loadings.
Thus, for determining the fatigue life the geometrical (peak) stress range has to be calculated for the various locations:

$$\Delta\sigma_{geom_{i,j,k}} = \Sigma(\Delta\sigma_{nom_{i,k}} \cdot SCF_{i,j,k}) \qquad (13.5)$$

The $\Delta\sigma$-N line to be considered is also based on the geometrical stress range.

Recent research has shown that the $\Delta\sigma$-N curves can be higher than those given in EC3 since at the time of drafting EC3 not all results were available. However, EC3 allows higher values than given if proven by appropriate tests. For 16 mm wall thickness, the fatigue class 114 (at 2 x 10^6 cycles) can be adopted for hollow section joints using the geometric stress approach. This deviates somewhat from the classifications given previously in [6]. The reanalysis in [123] showed that one set of curves with one general thickness correction factor is possible for connections of CHS and RHS.

The curves with the thickness correction included in the $\Delta\sigma$-N curves are given in Fig. 13.8. It has been shown that the stress or strain gradient influences the fatigue life. Since this influence is not incorporated in the geometrical stress range, joints with relatively high stress concentration factors show a larger thickness effect, i.e. the fatigue performance is better for thin walled connections than for those with thick walls.

It should be noted that no further thickness effect should be used for thicknesses below 4 mm, since the weld performance may overrule the geometrical influence, which may sometimes result in lower fatigue strengths [42].
For the designer it is important to have an insight into the parameters which determine the stress concentration factors. Optimal design requires the stress concentration factors to be as low as possible.

As an indication, the stress concentration factors are given for some joint configurations. Fig. 13.9 shows the stress concentration factors for axially loaded X-joints of circular hollow sections at four locations, i.e. for the chord and brace, at the crown and saddle. The following conclusions can be made:

For the chord

- Generally the highest SCF occurs at the saddle position
- Highest SCFs at the saddle are obtained for medium β ratios
- SCF decreases with decreasing τ value
- SCF decreases with decreasing 2γ value

For the brace

- Generally the same applies as for the chord; however, a decrease in τ value gives an increase in SCF at the crown position (in some cases the graphs are only given here for $\tau \simeq 1.0$).
- SCF in the brace may become critical compared to that in the chord for small τ values; however, the brace thickness is then smaller than the chord thickness. Considering the thickness effect, this still results mostly in a critical chord location.

For X-joints of square hollow sections the SCFs are given for various locations in Fig. 13.10. As mentioned before, similar observations can be made as for circular hollow section X-joints:
- For τ = 1 the highest SCFs generally occur in the chord at locations B and C
- The highest SCFs are found for medium β ratios
- The lower the 2γ ratio, the lower is the SCF
- The lower the τ ratio, the lower is the SCF in the chord, whereas it has less influence for the brace.

Fig. 13.11 shows the SCFs for an axially loaded K-gap joint of circular hollow sections with $g = 0.1\ d_0$. Here the same observations are valid as for X-joints, but the SCFs are considerably lower due to the stiffening effect of the opposite loadings on the chord face. Here only maximum SCF values for chord and brace are given (i.e. no differentiation is made between the saddle and crown positions).

The effect of the brace angle is not included in the figures, but a decrease in the angle between brace and chord results in a considerable decrease in SCF.
If the chord is loaded, the geometrical or hot spot stress range at the chord locations at the crown (CHS) or at the locations C and D (RHS) (see Fig. 13.7) has to be increased by the chord nominal stress range multiplied by the stress concentration factor produced by the chord stresses. As shown in Fig. 13.12, this SCF varies between 1 and 3, for RHS T- and X-joints depending on the loading, type of joint and geometrical parameters [122].

Another aspect to be considered is multiplanar loading. For the same type of joint and the same geometry, different SCFs can be obtained for different loading conditions (see Fig. 13.13).
All the SCFs are based on measurements taken at the

toe of the weld, since this location is generally critical.

However, for very low SCFs, crack initiation can start at the weld root. Therefore a minimum SCF = 2.0 is recommended. Further, the SCF values have been determined for butt welded joints. Fillet welds cause somewhat lower SCFs in the chord, but due to local wall bending effects considerably higher SCFs in the braces. It is therefore recommended to increase the SCFs in RHS braces of T- and X-joints by a factor of 1.4 [122] when fillet welds are used..

Considering all these aspects, it can be concluded that optimal design can be achieved if the SCFs are as low as possible. Thus the following guidelines can be given:
- Avoid medium β ratios.
  β ratios close to 1.0 give the lowest SCFs.
- Make the wall thickness of the brace as low as possible (low τ)
- Take relatively thick walled chords (low $2g$ ratio).

In this way, SCFs of about 2 to 4 are possible resulting in an economic design.

Note : If the bending moments in girders have not been accurately determined by finite element analyses or other methods, the effect of bending moment can be in corporated in a simplified manner as discussed in 13.6.2.

13.6.2 Classification method based on nominal stress ranges

For simple design methods it would be easier if the SCFs could already be incorporated in the design class taking account of the main influencing parameters.
This, however, is impossible for T-, Y- and X-joints, since the variation in SCF is considerable. For K-joints, however, this is possible to a certain extent and has been done in Eurocode 3. The thickness effect is indirectly taken into account. The method can only be used for thin walled sections (see recommended range of validity).
The classification only depends on the gap, overlap and τ ratio (Table 13.3). It must be stated that the design classes are based on test results and on an independent analysis, and do not fully comply with the stress concentration factor method. The design classes given show clearly the advantage of using a low T ratio or high t_0/t_i.
Since it is sometimes difficult for designers to determine the secondary bending moments, EC3 allows a calculation based on the assumption that braces are pin connected to a continuous chord. However, the stress ranges in chord and braces caused by the axial loading in the braces have to be multiplied by the factors given in Tables 13.4 and 13.5 to account for the secondary bending moments.
These values are based on measurements in actual girders.

13.7 FATIGUE CAPACITY OF BOLTED CONNECTIONS

High strength friction grip (HSFG) bolted connections show a more favourable fatigue behaviour than ordinary untentioned bolted connections. High strength bolted connections loaded in tension can, for example, be designed in such a way that the fatigue load does not critically affect the joints. Prestressed high strength bolted connections subjected to shear or friction loads can bear higher fatigue stresses than welded joints, which means that in general, these bolted connections in shear do not represent the most critical elements. Bolted connections should be designed in such a way that there is no play and no sliding motion between the parts.

13.7.1 Bolted connections under tensile load

Theoretical investigations and experimental results [128] indicate that the fatigue behaviour of prestressed bolted connections is significantly influenced by the way in which the load is transmitted. A few examples of bolted connections in tension are shown in Fig. 13.14.

For configurations a_1 and a_2 (Fig. 13.14) the contact face pressure is, by design, co-axial with the external load. As the load increases, there is at first, in this case, a significant decrease in the contact pressure. It is only when the applied load exceeds the contact pressure, that the load in the high strength bolts begins to increase appreciably. For configurations c_1 and c_2, the load in the high strength bolts increases from the very beginning with growing applied load. This leads to the conclusion that connection types a_1 and a_2 are better in fatigue than the other types.

The rigidity of the flanges is distinctly higher with the a_1 and a_2 configurations than with the axial load transmission through the bolts accompanied by flange bending. This leads to a small stress increase in bolts

under fatigue load. This change in stresses due to fatigue loading can be neglected, when the external bolt load F_t is smaller than the bolt preload F_v.

Should the load transmitting parts not be located on the same plane, the connections must then be designed in such a manner that the load transmission is mainly effected through the reduction of contact loads. The arrangements shown in Fig. 13.15 are recommended for bolted ring flange connections between hollow sections. These proposed flange connections require expensive machining and finishing. However, the same level of load transmission can be achieved simply with the help of packing plates (shims). It is further recommended that high strength bolts be located as closely as possible to the load carrying structural parts. *Snug tight bolted connections without prestressing should be avoided, since the fatigue behaviour is bad.*

13.7.2 Bolted connections under shear load

The fatigue stress values of high strength bolted connections under shear load are generally higher than those pertaining to welds that connect hollow sections to end plates. As shown in Fig. 13.16, the stress distribution in prestressed bolted connections is significantly better than that in bolted connections without preload. The reason is that part of the external load is transmitted by the frictional force before the bolt hole. After a high strength bolted connection has slipped, a more unfavourable stress distribution applies than before, since part of the force is now transmitted by pressure on the face of the hole as well as by the frictional force (see Fig. 13.16c).
Non-prestressed, non-fitted bolts should be avoided for structural parts subjected to fatigue loading.

Recommendations for the design class of high strength bolted connections are given in Eurocode 3 (see Table 13.6).
It is noted that depending on the conditions, load factors have to be used; see e.g. Table 13.2.

13.8 FATIGUE DESIGN

In the previous sections the fatigue resistance of hollow section joints has been discussed in relation to the geometry. However, when a designer starts with the design process, the geometry is not known and he or she has first to determine the geometry, e.g. for a truss. Here, several steps have to be followed:

Step A:
For the determination of the geometry, use has to be made of the knowledge obtained in the previous sections. For a good performance of joints, the following points have to be considered to obtain the best fatigue behaviour:
- Select joints with high or low β values, avoid intermediate values. Considering fabrication, $\beta = 0.8$ is preferred to $\beta = 1.0$.
- Choose the chord diameter or chord width-to-thickness ratio 2γ to be as low as possible; e.g. for tension chords about 20 or lower and for compression chords about 25 or lower.
- Design the braces to be as thin as possible to achieve preferably brace to chord thickness ratios $\tau \leq 0.5$ and to minimise welding.
- Design girders in such a way that the angles θ between braces and chord are preferably about 40°.

Considering the above, joints with relatively low stress concentration factors can be achieved: e.g. for a K-joint of circular hollow sections (Fig. 13.11) with

$\beta = 0.8$
$2\gamma = 20$ } SCF chord ≈ 2.1
$\tau = 0.5$ } SCF brace ≈ 2.0
$\theta = 40°$

Step B:
Based on the required lifetime the number of cycles N has to be determined.

Step C:
For the number of cycles N (from B) the geometric stress range $\Delta\sigma_{geom.}$ can be determined from the $\Delta\sigma$-N line assuming a certain thickness, see Fig. 13.8.

Step D:
Depending on the inspection frequency and the type of structure ("failsafe" or "non failsafe") the partial load factor γ_{Mf} can be determined (Table 13.2).

Step E:
Determine the factors C to account for secondary bending moments (Tables 13.4 and 13.5).

Step F:
Based on steps A, C, D and E, the allowable nominal stress range for the braces can be determined:

$$\Delta\sigma_{nom.brace} = \frac{\Delta\sigma_{geom.}}{\gamma_{Mf} \cdot C \cdot SCF}$$

For a particular R ratio the $\sigma_{max.}$ can be determined as follows:

$$\left.\begin{aligned} R &= \frac{\sigma_{min.}}{\sigma_{max.}} \\ \Delta\sigma &= \sigma_{max} - \sigma_{min} \end{aligned}\right\} \quad \sigma_{max.} = \frac{\Delta\sigma}{1-R}$$

Thus:

$$\sigma_{max.nom.brace} = \frac{\Delta\sigma_{geom.}}{\gamma_{Mf} \cdot C \cdot (1-R) \cdot SCF}$$

With this maximum brace stress the cross section of the braces can be determined and, with the parameters selected under step A, the chord dimensions and the joint.
If the chord has large chord loads, a larger cross section should be taken to account for this.

Step G:
The configuration now determined should be checked for ease of fabrication, inspection and the validity range for joints.
If the design satisfies the requirements, the final calculation can be carried out, however, now starting from the loading and the known geometry.

The procedure is now as follows:

1. Determine loads and moments in members and from these the stresses in braces and chord, e.g. assuming continuous chords and pin ended connections to rigid stiff members if the members are not noding, see Fig. 13.17.
2. Determine from (1) the nominal stress range $\Delta\sigma_{nom.brace}$ in the brace and the $\Delta\sigma_{nom\ chord}$ in the chord.
3. Multiply the nominal stress ranges by the partial safety factor γ_{Mf}, the factors to account for secondary bending moments (step E) and the SCFs to obtain the maximum geometric stress ranges for chord and braces.
4. Determine the number of cycles to failure in the $\Delta\sigma$-N curve for geometric stress for the relevant thickness and thus the fatigue life.

If this meets or exceeds the required fatigue life, the design will satisfy the requirements. Otherwise modifications have to be made.

If a spectrum (variable amplitude) loading is acting, the spectrum can be divided into stress blocks and for each stress range the number of cycles to failure can be determined. Using the Palmgren-Miner rule (eq. 13.1) will give the cumulative damage which should not exceed 1.0.

Table 13.1 Detail category EC3: Hollow sections and simple connections

Details loaded by nominal normal stresses		
Detail m = -3	Construction detail	Description
160	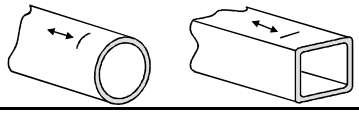	Rolled and extruded products Non-welded elements. Sharp edges and surface flaws to be improved by grinding
140	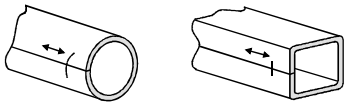	Continuous longitudinal welds Automatic longitudinal welds with no stop-start positions, proven free of detectable discontinuities.
71	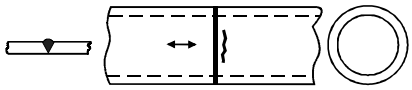	Transverse butt welds Butt welded end-to-end connection of circular hollow sections Requirements - Height of the weld reinforcement less than 10% of weld with smooth transitions to the plate surface - Welds made in flat position and proven free of detectable discontinuities - *Details with wall thickness greater than 8 mm may be classified two Detail categories higher (90)*
56	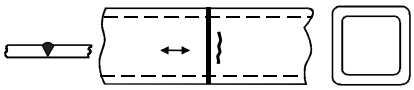	Transverse butt welds Butt welded end-to-end connection of rectangular hollow sections Requirements: - Height of the weld reinforcement less than 10% of weld with smooth transitions to the plate surface - Welds made in flat position and proven free of detectable discontinuities - *Details with wall thicknesses greater than 8 mm may be classified two Detail categories higher (71)*
71	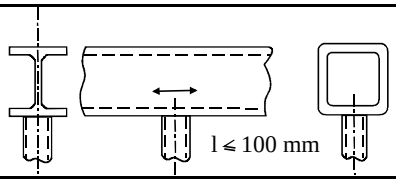	Welded attachments (non-load-carrying welds) Circular or rectangular section, fillet welded to another section. Section width parallel to stress direction 100 mm.
50	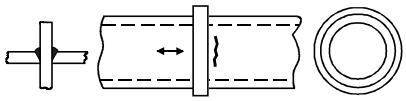	Welded connections (load carrying welds) Circular hollow sections, end-to-end butt welded with an intermediate plate. Requirements: - Welds proven free of detectable discontinuities - *Details with wall thicknesses greater than 8 mm may be classified one Detail category higher (56)*
45	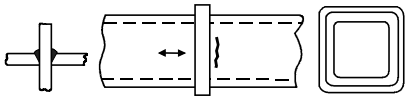	Welded connections (load carrying welds) Rectangular hollow sections, end-to-end butt welded with an intermediate plate. Requirements: - Welds proven free of detectable discontinuities - *Details with wall thicknesses greater than 8 mm may be classified one Detail category higher (50)*
40	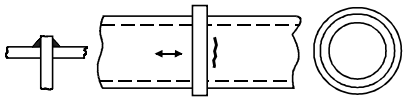	Welded connections (load-carrying welds) Circular hollow sections, end-to-end fillet welded with an intermediate plate. Requirements: - Wall thickness less than 8 mm.
36	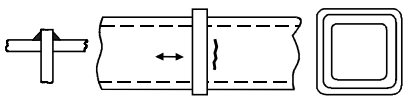	Welded connections (load-carrying welds) Rectangular hollow sections, end-to-end fillet welded with an intermediate plate Requirements: - Wall thickness less than 8 mm

Table 13.2 Partial safety factors γ_M according to Eurocode 3

Inspection and access	"Fail safe" structures	Non "fail safe" structures
Periodic inspection and maintenance Accessible joint detail	$\gamma_M = 1.00$	$\gamma_M = 1.25$
Periodic inspection and maintenance Poor accessibility	$\gamma_M = 1.15$	$\gamma_M = 1.35$

Table 13.3 See next page

Table 13.4 Coefficients to account for secondary bending moments in joints of lattice girders made from circular hollow sections

Type of joint		Chords	Verticals	Diagonals
Gap joints	K	1.5	-	1.3
	N	1.5	1.8	1.4
Overlap joints	K	1.5	-	1.2
	N	1.5	1.65	1.25

Table 13.5 Coefficients to account for secondary moments in joints of lattice girders made from rectangular hollow sections

Type of joint		Chords	Verticals	Diagonals
Gap joints	K	1.5	-	1.5
	N	1.5	2.2	1.6
Overlap joints	K	1.5	-	1.3
	N	1.5	2.0	1.4

Table 13.6 - Recommended fatigue class for bolted connections according to Eurocode 3

Detail	Class	Slope m
Bolts loaded in tension based on tensile stress area	36	-5
Double-sided, slip-resistant connections, e.g. splices or cover plates (based on stress in gross section)	112	-3

Table 13.3 Detailed category EC3: Classes for classification method

Detail categories for lattice girder joints based on nominal stresses			
Detail m = -5	Construction Details		Description
90	$t_o/t_i \geq 2.0$	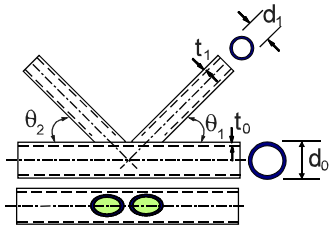	Joints with gap Circular hollow sections, K and N joints
45	$t_o/t_i = 1.0$		
71	$t_o/t_i \geq 2.0$	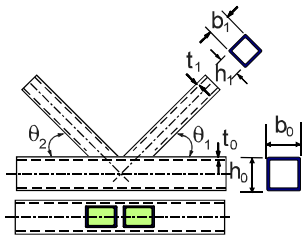	Joints with gap Rectangular hollow sections, K and N Joints Requirements $-0.5\,(b_o-b_i) \leq g \leq 1.1\,(b_o-b_i)$ $g \geq 2\,t_o$
36	$t_o/t_i = 1.0$		
71	$t_o/t_i \geq 1.4$	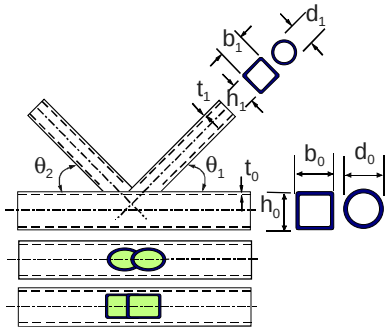	Joints with overlap K joints Requirements overlap between 30 and 100%
56	$t_o/t_i = 1.0$		
71	$t_o/t_i \geq 1.4$	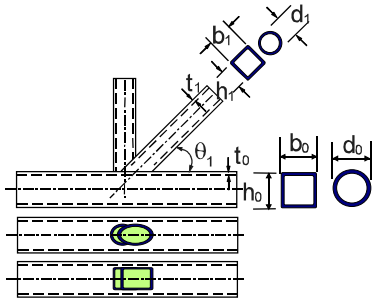	Joints with overlap N joints
50	$t_o/t_i = 1.0$		

General Requirements

$d_o \leq 300$ mm	$0.25 \leq d_i/d_o \leq 1.0$	$d_o/t_o \leq 25$*	$-0.5d_o \leq e \leq 0.25d_o$
$b_o \leq 200$ mm	$0.4 \leq b_i/b_o \leq 1.0$	$b_o/t_o \leq 25$*	$-0.5h_o \leq e \leq 0.25h_o$
$t_o, t_i \leq 12.5$mm*	$35^0 \leq \theta \leq 50^0$		

Out of plane eccentricity : $\leq 0.02b_o$ or $\leq 0.02d_o$

Fillet welds are permitted in braces with wall thickness ≤ 8 mm

- For intermediate t_o/t_i values, use linear interpolation between nearest Detail Categories
- Note that the detail class is based on the stress range in the braces

** Regarding general requirements, it is recommended to use the limits of the tests:*
$4 \leq (t_o$ and $t_1) \leq 8$ mm instead of ≤ 12.5 mm
$b_o/t_o \cdot t_o/t_1$ or $d_o/t_o \cdot t_o/t_1 \leq 25$ instead of b_o/t_o or $d_o/t_o \leq 25$

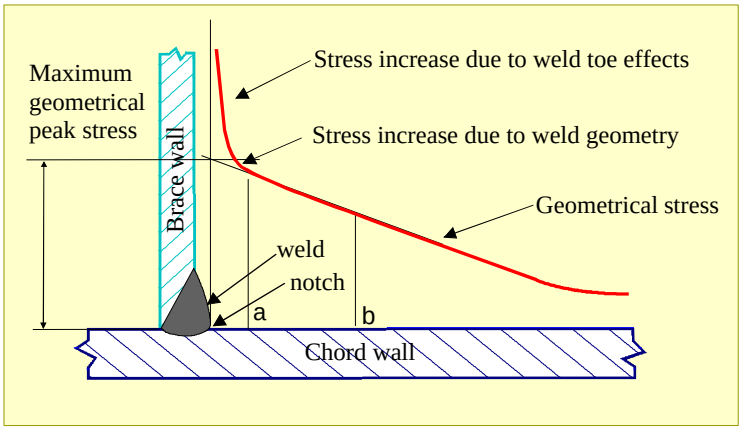

Fig. 13.1 Peak stress due to weld discontinuity

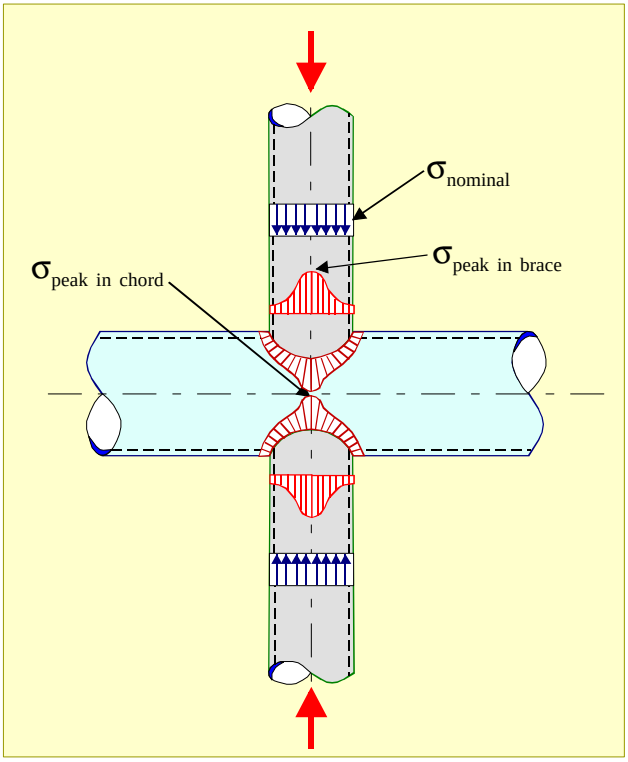

Fig. 13.2 Geometrical stress distribution in an axially loaded X-joint of circular hollow sections

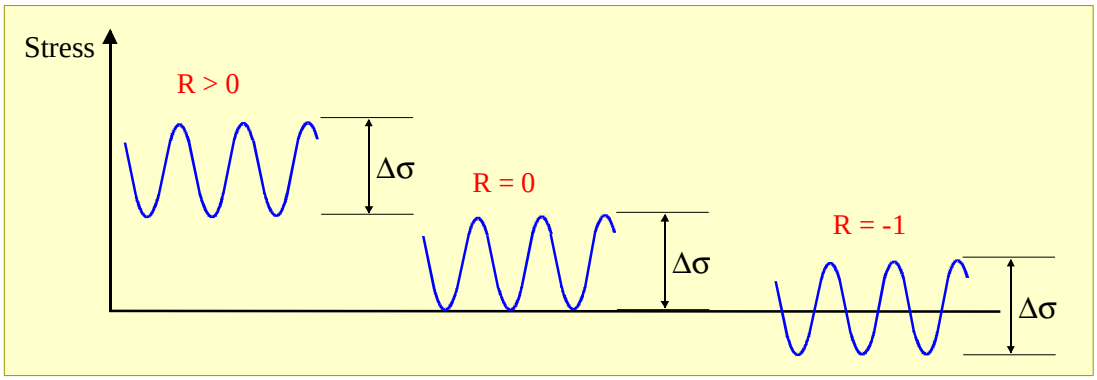

Fig. 13.3 Stress range and stress ratio R

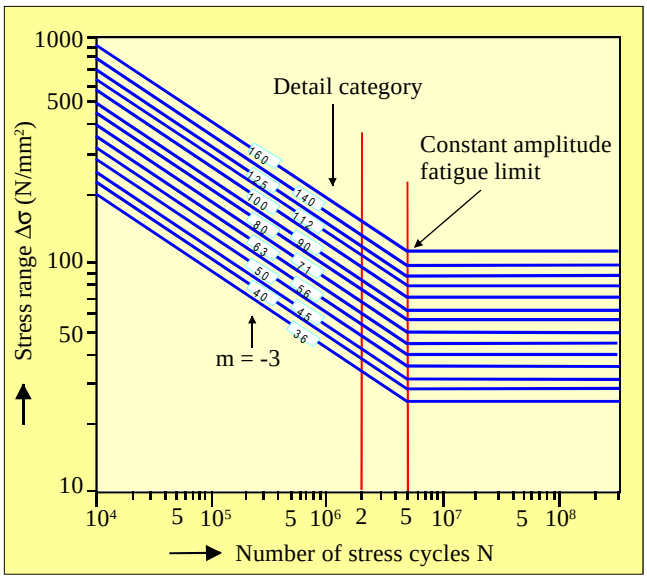

Fig. 13.4 -N curves for classified details and constant amplitude loading (EC3)

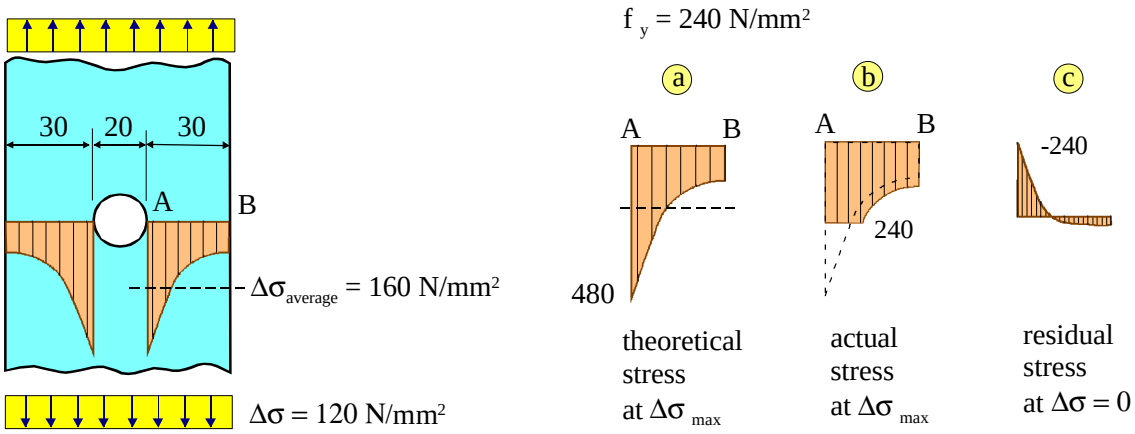

Fig. 13.5 Plate with a hole

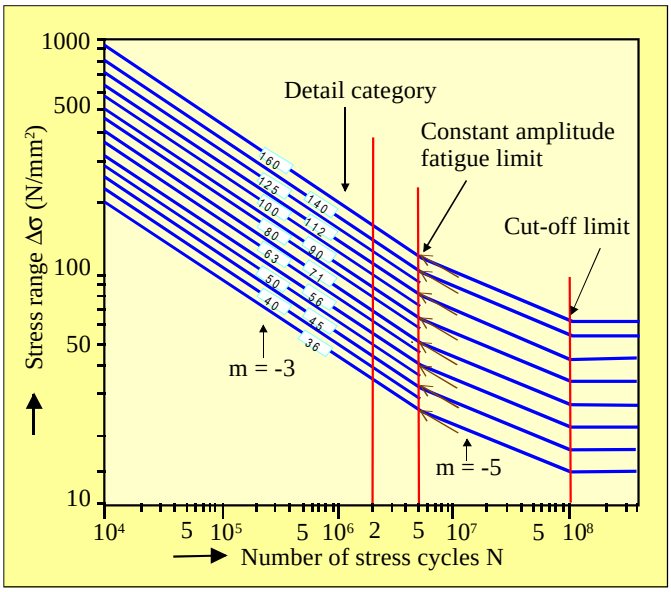

Fig. 13.6 -N curves for classified details and variable amplitude loading (EC3)

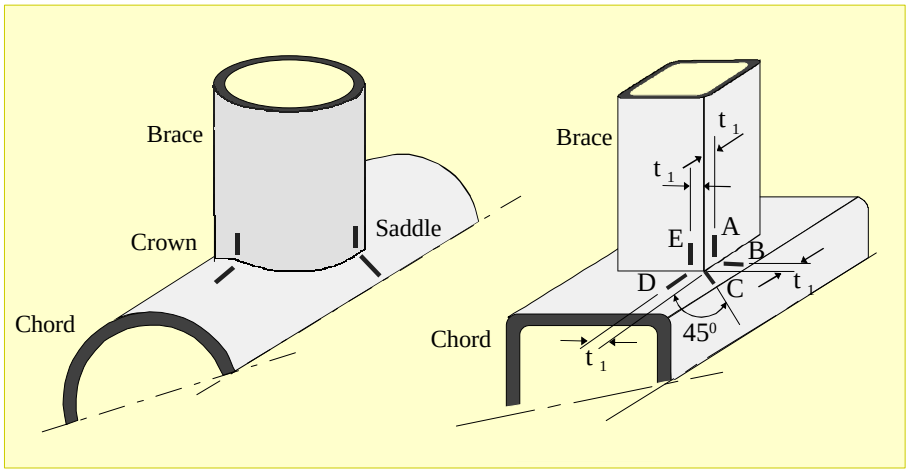

Fig. 13.7 Locations of extrapolation of geometric peak stresses for a T-joint

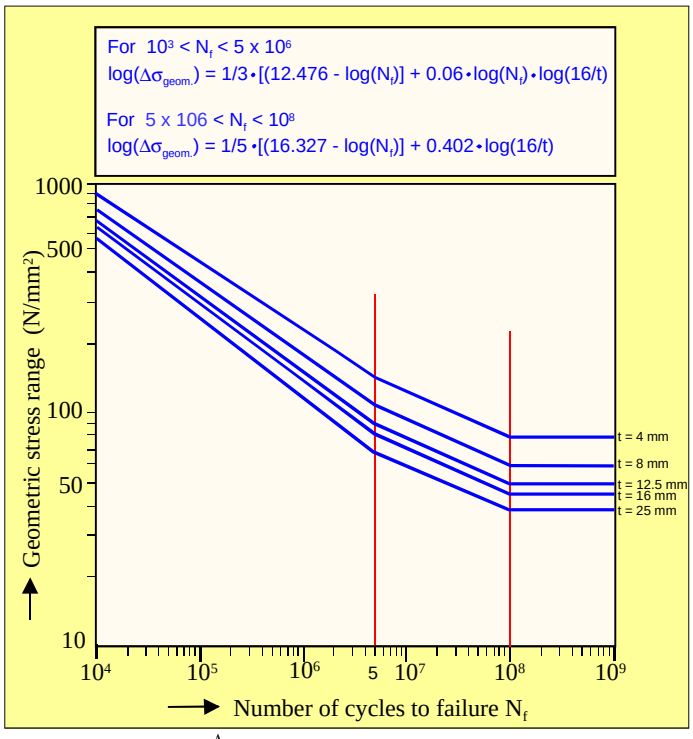

Thickness correction
for uniplanar joints with t ≠ 16 mm
(for N = 5 x 10⁶)

$$\frac{\Delta\sigma_{geom.(\,t\,)}}{\Delta\sigma_{geom.\ (t=16mm)}} = \left(\frac{16}{t}\right)^{0.402}$$

Limitation
CHS : 4 ≤ t ≤ 50 mm
RHS : 4 ≤ t ≤ 16 mm

Fig. 13.8 Basic $\Delta\sigma_{geom.}$ - N_f design curve for the geometrical stress method for hollow section joints

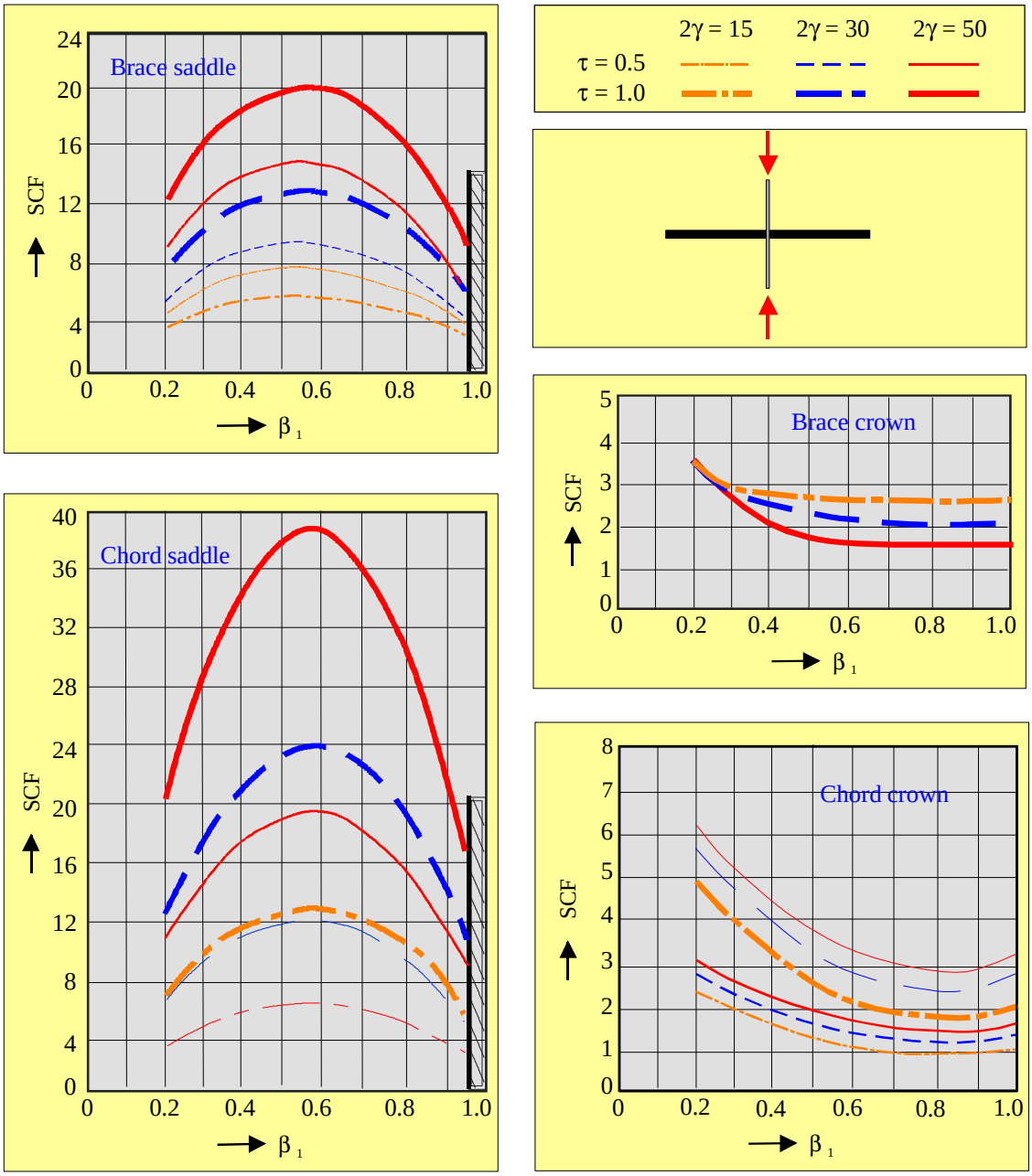

Fig. 13.9 SCFs for axially loaded circular hollow sections X-joints [122]

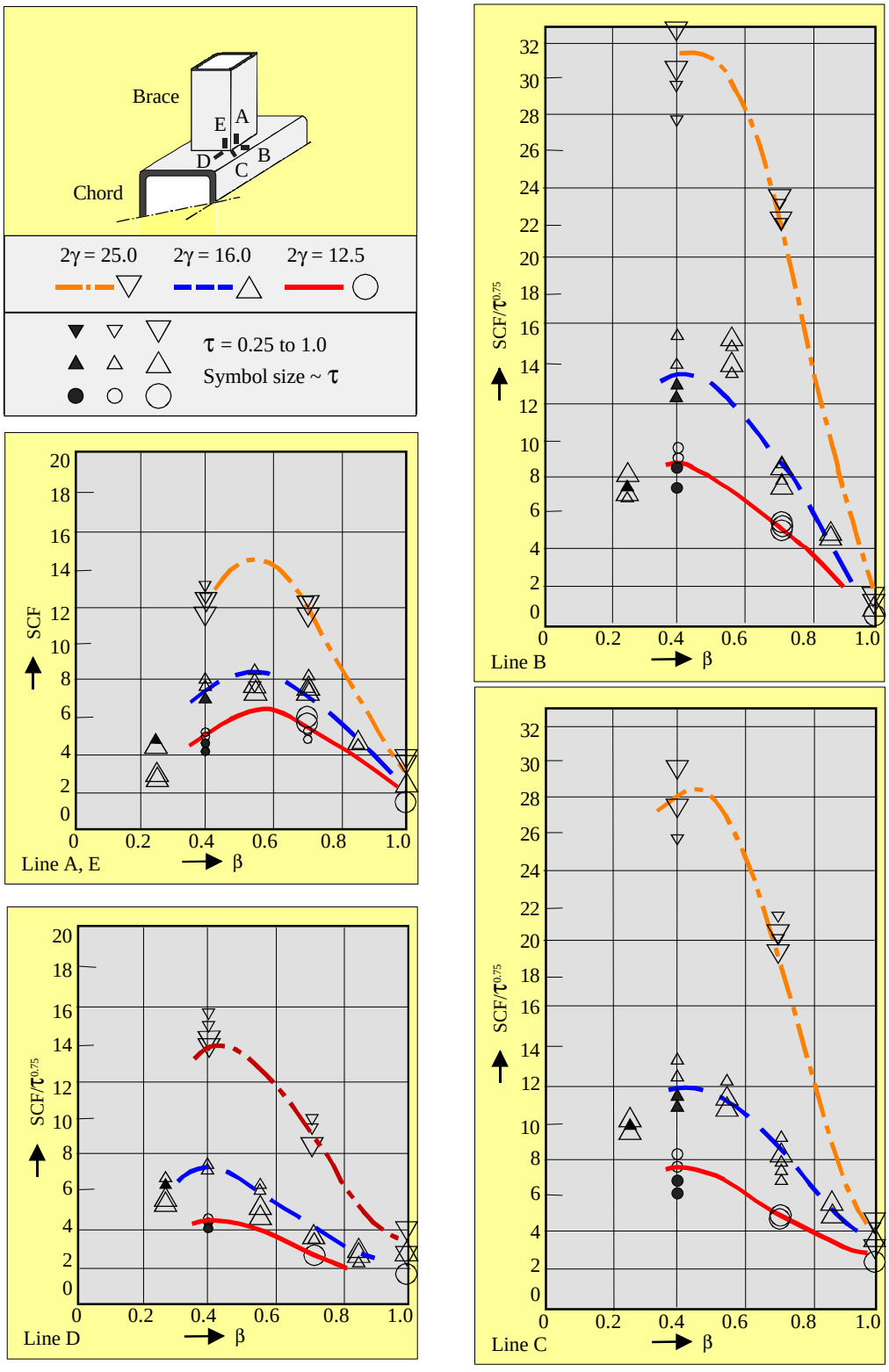

Fig. 13.10 SCFs for butt-welded, T- and X-joints of square hollow sections, loaded by an axial force on the brace (parametric formulae compared with FE calculations) [122].

Notes: 1) The effect of bending in the chord for a T-joint due to the axial force on the brace should be separately included in the analysis
2) For fillet welded connections: multiply SCFs for the brace by 1.4
3) A minimum SCF= 2.0 is recommended to avoid crack initiation from the root.

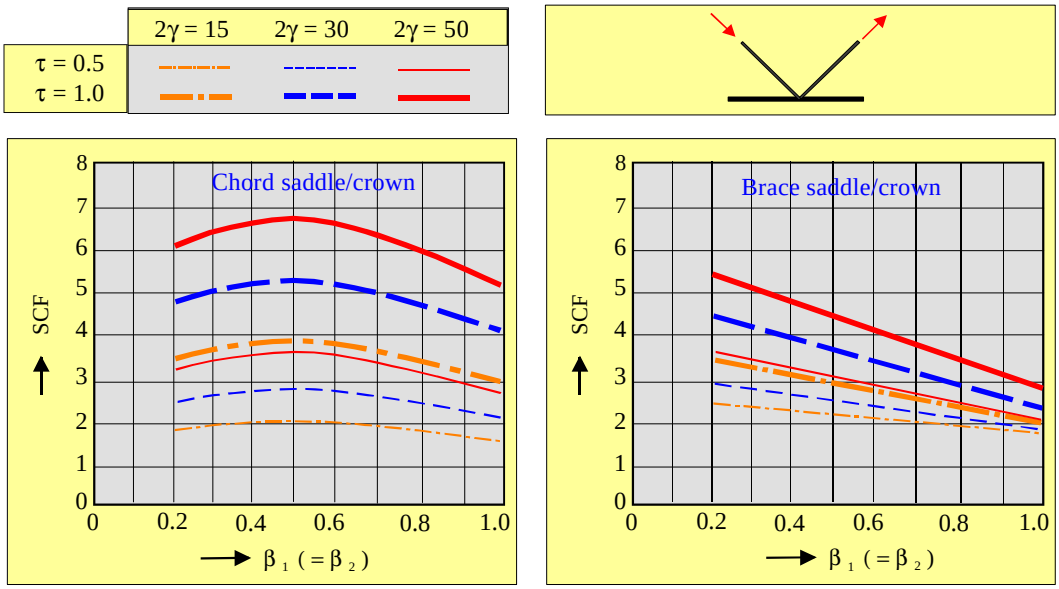

Fig. 13.11 Maximum SCFs for axially loaded K-joints of circular hollow sections with a gap g = 0.1 d_0

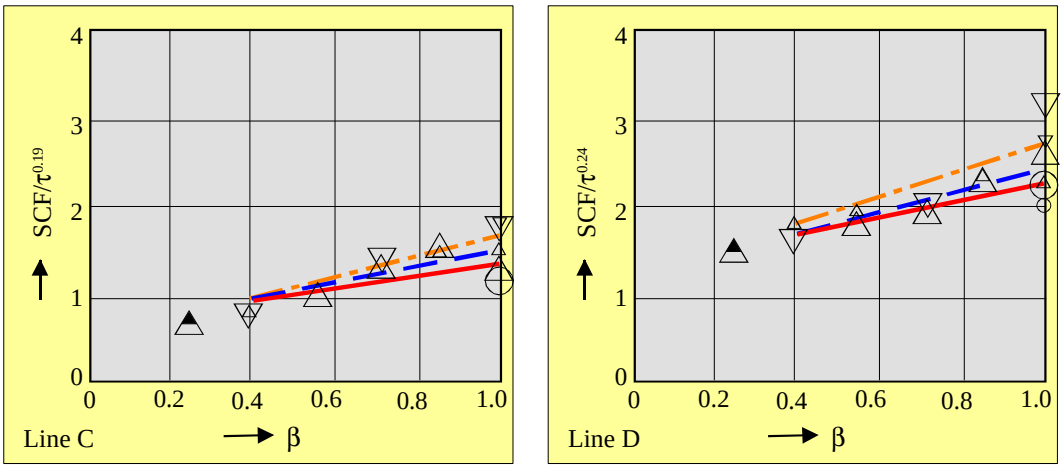

Fig. 13.12 SCFs for T- and X-joints (chord locations C and D of fig. 13.7 only), loaded by an in-plane bending moment or axial force on the chord [122]

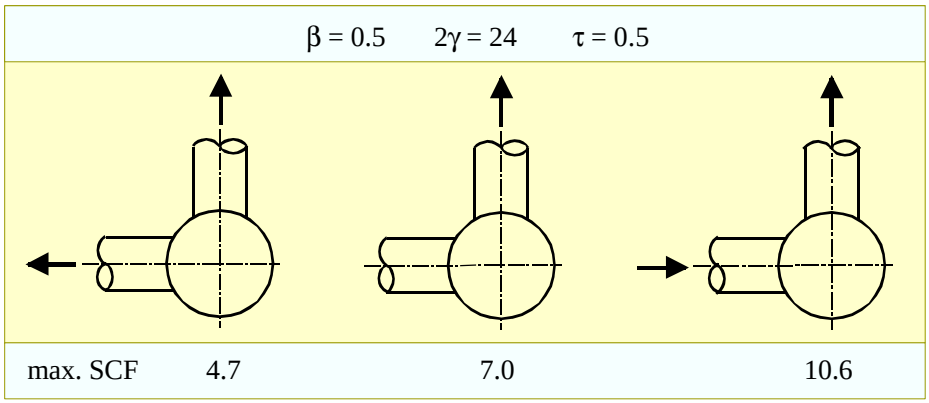

Fig. 13.13 Effect of multiplanar loading on the SCF

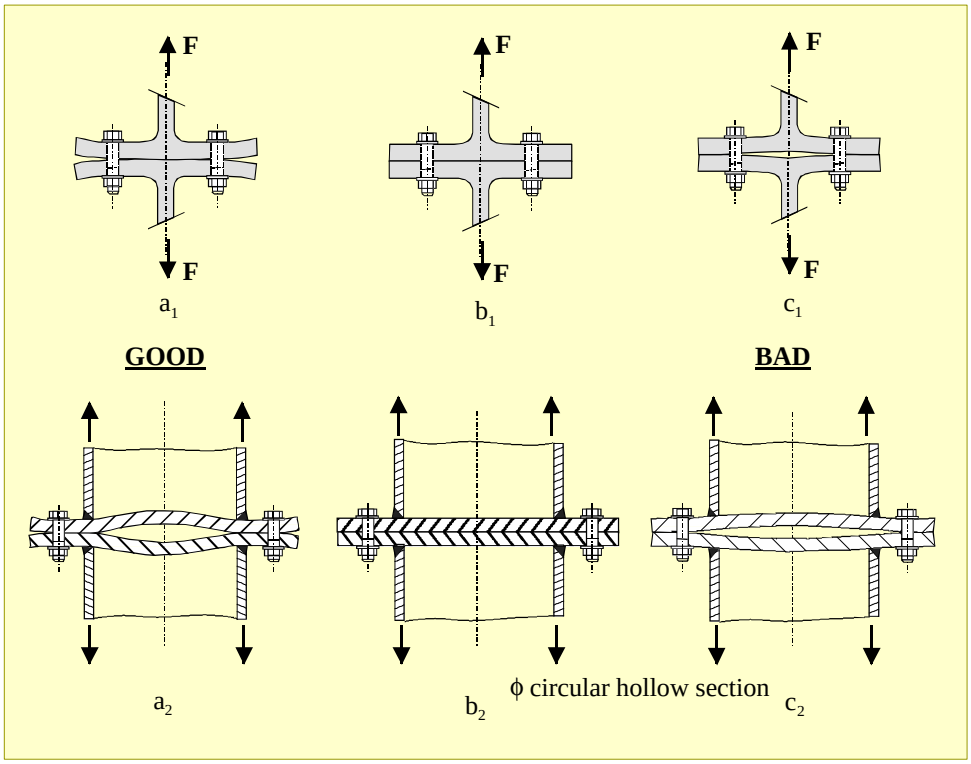

Fig. 13.14 Examples of bolted connections (with deformed flanges) in tension

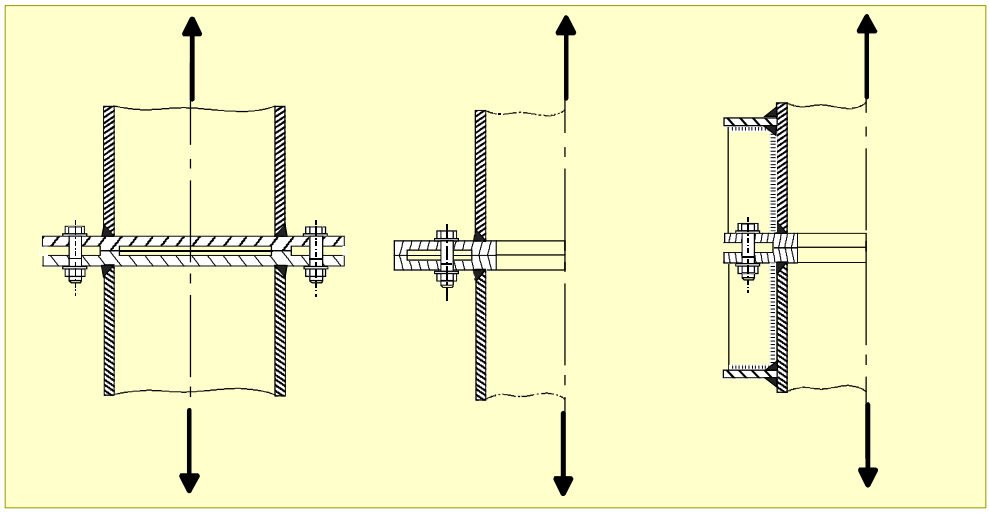

Fig. 13.15 Recommended bolted ring flange connection for fatigue loading

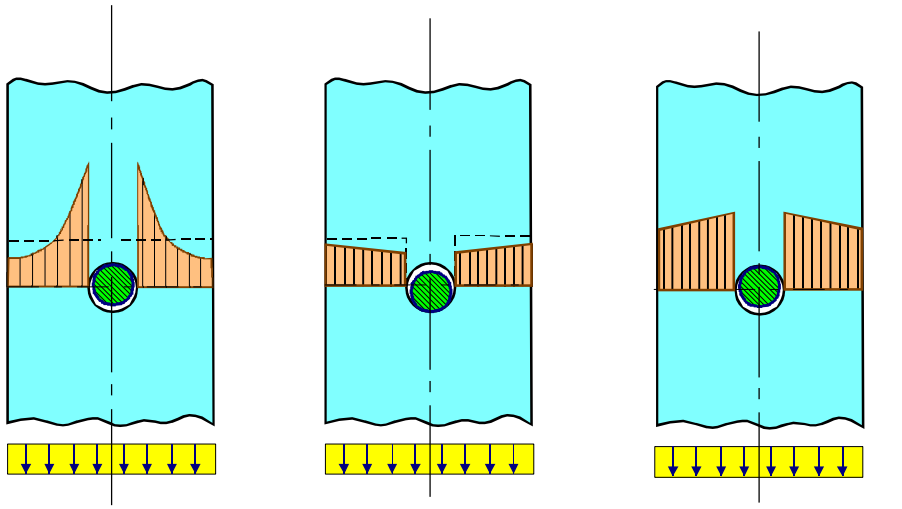

a. No preload b. Preloaded c. Preloaded, after slip

Fig. 13.16 Possible stress distributions in bolted shear connections

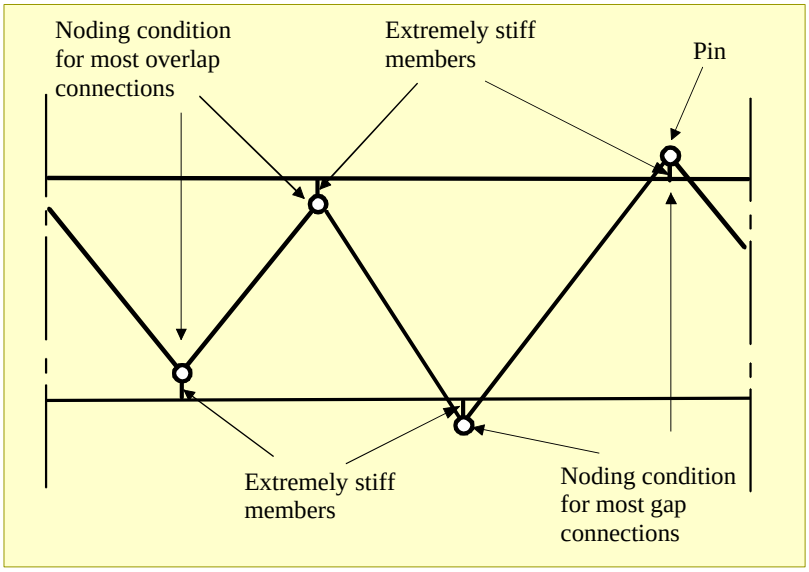

Fig. 13.17 Plane frame joint modelling assumptions

14. DESIGN EXAMPLES

14.1 UNIPLANAR TRUSS IN CIRCULAR HOLLOW SECTIONS

● *Truss layout and member loads*

With this example [1] the design principles of chapter 6 are illustrated as well as the joint design methods. A Warren type truss with low brace member angles is chosen to limit the number of joints, see Fig. 14.1.

The trusses are spaced at 12 m intervals and the top chord is considered to be laterally supported at each purlin position at 6 m centre on centre. The span to depth ratio is 15, which is around the optimal limit considering service load deflections and overall costs.

For this example, hot formed members are chosen and the member resistances are calculated according to Eurocode 3, *assuming a partial safety factor γ_M = 1.0 (this factor will be different for various countries).*

The factored design load P from the purlins including the weight of the truss has been calculated as P = 108 kN.

A pin-jointed analysis of the truss gives the member forces shown in Fig. 14.2.

● *Design of members*

In this example the chords are made from steel with a yield stress of 355 N/mm^2 and the braces from steel with a yield stress of 275 N/mm^2.

For member selection, use can be made of either member resistance tables with the applicable effective length or the applicable strut buckling curve. The availability of the member sizes selected has to be checked. Since the joints at the truss ends are generally decisive, the chords should not be too thin walled. As a consequence, a continuous chord with the same wall thickness over the whole truss length is often the best choice.

Top chord

Use a continuous chord with an effective in-plane and out-of-plane length of:

ℓ_e = 0.9 x 6000 = 5400 mm [1, 2], see chapter 2.

Maximum chord force N_o = 1148 kN (compression).

Possible section sizes are shown in table 14.1, along with their compressive resistances.

From a material point, the sections ϕ 244.5 - 5.6 and ϕ 219.1 - 7.1 are most efficient. However, for the supplier considered in this example, these two dimensions are not available from stock (only deliverable from factory). These dimensions can only be used if a large quantity is required, which is assumed in this example.

Bottom chord

For the connection capacity it is best to keep the tension chord as compact and stocky as possible. However, to allow gap joints and to keep the eccentricity within the limits, a larger diameter may be needed. Possible section sizes are given in table 14.2.

Diagonals

Try to select members which satisfy

$\frac{f_{yo} \cdot t_o}{f_{yi} \cdot t_i} \geq 2.0$; i.e. $\frac{355 \cdot (7.1)}{275 \cdot t_i} \geq 2.0$ or $t_i \leq 4.5$ mm, see chapter 8.

For the braces loaded in compression, use an initial effective length of

$0.75\ell = 0.75 \sqrt{2.4^2 + 3.0^2} = 2.88$ m [1, 3], see chapter 2.

The possible sizes for the compression diagonals are given in table 14.3 and for the tension diagonals in table 14.4.

Member selection

The number of sectional dimensions depends on the total tonnage to be ordered. In this example, for the braces only two different dimensions will be selected. Comparison of the members suitable for the tension members and those suitable for the compression members shows that the following sections are most convenient:

- braces: ϕ 139.7 - 4.5
  ϕ 88.9 - 3.6
- top chord: ϕ 219.1 - 7.1
- bottom chord: ϕ 193.7 - 6.3 (These chord sizes allow gap joints; no eccentricity is required.)

It is recognized that the d_o/t_o ratios of the chords selected are high. This may give joint strength problems in joints 2 and 5. The check for joint resistance is given in table 14.5.

Commentary and revision

Joint 1

In joint 1 between plate and brace a gap g = $2t_o$ is

chosen, see Fig. 14.4. This joint will be checked as a K (N) joint. Attention should be paid to the top chord shear capacity, i.e. cross section A should be able to resist the shear of 2.5 P=2.5x108=270 kN. Since joint 1 is rather heavily loaded, it is recommended to use the elastic shear capacity of the top chord conservatively, i.e.:

$$0.5\, A_o \cdot \frac{f_{yo}}{\sqrt{3}} =$$

$$0.5 \cdot 4728 \cdot \frac{0.355}{\sqrt{3}} = 485 \text{ kN} > 270 \text{ kN}$$

Joint 2

The strength of joint 2 is not sufficient. The easiest way to obtain sufficient joint strength will be to decrease the gap from 12.8 t_o to 3 t_o (Fig. 14.5) resulting in a joint efficiency of 0.86 > 0.82. However, this means that a (negative) eccentricity of e = 28 mm is introduced resulting in a moment due to eccentricities of:

$M = (878 - 338) \cdot 28 \cdot 10^{-3} = 15.1$ kNm.

Since the length and the stiffness EI of the top chord members between joints 1 - 2 and 2 - 3 are the same (see Fig. 14.3), this moment can be equally distributed over both members, i.e. both members have to be designed additionally for M_o = 7.6 kNm. The chord members between joints 1 - 2 and 2 - 3 now have to be checked as beam-columns. Of these, the chord member 2 - 3 is most critical. This check depends on the national code to be used.

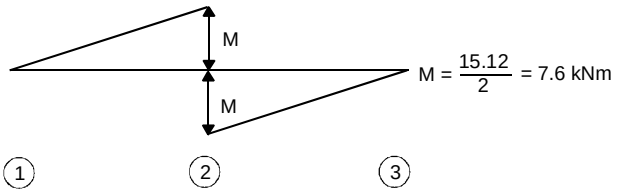

According to Eurocode 3 the following criterion has to be checked:

$$\frac{N_o}{\chi \cdot A_o \cdot f_{yo}} + k \cdot \frac{M_o}{M_{p\ell,o}} \leq 1.0$$

where:

$M_{p\ell,o}$ = plastic resistance ($W_{p\ell,o} \cdot f_{yo}$) of the chord (class 1 or 2 sections); for class 3, use the elastic moment resistance ($W_{eo} \cdot f_{yo}$)

k = factor including second order effects depending on slenderness, section classification and moment diagram (in this case triangular). $k \leq 1.5$.

$$\frac{878}{1189} + k \cdot \frac{7.6}{113.3} = 0.74 + 0.07\, k < 1.0$$

(regardless of the code used, this will not be critical).

Purlin connections

Depending on the type of purlins, various purlin connections are possible. If corrosion will not occur, a cut out of a channel section welded on top of the chord at the purlin support location and provided with bolt stubs provides an easy support.

If single beam purlins are used, a plate as shown in Fig. 12.18 (b) can be used.

Site-bolted flange connections

These lecture notes do not give complete design procedures for bolted flange connections.
However, in ref. [1] this example is worked out further, e.g. resulting in a connection according to Fig. 12.1 with 10 bolts ϕ 24 Grade 10.9 with an end plate thickness of 22 mm (f_y = 355 N/mm^2) for the bottom tensile chord connection. To avoid displacements in the connection it is recommended to pretension the bolts. For fatigue loaded connections the bolts have to be pretensioned.

14.2 UNIPLANAR TRUSS IN SQUARE HOLLOW SECTIONS

In ref. [3] a truss with the same configuration and loading has been designed in hot formed square hollow sections, all with a yield stress of 355 N/mm^2. In principle, the approach is similar, resulting in the member dimensions of Fig.14.7.

14.3 MULTIPLANAR TRUSS (TRIANGULAR GIRDER)

For an easy comparison, for this example a multiplanar truss (Fig. 14.8) is chosen with the side elevation dimensions equivalent to the uniplanar truss discussed under 14.1.

● *Member loads*

The member loads can be determined in a similar way as for the uniplanar truss, assuming pin ended members. The load in the bottom chord follows by

dividing the relevant moment by the girder depth. Since two top chords are used, the load at the top has to be divided by 2. The loads in the braces follow from the shear forces V in the girder (Fig. 14.9).
The top chords should be connected in the top plane for equilibrium of loading, see Fig. 14.10. This can be achieved by a bracing system which connects the loading points. Connection of the loading points only results in a triangular truss which has no torsional rigidity. A combination with diagonals gives torsional resistance.

It is also possible to use the purlins or the roof structure as the connecting parts between the loading points. Now the loads in one plane are known and the design can be treated in a similar way as for uniplanar trusses.

● *Joints*
The joints can also be treated in a similar way as for uniplanar joints, however, taking account of the reduction factor of 0.9 for the joints. From a fabrication point of view it is better to avoid overlaps of the intersecting braces from both planes. Sometimes this may result in an offset.

The offset (if $e \leq 0.25d_o$) does not need to be incorporated in the joint design. For chords loaded in tension, this offset moment can also be neglected in the member design. For compression-loaded chords, the moments due to this offset have to be distributed into the chord members and taken into account in the member design.

● *Design calculation*
Assume P = 187 kN factored load.
This means that the loads acting in the side planes of the triangular truss (Fig. 14.12) are:

$$\frac{P}{2\cos 30°} = 108 \text{ kN}$$

This is equal to the purlin loads used in the design example for the uniplanar truss in 14.1. As a consequence, the top chord and the diagonals can be the same as those for the uniplanar truss, provided the same steel grades are used.
Only for the bottom chord the required cross section should be twice that required for the uniplanar truss, i.e. ϕ 219.1x 11.0 with A_o = 7191 mm^2. (This section may have a longer delivery time.)
The resulting sections are shown in Fig. 14.13.

The braces between the top chords are determined by the horizontal loads of 54 kN at each purlin support or by loads resulting from non-equally distributed loading on the roof. Since transport is simpler for V-trusses than for triangular trusses, it is also possible to use the purlins as connection between the top chords.
A simple bolted connection as given in Fig. 14.6 can easily transfer the shear load of 54 kN. However, in this way, the truss has no torsional rigidity and cannot act as horizontal wind bracing for the roof. If this is required, braces between the top chords have to be used.

● *Check for joint strength*
In table 14.6 the joints have been checked in a similar way as for the uniplanar truss in 14.1. However, the multiplanar correction factor 0.9 has been included for the strength of joints 5, 6 and 7.
A connection without any eccentricity would result in an overlap of the braces in the two planes (Fig. 14.14a). To allow welding, an out-of-plane gap of 22.5 mm is chosen, which results in an eccentricity of 50 mm (in-plane 43 mm). As a consequence, the in-plane gap increases, resulting in lower C_k values, which are given between brackets in table 14.6.

14.4 MULTIPLANAR TRUSS IN SQUARE HOLLOW SECTIONS

The approach for a multiplanar truss in square hollow sections is similar to that used in 14.3. Generally, the braces in the two side planes are connected at different faces of the bottom chord, giving no problems with out-of-plane overlaps as would be possible for circular hollow sections.
Working out the example used in 14.3 for square hollow sections (all with f_y = 355 N/mm^2), results for the top chords and braces in the same dimensions as those given in Fig. 14.7. Only for the bottom chord, a section with twice the cross sectional area has to be chosen.

14.5 JOINT CHECK USING FORMULAE

The joints used in the previous examples can also be checked using the formulae given in chapters 8 and 9. Here, in these examples, only joint No. 2 of the uniplanar truss of Fig. 14.3 (CHS) and that of Fig. 14.7 (RHS) will be checked.

14.5.1 Joint No. 2 in CHS

The loading and dimensions are given in Figs. 14.1 to 14.3 with detailed information in Fig. 14.5.
According to chapter 8, table 8.1, the joint has to be checked as follows:

Check for chord plastification:

$$N_1^* = \frac{f_{yo} \cdot t_o^2}{\sin\theta_1} \cdot \left(1.8 + 10.2\,\frac{d_1}{d_o}\right) \cdot f(\gamma, g') \cdot f(n')$$

with: $f(\gamma, g') = \gamma^{0.2} \cdot \left[1 + \frac{0.024\gamma^{1.2}}{\exp(0.5g' - 1.33) + 1}\right]$

$f(n') = 1 + 0.3\,n' - 0.3\,n'^2 \le 1.0$

Check of validity range:

$\frac{d_1}{d_o} = \frac{139.7}{219.7} = 0.64 > 0.2$ (O.K.)

≤ 1.0

$\gamma = \frac{219.7}{2 \cdot (7.1)} = 15.5 \le 25$ (O.K.)

$\theta = 38.7° \ge 30°$ (O.K.)

$g = 3t_o \ge t_1 + t_2$ (O.K.)

Parameters and functions:

$g' = \frac{g}{t_o} = 3$

$f(\gamma, g') = 15.5^{0.2} \cdot \left[1 + \frac{0.024 \cdot (15.5)^{1.2}}{\exp(0.5 \cdot (3) - 1.33) + 1}\right] = 2.24$

$n' = \frac{N_{op}}{A_o \cdot f_{yo}} = \frac{-388}{4728 \cdot (0.355)} = -0.20$

$f(n') = 1 + 0.3\,(-0.20) - 0.3\,(-0.20)^2 = 0.93$

$N_1^* = \frac{0.355 \cdot (7.1)^2}{\sin(38.7°)} \cdot [1.8 + 10.2 \cdot (0.64)] \cdot (2.24) \cdot (0.93)$

$= 496.5$ kN

Thus 496.5 kN > 432 kN (O.K.)

Comparison with the efficiency method:

$A_1 \cdot f_{y1} = 1911 \times 0.275 = 525.5$ kN (O.K.)

Thus efficiency $\frac{N_1^*}{A_1 \cdot f_{y1}} = \frac{496.5}{525.5} = 0.94$

In the simplified method with graphs 0.86 was given, which is about 9% too conservative.

acting efficiency $\frac{N_1}{A_1 \cdot f_{y1}} = \frac{432}{525.5} = 0.82$

In case the gap g would have been 12.8 t_o:

$f(\gamma, g') =$

$15.5^{0.2} \cdot \left[1 + \frac{0.024 \cdot (15.5)^{1.2}}{\exp(0.5 \cdot (12.8) - 1.33) + 1}\right] = 1.73$

Thus $N_1^* = 496.5 \cdot \left(\frac{1.73}{2.24}\right) = 385$ kN (<432 kN)

which results in an efficiency:

$\frac{385}{525.5} = 0.73$, which is slightly higher than the 0.7 (see table 14.5) used in the efficiency method.

These comparisons show that due to simplifications the efficiency method is somewhat conservative compared to the method with formulae.

Check for punching shear:

$$N_i^* = \pi \cdot d_i \cdot t_o \cdot \frac{f_{yo}}{\sqrt{3}} \cdot \frac{1 + \sin\theta_i}{2\sin^2\theta_i}$$

d_2 is the smallest diagonal, but the other (larger) member has the larger force.

$$N_2^* = \pi \cdot (88.9) \cdot (7.1) \cdot \frac{0.355}{\sqrt{3}} \cdot \frac{1 + \sin(38.7°)}{2\sin^2(38.7°)}$$

$= 844.8$ kN ≥ 259 kN (O.K.)

Also $N_1^* > N_2^* > 432$ kN (O.K.)

14.5.2 Joint No. 2 in RHS

The dimensions of the sections and the yield stresses are given in Fig. 14.7. All other information remains the same as given in Figs. 14.1 and 14.2.

Check for chord plastification:

$$N_1^* = 8.9 \cdot \frac{f_{yo} \cdot t_o^2}{\sin\theta_1} \cdot \left[\frac{b_1 + b_2}{2b_o}\right] \cdot \gamma^{0.5} \cdot f(n)$$

$$\frac{b_1 + b_2}{2b_o} = \frac{120 + 80}{2 \cdot (180)} = 0.56$$

$$\gamma = \frac{180}{2 \cdot (8)} = 11.25$$

$$n = \frac{-878}{5410 \cdot (0.355)} = -0.46$$

$$f(n) = 1.3 + \frac{0.4}{\beta} \cdot n = 0.97$$

$$N_1^* = 8.9 \times \frac{0.355 \cdot (8)^2}{\sin(38.7^o)} \cdot (0.56) \cdot (11.25)^{0.5} \cdot (0.97)$$

$$= 589 \text{ kN} > 432 \text{ kN} \quad \text{(O.K.)}$$

Compared with the efficiency method:

efficiency according to formula

$$= \frac{N_1^*}{A_1 \cdot f_{y1}} = \frac{589}{1850 \cdot (0.355)} = 0.90$$

actual efficiency

$$= \frac{432}{1850 \cdot (0.355)} = 0.66 < 0.90$$

Thus these figures are about the same as those obtained with the efficiency graphs (see ref. 3, table 8).

Check of validity range:

$$\frac{b_{min}}{b_o} = \frac{80}{180} = 0.44 \rightarrow 0.44 \geq 0.1 + 0.01\frac{b_o}{t_o} = 0.325 \text{ (O.K.)}$$

$$\frac{b_1}{t_1} = \frac{120}{4} = 30 \rightarrow 30 \leq 1.25\sqrt{\frac{E}{f_{y1}}} = 30.4 \quad \text{(O.K.)}$$

$$\frac{b_o}{t_o} = \frac{180}{8} = 22.5 \rightarrow 15 \leq 22.5 \leq 35 \quad \text{(O.K.)}$$

$$\frac{b_1 + b_2}{2b_i} = 0.83 \rightarrow 0.6 \leq 0.83 \leq 1.3 \quad \text{(O.K.)}$$

$$g = \frac{b_o}{\tan\theta} - \frac{b_1 + b_2}{2\sin\theta} = 64.9 \text{ mm, thus } \frac{g}{b_o} = 0.36$$

$$\rightarrow 0.22 \leq 0.36 \leq 0.66 \quad \text{(O.K.)}$$

If rectangular sections would have been used, the joint resistance check would have been considerably more complicated, which is evident if table 9.1 is compared to table 9.3.
The extra checks are:
- chord shear
- brace effective width
- punching shear

14.6 CONCRETE-FILLED COLUMN WITH REINFORCEMENT

Here the example is taken from ref. 5.
A concrete filled circular hollow section is considered with a cross section and reinforcement as shown in Fig. 14.15 with the γ according to table 4.1.

Concrete	C 30	with	$\gamma_c = 1.5$
CHS	S 275	with	$\gamma_a = 1.1$
reinforcement	S 500	with	$\gamma_s = 1.15$

assumption for the analysis:

$\bar{\lambda} = 0.15$
$N_{Sd} = 6000$ kN
$M_{max,Sd} = 60$ kNm

strength:
$f_{yd} = 275/1.1 = 250$ /Nmm^2
$f_{sd} = 500/1.15 = 435$ /Nmm^2
$f_{cd} = 30/1.5 = 20$ /Nmm^2

cross sectional area:
$A_a = 11000$ mm^2
$A_s = 7850$ mm^2
$A_c = \pi \times 406.4^2/4 - 11000 - 7850 = 110867$ mm^2

reinforcement ratio (for fire design):
$\rho = 7850 / (\pi \times 406.4^2/4 - 11000) \Rightarrow 6.6\% > 4\%$

The ratio of reinforcement ρ has to be limited to 4% for the calculation (see 4.3.1). This may be achieved by considering only reinforcing bars which lie in the most favourable position of the section so that $\rho \leq 4\%$.

Here the outer and the next following two layers of reinforcement are considered:

$A_s = 10 \times 491 = 4910\ mm^2$

$A_c = \pi \times 406.4^2/4 - 11000 - 4910 = 113807\ mm^2$

$\rho = 4910 / (\pi \times 406.4^2/4 - 11000) \Rightarrow 4.1\% \approx 4\%$

$N_{pl,Rd} = 11000 \times 250 + 4910 \times 435 + 113807 \times 20$

$= 7162 \times 10^3\ N$

$= 7162\ kN$

$0.2 < \delta = 11000 \times 0.25/7162 = 0.38 < 0.9$

Check of local buckling:

$$\frac{d}{t} = \frac{406.4}{8.8} = 46.2 < 77$$

An increase in the bearing capacity caused by confinement effects is neglected.

Note: The partial factors γ are still different for various countries. Here $\gamma_a = 1.1$ is taken although in the other examples $\gamma_a = 1.0$ is assumed.

Table 14.1 - Possible section sizes for top (compression) chord

f_y N/mm^2	N_o (kN)	ℓ_e (m)	possible sections (mm)	A_o (mm^2)	d_o/t_o	$\bar{\lambda}$ 1)	χ 1)	$\chi \cdot f_{yo} \cdot A_o$ (kN)
355	1148	5.400	ϕ 193.7 - 10.0	5771	19.4	1.09	0.61	1245
			ϕ 219.1 - 7.1	4728	30.9	0.94	0.71	1189
			ϕ 219.1 - 8.0	5305	27.4	0.95	0.71	1329
			ϕ 244.5 - 5.6	4202	43.7	0.84	0.78	1159
			ϕ 244.5 - 6.3	4714	38.8	0.84	0.78	1298

1) Eurocode 3 buckling curve "a"

Table 14.2 - Possible section sizes for bottom (tension) chord

f_y N/mm^2	N_o (kN)	possible sections (mm)	A_o (mm^2)	d_o/t_o	$f_{yo} \cdot A_o$ (kN)
355	1215	ϕ 168.3 - 7.1	3595	23.7	1276
		ϕ 177.8 - 7.1	3807	25.0	1351
		ϕ 193.7 - 6.3	3709	30.7	1317

Table 14.3 - Possible section sizes for compression diagonals

f_y N/mm^2	N_i (kN)	ℓ_e (m)	possible sections (mm)	A_1 (mm^2)	$\bar{\lambda}$ 1)	χ 1)	$\chi \cdot f_{y1} \cdot A_1$ (kN)
275	432	2.88	ϕ 168.3 - 3.6	1862	0.57	0.90	462
			ϕ 139.7 - 4.5	1911	0.69	0.85	448
275	259	2.88	ϕ 114.6 - 3.6	1252	0.85	0.77	266
			ϕ 101.6 - 4.0	1226	0.96	0.70	235
275	86	2.88	ϕ 88.9 - 2.0*	546	1.08	0.61	92
			ϕ 76.1 - 2.6	600	1.28	0.49	80

1) Eurocode 3 buckling curve "a"

* the wall thickness is rather small for welding

Table 14.4 - Possible section sizes for tension diagonals

f_y N/mm^2	N_i (kN)	possible sections (mm)	A_2 (mm^2)	$f_{y2} \cdot A_2$ (kN)
275	432	ϕ 133.3 - 4.0	1621	445
275	259	ϕ 88.9 - 3.6	964	265
275	86	ϕ 48.3 - 2.3	332	91

Table 14.5: Check joint resistance for a uniplanar truss

			joint parameter				actual efficiency	joint strength efficiency (see Fig. 8.19)				remarks
joint	chord (mm)	braces (mm)	d_1/d_o	d_o/t_o	$\frac{g}{t_o}$	$n' = \frac{f_{op}}{f_{yo}}$	$\frac{N_i}{A_i \cdot f_{yi}}$	C_k	$\frac{f_{yo} \cdot t_o}{f_{yi} \cdot t_i}$	$\frac{f(n')}{\sin\theta_1}$	$\frac{N_1^*}{A_i \cdot f_{yi}}$	$N_1^* \geq N_i$
1	219.1 - 7.1	plate	0.64	30.9		not appl.						
		139.7 - 4.5			2.0		0.82	0.32	2.04	1.60	>1.00	yes*
2	219.1 - 7.1	139.7 - 4.5	0.64	30.9	12.8*	- 0.20	0.82	0.23	2.04	1.49	0.70	no*
		88.9 - 3.6					0.98		2.55		>1.00	yes
3	219.1 - 7.1	139.7 - 4.5	0.64	30.9	12.8	- 0.52	0.49	0.23	2.04	1.22	0.58	yes
		88.9 - 3.6					0.32		2.55		>1.00	yes
4	219.1 -7.1	88.9 - 3.6	0.41	30.9	18.5	- 0.68	0.32	0.26	2.55	1.05	0.70	yes*
		88.9 - 3.6					0.32		2.55		0.70	yes*
5	193.7 - 6.3	139.7 - 4.5		30.7		+	0.82		1.81		0.85	yes
		139.7 - 4.5	0.72		2.9		0.82	0.29	1.81	1.60	0.85	yes
6	193.7 - 6.3	88.9 - 3.6		30.7		+	0.98		2.26		>1.00	yes
		139.7 - 4.5	0.72		9.4		0.49	0.23	1.81	1.60	0.67	yes
7	193.7 - 6.3	88.9 - 3.6		30.7		+	0.32		2.26		0.91	yes
		88.9 - 3.6	0.46		15.8		0.32	0.25	2.26	1.60	0.91	yes

*See commentary and revision: Here, joint 4 is treated as a K-joint because the plates stiffen the joint, although the loading is similar to an X-joint.

Table 14.6: Check joint resistance for multiplanar truss

			joint parameter				actual efficiency	joint strength efficiency (see Fig. 8.19)				multi-planar factor	remarks
joint	chord (mm)	braces (mm)	d_1/d_o	d_o/t_o	$\frac{g}{t_o}$	$n' = \frac{f_{op}}{f_{yo}}$	$\frac{N_i}{A_i \cdot f_{yi}}$	C_k	$\frac{f_{yo} \cdot t_o}{f_{yi} \cdot t_i}$	$\frac{f(n')}{\sin\theta_1}$	$\frac{N_1^*}{A_i \cdot f_{yi}}$		$N_1^* \geq N_i$
1-4	The checks for joints 1 to 4 are given in table 14.5												
5	219.1 - 11.0	139.7 - 4.5 139.7 - 4.5	0.64	19.9	4.5 (9.4)	+	0.82 0.82	0.38 (0.33)	3.16 3.16	1.60	>1.00 >1.00 (>1.00)	0.9	yes yes yes
6	219.1 - 11.0	88.9 - 3.6 139.7 - 4.5	0.64	19.9	8.2 (17.7)	+	0.98 0.49	0.35 (≈0.31)	3.94 3.16	1.60	>1.00 >1.00 (>1.00)	0.9	yes yes yes
7	219.1 - 11.0	88.9 - 3.6 88.9 - 3.6	0.41	19.9	11.9 (21.4)	+	0.32 0.32	0.39 (≈0.35)	3.94 3.94	1.60	>1.00 >1.00 (>1.00)	0.9	yes yes yes

Notes: - An eccentricity e ≈ 38 mm has to be introduced to satisfy the condition $g \geq t_1 + t_2$. However, for welding, a gap of 22.5 mm is chosen between the diagonals of both planes, which results in an eccentricity of 50 mm (≈ $0.23d_o$).

- The figures between brackets ( ) show the estimated $g' = g/t_o$ values for an in-plane eccentricity of 50·cos(30°) = 43 mm.

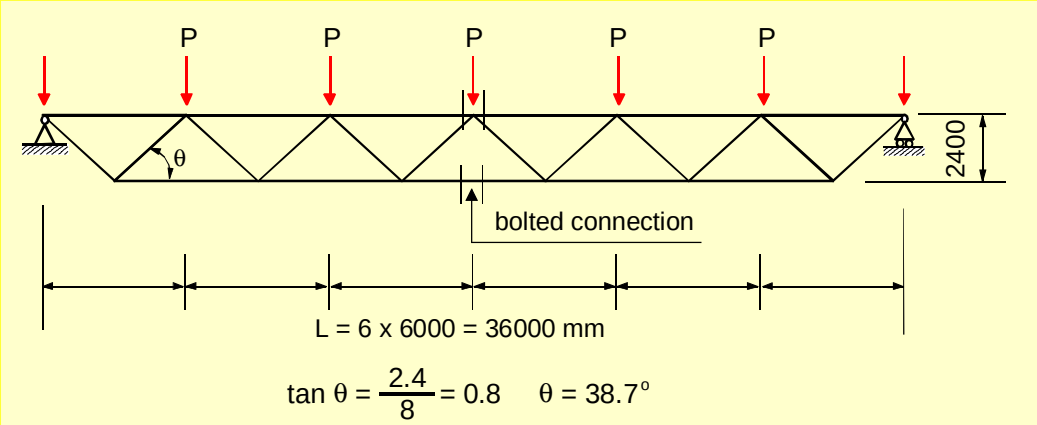

Fig. 14.1 Truss layout

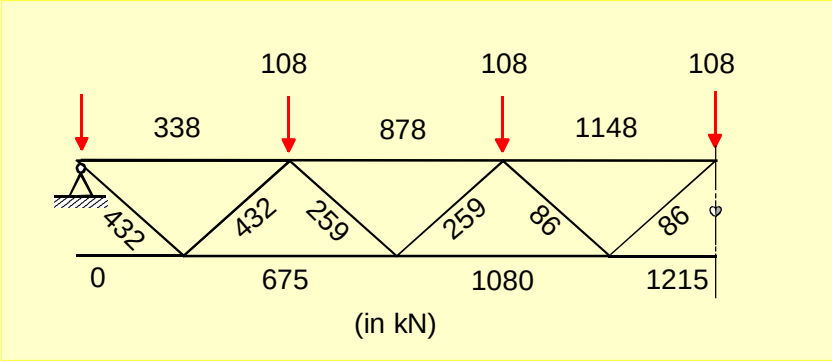

Fig. 14.2 Truss member axial loads

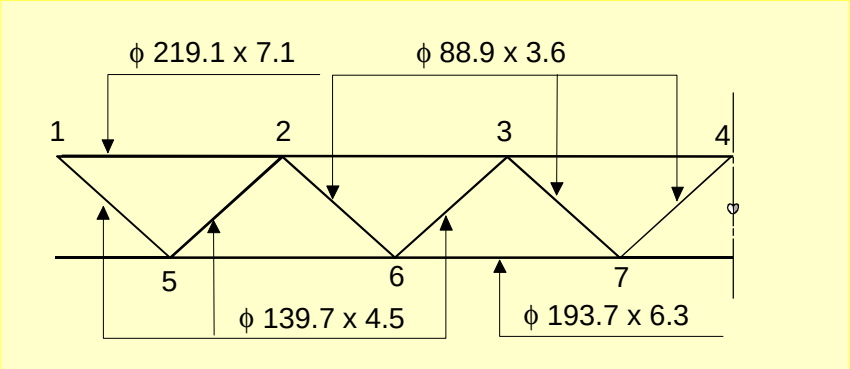

Fig. 14.3 Member dimensions

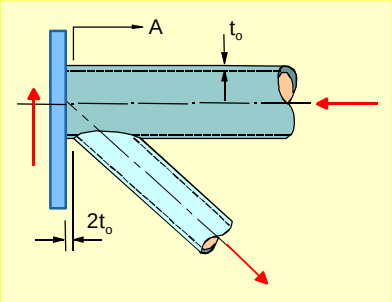

Fig. 14.4 Joint 1

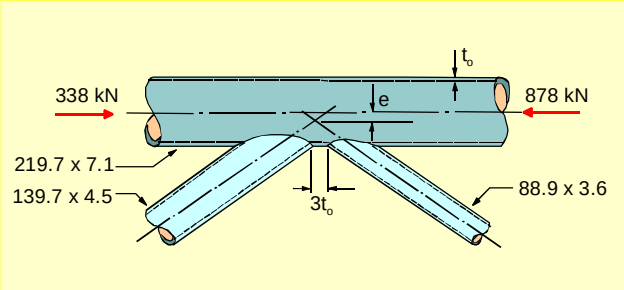

Fig. 14.5 Joint 2

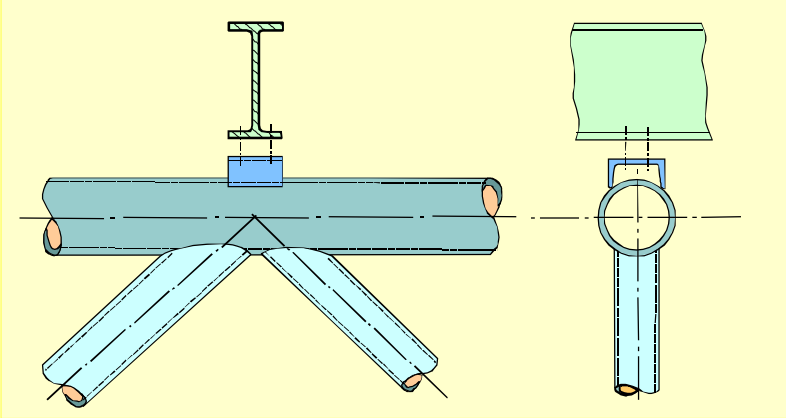

Fig. 14.6 Purlin connection

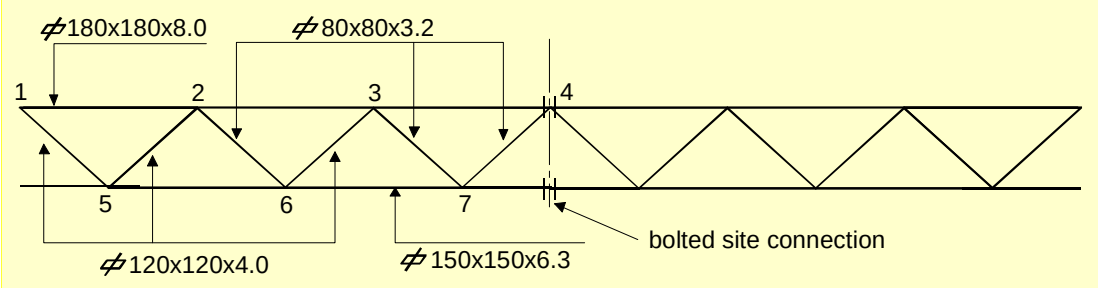

Fig. 14.7 Member dimensions and connection numbers for RHS truss ($f_{y0} = f_{yi} = 355$ N/mm^2)

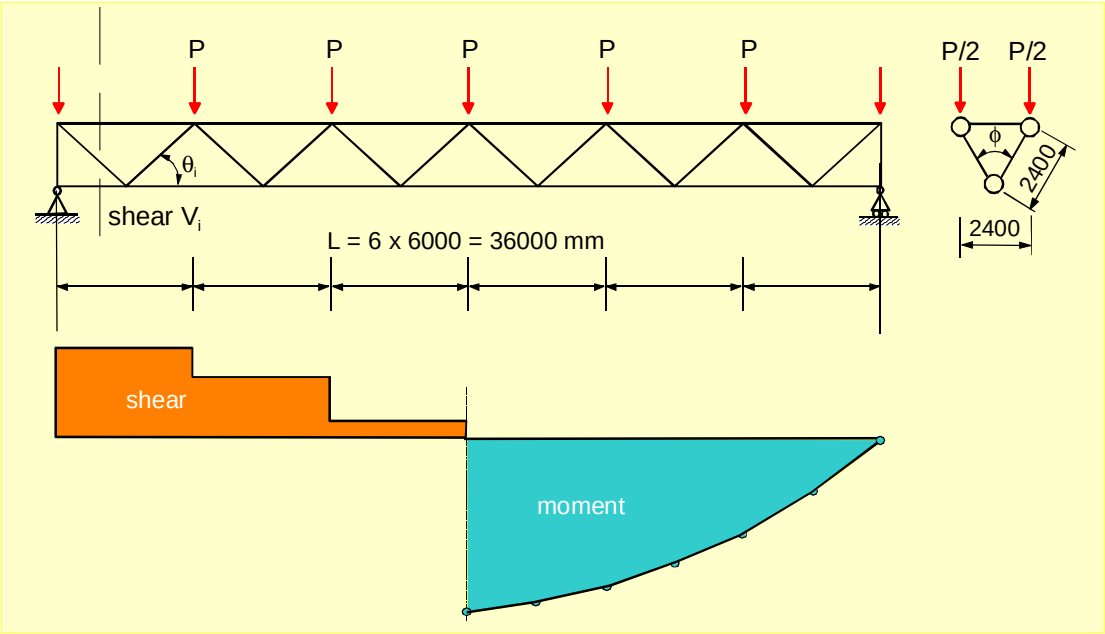

Fig. 14.8 Triangular truss

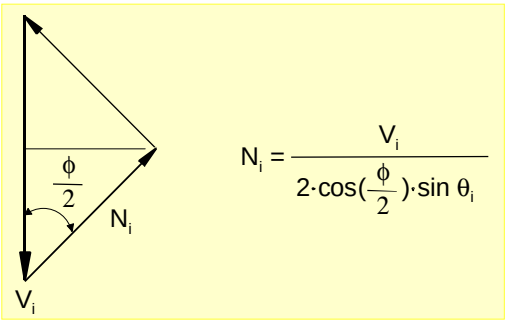

Fig. 14.9

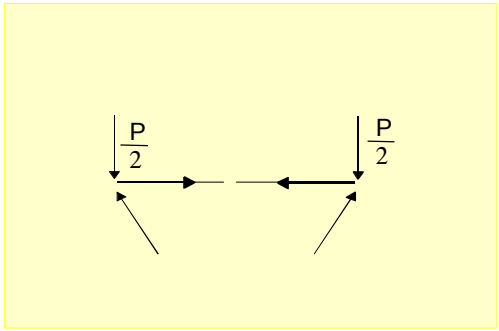

Fig. 14.10

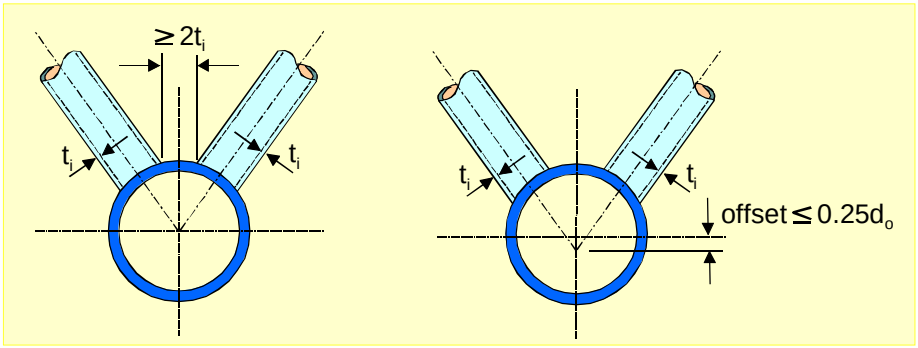

Fig. 14.11 Gap and offset

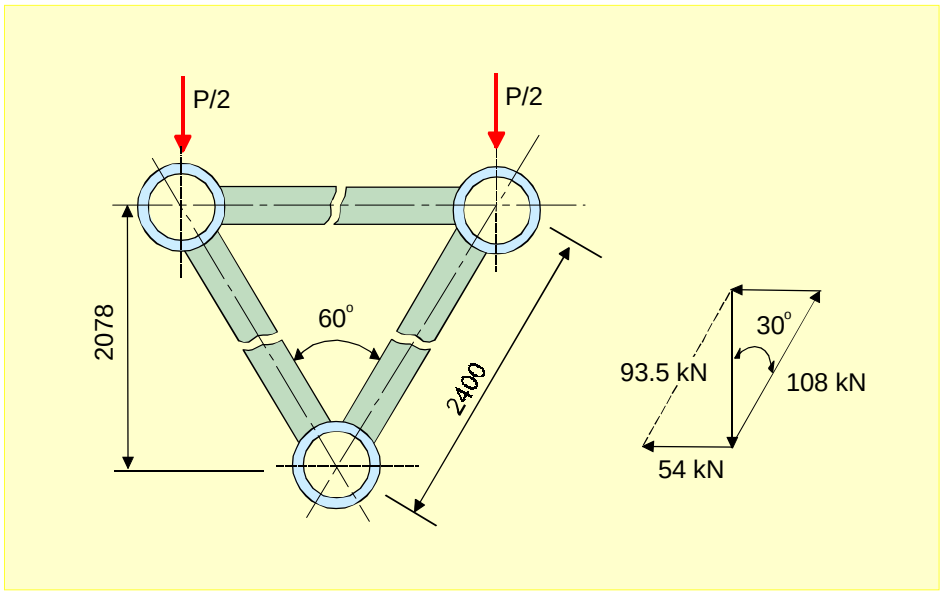

Fig. 14.12 Cross section of the triangular truss in circular hollow sections

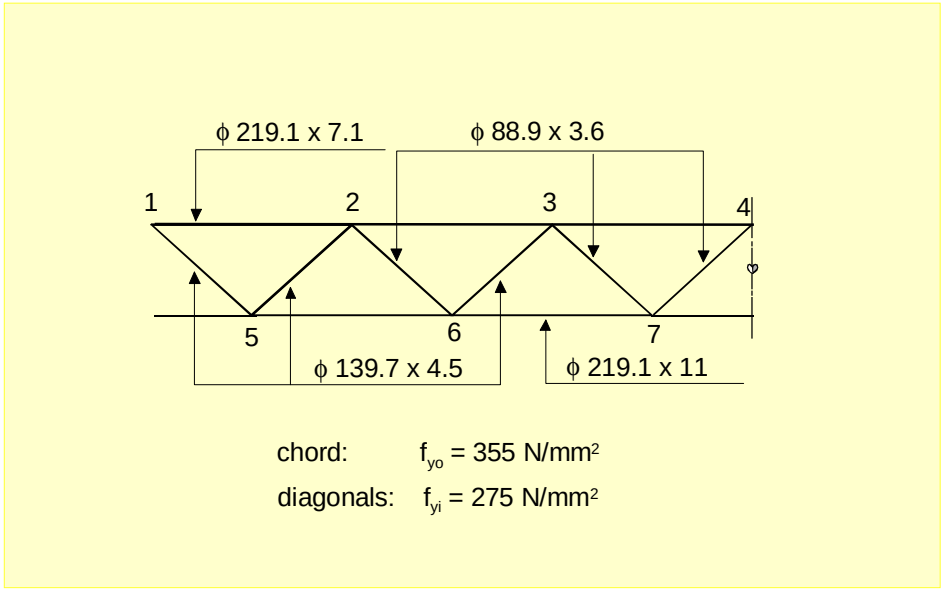

Fig. 14.13 Member dimensions and steel grades

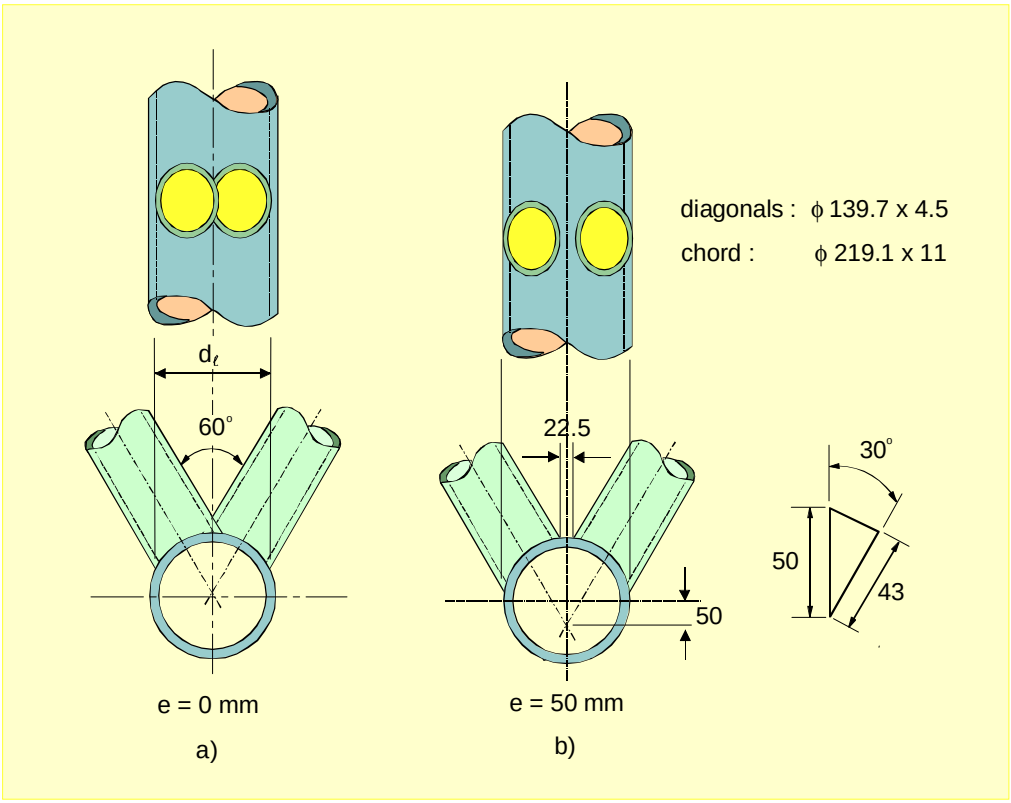

Fig. 14.14 Connection diagonals with bottom chord

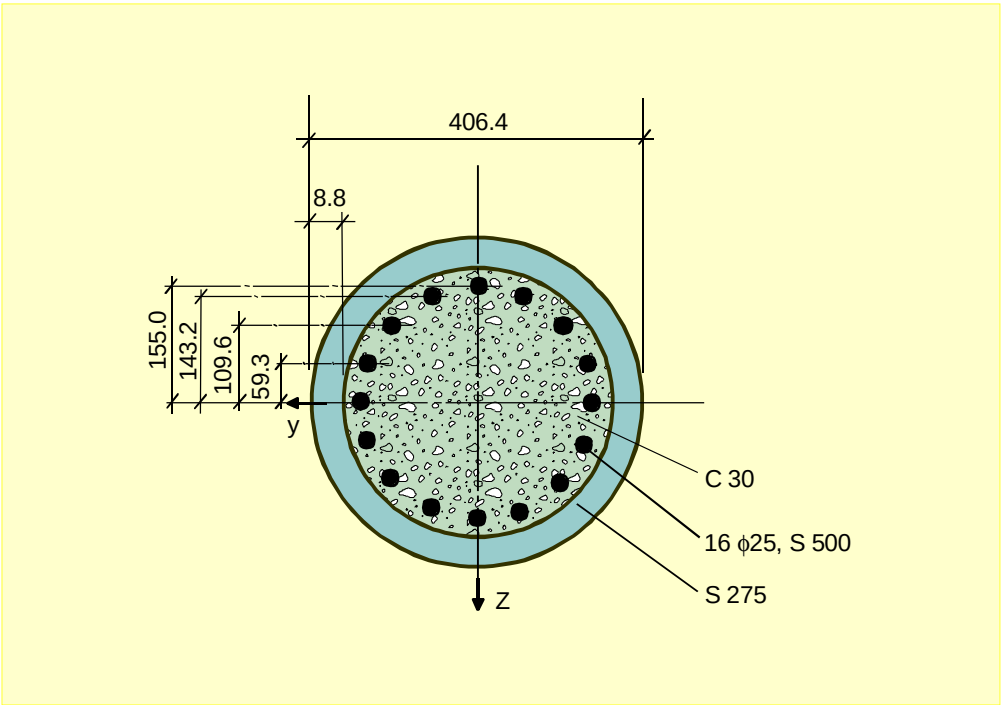

Fig. 14.15 Concrete filled column

15. REFERENCES

CIDECT Design Guides

1. Wardenier, J., Kurobane, Y., Packer, J.A., Dutta, D. and Yeomans, N.: Design guide for circular hollow section (CHS) joints under predominantly static loading (1). CIDECT (Ed.) and Verlag TÜV Rheinland, Cologne, Germany, 1991. ISBN3-88585-975-0.

2. Rondal, J., Würker, K.G., Wardenier, J., Dutta, D. and Yeomans, N.: Structural stability of hollow sections (2). CIDECT (Ed.) and Verlag TÜV Rheinland, Cologne, Germany, 1991. ISBN 3-8249-0075-0.

3. Packer, J.A., Wardenier, J., Kurobane Y., Dutta, D. and Yeomans, N.: Design guide for rectangular hollow section (RHS) joints under predominantly static loading (3). CIDECT (Ed.) and Verlag TÜV Rheinland, Cologne, Germany, 1992. ISBN 3-8249-0089-0.

4. Twilt, L., Hass, R., Klingsch, W., Edwards, M. and Dutta, D.: Design guide for structural hollow section columns exposed to fire (4). CIDECT (Ed.) and Verlag TÜV Rheinland, Cologne, Germany, 1994. ISBN 3-8249-0171-4.

5. Bergmann, R., Dutta, D., Matsui, C. and Meinsma, C.: Design guide for concrete-filled hollow section columns (5). CIDECT (Ed.) and Verlag TÜV Rheinland, Cologne, Germany, 1995. ISBN 3-8249-0298-2.

6. Wardenier, J., Dutta, D., Yeomans, N., Packer, J.A. and Bucak, Ö.: Design guide for structural hollow sections in mechanical applications (6). CIDECT (Ed.) and Verlag TÜV Rheinland, Cologne, Germany, 1995. ISBN 3-8249-0302-4.

7. Dutta, D., Wardenier, J., Yeomans, N., Sakae, K., Bucak, Ö. and Packer, J.A.: Design Guide for Fabrication, Assembly and Erection of Hollow Section Structures (7). CIDECT (Ed.) and TÜV Verlag, Cologne, Germany, 1998. ISBN 3-8249-0443-8.

8. Zhao, X-L., Herion, S., Packer, J A., Puthli, R.S., Sedlacek, G., Wardenier, J., Weynand, K., Wingerde, A.M. van. and Yeomans, N.F.: Design Guide for Circular and Rectangular Hollow Section Welded Joints under Fatigue Loading (8). CIDECT (Ed.) and TÜV Verlag, Cologne, Germany, 2000. ISBN 3-8249-0565-5.

9. Eekhout, M.: Tubular structures in architecture. CIDECT, 1996. ISBN 90-75095-26-0.

Standards and Recommendations

10. ENV 1991-1-1: 1994, Eurocode No.1, Basis of Design and Actions on Structures, CEN, 1994.

11. ENV 1992-1-1:1991. Eurocode No. 2: Design of Concrete Structures, part 1: General Rules and Rules for Buildings, CEN 1991.

12. ENV 1993-1-1: 1992,Eurocode No. 3, Design of Steel Structures, part 1.1 - General Rules and Rules for Buildings, CEN, 1992.

13. ENV 1994-1-1: 1992. Eurocode No. 4: Design of Composite Steel and Concrete Structures, part 1.1: General Rules and Rules for Buildings.

14. A.I.J.: Recommendations for the design and fabrication of tubular structures in steel, 3rd ed., Architectural Institute of Japan, 1990.

15. A.P.I. Recommended practice for planning, designing and constructing fixed offshore Platforms RP-2A. American Petroleum Institute, U.S.A., 1997.

16. A.W.S.: Structural Welding Code - Steel. ANSI/AWS D1.1-2000, 17th Edition, American Welding Society, Miami, Florida, U.S.A., 2000.

17. Det Norske Veritas: Rules for classification, fixed offshore installations. Part 3, Chapter 1: Structural Design, General. DNV, Hø vik, Norway, 1989.

18. Internal Institute of Welding, Subcommission XV-E: Design recommendations for hollow section joints - predominantly statically loaded, 2nd ed., IIW Doc. XV-701-89, International Institute of Welding Annual Assembly, Helsinki, Finland, 1989.

19. International Institute of Welding, Subcommission XV-E: Recommended Fatigue Design Procedure for Welded Hollow Section Joints, Part 1: Recommendations and Part 2: Commentary. Docs XV-1035-99/XIII-1804-99.

20. ISO 657/14: Hot rolled steel sections, Part 14: Hot formed structural hollow sections - Dimensions and sectional properties. International Organization for Standardization.

21. ISO 4019: Cold finished steel structural hollow sections - Dimensions and sectional properties. International Organization for Standardization.

22. ISO 834: "Fire resistance tests - Elements of building construction", International Organization for Standardization, first edition, 1975.

23. ISO TC67/SC7/WG3/P3: Draft Code Provisions for Section E. Revision R6, International Organization for Standardization, 1997.

24. HSE: Offshore Installations: Guidance on design, construction and certification. Health and Safety Executive, U.K., 1990.

25. UEG: Design of Tubular Joints for Offshore Structures, Underwater Engineering Group UEG, London, U.K., 1985.

26. EN 10210-1: Hot finished structural hollow sections of non-alloy and fine grain structural steels - part 1: Technical delivery conditions, 1998.

27. EN 10210-2: Hot finished structural hollow sections of non-alloy and fine grain structural steels - Part 2: Tolerances, dimensions and sectional properties, 1998.

28. EN 10219-1: Cold formed structural hollow sections of non-alloy and fine grain structural steels - part 1: Technical delivery conditions, 1998.

29. EN 10219-2: Cold formed structural hollow sections of non-alloy and fine grain structural steels - Part 2: Tolerances, dimensions and sectional properties, 1998.

Books

30. Brodka, J.: Stahlrohrkonstruktionen. Verlagsgesellschaft Rüdolf Müller, Köln-Braunsfeld, Germany, 1968.

31. CIDECT: Construction with hollow steel sections. British Steel plc, Corby, Northants, U.K., 1984. ISBN 0-9510062-0-7.

32. Dutta, D., Würker, K.G.: Handbuch Hohlprofile in Stahlkonstruktionen, Verlag TÜV Rheinland GmbH, Köln, Germany, 1988. ISBN 3-88585-528-3.

33. Dutta, D.: Hohlprofilkonstruktionen. Ernst & Sohn, Berlin, Germany, 1999. ISBN 3-433-01310-1.

34. Kurobane, Y.: New Developments and Practices in Tubular Joint Design (+ Addendum), International Institute of Welding, Annual Assembly, Oporto, Portugal, 1981, Doc. XV-488-81.

35. Mang, F., Bucak, Ö.: Hohlprofilkonstruktionen, Stahlbau-Handbuch, Bd. I, Stahlbau-Verlag, Köln, Germany, 1983.

36. Marshall, P.W.: Design of welded tubular connections. Elsevier, Amsterdam, The Netherlands, 1992.

37. Packer, J.A. and Henderson, J.E.: Hollow Structural Section Connections and Trusses - A Design Guide. Canadian Institute of Steel Construction, Toronto, Canada, 1997. ISBN 0-88811-086-3.

38. Puthli, R.S.: Hohlprofilkonstruktionen aus Stahl nach DIN V ENV 1993 (EC3) und DIN 18 800 (11.90), Werner Verlag GmbH & Co. K.G., Düsseldorf, Germany, 1998. ISBN 3-8041-2975-7.

39. Rautaruukki: Design Handbook for Rautaruukki Structural Hollow Sections. Hämeenlinna, Finland, 1998. ISBN 952-5010-22-8.

40. Stahlrohr-Handbuch: 9. Aufl. Vulkan-Verlag, Essen, Germany, 1982.

41. Syam, A.A. and Chapman, B.G.: Design of structural steel hollow section connections. 1st Edition, Australian Institute of Steel Construction, Sydney, Australia, 1996. ISBN 0 9099 45 58 6.

42. Wardenier, J.: Hollow Section Joints, Delft University Press, Delft, The Netherlands, 1982. ISBN 90.6275.084.2.

43. Wardenier, J. and Packer, J.A.: Connections between hollow sections, Chapter 3.5 in "Constructional Steel Design - An International Guide", Elsevier, London, U.K., 1992.

44. Wanke, J.: Stahlrohrkonstruktionen. Springer Verlag, Vienna, Austria, 1966.

Publications and documentation

45. Jamm, W.: Form strength of welded tubular connections and tubular structures under static loading. (Translation from German). Schweissen und Schneiden, Vol. 3, Germany, 1951.

46. Natarajan, M. and Toprac, A.A.: Studies on tubular joints in Japan: Review of research reports. University of Texas Report, U.S.A., 1968.

47. Togo, T.: Experimental study on mechanical behaviour of tubular joints. PhD thesis, Osaka University, Japan, 1967 (in Japanese).

48. Natarajan, M. and Toprac, A.A.: Studies on tubular joints in USA: Review of research reports. University of Texas Report, U.S.A., 1969.

49. Bouwkamp, J.G.: Concept on tubular joints design. Proceedings of ASCE, Vol. 90, No. ST2, U.S.A., 1964.

50. Marshall, P.W. and Toprac, A.A.: Basis for tubular design. ASCE preprint 2008, April 1973, also Welding Journal, U.S.A., 1974.

51. Lind, N.C. and Schroff, D.K.: Utilization of cold work in light gauge steel.

52. Packer, J.A.: Overview of Current International Design Guidance on Hollow Structural Section Connections. Proceedings of the Third International Offshore and Polar Engineering Conference, Singapore, 1993.

53. Baar, S.: Etude théorique et expérimentale du déversement des poutres à membrures tubulaires. Collection des publications de la Faculté des Sciences Appliquées de Université de Liège, No. 10, Liège, Belgium, 1968.

54. Mouty, J.: Effective lengths of lattice girder members. CIDECT Monograph No. 4, 1991.

55. Korol, R.M. and Hudoba, J.: Plastic Behaviour of Hollow Structural Sections. Journal of the Structural Division, ASCE, 98(5), U.S.A., 1972.

56. Wilkinson, T. and Hancock, G.: Compact or class 1 limits for rectangular hollow sections in bending. Proceedings of the Eighth International Symposium on Tubular Structures, Singapore, 1998.

57. Marshall, J.: Torsional behaviour of structural rectangular hollow sections. The Structural Engineer, No. 8, Vol. 49, 1971.

58. Deutscher Dampfkesselausschuß: Glatte Vierkantrohre und Teilkammern unter innerem Überdruck, Technische Regeln für Dampfkessel (TRD 320), Vereinigung der Technischen Überwachungsvereine e.V., Essen, Germany, 1975.

59. Brockenbrough, R.L.: Strength of square tube connections under combined loads. Proceedings of ASCE, Journal of Structural Division, St. 12, U.S.A., 1972.

60. Roik, K. and Wagenknecht, G.: Traglastdiagramme zur Bemessung von Druckstäben mit doppelsymmetrischem Querschnitt aus Baustahl. Mitteilungen des Instituts für konstruktiven Ingenieurbau, Universität Bochum, Heft 27, Germany, 1977.

61. Schulz, G.: Der Windwiderstand von Fachwerken aus zylindrischen Stäben und seine Berechnung. Internationaler Normenvergleich für die Windlasten auf Fachwerken. Monograph No. 3, CIDECT, 1970.

62. Tissier, P.: Resistance to corrosion of the interior of hollow steel sections. Acier, Stahl, Steel 2/1978.

63. British Steel: Tubular Structures (various numbers), The Tubemasters, Welded Tubes Business BSC, Corby, U.K.

64. Mannesmanröhren Werke A.G.: Mannesmann Stahlbauhohlprofile (MSH) Anwendungsbeispiele, Technical Documentation, Düsseldorf, Germany, 1991.

65. IISI: Innovation in steel - Bridges around the world. International Iron and Steel Institute (1997).

66. Guiaux, P. and Janss, J.: Comportement au flambement de colonnes constituées de tubes en acier remplis de béton. Centre de Recherches Scientifiques et Techniques de l'Industrie des Fabrications Métalliques, MT 65, Brussels, Belgium, 1970.

67. Virdi, K.S. and Dowling, P.J.: A unified design method for composite columns. International Association for Bridge and Structrural Engineering. Mémoires Vol. 36-II, Zurich, Switzerland, 1976.

68. Roik, K., Bergmann, R., Bode H. and Wagenknecht, G.: Tragfähigkeit von ausbetonierten Hohlprofilen aus Baustahl, Ruhr-Universität Bochum, Institut für konstruktiven Ingenieurbau, TWM-Heft Nr. 75-4, Germany, 1975.

69. Twilt, L. and Both, C.: Technical Notes on the realistic behaviour and design of fire exposed steel and composite structures. Final report ECSC 7210-SA/112, Activity D: "Basis for Technical Notes", TNO Building and Construction Research, BI-91-069, The Netherlands, 1991.

70. Grandjean, G., Grimault, J.-P. and Petit, L.: Détermination de la Durée au Feu des Profiles Creux Remplis de Béton. Cometube, Paris, France, 1980 (also published as ECSC-report No. 7210-SA/302).

71. Twilt, L. and Haar, P.W. v.d.: Harmonization of the Calculation Rules for the Fire Resistance of Concrete Filled SHS-columns, CIDECT project 15F-86/7-0; IBBC-TNO report B-86-461, The Netherlands, 1986.

72. Draft user's manual POTFIRE, developed for CIDECT by CTICM and TNO, CIDECT progr. 15N - 21/98.

73. Hönig, O., Klingsch, W. and Witte, H.: Baulicher Brandschutz durch wassergefüllte Stützen in Rahmentragwerken (Fire resistance of water filled columns). Research Report, Studiengesellschaft für Stahlanwendung e.V., Forschungsbericht p. 86/4.5, Düsseldorf, Germany, 1985.

74. Packer, J.A. and Wardenier, J.: Design rules for welds in RHS, K, T, Y and X connections, Proceedings IIW International Conference on Engineering Design in Welded Constructions, Madrid, Spain, 1992.

75. Lu, L.H., De Winkel, G.D., Yu, Y. and Wardenier, J.: Deformation limit for the ultimate strength of hollow section joints. Proceedings of the Sixth International Symposium on Tubular Structures, Melbourne, Australia, 1994.

76. Vegte, G.J. van der: The static strength of uniplanar and multiplanar tubular T- and X-joints, PhD thesis, Delft University Press, Delft, The Netherlands, 1995.

77. Makino, Y., Kurobane, Y., Ochi, K., Vegte, G.J. van der and Wilmhurst, S.R.: Database of test and numerical analysis results for unstiffened tubular joints. IIW Doc. XV-E-96-220, Dept. of Architecture, Kumamoto University, Japan, 1996.

78. Liu D.K. and Wardenier, J.: Effect of boundary conditions and chord preloads on the strength of RHS multiplanar K-joints. Proceedings 8th Int. Symposium on Tubular Structures, Singapore, 1998.

79. Marshall, P.W.: Connections for Welded Tubular Structures. Houdremont lecture. Proceedings 2nd International IIW Conference, Boston. U.S.A., 1984.

80. Yura, J.A., Zettlemoyer, N. and Edwards, I.F.: Ultimate capacity equations for tubular joints, OTC 3690, U.S.A., 1980.

81. Kurobane, Y. and Makino, Y.: Analysis of existing and forthcoming data for multiplanar KK-joints with circular hollow sections. CIDECT final report 5BF-10/98.

82. Makino, Y., Kurobane, Y., Paul, J.C., Orita, Y., Hiraishi, K.: Ultimate capacity of gusset plate-to-tube joints under axial and in-plane bending loads. Proceedings of 4th International Symposium on Tubular Structures, Delft, The Netherlands, 1991.

83. Akiyama, N., Yayima, M., Akiyama, H. and Otake, F.: Experimental study on strength of joints in steel tubular structures. JSSC Vol. 10, No. 102, Japan, 1974 (in Japanese).

84. Lee, M.S. and Cheng, M.P.: Plastic consideration on punching shear strength of tubular joints. OTC 2641, U.S.A., 1976.

85. Hoadley, P.W. and Yura, J.A.: Ultimate strength of tubular joints subjected to combined loads. PMFSEL, Report No. 8303, University of Texas, Austin, U.S.A., 1983.

86. Yamada, Y., Morita, M., Makino, Y. and Wilmshurst, S.R.: A new ultimate capacity formula for unstiffened CHS T-, TT-, X-, K- and KK-joints under axial brace loads. Proceedings of the Eighth International Symposium on Tubular Structures, Singapore, 1998.

87. Paul, J.C.: The ultimate behaviour of multiplanar TT- and KK-joints made of circular hollow sections. PhD thesis, Kumamoto University, Japan, 1992.

88. Zettlemoyer, N.: ISO Harmonisation of offshore guidance on strength of tubular joints. Proceedings of the Sixth ISOPE Conference, Los Angeles, U.S.A., 1996.

89. Lalani, M.: Developments in tubular joint technology for offshore structures. Proceedings of the Second ISOPE Conference, San Francisco, U.S.A., 1992.

90. Thiensiripipat, N.: Statical behaviour of cropped web joints in tubular trusses. PhD thesis, University of Manitoba, Canada, 1979.

91. Rondal, J.: Study of maximum permissible Weld Gaps in Connections with Plane End Cuttings (5AH2); Simplification of Circular Hollow Section Welded Joints (5AP), CIDECT Report 5AH2/4AP-90/20.

92. Packer, J.A.: Theoretical behaviour and analysis of welded steel joints with RHS chord sections. PhD thesis, University of Nottingham, U.K., 1978.

93. Zhao, X.L.: The behaviour of cold formed RHS beams under combined actions. PhD thesis, The University of Sydney, Australia, 1992.

94. Yu, Y.: The static strength of uniplanar and multiplanar connections in rectangular hollow sections, PhD thesis, Delft University Press, Delft, The Netherlands, 1997.

95. Wardenier, J. and Giddings, T.W.: The strength and behaviour of statically loaded welded connections in structural hollow sections. Monograph No. 6, CIDECT, Corby, U.K., 1986.

96. Davies, G. and Crocket, P.: Effect of the hidden weld on RHS partial overlap K-joint capacity. Proceedings International Symposium on Tubular Structures, Melbourne, Australia, 1994.

97. Frater, G.: Performance of welded rectangular hollow structural section trusses. PhD thesis, University of Toronto, Canada, 1991.

98. Bauer, D. and Redwood, R.G.: Triangular truss joints using rectangular tubes. Journal of Structural Engineering, ASCE, 114(2), U.S.A., 1988.

99. Korol, R.M., El-Zanaty, M. and Brady, F.J.: Unequal width connections of square hollow sections in Vierendeel trusses. Canadian Journal of Civil Engineering, Vol. 4, No.2, Canada, 1977.

100. Ono, T., Iwata, M. and Ishida, K.: An experimental study on joints of new truss system using rectangular hollow sections. Proceedings 4th Internatonal Symposium on Tubular Structures, Delft, The Netherlands, 1991.

101. Szlendak, J.: Ultimate load of welded beam-column connections in rectangular hollow sections. PhD thesis, Technical University of Warsaw, Poland, 1982 (in Polish).

102. Wardenier, J. and Mouty, J.: Design rules for predominantly statically loaded welded joints with hollow sections as bracings and an I- or H-section as chord. Welding in the World, Vol. 17, No. 9/10, 1979.

103. Aribert, J.M., Ammari, F. and Lachal, A.: Influence du mode d'application d'une charge de compression locale sur la résistance plastique de l'âme d'un profilé cas des assemblages tubulaires. Construction Métallique No. 2, France, 1988.

104. Kamba, T. and Tabuchi, M.: Database for tubular column to beam connections in moment resisting frames. IIW Doc. XV-E-94-208, Dept. of Architecture, Kobe University, Japan, 1994.

105. De Winkel, G.D.: The Static strength of I-beam to circular hollow section column connections, PhD thesis, Delft University Press, Delft, The Netherlands, 1998.

106. Lu, L.H.: The static strength of I-beam to rectangular hollow section column connections, PhD thesis, Delft University Press, Delft, The Netherlands, 1997.

107. Shanmugan N.E., Ting, L.C. and Lee, S.L.: Static behaviour of I-beam to box column connections with external stiffeners. The Structural Engineer 71(15), London, U.K., 1993.

108. Kato, B. and Hirose, A.: Bolted tension flanges joining circular hollow section members. CIDECT report 8C-84/24-E.

109. Igarashi, S., Wakiyama, K., Inoue, K., Matsumoto, T. and Murase, Y.: Limit design of high strength bolted tube flange joint, Parts 1 and 2. Journal of Structural and Construction Engineering Transactions of AIJ, Department of Architecture reports, Osaka University, Japan, 1985.

110. Packer, J.A., Bruno, L. and Birkemoe, P.C.: Limit analysis of bolted RHS flange plate joints, Journal of Structural Engineering, American Society of Civil Engineering, Vol. 115, No. 9, U.S.A., 1989.

111. Struik, J.H.A. and De Back, J.: Tests on bolted T-stubs with respect to a bolted beam-to-column connection. Stevin Laboratory report 6-69-13, Delft University of Technology, The Netherlands, 1969.

112. Fisher, J.W. and Struik, J.H.A.: Guide to design criteria for bolted and riveted joints. John Wiley & Sons. New York, London, Sydney, 1973.

113. Yeomans, N.F.: Rectangular hollow section connections using the Lindapter Hollo-Bolt. Proceedings International Symposium on Tubular Structures, Singapore, 1998.

114. Yeomans, N.F.: I-Beam/rectangular hollow section column connections using the Flowdrill system. Proceedings Sixth International Symposium on Tubular Structures, Melbourne, Australia, 1994.

115. Packer, J.A. . and Krutzler, R.T.: Nailing of steel tubes. Proceedings Sixth International Symposium on Tubular Structures, Melbourne, Australia, 1994.

116. Packer, J.A. .: Nailed tubular connections under axial loading. Journal of Structural Engineering, Vol. 122, No. 8, U.S.A., 1996.

117. Kosteski, N., Packer, J.A. and Wingerde, A.M. van: Fatigue behaviour of nailed tubular connections. Proceedings of the Ninth International Offshore and Polar Engineering Conference, Brest, France, 1999.

118. Zirn, R.: Schwingfestigkeitsverhalten geschweißter Rohrknotenpunkte und Rohrlasschenverbindungen. Techn. Wiss. Bericht MPA Stuttgart, Heft 75-01, Germany, 1975.

119. De Back, J.: Testing tubular joints. Session developer's report, International Conference on Steel in Marine Structures, Paris, France, 1981.

120. Vegte, G.J. van der, Back, J. de, and Wardenier, J.: Low cycle fatigue of welded structures. Delft University of Technology, Stevin report 25.6.89.10/A1, Delft, The Netherlands, 1989.

121. Thorpe, T.W. and Sharp, J.V.: The fatigue performance of tubular joints in air and sea water. MaTSU Report, Harwell Laboratory, Oxfordshire, U.K., 1989.

122. Wingerde, A.M. van: The fatigue behaviour of T- and X-joints made of square hollow sections, Heron, Vol. 37, No. 2, Delft University of Technology, Delft, The Netherlands, 1992.

123. Wingerde, A.M. van, Wardenier, J. and Packer, J.A.: Commentary on the draft specification for fatigue design of hollow section joints. Proceedings 8th International Symposium on Tubular Structures, Singapore, 1998.

124. Romeijn, A.: Stress and strain concentration factors of welded multiplanar tubular joints, Heron, Vol. 39, No. 3, Delft University of Technology, Delft, The Netherlands, 1994.

125. Herion, S.: Räumliche K-Knoten aus Rechteck-Hohlprofilen, PhD thesis, University of Karlsruhe, Germany, 1994.

126. Panjeh Shahi, E.: Stress and strain concentration factors of welded multiplanar joints between square hollow sections, PhD thesis, Delft University Press, Delft, The Netherlands, 1995.

127. Niemi, E.J.: Fatigue resistance predictions for RHS K-joints, using two alternative methods. Proceedings Seventh International Symposium on Tubular Structures, Miskolc, Hungary, 1996.

128. Bouwman, L.P.: Bolted connections dynamically loaded in tension, ASCE, Journal of the Structural Division, Vol. 108, No. ST, U.S.A., 1982.

129. Packer, J.A. and Fear, C.E.: Concrete-filled rectangular hollow section X and T connections. Proceedings 4th International Symposium on Tubular Structures, Delft, The Netherlands, 1991.

130. ESDEP: European Steel Design Education Programme, Lectures Working Group 13: Hollow Section Structures and Working Group 12: Fatigue, The Steel Construction Institute, U,K., 1994.

131. Proceedings International Symposia on Tubular Structures (general), 1984, 1986, 1989, 1991, 1993, 1994, 1996, 1998.

Acknowledgements for figures and photographs:

The author expresses his appreciation to the following organisations, firms and institutes for making available the photographs and figures used in this lecture book.

- Corus Tubes, U.K.
- CIDECT
- Delft University of Technology, The Netherlands
- Instituto para la Construccion Tubular, Spain
- Kumamoto University, Dept. of Architecture, Japan
- Ruhr University, Bochum, Faculty of Civil Engineering, Germany
- Stichting Bouwen met Staal, Rotterdam
- Tubeurop, France
- University of Toronto, Dept. of Civil Engineering, Canada
- Vallourec & Mannesmann Tubes, Germany

COMITE INTERNATIONAL POUR LE DEVELOPPEMENT ETL'ETUDE DE LA CONSTRUCTION TUBULAIRE

INTERNATIONAL COMMITTEE FOR THE DEVELOPMENT AND STUDY OF TUBULAR STRUCTURES

CIDECT, founded in 1962 as an international association, joins together the research resources of the principal hollow steel section manufacturers to create a major force in the research and application of hollow steel sections world-wide.

The objectives of CIDECT are:

- to increase the knowledge of hollow steel sections and their potential application by initiating and participating in appropriate research and studies.
- to establish and maintain contacts and exchanges between producers of the hollow steel sections and the ever increasing number of architects and engineers using hollow steel sections throughout the world.
- to promote hollow steel section usage wherever this makes good engineering practice and suitable architecture, in general by disseminating information, organising congresses, etc.
- to co-operate with organisations concerned with practical design recommendations, regulations or standards at national and international level.

Technical activities

The technical activities of CIDECT have centred on the following research aspects of hollow steel section design:

- Buckling behaviour of empty and concrete filled columns
- Effective buckling ths of members in trusses
- Fire resistance of concrete filled columns
- Static strength of welded and bolted joints
- Fatigue resistance of welded joints
- Aerodynamic properties
- Bending strength of hollow steel section beams
- Corrosion resistance
- Workshop fabrication, including section bending

The results of CIDECT research form the basis of many national and international design requirements for hollow steel sections.

CIDECT Publications

The current situation relating to CIDECT publications reflects the ever increasing emphasis on the dissemination of research results.

The list of CIDECT Design Guides, in the series “Construction with Hollow Steel Sections”, already published, or in preparation, is given below. These design guides are available in English, French, German and Spanish.

1. Design guide for circular hollow section (CHS) joints under predominantly static loading (1991)

2. Structural stability of hollow sections (1992, reprinted 1996)

3. Design guide for rectangular hollow section (RHS) joints under predominantly static loading (1992)

4. Design guide for structural hollow section columns in fire (1995, reprinted 1996)

5. Design guide for concrete filled hollow section columns under static and seismic loading (1995)

6. Design guide for structural hollow sections in mechanical applications (1995)

7. Design guide for fabrication, assembly and erection of hollow section structures (1998)

8. Design guide for circular and rectangular hollow section joints under fatigue loading (to be published 2001)

In addition, taking into account the ever increasing place of steel hollow sections in internationally acclaimed "high tech" structures a book "Tubular Structures in Architecture" has been published with the sponsorship of the European Community.

Copies of the Design Guides, the architectural book and research papers may be obtained from:

The Steel Construction Institute
Attn. Dr. Farooq Awan
Silwood Park
Ascot
Berkshire SL5 7QN
England
Tel: +44-(0)1344-23345
Fax: +44-(0)1344-22944
E-mail: publications@steel-sci.com
Web site: http://www.steel-sci.org

CIDECT Organisation (2000)

- President: B. Becher - Germany
  Vice -President: C.L. Bijl - The Netherlands

- A General Assembly of all members meeting once a year and appointing an Executive Committee responsible for administration and execution of established policy.

- A Technical Commission and Promotions Group; meeting at least once a year and direclty responsible for the research and technical promotion work.

Present members of CIDECT are:

- Aceralia Transformados, Spain
- A.G. Tubos Europa, S.A., Spain
- Borusan, Turkey
- Corus, United Kingdom
- IPSCO Inc., Canada
- Onesteel (formerly BHP Steel), Australia
- Rautaruukki Oy, Finland
- Tubeurop, France
- Vallourec & Mannesmann Tubes, Germany
- Voest Alpine Krems, Austria